



*A National Center of Excellence in Advanced Technology Applications*

ISSN 1520-295X

---

# Experimental and Analytical Studies of Structures Seismically Isolated with an Uplift-Restraint Isolation System

by

Panayiotis C. Roussis and Michael C. Constantinou  
University at Buffalo, State University of New York  
Department of Civil, Structural and Environmental Engineering  
Ketter Hall  
Buffalo, New York 14260

Technical Report MCEER-05-0001

January 10, 2005

This research was conducted at the University at Buffalo, State University of New York and was supported primarily by the Earthquake Engineering Research Centers Program of the National Science Foundation under award number EEC-9701471.

## NOTICE

This report was prepared by the University at Buffalo, State University of New York as a result of research sponsored by the Multidisciplinary Center for Earthquake Engineering Research (MCEER) through a grant from the Earthquake Engineering Research Centers Program of the National Science Foundation under NSF award number EEC-9701471 and other sponsors. Neither MCEER, associates of MCEER, its sponsors, the University at Buffalo, State University of New York, nor any person acting on their behalf:

- a. makes any warranty, express or implied, with respect to the use of any information, apparatus, method, or process disclosed in this report or that such use may not infringe upon privately owned rights; or
- b. assumes any liabilities of whatsoever kind with respect to the use of, or the damage resulting from the use of, any information, apparatus, method, or process disclosed in this report.

Any opinions, findings, and conclusions or recommendations expressed in this publication are those of the author(s) and do not necessarily reflect the views of MCEER, the National Science Foundation, or other sponsors.

# Experimental and Analytical Studies of Structures Seismically Isolated with an Uplift-Restraint Isolation System

by

Panayiotis C. Roussis<sup>1</sup> and Michael C. Constantinou<sup>2</sup>

Publication Date: January 10, 2005  
Submittal Date: October 19, 2004

Technical Report MCEER-05-0001

Task Number 2.4a and 03/2.2

NSF Master Contract Number EEC-9701471

- 1 Postdoctoral Associate, Department of Civil, Structural and Environmental Engineering, University at Buffalo, State University of New York
- 2 Professor, Department of Civil, Structural and Environmental Engineering, University at Buffalo, State University of New York

MULTIDISCIPLINARY CENTER FOR EARTHQUAKE ENGINEERING RESEARCH  
University at Buffalo, State University of New York  
Red Jacket Quadrangle, Buffalo, NY 14261

---



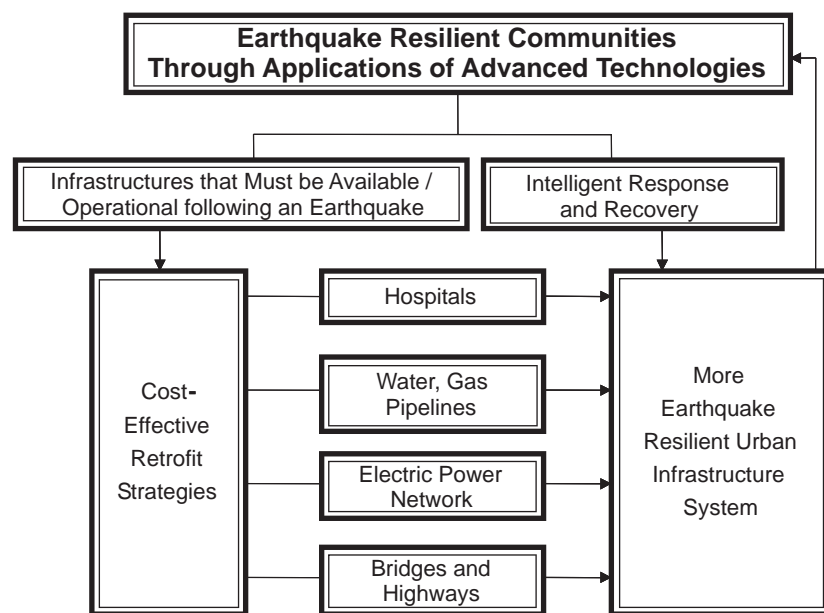
## Preface

The Multidisciplinary Center for Earthquake Engineering Research (MCEER) is a national center of excellence in advanced technology applications that is dedicated to the reduction of earthquake losses nationwide. Headquartered at the University at Buffalo, State University of New York, the Center was originally established by the National Science Foundation in 1986, as the National Center for Earthquake Engineering Research (NCEER).

Comprising a consortium of researchers from numerous disciplines and institutions throughout the United States, the Center's mission is to reduce earthquake losses through research and the application of advanced technologies that improve engineering, pre-earthquake planning and post-earthquake recovery strategies. Toward this end, the Center coordinates a nationwide program of multidisciplinary team research, education and outreach activities.

MCEER's research is conducted under the sponsorship of two major federal agencies: the National Science Foundation (NSF) and the Federal Highway Administration (FHWA), and the State of New York. Significant support is derived from the Federal Emergency Management Agency (FEMA), other state governments, academic institutions, foreign governments and private industry.

MCEER's NSF-sponsored research objectives are twofold: to increase resilience by developing seismic evaluation and rehabilitation strategies for the post-disaster facilities and systems (hospitals, electrical and water lifelines, and bridges and highways) that society expects to be operational following an earthquake; and to further enhance resilience by developing improved emergency management capabilities to ensure an effective response and recovery following the earthquake (see the figure below).



A cross-program activity focuses on the establishment of an effective experimental and analytical network to facilitate the exchange of information between researchers located in various institutions across the country. These are complemented by, and integrated with, other MCEER activities in education, outreach, technology transfer, and industry partnerships.

*This report describes the development of a novel uplift-prevention Friction Pendulum isolator called the XY-FP. It presents the principles of operation and mathematical model of the XP-FP isolator, describes its mechanical behavior through testing of a single isolator, and demonstrates its effectiveness through testing of a quarter-scale steel-frame model structure. The computer program 3D-BASIS-ME was modified to include an element representative of the mechanical behavior of the new XY-FP isolator, and the validity and accuracy of analytical methods to predict its behavior is assessed. The study shows that the XY-FP isolator provides effective uplift prevention regardless of the state of displacement in the bearing, allows for decoupling of the bi-directional horizontal motion along two orthogonal directions, and has the capability to provide distinct stiffness and energy dissipation along the principal directions of the bearing. In addition, by encompassing much less structural material, the isolator offers a lighter and more economical alternative to the standard Friction Pendulum bearing. Moreover, it provides an architecturally flexible solution in terms of integration into a structural system when space considerations are important.*

## ABSTRACT

Notwithstanding its pervasive influence on seismic-resistant engineering, the efficacy of seismic isolation in structures subjected to strong ground excitation, including near-fault effects, is potentially compromised by excessive overturning moments capable of inducing undesirable uplift or tension in the isolation bearings. This report aims at extending the scope of seismic isolation by studying a novel sliding isolation bearing, denoted as XY-FP, that is capable of sustaining tensile forces, thereby preventing uplift.

This report primarily focuses on: (i) introducing the concept and establishing the principles of operation and mathematical model of the new XY-FP isolator; (ii) developing an understanding of the mechanical behavior of the XY-FP isolator through testing of a single isolator; (iii) generating experimental results through earthquake simulator testing of a quarter-scale five-story model to validate the effectiveness of these isolators in preventing uplift; (iv) modifying the computer program 3D-BASIS-ME to include an element representative of the XY-FP isolator; and (v) assessing the validity and accuracy of analytical methods to predict the behavior of such systems.

The XY-FP isolation bearing consists of two opposing concave beams interconnected through an element which permits tension to develop in the bearing, thereby preventing uplift. Salient properties that distinguish the XY-FP isolator from the conventional Friction Pendulum (FP) isolator include: (i) effective uplift restraint regardless of the state of displacement in the bearing; (ii) decoupling of the bi-directional horizontal motion along two orthogonal directions; and (iii) capability of providing distinct stiffness and energy dissipation along the principal directions of the bearing.

To demonstrate the validity of the concept and provide evidence for the effectiveness of the XY-FP isolator in uplift restraint, an extensive testing program on the earthquake simulator at the University at Buffalo was conducted on a slender quarter-scale five-story base-isolated model structure. The isolation system, comprised of four XY-FP isolators, was installed beneath a base and rotated for testing in different directions. The range of tests conducted represent the only available experimental data on XY-FP isolators and form the basis for comparison with and validation of the analytical predictions.

A comprehensive mathematical model capable of accommodating the mechanical behavior of the XY-FP isolator was developed and implemented in program 3D-BASIS-ME. The new element representing the XY-FP isolator was synthesized by two independent uniaxial hysteretic elements allowing different frictional interface properties along the principal isolator directions under compressive or tensile isolator normal force. Contrary to the element representing the conventional FP isolator, the new element is capable of developing tension. This enhancement augments the potential of 3D-BASIS-ME by providing a versatile tool for analysis of seismically isolated structures with XY-FP isolators.

The dynamic response of the five-story seismically isolated model was predicted analytically using 3D-BASIS-ME. The validity of the analytical model, with reference to the newly introduced element representing the XY-FP isolator, was investigated by comparison of analytical predictions with experimental results.

Finally, a case study involving nonlinear response-history analysis of a seismically isolated structure subjected to bi-directional horizontal seismic excitation is presented to assess the impact of XY-FP isolator on the response of a real structure.

## **ACKNOWLEDGEMENTS**

Financial support for this project was provided by the Multidisciplinary Center for Earthquake Engineering Research (Task 2.4a and Task 03/2.2) and Earthquake Protection Systems, Inc., Vallejo, CA. This support is gratefully acknowledged.

The assistance of Professor Panagiotis Tsopelas of the Catholic University of America in modifying program 3D-BASIS-ME is also gratefully acknowledged.

This report is nearly identical to the doctoral dissertation of Panayiotis C. Roussis. The dissertation committee consisted of Professors Michael C. Constantinou (Chair), Andrei M. Reinhorn, Andrew S. Whittaker, and Andres Soom (outside reviewer, Department of Mechanical and Aerospace Engineering).



# TABLE OF CONTENTS

SECTION	TITLE	PAGE
<b>1</b>	<b>INTRODUCTION</b> .....	<b>1</b>
1.1	Background.....	1
1.2	Motivation .....	5
1.3	Objective.....	6
1.4	Outline .....	6
<b>2</b>	<b>DESCRIPTION AND MATHEMATICAL MODEL OF XY-FP ISOLATOR</b> .....	<b>9</b>
2.1	Introduction .....	9
2.2	Principles of Operation.....	9
2.3	Mathematical Model.....	10
<b>3</b>	<b>TESTING OF XY-FP ISOLATOR</b> .....	<b>19</b>
3.1	Introduction .....	19
3.2	Theoretical Background .....	19
3.3	Testing Machine Description.....	21
3.4	Testing Program .....	21
3.5	Test Results .....	24
<b>4</b>	<b>MODEL FOR EARTHQUAKE SIMULATOR TESTING</b> .....	<b>31</b>
4.1	Introduction .....	31
4.2	Model Description .....	31
4.3	Pushover Analysis .....	34
4.4	Instrumentation.....	34
4.5	Testing Program .....	36
4.6	Identification of Dynamic Characteristics of Model Structure.....	48
<b>5</b>	<b>EARTHQUAKE SIMULATOR TESTING RESULTS</b> .....	<b>55</b>
5.1	Introduction .....	55
5.2	Test Results .....	55
5.3	Interpretation of Results .....	57
<b>6</b>	<b>MODIFICATION OF PROGRAM 3D-BASIS-ME</b> .....	<b>69</b>
6.1	Introduction .....	69
6.2	Overview of Program 3D-BASIS .....	69
6.3	Enhancements Introduced in Program 3D-BASIS-ME .....	71
6.3.1	New Hysteretic Element for XY-FP Isolator .....	71
6.3.2	Account for Initial Non-zero Displacement of the Isolators .....	75
6.3.3	A More Accurate Description of the Additional Bearing Axial Forces due to Overturning Moment Effects .....	75
<b>7</b>	<b>ANALYTICAL PREDICTION OF RESPONSE</b> .....	<b>79</b>
7.1	Introduction .....	79
7.2	Analytical Model.....	79
7.3	Comparison of Experimental and Analytical Results.....	80

## TABLE OF CONTENTS (Continued)

SECTION	TITLE	PAGE
<b>8</b>	<b>A CASE STUDY</b> .....	87
8.1	Introduction .....	87
8.2	Description of Seismically Isolated Structure .....	87
8.3	Analytical Model in SAP2000 and 3D-BASIS-ME .....	89
8.4	Analysis Results .....	93
<b>9</b>	<b>SUMMARY AND CONCLUSIONS</b> .....	111
<b>10</b>	<b>REFERENCES</b> .....	117
<b>APPENDIX A</b>	<b>PUSHOVER ANALYSIS OF 5-STORY MODEL FRAME</b> .....	*
<b>APPENDIX B</b>	<b>EXPERIMENTAL RESULTS FOR THE 5-STORY MODEL STRUCTURE SEISMICALLY ISOLATED WITH XY-FP ISOLATORS</b> .....	*
<b>APPENDIX C</b>	<b>COMPARISON OF ANALYTICAL AND EXPERIMENTAL RESULTS FOR THE 5-STORY MODEL STRUCTURE SEISMICALLY ISOLATED WITH XY-FP ISOLATORS</b> .....	*
<b>APPENDIX D</b>	<b>COMPARISON OF ANALYTICAL PREDICTIONS OF SAP2000 AND 3D-BASIS-ME FOR THE CASE-STUDY STRUCTURE SEISMICALLY ISOLATED WITH SOLELY FP ISOLATORS</b> .....	*
<b>APPENDIX E</b>	<b>COMPARISON OF 3D-BASIS-ME ANALYTICAL PREDICTIONS OF THE CASE-STUDY STRUCTURE SEISMICALLY ISOLATED WITH (a) SOLELY FP ISOLATORS AND (b) BOTH FP AND XY-FP ISOLATORS</b> .....	*

\* The appendices are provided on the enclosed CD.

## LIST OF FIGURES

FIGURE	TITLE	PAGE
1-1	Uplift-restraint system used on Excel Minami-Koshigaya building, Koshigaya City, Japan (Sumitomo Construction, 1990) .....	2
1-2	Displacement-control, uplift-restraint device incorporated in elastomeric bearing (Kelly et al., 1987).....	3
1-3	Uni-directional flat sliding bearing with uplift-restraint device (Nagarajaiah et al., 1992) .....	4
1-4	View of uni-directional FP bearing with uplift restraint installed at the San Francisco approach to the Oakland Bay Bridge .....	4
1-5	View of the novel uplift-prevention XY-FP isolator .....	5
2-1	Three-dimensional view of the uplift-restraint XY-FP isolator.....	9
2-2	Plan view of XY-FP isolator in its deformed position.....	11
2-3	Free body diagrams of (a) connecting slider for motion along local axis 1, and (b) upper concave beam for motion along local axis 2, under compressive and tensile normal force .....	12
2-4	Effect of lateral force interaction in XY-FP isolator .....	15
2-5	Force-displacement relation of XY-FP isolator under (a) compressive and (b) tensile normal force.....	16
2-6	Behavior of system of two isolators: FP vs. XY-FP isolators .....	18
3-1	Dependency of coefficient of friction on velocity .....	20
3-2	Variation of friction parameter $f_{\max}$ with pressure.....	20
3-3	Schematic of isolator testing apparatus .....	21
3-4	Photograph of isolator testing apparatus.....	22
3-5	Two-dimensional view of the uplift-restraint XY-FP isolator used in this study.....	22
3-6	Views of XY-FP isolator during testing in 0°, 45°, and 90° orientation.....	23
3-7	Imposed displacement history for XY-FP isolator testing.....	23
3-8	Recorded normalized force-displacement loops of XY-FP isolator demonstrating the effect of (a) normal force, and (b) sliding velocity .....	25
3-9	Dependency of coefficient of friction on velocity of sliding.....	27
3-10	Recorded normalized force-displacement loops of XY-FP isolator for different isolator orientations for (a) compressive and (b) tensile normal load.....	28
4-1	Photograph of tested five-story isolated model structure on the seismic simulator at the University at Buffalo .....	32
4-2	Schematic of tested 5-story isolated model structure .....	33
4-3	Member cross sections for model structure .....	33
4-4	Instrumentation diagram for the 5-story test frame .....	35
4-5	Histories and response spectra of shake table motion for El Centro S00E 200% excitation.....	39
4-6	Histories and response spectra of shake table motion for Taft N21E 400% excitation.....	40

## LIST OF FIGURES (Continued)

FIGURE	TITLE	PAGE
4-7	Histories and response spectra of shake table motion for Newhall 90 100% excitation.....	41
4-8	Histories and response spectra of shake table motion for Newhall 360 100% excitation.....	42
4-9	Histories and response spectra of shake table motion for Sylmar 90 100% excitation.....	43
4-10	Histories and response spectra of shake table motion for Kobe N-S 100% excitation.....	44
4-11	Histories and response spectra of shake table motion for Pacoima S74W 100% excitation.....	45
4-12	Histories and response spectra of shake table motion for Pacoima S16E 100% excitation.....	46
4-13	Histories and response spectra of shake table motion for Hachinohe N-S 100% excitation.....	47
4-14	Floor transfer function amplitudes for banded (0-40 Hz) white noise base excitation .....	52
4-15	Schematic of influential mode shapes of fixed-based model structure.....	53
5-1	Typical isolation system displacement history .....	56
5-2	History of permanent displacements from testing in different isolator orientations .....	62
5-3	Experimental results in El Centro S00E 200% for bearing orientation of 0° .....	63
5-4	Experimental results in Newhall 360 100% for bearing orientation of 0° .....	64
5-5	Experimental results in Newhall 360 100% for bearing orientation of 90° .....	65
5-6	Experimental results in Newhall 360 100% for bearing orientation of 45° .....	66
5-7	Comparison of experimental results in Pacoima S74W 100% and Pacoima S74W+Vertical 100% excitations for bearing orientation of 0° .....	67
6-1	Force interaction curves for XY-FP and FP isolators.....	73
6-2	Definition of overturning moments OVMX and OVMY, and additional force FOVM .....	74
7-1	Comparison of experimental and analytical results for bearing orientation of 0° for 100% Kobe N-S excitation.....	82
7-2	Comparison of experimental and analytical results for bearing orientation of 0° for 100% Newhall 360+vertical excitation .....	83
7-3	Comparison of experimental and analytical results for bearing orientation of 90° for 100% Newhall 360+vertical excitation.....	84
7-4	Comparison of experimental and analytical results for bearing orientation of 45° for 100% Sylmar 90+vertical excitation .....	85

## LIST OF FIGURES (Continued)

FIGURE	TITLE	PAGE
7-5	Comparison of experimental and analytical results for bearing orientation of 45° for 100% Newhall 360+vertical excitation .....	86
8-1	View of the new Acropolis Museum in Athens, Greece directly at the foot of the Acropolis. ( <a href="http://www.archpedia.com/Projects-Bernard-Tschumi_01.html">http://www.archpedia.com/Projects-Bernard-Tschumi_01.html</a> ) .....	88
8-2	Plan view of isolated structure.....	88
8-3	Schematic of SAP2000 model of the seismically isolated building used in the case study .....	90
8-4	Plan view of the base of the building model in SAP2000 showing the spatial distribution of seismic isolation bearings .....	90
8-5	Comparison of SAP2000 and 3D-BASIS-ME generated results in terms of superstructure response in X direction for the model with 94 FP isolators in scaled (factor 4.5) Lower California 270-180 excitation .....	95
8-6	Comparison of SAP2000 and 3D-BASIS-ME generated results in terms of superstructure response in Y direction for the model with 94 FP isolators in scaled (factor 4.5) Lower California 270-180 excitation .....	96
8-7	Comparison of SAP2000 and 3D-BASIS-ME generated results in terms of isolation system response in X direction for the model with 94 FP isolators in scaled (factor 4.5) Lower California 270-180 excitation .....	97
8-8	Comparison of SAP2000 and 3D-BASIS-ME generated results in terms of isolation system response in Y direction for the model with 94 FP isolators in scaled (factor 4.5) Lower California 270-180 excitation .....	98
8-9	Comparison of SAP2000 and 3D-BASIS-ME generated results in terms of response of bearing No. 55 in X direction for the model with 94 FP isolators in scaled (factor 4.5) Lower California 270-180 excitation .....	99
8-10	Comparison of SAP2000 and 3D-BASIS-ME generated results in terms of response of bearing No. 55 in Y direction for the model with 94 FP isolators in scaled (factor 4.5) Lower California 270-180 excitation .....	100
8-11	Number of bearings in uplift per time instant.....	102
8-12	Comparison of 3D-BASIS-ME generated results in terms of superstructure response in X direction between the model with 94 FP isolators and the model with 25 XY-FP + 69 FP isolators in scaled (factor 2.0) El Centro 180-270 excitation .....	103
8-13	Comparison of 3D-BASIS-ME generated results in terms of superstructure response in Y direction between the model with 94 FP isolators and the model with 25 XY-FP + 69 FP isolators in scaled (factor 2.0) El Centro 180-270 excitation .....	104
8-14	Comparison of 3D-BASIS-ME generated results in terms of isolation system response in X direction between the model with 94 FP isolators and the model with 25 XY-FP + 69 FP isolators in scaled (factor 2.0) El Centro 180-270 excitation.....	105
8-15	Comparison of 3D-BASIS-ME generated results in terms of isolation system response in Y direction between the model with 94 FP isolators and the model with 25 XY-FP + 69 FP isolators in scaled (factor 2.0) El Centro 180-270 excitation.....	106

## LIST OF FIGURES (Continued)

FIGURE	TITLE	PAGE
8-16	Comparison of 3D-BASIS-ME generated results in terms of response of bearing No. 67 in X direction between the model with 94 FP isolators and the model with 25 XY-FP + 69 FP isolators in scaled (factor 2.0) El Centro 180-270 excitation.....	107
8-17	Comparison of 3D-BASIS-ME generated results in terms of response of bearing No. 67 in Y direction between the model with 94 FP isolators and the model with 25 XY-FP + 69 FP isolators in scaled (factor 2.0) El Centro 180-270 excitation.....	108

## LIST OF TABLES

<b>TABLE</b>	<b>TITLE</b>	<b>PAGE</b>
3-1	Values of parameters used in isolator testing program.....	23
3-2	Parameters used in calibration of the equation describing the dependency of coefficient of friction on velocity (Equation (3-1)).....	26
4-1	Scale factors for model structure .....	34
4-2	List of data acquisition channels (with reference to Figure 4-4) .....	36
4-3	List of earthquake motions and their characteristics in prototype scale .....	38
4-4	List of earthquake simulator tests conducted on the 5-story model structure .....	48
4-5	Dynamic characteristics of fixed-based model structure .....	53
5-1	Experimentally recorded peak structure response for isolator angle of 0° .....	58
5-2	Experimentally recorded peak structure response for isolator angle of 90° .....	59
5-3	Experimentally recorded peak structure response for isolator angle of 45° .....	60
8-1	Properties of analyzed structure.....	91
8-2	Periods of free vibration of the fixed-base structure .....	91
8-3	Selected ground motions and scale factors used in analysis.....	93
8-4	FP isolators undergoing uplift identified from 3D-BASIS-ME analysis.....	101



# SECTION 1

## INTRODUCTION

### 1.1 Background

Having found a plethora of applications in many parts of the world, seismic isolation has emerged as a pragmatic approach to providing earthquake resistance to structural systems. Research developments in the areas of analytical modeling and experimental validation techniques paralleled by notable advances of seismic isolation device hardware, have provided the impetus for the increasing acceptance of seismic isolation.

The fundamental principle underlying seismic isolation involves decoupling the structure from the damaging horizontal ground motion by means of additional flexibility and energy dissipation capability, thereby mitigating the severity of structural vibration and damage during seismic events (Naeim and Kelly, 1999; Skinner et al., 1993). Typified by either elastomeric or sliding bearings, the application of seismic isolation systems can result in significant reduction of the inertial forces developed in a structure during a severe earthquake. While this entails a desired reduction of the sustained overturning moments, the uplift forces may still be potentially large enough to be of concern, on account of the inherent incapacity of elastomeric and sliding bearings to resist uplift forces.

In fact, a variety of conditions may contribute to the development of either tensile forces (in bolted rubber bearings) or uplift (in sliding bearings and doweled rubber bearings). These include slender structures with a large height-to-width aspect ratio, certain types of bridges with large ratio of height of the centroidal axis to the distance between the bearings, and bearings below braced columns or stiff walls.

Tensile forces or uplift in isolation bearings may produce, under certain conditions, detrimental effects in the form of local instability or rupture of elastomeric bearings, and damage on sliding bearings due to large compressive forces upon impact following uplift. Loss of contact and impact on return can yield higher-mode response and large axial forces in columns.

A number of uplift-restraint seismic isolation systems have been proposed and some have been implemented. A brief account of these systems and their limitations is given below.

- An uplift-restraint system consisting of two massive orthogonal steel arms (Figure 1-1) was developed by Sumitomo Construction in Japan and used on the Excel Minami-Koshigaya 10-story building in Koshigaya City (Sumitomo Construction, 1990). The opposing arms, connected to the superstructure and foundation, interlock upon uplift equal to the 1-cm default clearance, thus preventing further uplift of the superstructure. The system has not been tested and its impact on the behavior of the isolation system has not been assessed to the knowledge of the author.

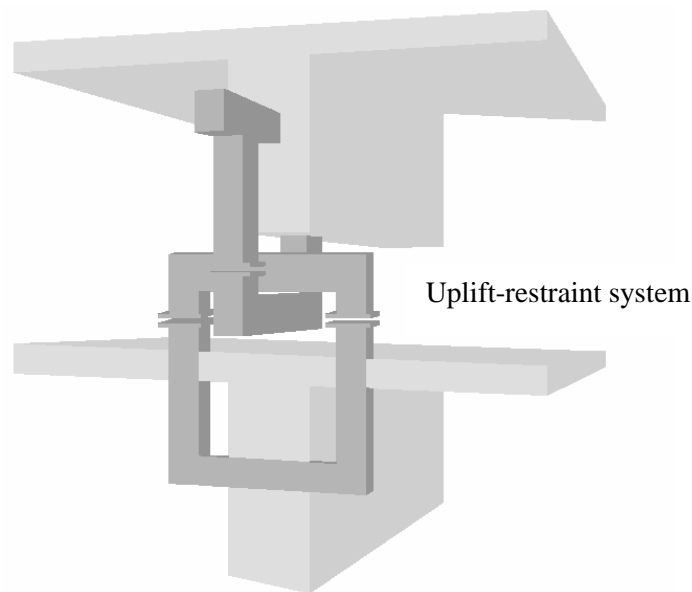


Figure 1-1: Uplift-restraint system used on Excel Minami-Koshigaya building, Koshigaya City, Japan (Sumitomo Construction, 1990).

- A mechanism that claims to provide uplift restraint and displacement control for elastomeric bearings was described by Kelly et al. (1987) and Griffith et al. (1988a, 1988b, 1990). The system has been studied in earthquake simulator tests of seismically isolated structures. Incorporated within a central hole in elastomeric bearings, the device consists of two high-strength bolts contained in a cylindrical sleeve that allows a certain amount of free movement of the bolts (Figure 1-2). This mechanism can be activated only when the bearing undergoes substantial uplift or substantial lateral deformation. In effect, the system does not prevent uplift but rather

may restrict uplift to a limit, which is too large due to the dual function of the mechanism to also provide lateral displacement control. In addition to this limitation, the mechanism is hidden within the bearing inhibiting inspection without removal and disassembly of the bearing.

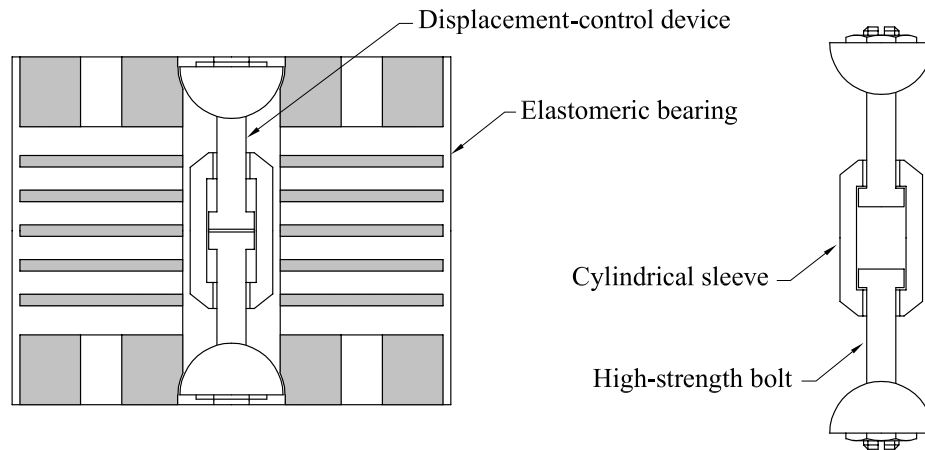


Figure 1-2: Displacement-control, uplift-restraint device incorporated in elastomeric bearing (Kelly et al., 1987).

- The technique of prestressing for the prevention of tensile force and uplift in isolators was described in Logiadis (1996) and Kasalanati and Constantinou (1999). Prestressing tendons were used to develop sufficient additional compressive force on the bearings so that tension or uplift was prevented. This system, while effective and predictable in behavior as demonstrated by testing, is complex and may impact the performance of the isolation system.
- Uni-directional flat sliding bearings encompassing uplift-restraint devices as shown in Figure 1-3 were tested by Nagarajaiah et al. (1992) in an isolation system together with helical steel springs for providing restoring force. The same concept in uplift prevention may be used in sliding bearings with a curved surface as it has been done at the San Francisco approach to the Oakland Bay Bridge, where uni-directional FP bearings are utilized (Figure 1-4). It may be noted that this uplift restrainer allows for some uplift before it engages due to the cylindrical shape of the sliding surface. Extension of this type of restrainer to multi-directional sliding bearings is feasible if the displacement demand is low.

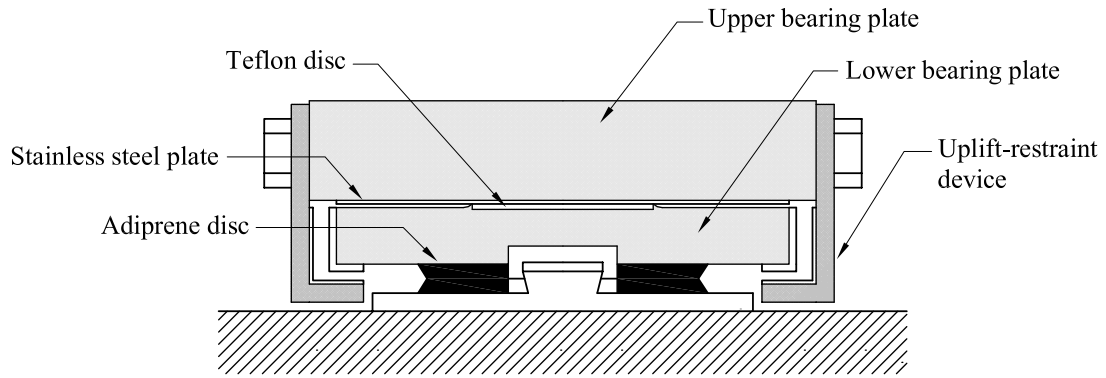


Figure 1-3: Uni-directional flat sliding bearing with uplift-restraint device (Nagarajaiah et al., 1992).



Figure 1-4: View of uni-directional FP bearing with uplift restraint installed at the San Francisco approach to the Oakland Bay Bridge.

Studied in this report is a novel uplift-prevention Friction Pendulum isolator, abbreviated hereafter as XY-FP (Figure 1-5). The XY-FP isolation bearing has the following unique properties: (i) it provides effective uplift prevention regardless of the state of displacement in the bearing; (ii) it allows for decoupling of the bi-directional horizontal motion along two orthogonal directions; and (iii) it has the capability of providing distinct stiffness and energy dissipation along the principal directions of the bearing. Additional benefits can be derived from the unique morphology of the new bearing. In particular, by encompassing much less structural material, the isolator offers a lighter and more economical alternative to the standard Friction Pendulum (FP) bearing. Moreover, it provides an architecturally flexible solution in terms of integration into a structural system for cases where space considerations are important.



Figure 1-5: View of the novel uplift-prevention XY-FP isolator.

## 1.2 Motivation

Thus far, seismically isolated structures have been designed so that uplift in sliding bearings or tension in elastomeric bearings is avoided. To accommodate this practice, changes to the structural system above the isolators were often deemed necessary. However, such changes may be extensive as illustrated in the Oakland City Hall (Honeck et al., 1993) with the construction of a large truss at the basement level to “spread out” the reactions, and in the Corinth Canal Bridges (Constantinou, 1998) with use of counterweights at the abutments.

Uplift or tension in bearings is often undesirable due to concerns for failure of elastomeric bearings in tension or concerns for large bearing compressive forces on engagement following uplift (which may include impact effects).

Recent applications of seismic isolation in California deal with substantial seismic loading, which includes near-fault effects, and desire to achieve specific performance levels. Tension or uplift in isolation bearings is often encountered. Cost, architectural and functionality constraints prevent the modification of the structural system to avoid uplift or tension in bearings. Accordingly, a need evolved to develop acceptable isolators with tension (or uplift restraint) capability and to better understand the phenomena of uplift or tension of isolators and their impact on the performance of structural and non-structural systems.

Prompted by the need to respond to these developments, this research aims at extending the scope of seismic isolation by studying a novel uplift-restraint isolation bearing. With

the isolators capable of sustaining tension, the application of seismic isolation could be widely facilitated.

### **1.3 Objective**

The principal objectives of this report can be summarized as follows: (i) to introduce the concept and establish the principles of operation and mathematical model of the newly introduced XY-FP isolator; (ii) to gain an understanding of the mechanical behavior of the XY-FP isolator through testing of a single isolator; (iii) to generate experimental results through testing of a quarter-scale steel-frame model structure on the earthquake simulator at the University at Buffalo to validate the effectiveness of these isolators in preventing uplift; (iv) to modify the computer program 3D-BASIS-ME to include an element representative of the mechanical behavior of the new XY-FP isolator; and (v) to assess the validity and accuracy of analytical methods to predict the behavior of such systems.

### **1.4 Outline**

This report is thematically organized into nine sections. The introductory section presents background information and embodies the prime motivation, objectives, and organization of the report.

Section 2 describes the concept and presents the underlying principles of operation of the XY-FP isolator. A distinguishing feature of the new isolator is its capability to prevent uplift through a mechanism which permits tension to develop in the bearing. Further, the mathematical model for the new XY-FP isolator is formulated upon development of the force-displacement constitutive relationship.

Section 3 presents experimental results from tests of a single XY-FP isolator conducted using the isolator testing machine currently available at the Structural Engineering and Earthquake Simulation Laboratory of the University at Buffalo. This section aims at gaining a better understanding of the behavior and mechanical properties of the isolators at hand.

Section 4 provides information on the testing program on the earthquake simulator at the

University at Buffalo. The program involved a quarter-scale five-story base-isolated model structure subjected to a number of recorded ground motions having a broad range of frequency contents and amplitudes. The properties and dynamic characteristics of the non-isolated superstructure model were identified and are presented in this section. The isolation system, installed beneath a rigid base, was comprised of four XY-FP isolators. The instrumentation scheme employed in the testing program along with a complete list of tests conducted are presented.

Section 5 includes a representative sample of experimental results from the earthquake simulator testing program described in Section 4. Interpretation of these results provides evidence for the effectiveness of the XY-FP isolator in uplift prevention. In addition, the experimental response forms the basis for comparison with and validation of the analytical predictions presented in Section 7.

Section 6 outlines the modifications made in computer program 3D-BASIS-ME (Tsopelas, et al., 1994). While maintaining the main features of the program, the following enhancements are incorporated: (i) a new hysteretic element capable of modeling the behavior of the new XY-FP isolator; (ii) capability of accounting for initial non-zero displacement of the isolators; and (iii) a more accurate description of the additional bearing axial forces due to overturning effects.

Section 7 is devoted to the analytical prediction of response. The validity of the analytical model, with reference to the newly introduced element representing the XY-FP isolator, was investigated by comparison of analytical predictions with experimental results. The good agreement attests to the accuracy of the analytical model even under extreme dynamic conditions.

Section 8 presents a case study which involves analysis of a seismically isolated structure and assessment of the impact of XY-FP bearing on its response. Nonlinear response-history analysis of the seismically isolated structure subjected to bi-directional horizontal seismic excitation was performed using programs SAP2000 and 3D-BASIS-ME. First, a comparison is made between results from SAP2000 and 3DBASIS-ME analysis based on an isolation system model consisting solely of FP isolators. Moreover, results from 3DBASIS-ME analysis of the model with only FP isolators are compared to results from

analysis of the model with isolators prone to uplift being replaced with XY-FP isolators.

Section 9 presents a summary of key findings and conclusions drawn from this report.

The report is further augmented by five appendices. Appendix A presents information on the pushover analysis of the five-story frame model considered in this study. The complete presentation of experimental results of the five-story base-isolated model structure from the earthquake simulator testing program is given in Appendix B. Appendix C presents comparisons of experimental and 3D-BASIS-ME analytical results for the isolated structure at hand. Appendices D and E include comparison of analytical results pertaining to the case study considered in this report. Presented in Appendix D are results generated by programs SAP2000 and 3DBASIS-ME from analyses of the model with solely FP isolators. In Appendix E results from 3DBASIS-ME analysis of the model with only FP isolators are compared to results from analysis of the model with isolators prone to uplift being replaced with XY-FP isolators.

## SECTION 2

### DESCRIPTION AND MATHEMATICAL MODEL OF XY-FP ISOLATOR

#### 2.1 Introduction

A novel uplift-restraint Friction Pendulum isolator, abbreviated hereafter as XY-FP, is studied in this report. This section introduces the principles of operation and establishes a mathematical model of the new XY-FP isolator.

#### 2.2 Principles of Operation

While a conventional Friction Pendulum in principle (Zayas et al., 1987; Mokha et al., 1988), the new isolator consists of two opposing concave stainless steel-faced beams forming a bi-directional (XY) motion mechanism (Figure 2-1). Under the imposed constraint to remain mutually perpendicular (except for small rotation about the vertical axis), the two beams can move independently relative to each other. In particular, the kinematics involved consists of two independent components: (1) sliding of the upper beam along the (fixed) lower beam; and (2) sliding of the upper beam with respect to the connecting block in a direction perpendicular to the axis of the lower beam. Moreover, the XY-FP isolator is designed for the capability of small rotation (approximately 4 degrees) about the vertical axis to accommodate torsion of the structure.

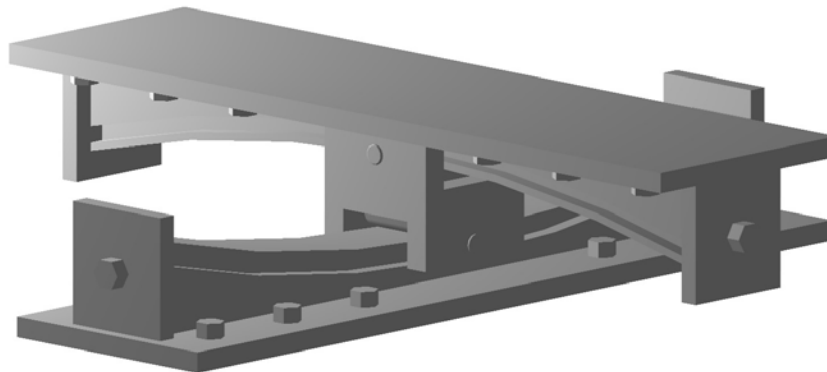


Figure 2-1: Three-dimensional view of the uplift-restraint XY-FP isolator.

In addition to geometric considerations, a distinguishing feature of the new XY-FP isolator is its capability to prevent uplift. The configuration through which the two parts are interconnected permits tension to develop in the bearing, thereby preventing uplift.

The XY-FP isolation bearing has the following unique properties: (1) it provides effective uplift prevention; (2) it allows for decoupling of the bi-directional motion along two orthogonal directions; and (3) it has the capability of providing distinct stiffness and energy dissipation along the principal horizontal directions of the bearing. The latter property can be exploited, for example, in bridges where different response in terms of displacement may be desired along the longitudinal and transverse directions. Neither a conventional FP nor a rubber bearing can offer feasible displacement control in orthogonal directions. Additional benefits can be derived from the unique morphology of the new bearing. In particular, by encompassing much less structural material, the XY-FP isolator offers a lighter and more economical alternative to the FP bearing. Moreover, it provides an architecturally flexible solution in terms of integration into a structural system for cases where space consideration is important, e.g., where the cylindrical shape of the conventional FP bearing becomes awkward or problematic under walls, as in the proximity of elevators and stairs.

### 2.3 Mathematical Model

In formulating the mathematical model for the new XY-FP isolator, separate force-displacement constitutive relationships were developed discretely for compressive and tensile bearing normal load. It is also important to note that the bi-directional motion admits decoupling along the principal axes of the bearing. Accordingly, the constitutive relationship can be conveniently stated with respect to the local co-ordinate system.

Figure 2-2 depicts a plan view of the bearing, whose orientation is defined by the angle  $\theta$  the bottom beam makes with the global X axis, in its deformed position  $U = [U_x \ U_y]^T$  under the action of a horizontal force  $F = [F_x \ F_y]^T$ . The corresponding displacement vector in the local axis system is given by

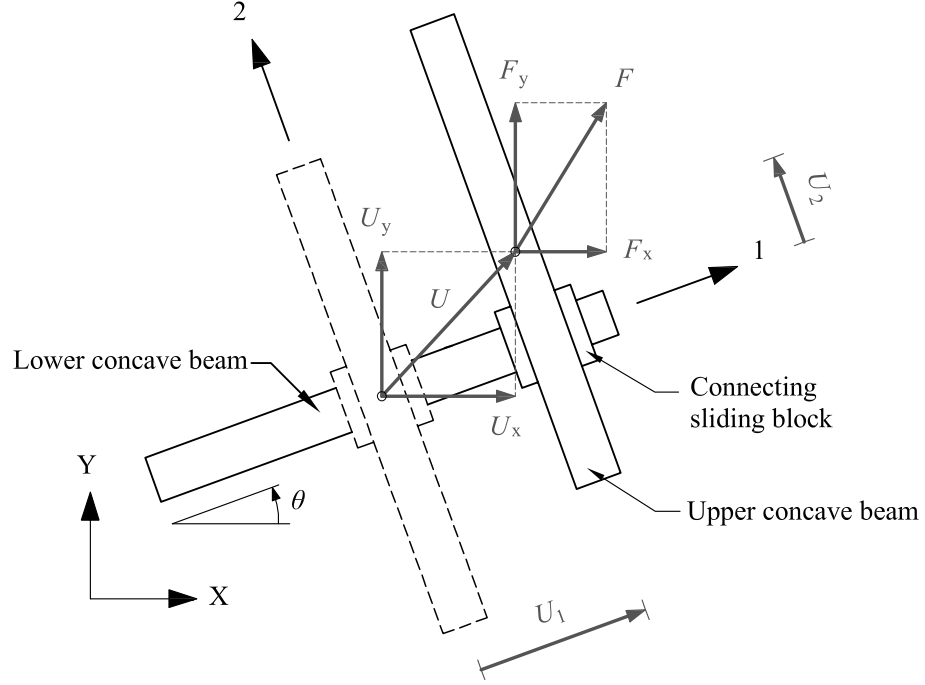


Figure 2-2: Plan view of XY-FP isolator in its deformed position.

$$\begin{Bmatrix} U_1 \\ U_2 \end{Bmatrix} = \begin{bmatrix} \cos \theta & \sin \theta \\ -\sin \theta & \cos \theta \end{bmatrix} \begin{Bmatrix} U_x \\ U_y \end{Bmatrix} \quad (2-1)$$

The displacement components  $U_1$  and  $U_2$  are associated with independent motions along the bearing principal axes, namely sliding of upper beam along the lower beam (local axis 1), and sliding of upper beam in direction perpendicular to the lower beam (local axis 2). Figure 2-3 shows free body diagrams of the mobilized bearing segments under compressive and tensile bearing normal force.

Equilibrium of forces in the horizontal (along axes 1 and 2) and vertical directions for each configuration of Figure 2-3 requires that

$$F_i - F_{f_i} \cos \varphi - S \sin \varphi = 0 \quad (2-2)$$

$$-N - F_{f_i} \sin \varphi + S \cos \varphi = 0 \quad (2-3)$$

where  $i = 1, 2$  denotes the two principal isolator directions;  $F_i$  is the horizontal force of the isolator in the  $i$ -direction;  $F_{f_i}$  is the friction force mobilized on each beam;  $N$  is the

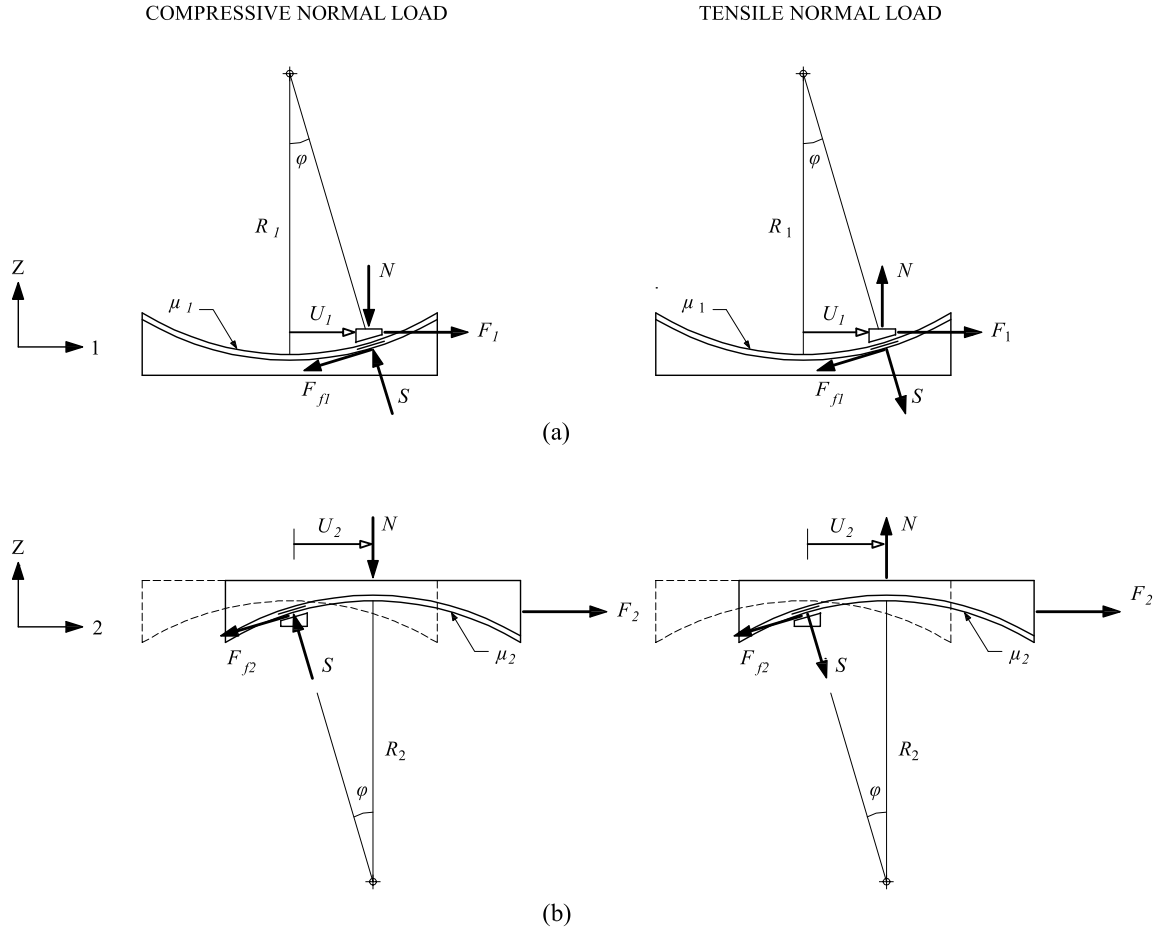


Figure 2-3: Free body diagrams of (a) connecting slider for motion along local axis 1, and (b) upper concave beam for motion along local axis 2, under compressive and tensile normal force.

normal force on the bearing, positive when compressive;  $S$  is the reaction force component normal to the sliding surface; and  $\varphi$  is the angle between the normal to the sliding surface and vertical direction. (It should be noted that the points of application of forces are not clearly shown in Figure 2-3. The exact location of these points is only important for the consideration of moment equilibrium and not of equilibrium of forces as considered herein).

Combining Equations (2-2) and (2-3) gives

$$F_i = N \tan \varphi + \frac{F_{f_i}}{\cos \varphi} \quad (2-4)$$

In view of the dependency of  $\varphi$  on the displacement component  $U_i$  given by

$$U_i = R_i \sin \varphi \quad (2-5)$$

Equation (2-4) can be written as

$$F_i = \frac{N}{R_i \cos \varphi} U_i + \frac{F_{f_i}}{\cos \varphi} ; \quad i = 1, 2 \quad (2-6)$$

where  $R_i$  is the radius of curvature of the circular trajectory of the pivot point of the slider on top of each beam. This radius is equal to the radius of curvature of the surface of each beam minus the small height of the pivot point to the surface. Equation (2-6) describes the resisting force of the isolator along the  $i$ -direction in the general case of large values of angle  $\varphi$ . It is synthesized by two components, one representing the pendulum effect associated with a restoring force (in the case of compressive normal load), and the other representing the contribution of friction developed at the sliding interface.

Assuming small angles of rotation  $\varphi$ , Equation (2-6) reduces to the linearized form

$$F_i = \frac{N}{R_i} U_i + F_{f_i} ; \quad i = 1, 2 \quad (2-7)$$

in which the friction forces associated with the two beams are

$$F_{f_1} = \mu_1 |N| \operatorname{sgn}(\dot{U}_1) + \mu_{side} \left| \frac{N}{R_2} U_2 + \mu_2 |N| \operatorname{sgn}(\dot{U}_2) \right| \operatorname{sgn}(\dot{U}_1) \quad (2-8)$$

$$F_{f_2} = \mu_2 |N| \operatorname{sgn}(\dot{U}_2) + \mu_{side} \left| \frac{N}{R_1} U_1 + \mu_1 |N| \operatorname{sgn}(\dot{U}_1) \right| \operatorname{sgn}(\dot{U}_2) \quad (2-9)$$

where  $\mu_1$  and  $\mu_2$  are the sliding friction coefficients of the lower and upper concave beams, respectively;  $\mu_{side}$  is the coefficient of friction associated with side contact surface between the connecting block and the beams; and  $\operatorname{sgn}(\ )$  is the signum function operating on the sliding velocities.

Equations (2-8) and (2-9) reveal the interaction between lateral forces and friction forces. For instance, when the bearing upper beam moves with respect to the connecting block in direction perpendicular to the lower beam (along axis 2), the developed shear force  $F_2$  is transferred onto one side of the lower beam. Thus, the side contact surface of the lower beam is acted upon a normal force of magnitude  $|F_2|$ , which results in increasing the friction force on the lower beam, should motion along axis 1 occurs. Analogous considerations can be made for the effect of lateral force  $F_1$  on  $F_{f_2}$  as dictated by Equation (2-9).

It should be noted that, the contribution of lateral forces  $F_1$  and  $F_2$  in friction forces  $F_{f_2}$  and  $F_{f_1}$ , respectively, is small, on account of the fact that,  $\mu_{side}\mu_i|N|$  is of higher order and can be neglected, and  $(N/R_i)U_i$  is less than  $0.2|N|$ , since FP bearings are typically designed for displacement  $U < 0.2R$ . Therefore, the additional friction force is always less than  $0.2\mu_{side}|N|$ , with the maximum value attained only at the extreme displacement.

Supportive evidence of the small effect of lateral force interaction is provided graphically in Figure 2-4 wherein simulated isolator force–displacement loops under bi-directional motion are plotted against loops under uni-directional (along local axis 1) motion. In particular, the imposed bi-directional motion in the upper graph of Figure 2-4 consists of a linear displacement pattern in which  $U_1 = U_2 = U_0 \sin \omega t$ , whereas the bi-directional motion in the lower graph consists of an 8-shaped displacement pattern in which  $U_1 = U_0 \sin \omega t$  and  $U_2 = U_0 \sin 2\omega t$ , with  $U_0 = 200$  mm and  $\omega = \pi$  rad/sec. Identical isolator interface conditions were assumed with sliding friction coefficient  $\mu_1 = \mu_2 = \mu_{side} = 0.05$  and radius of curvature  $R = 990$  mm. It can be seen from these plots that the error in the isolator force  $F_1$  neglecting the effect of lateral force  $F_2$  is only about 5 percent.

Neglecting the effect of lateral force on friction force, as will be considered hereafter, the forces needed to induce displacement  $U = [U_1 \ U_2]^T$  on the bearing in the local coordinate system are given collectively by

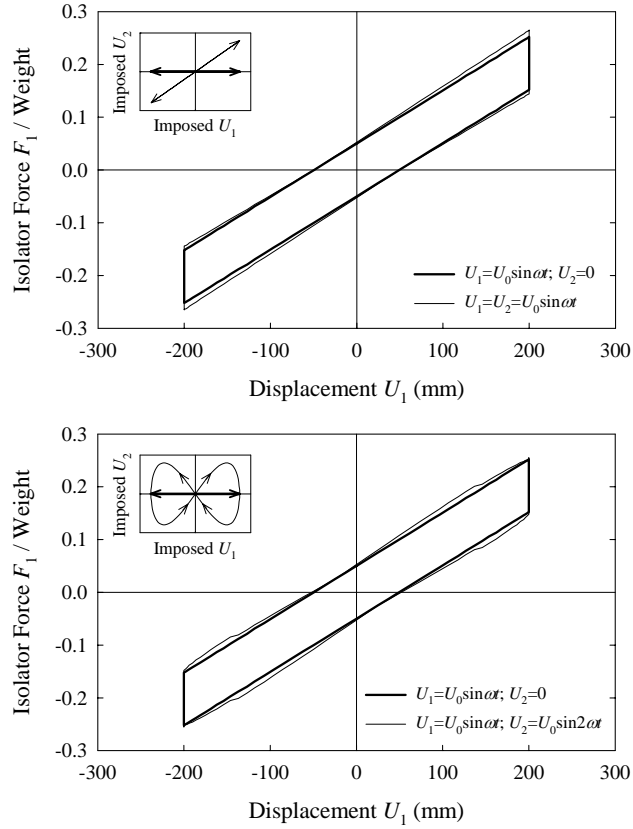


Figure 2-4: Effect of lateral force interaction in XY-FP isolator.

$$\begin{Bmatrix} F_1 \\ F_2 \end{Bmatrix} = \begin{bmatrix} N/R_1 & 0 \\ 0 & N/R_2 \end{bmatrix} \begin{Bmatrix} U_1 \\ U_2 \end{Bmatrix} + \begin{bmatrix} \mu_1 |N| & 0 \\ 0 & \mu_2 |N| \end{bmatrix} \begin{Bmatrix} \text{sgn}(\dot{U}_1) \\ \text{sgn}(\dot{U}_2) \end{Bmatrix} \quad (2-10)$$

The error involved in the linearization of Equation (2-6) is insignificant for all practical purposes, since, as mentioned above, FP bearings are typically designed for displacement  $U < 0.2R$ , so that  $\cos \varphi \approx 1$ .

In general, the normal force on the isolation bearing is a fast-varying function of time due to the effect of vertical earthquake motion and the overturning moment effects. For a vertically rigid superstructure, the normal force on the bearing at any given time is synthesized by

$$N = W \left( 1 + \frac{\ddot{u}_{gv}}{g} + \frac{N_{OM}}{W} \right) \quad (2-11)$$

where  $W$  is the weight acting on the isolator;  $\ddot{u}_{gv}$  is the vertical ground acceleration (positive when the direction is upwards); and  $N_{OM}$  is the additional axial force due to overturning moment effects (positive when compressive).

Evaluation of the bearing normal force according to Equation (2-11) is of utmost importance for the accuracy of the XY-FP model. The fluctuation in the bearing axial force caused by the vertical component of ground motion and overturning moments can be large enough to cause reversal of the axial force from compression to tension.

The theoretical force-displacement relation of the XY-FP isolator under compressive and tensile normal force is depicted in Figure 2-5. Coefficients  $\mu_1$  and  $\mu_2$  can have different values depending on whether the bearing is in compression or tension. It may be noted that under tension the bearing has negative stiffness. This does not imply system instability, since it is virtually impossible to have all bearings in tension at the same time.

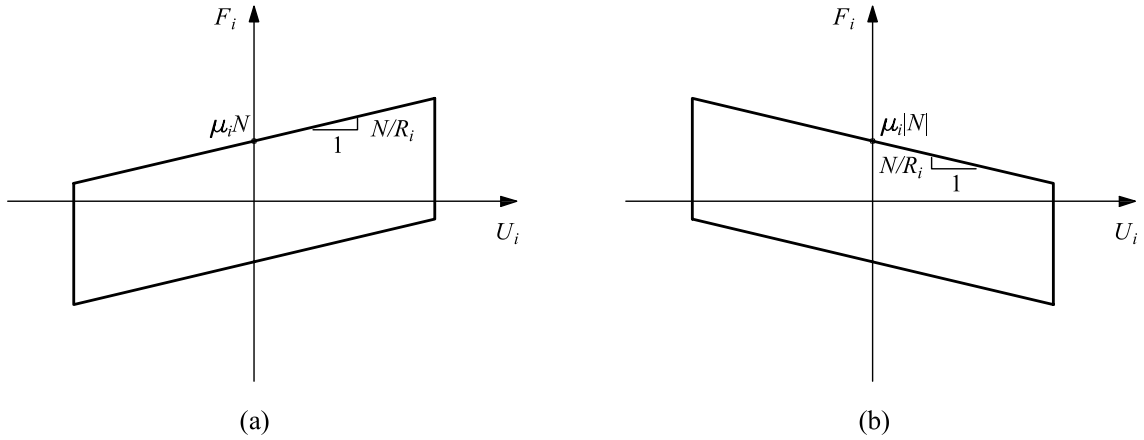


Figure 2-5: Force-displacement relation of XY-FP isolator under (a) compressive and (b) tensile normal force.

In view of Equation (2-10), the horizontal stiffness of the isolator along the  $i$ -th principal direction is derived as

$$K_i = \frac{N}{R_i} \tag{2-12}$$

which yields the period of free vibration as

$$T_i = 2\pi \sqrt{\frac{W}{(W/R_i)g}} = 2\pi \sqrt{\frac{R_i}{g}} \quad (2-13)$$

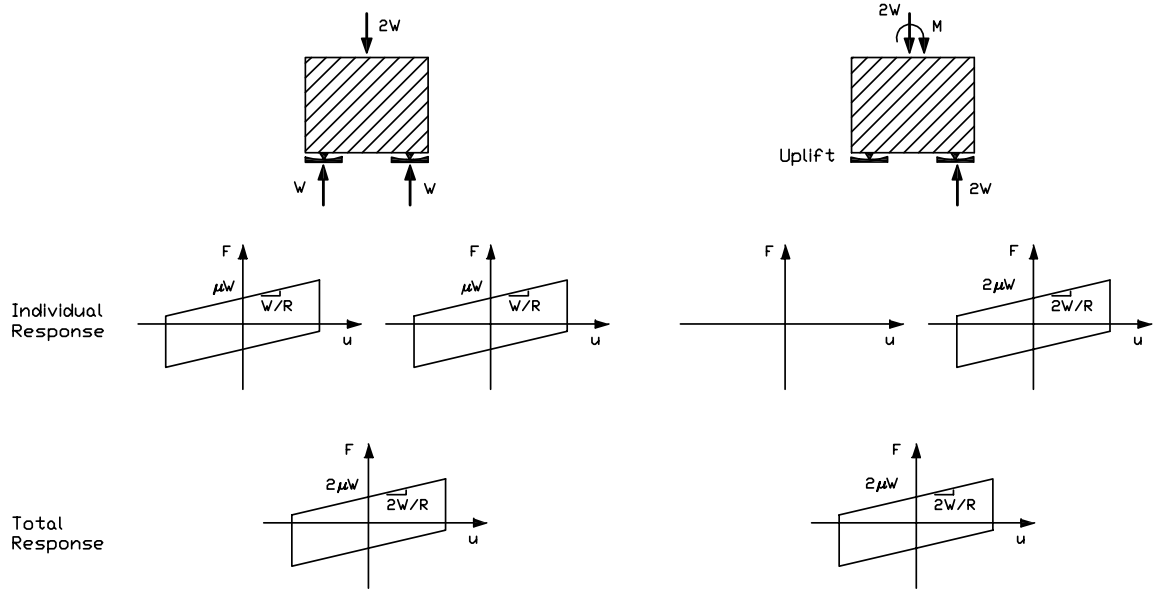
where  $i = 1, 2$  denotes the two principal isolator directions and  $W$  is the weight acting on the isolator. As in the conventional FP isolator, the period is independent of the supported mass and dependent only on the geometry of the bearing.

Having defined the constitutive relation of the bearing with respect to the local coordinate system (Equation (2-10)), the corresponding force-displacement relationship in the global co-ordinate system can be readily derived as

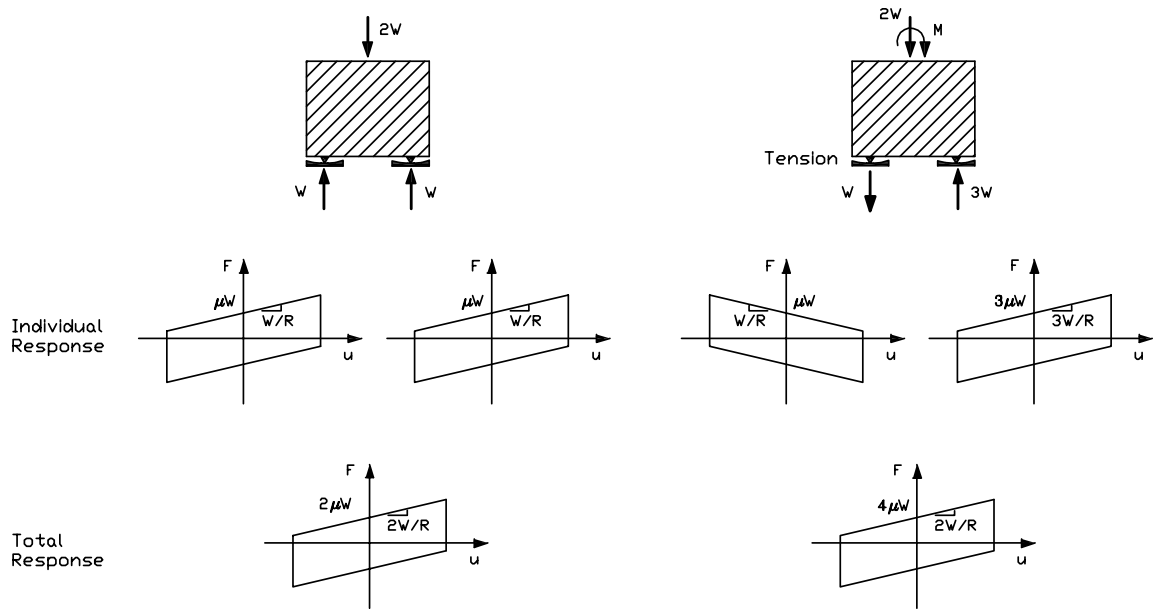
$$\begin{Bmatrix} F_x \\ F_y \end{Bmatrix} = \begin{bmatrix} \cos \theta & \sin \theta \\ -\sin \theta & \cos \theta \end{bmatrix}^T \begin{Bmatrix} F_1 \\ F_2 \end{Bmatrix} \quad (2-14)$$

To gain insight of the global behavior of the isolation system, it is appropriate to extend this discussion by considering a system of two isolators. First, the case of an isolation system consisting of two conventional FP isolators supporting a wall of weight  $2W$  is considered (Figure 2-6(a)). In the presence of sufficient overturning moment  $M$ , where one of the isolators experiences uplift, redistribution of loads occurs and the total weight,  $2W$ , is sustained by the other isolator. It is evident that, both the restoring force and the friction force of the system as a whole remain unchanged.

Next, consider the case where the isolation system is comprised of two uplift-restraint XY-FP isolators (Figure 2-6(b)). Under significant overturning moment, one of the isolators will develop tension, with the sustained compressive load on the adjacent isolator increased to satisfy equilibrium. The negative stiffness of the isolator in tension is balanced by the increased stiffness of the isolator in compression, resulting in the same total system stiffness (restoring force). However, tension development in the XY-FP isolator impacts the friction force of the isolation system. For the exaggerated conditions prevailed in this example, in which 50% of the isolators sustain tension and the magnitude of the tensile force is 100% of the initial compressive load  $W$ , the global friction force increases from  $2\mu W$  to  $4\mu W$ .



(a) FP isolators



(b) XY-FP isolators

Figure 2-6: Behavior of system of two isolators: FP vs. XY-FP isolators.

## SECTION 3

### TESTING OF XY-FP ISOLATOR

#### 3.1 Introduction

To gain a better understanding of the behavior and mechanical properties of the XY-FP isolators, tests of a single isolator were conducted using the isolator testing machine in the Structural Engineering and Earthquake Simulation Laboratory of the University at Buffalo (Kasalanati and Constantinou, 1999).

#### 3.2 Theoretical Background

Presented briefly herein, is the theoretical basis of certain aspects of frictional behavior that are relevant to the interpretation of experimental results at the macroscopic level. A detailed presentation of frictional aspects pertaining to sliding isolators can be found in Constantinou et al. (1999).

The coefficient of sliding friction mobilized on a typical sliding bearing interface is modeled by the following equation:

$$\mu_s = f_{\max} - (f_{\max} - f_{\min})e^{-a|v|} \quad (3-1)$$

where  $f_{\min}$  and  $f_{\max}$  are the minimum and maximum values of the coefficient of friction, respectively, and  $a$  is a parameter which controls the variation of the coefficient of friction with velocity (Constantinou et al., 1990). The dependency of the coefficient of friction on velocity is illustrated in Figure 3-1.

In general, parameters  $f_{\max}$ ,  $f_{\min}$ , and  $a$  are functions of bearing pressure and temperature. However, the dependency of  $f_{\min}$  and  $a$  on pressure is insignificant (compared with that of  $f_{\max}$ ) and can be neglected (Tsopelas et al., 1994). A representative expression describing the variation of parameter  $f_{\max}$  with pressure is given by

$$f_{\max} = f_{\max 0} - (f_{\max 0} - f_{\max p}) \tanh(\varepsilon p) \quad (3-2)$$

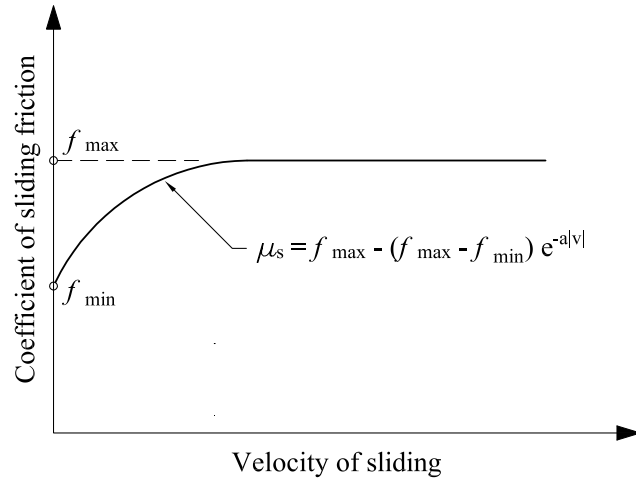


Figure 3-1: Dependency of coefficient of friction on velocity.

where  $p$  is the bearing pressure;  $f_{\max p}$  is the maximum value of the coefficient of friction at very high pressure;  $f_{\max 0}$  is the maximum value of the coefficient of friction at zero pressure; and  $\varepsilon$  is a constant that controls the variation of  $f_{\max}$  between very low and very high pressures.

Figure 3-2 presents the assumed variation of friction parameter  $f_{\max}$  with pressure, which is typical of the behavior of sliding bearings (Soong and Constantinou, 1994). Parameter  $f_{\max}$  is important in that it describes the maximum friction force that is transmitted through the bearing.

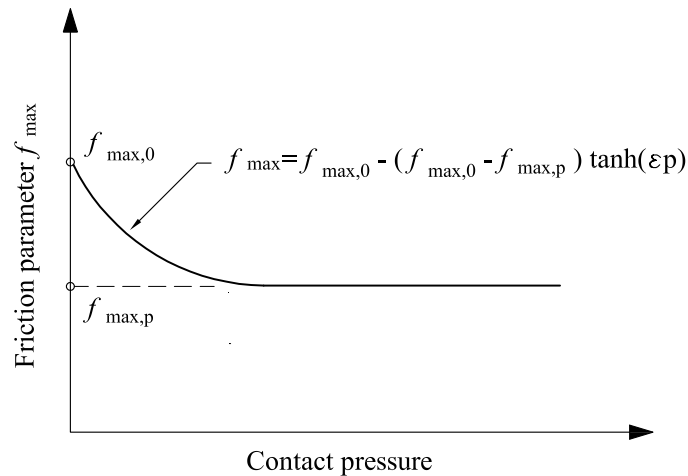


Figure 3-2: Variation of friction parameter  $f_{\max}$  with pressure.

### 3.3 Testing Machine Description

The apparatus shown in Figure 3-3 is comprised of the following components: (a) two horizontal beams – a lower support beam fixed to the rigid floor and an upper loading beam driven by a horizontal actuator; (b) three actuators – one horizontal actuator to impose the lateral displacement and two vertical actuators to both support the loading beam and maintain the axial load on the bearing; and (c) three load cells monitoring the load on the bearing – one reaction load cell (placed directly under the bearing) that measures directly both the axial and shear forces experienced by the bearing, and a load cell connected to each of the vertical actuators to control the vertical load.

The control strategy for these bearing tests consisted of maintaining the prescribed axial load on the bearing while imposing the desired lateral displacement. A detailed description and principles of operation of the testing machine can be found in Kasalanati and Constantinou (1999).

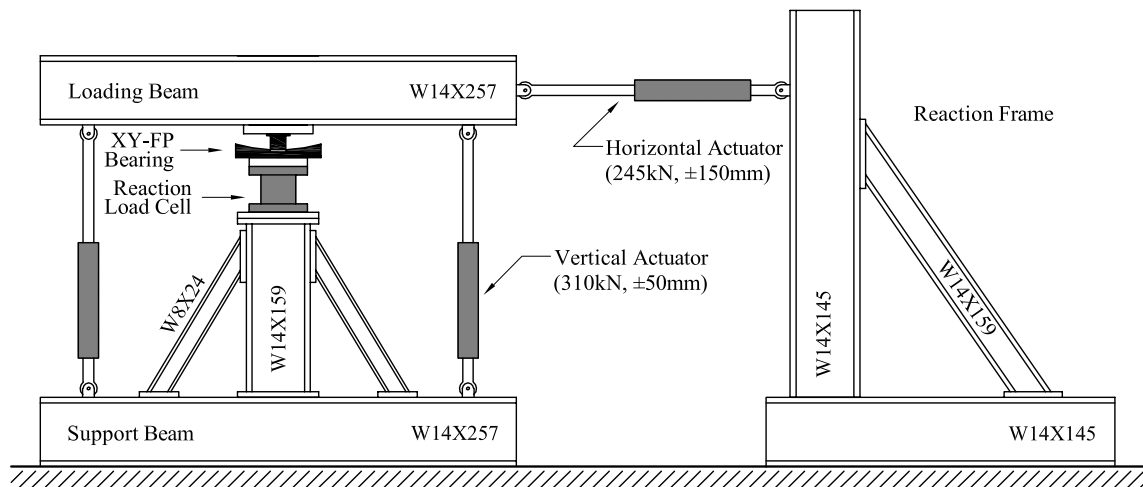


Figure 3-3: Schematic of isolator testing apparatus.

### 3.4 Testing Program

The isolator testing program involved a series of laboratory tests conducted on a single XY-FP isolator on the aforementioned apparatus (Figure 3-4). The isolator used in these tests was manufactured by Earthquake Protection Systems in Vallejo, California, with the dimensions shown in Figure 3-5. It was constructed of stainless steel and was designed to

have a displacement capacity of 203 mm (8 in). The radius of curvature of each concave beam is 990 mm (39 in.). Views of XY-FP isolator during testing in 0°, 45°, and 90° orientation are presented in Figure 3-6.

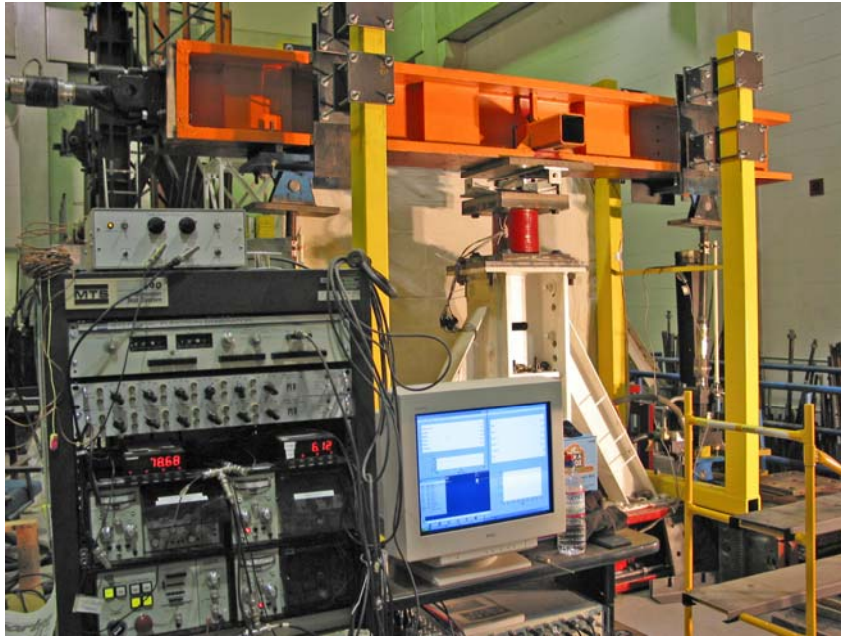


Figure 3-4: Photograph of isolator testing apparatus.

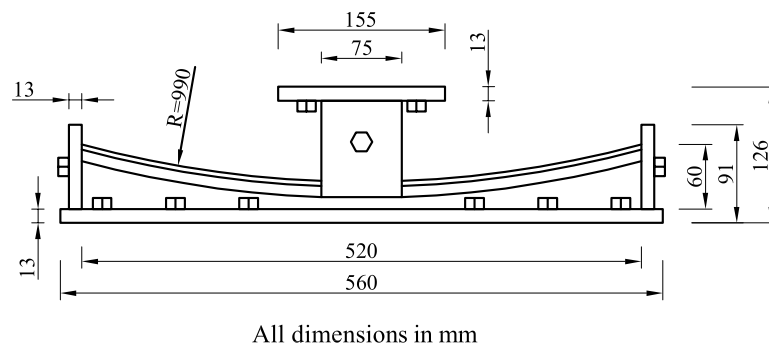


Figure 3-5: Two-dimensional view of the uplift-restraint XY-FP isolator used in this study.

The conditions pertaining to the displacement-controlled testing included a range of isolator orientation angles, normal loads (compressive and tensile), and peak sliding velocities. Table 3-1 presents the values of the variables used in the isolator testing program.



Figure 3-6: Views of XY-FP isolator during testing in 0°, 45°, and 90° orientation.

Table 3-1: Values of parameters used in isolator testing program.

Isolator Orientation	0°, 45°, 90°
Normal Load (kN)	27, 54, 108 : compression 27 : tension
Displacement Amplitude, $u_0$ (mm)	100
Frequency, $f$ (Hz)	0.01, 0.1, 0.3, 0.6, 0.8
Velocity Amplitude, $v_0 = 2\pi fu_0$ (mm/s)	6.3, 63, 188, 377, 503

The imposed displacement history is illustrated in Figure 3-7. The test started with an idle time of 10 sec fronted by a built-up segment of 60 sec in which a displacement amplitude  $u_0$  is reached under very low sliding velocity. During this build-up time, truly quasi-static conditions are present permitting measurements of the breakaway (or static) coefficient

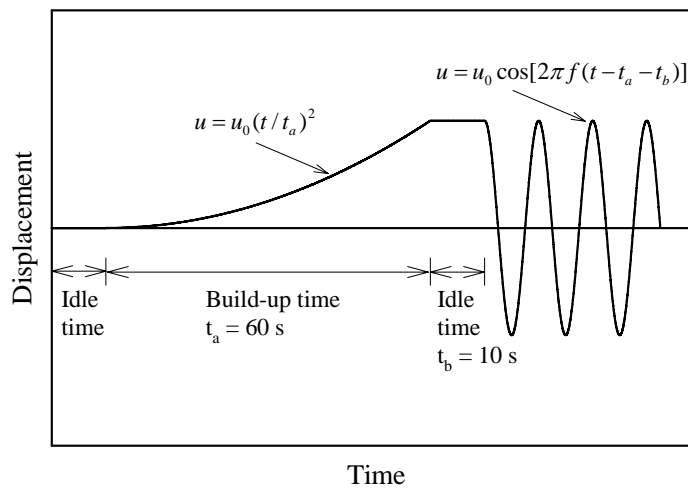


Figure 3-7: Imposed displacement history for XY-FP isolator testing.

of friction at initiation of motion and of the sliding coefficient of friction at very low velocity (parameter  $f_{\min}$ ). Subsequently, it is followed by an idle time of 10 sec and three-and-a-quarter cycles of harmonic displacement history as indicated in Figure 3-7.

### 3.5 Test Results

To expand our understanding of the behavior of the new XY-FP isolator, frictional force-displacement loops are plotted for different values of bearing pressure, peak sliding velocity, and bearing orientations. The recorded shear force was used to extract various frictional characteristics of interest. The frictional force during sliding in the “build-up time” interval upon division by the normal force results in the sliding friction coefficient at very low velocity,  $f_{\min}$ . The value of the coefficient of friction at peak velocity (zero displacement), occurring at the first cycle, is practically the maximum sliding coefficient of friction,  $f_{\max}$ . Information on the breakaway (or static) friction was not extracted since special specimen preparation was needed (see Constantinou et al., 1999 for details). In general, the breakaway coefficient of friction value is less than  $f_{\max}$  for the tested conditions of normal temperature.

Figure 3-8 shows representative force-displacement loops of the XY-FP isolator that demonstrate the effect of normal force and sliding velocity on the coefficient of friction. In particular, plotted in Figure 3-8(a) are force-displacement relationships for isolator angle of 0 degrees at peak sliding velocity of 503 mm/s for compressive normal loads of 27, 54, 108 kN and tensile normal load of 27 kN. These plots reveal the dependency of the coefficient of friction on the apparent pressure in a manner qualitatively analogous to the curve of Figure 3-2. The difference in the measured friction force between compression and tension tests for normal load of 27 kN is attributed to the fact that the contact area under tension is smaller so that the apparent pressure is larger, resulting in a smaller value for the coefficient of friction.

The array of loops in Figure 3-8(b) reveal the dependency of the coefficient of friction on the velocity of sliding. These results concern tests for isolator angle of 90 degrees at compressive normal load of 54 kN and peak sliding velocities of 6.3, 63, 188, and 377

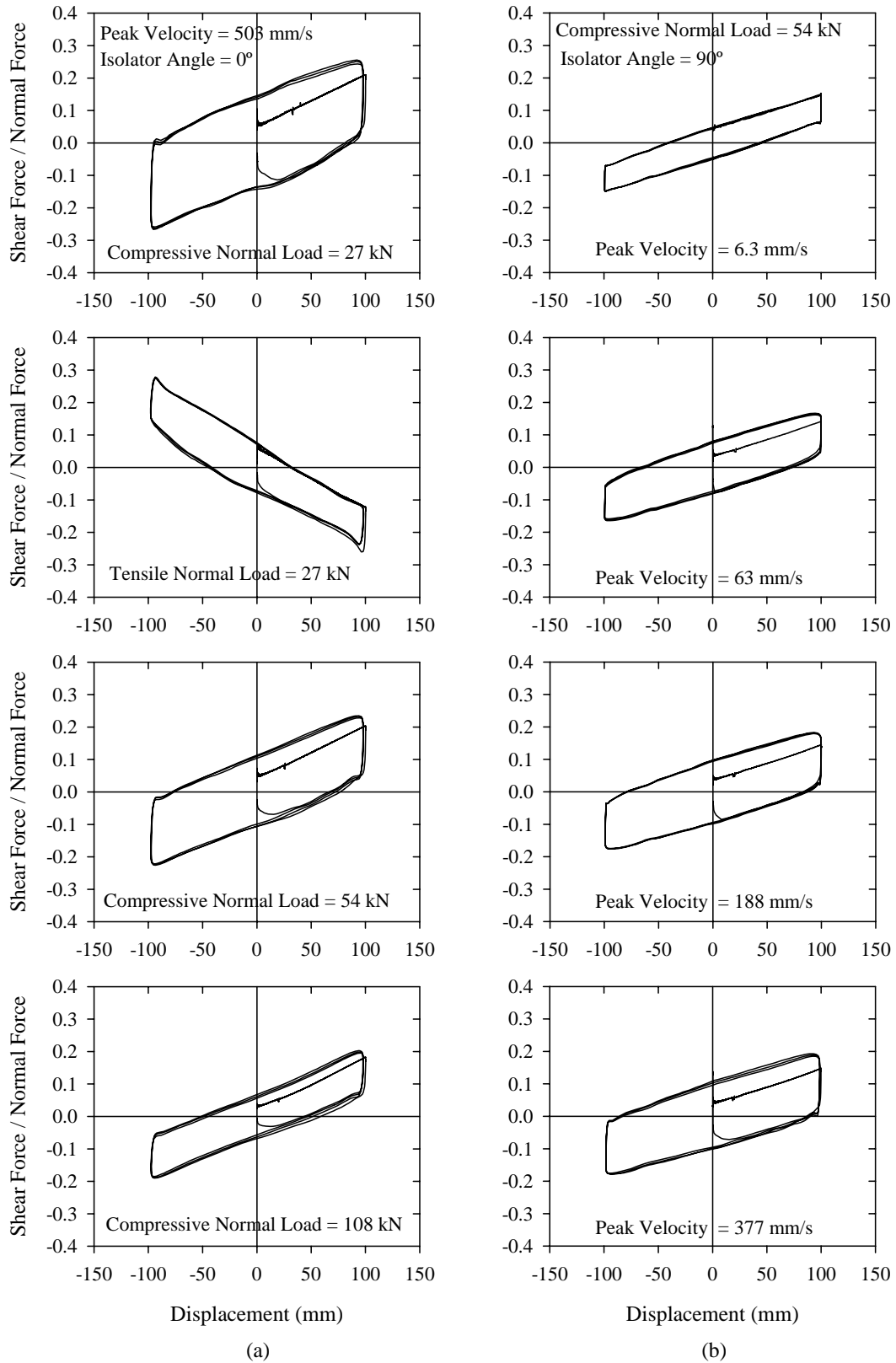


Figure 3-8: Recorded normalized force-displacement loops of XY-FP isolator demonstrating the effect of (a) normal force, and (b) sliding velocity.

mm/s. Collectively, the dependency of the coefficient of friction on the sliding velocity for each of the two component bearing beams is depicted in Figure 3-9. Superposed to the experimental results, are theoretical predictions of Equation (3-1) upon calibration with appropriate selection of parameters. Values of the parameters are presented in Table 3-2. Evidently, Equation (3-1) describes well the observed dependency of the sliding coefficient of friction on velocity.

Table 3-2: Parameters used in calibration of the equation describing the dependency of coefficient of friction on velocity (Equation (3-1)).

Parameters in Equation (3-1)	Lower Bearing Beam				Upper Bearing Beam			
	Normal Load (kN)				Normal Load (kN)			
	Compressive			Tensile	Compressive			Tensile
	27	54	108	27	27	54	108	27
$f_{\min}$	0.061	0.044	0.032	0.058	0.046	0.045	0.026	0.070
$f_{\max}$	0.142	0.110	0.070	0.079	0.137	0.106	0.066	0.083
$\alpha$ (s/m)	112	61.9	67.2	48.9	11.3	14.7	14.8	62.0

Figure 3-10 presents recorded normalized force-displacement loops for compressive and tensile normal loads and for isolator orientations of 0, 90, and 45 degrees. Results are plotted for the highest values of normal load and sliding velocity of Table 3-1, since more uncertainties in the frictional characteristics of the isolators and in the measurement system are to be expected under low velocity and pressure. These plots serve to verify that the equivalent friction force in any given direction can be approximated by the friction forces acting along the isolator principal axes 1 and 2 as the projection of their vectorial sum onto the direction of interest. With reference to Figure 3-10(a), the normalized friction force along the testing (global X) direction, from the 45-degree test for compressive normal load of 108 kN and sliding velocity of 503 mm/s is  $\mu_x = 0.087$ . Under the same values of testing parameters, the normalized friction forces from testing in 0- and 90-degree orientations are  $\mu_1 = 0.063$  and  $\mu_2 = 0.056$ , respectively. The vectorial sum of  $\mu_1$  and  $\mu_2$  gives a resultant of  $\mu_{res} = 0.084$  with practically the same projection onto the X direction,  $\mu_{res,X} = 0.084$ . Evidently, the recorded value of  $\mu_x$

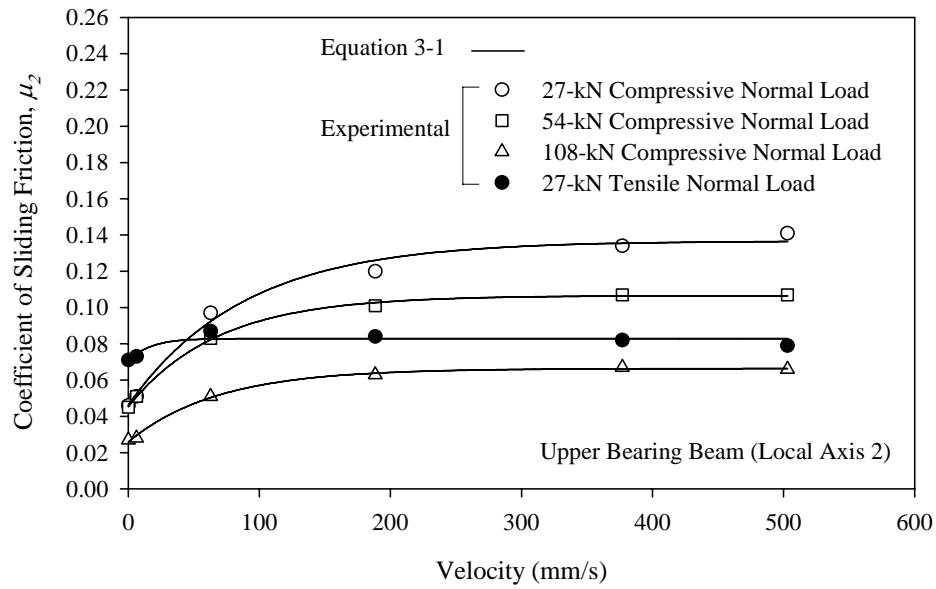
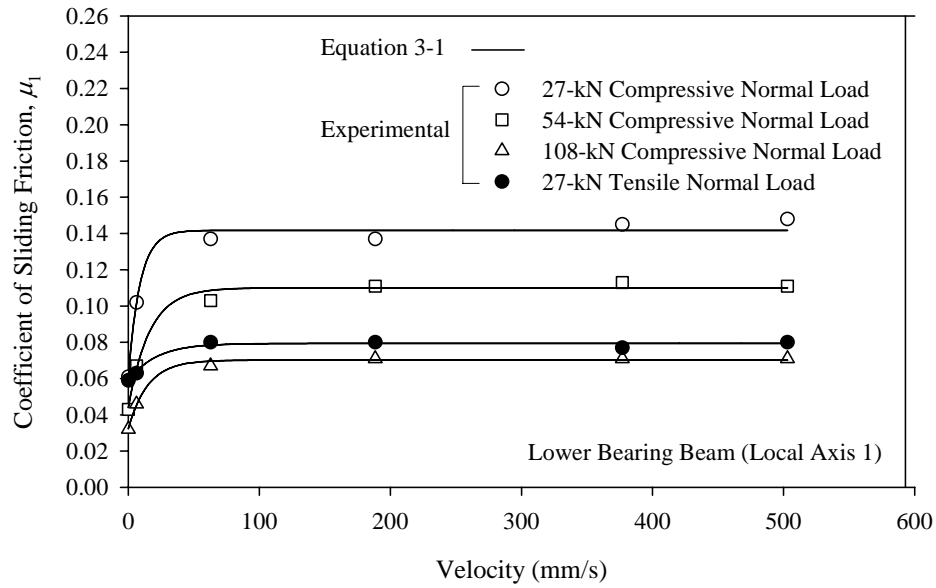


Figure 3-9: Dependency of coefficient of friction on velocity of sliding.

compares well with the calculated  $\mu_{res,X}$ . The minor discrepancy is attributed primarily to the variability in the friction values from test to test and secondarily to the interaction between lateral force and friction force as described in Section 2.3. Account for this effect could not be facilitated by the single-bearing testing machine used in the testing program.

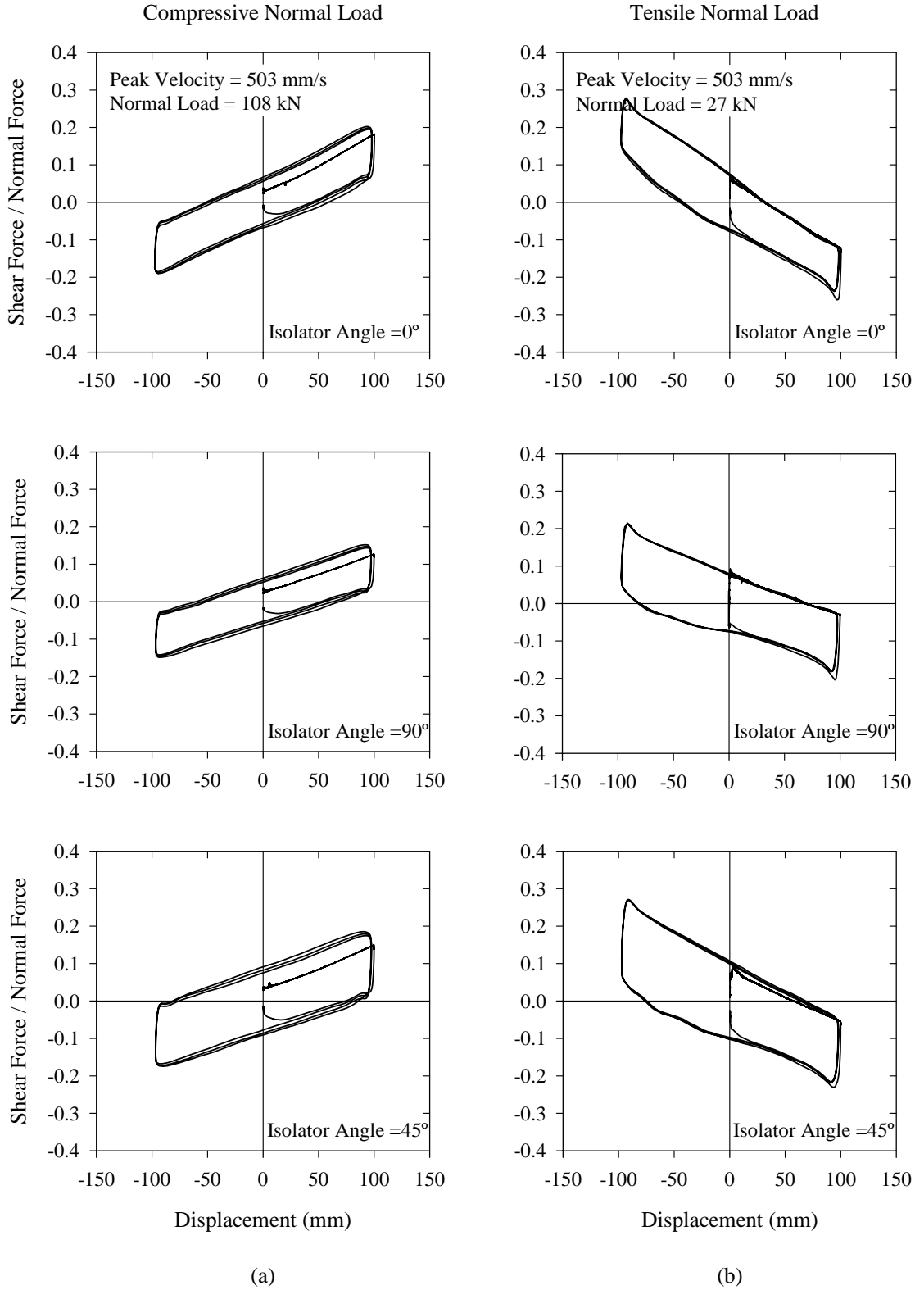


Figure 3-10: Recorded normalized force-displacement loops of XY-FP isolator for different isolator orientations for (a) compressive and (b) tensile normal load.

It can be argued that the comparison above involved friction forces based on incompatible velocities. Namely, all tests of Figure 3-10(a) were conducted under the same peak sliding velocity (503 mm/s) disregarding the fact that during the 45-degree test the velocity components along the isolator principal axes were smaller. This, clearly, is crossed out by considering high sliding velocity wherein friction becomes practically constant, as dictated by Equation (3-1).

One may observe in Figure 3-10 that the slopes of the normalized force-displacement loops, say in the portion corresponding to the built-up of displacement amplitude wherein velocity effects are not present to cause any distortion, are slightly different for isolator orientations of 0 and 90 degrees. The slopes (stiffnesses), theoretically given by  $1/R_t$ , were expected to be equal in view of identical radii of curvature of the two concave bearing beams confirmed through measurement and verified via analogous loops from shake-table testing (see Section 5). The discrepancy may be attributed to the fact that in the 0-degree configuration (see Figure 3-6) the  $P-\Delta$  moment is transferred directly on the load cell, while in the 90-degree configuration the moment is transferred above. This resulted in a difference in the state of stress in the load cell between the two configurations, which was reflected in the measurements due to channel cross-talk. The error in the measurements could not be corrected because of the nonlinear nature of the interaction between the electronic circuits in the load cells measuring axial force, shear force, and bending moment.



## SECTION 4

### MODEL FOR EARTHQUAKE SIMULATOR TESTING

#### 4.1 Introduction

The testing program on the earthquake simulator at the University at Buffalo involved a five-story base-isolated model structure. The superstructure consisted of a steel frame used in previous testing of energy dissipation systems at the University at Buffalo (e.g., Chang et al., 1993). The properties and dynamic characteristics of the model excluding the isolation system and fixed at the base were identified and are presented in Section 4.6. The isolation system, comprised of four XY-FP isolators, was installed beneath a base and rotated for testing in different directions. Specifically, tests were done at 0-degree, 45-degree, and 90-degree angle of lower bearing beam with respect to the direction of horizontal excitation. The testing program utilized a number of recorded ground motions with a wide range of both frequency content and amplitude.

#### 4.2 Model Description

Figures 4-1 and 4-2 show a photograph and a schematic of the model, respectively. At a quarter length scale, the single-bay moment-resisting steel frame is square in plan with a dimension of 1.321 m. The story heights are 1.092 m for the first story and 1.194 m for the other stories, for a total height of 5.868 m. The member layout is identical for all stories. The floors are comprised of MC6x12 channel sections. The cross sections of columns, beams, channels, and bracing are shown in Figure 4-3.

The model scale was chosen to be 4. In conforming to the similitude law, artificial mass, in the form of steel plates and lead blocks, was added to the structure at all floor levels. Table 4-1 presents the relevant scale factors associated with testing. The structure was attached to a rigid base under which the isolation system was installed. The distribution of mass is effectively 13.75 kN (3.1 kip) per floor and 37.8 kN (8.5 kip) for the base, for a total weight of 106.5 kN (24 kip). Installed beneath the rigid base, the isolation system consisted of four identical uplift-prevention XY-FP isolators. The isolator dimensions are shown in Figure 3-5.



Figure 4-1: Photograph of tested five-story isolated model structure on the seismic simulator at the University at Buffalo.

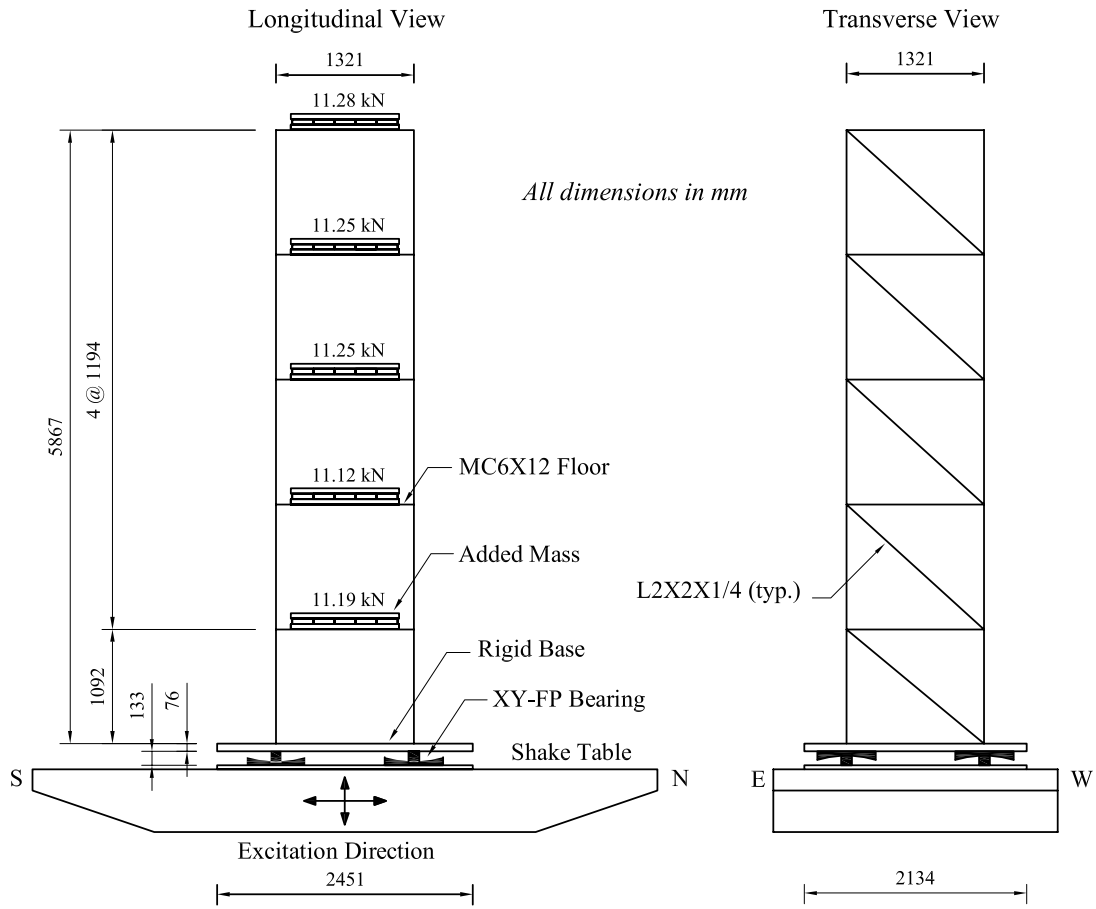


Figure 4-2: Schematic of tested 5-story isolated model structure.

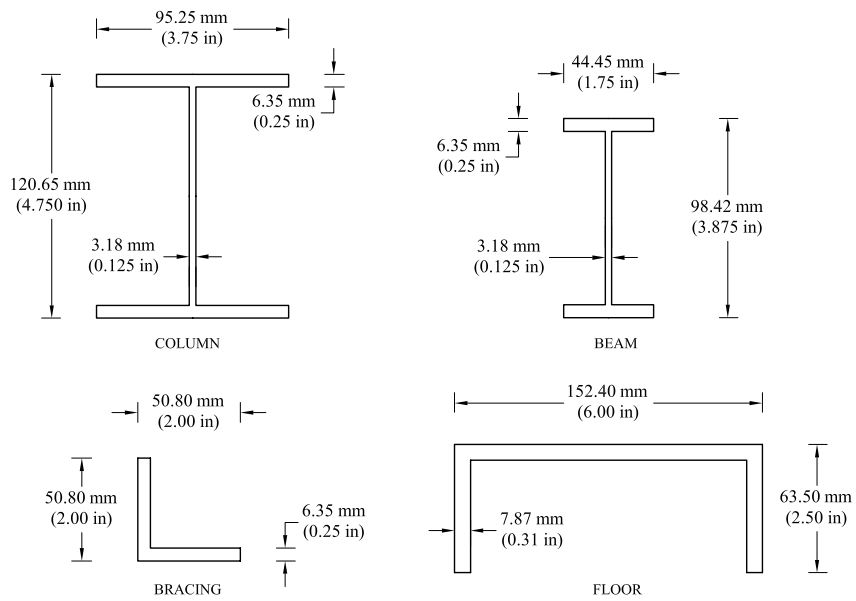


Figure 4-3: Member cross sections for model structure.

Table 4-1: Scale factors for model structure.

Quantity	Dimension	Scale Factor
Linear Dimension	L	4
Displacement	L	4
Time	T	2
Velocity	$LT^{-1}$	2
Acceleration	$LT^{-2}$	1
Frequency	$T^{-1}$	1/2
Stress / Pressure	$ML^{-1}T^{-2}$	1
Force	$MLT^{-2}$	16
Strain	-	1

### 4.3 Pushover Analysis

A pushover analysis of the model structure fixed at the base and exclusive of the isolation system was performed for the strong (N-S) direction of the model to identify its collapse mechanism and calculate the base shear strength. The base shear strength of the frame was also established using the method presented in Ramirez et al., 2001 (see Appendix A). These results are confirmed by pushover analysis using the program SAP2000 (Computers and Structures, 1998). The analysis determined that the model exhibits proper behavior with plastic hinges developing in the beams and that the base shear strength of the model is approximately equal to its weight.

### 4.4 Instrumentation

The instrumentation of the five-story model structure consisted of accelerometers and displacement transducers which recorded the horizontal accelerations and displacements of the frame at floor levels, the rigid base, and the shake table. In addition, the first-story columns were instrumented with strain gauged load cells to measure the first-story shear force. Figure 4-4 depicts the instrumentation scheme employed in the testing program. A list of monitored channels and their corresponding descriptions are given in Table 4-2.

As depicted in Figure 4-4 accelerations were recorded on the east and west side at each

floor, the base, and the table in the horizontal direction. In addition, the longitudinal, transverse, and vertical acceleration of the center of the base plate were recorded. Horizontal displacements with respect to a stationary frame were recorded on the east and west side at the 1st, 3rd, and 5th floor, the base, and the table. The 2nd and 4th floor accommodated only one displacement transducer on the west side. Furthermore, two displacement transducers were installed to measure the relative displacement of the base with respect to the table.

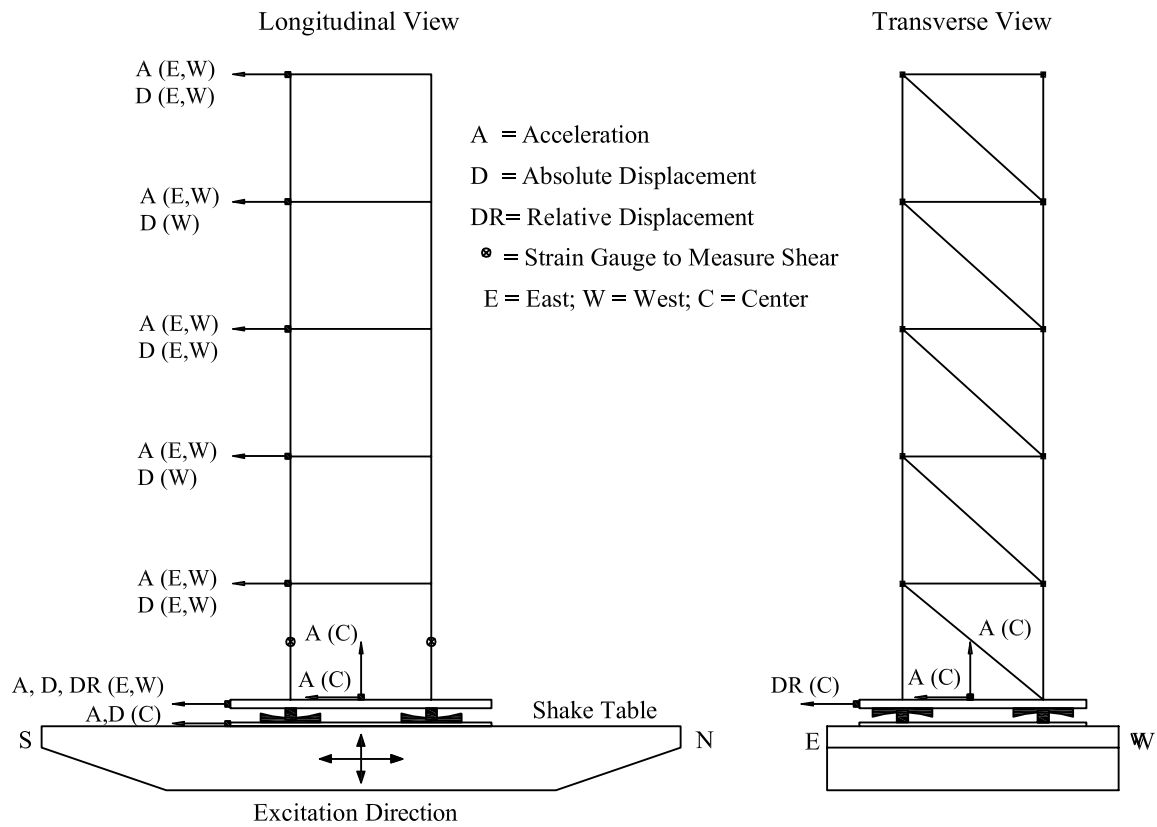


Figure 4-4: Instrumentation diagram for the 5-story test frame.

To assess the accuracy of important recordings, measurements were contrasted with corresponding calculated quantities. For example, to check the direct acceleration measurements, recorded floor absolute displacements were double-differentiated to obtain floor acceleration histories. In addition, the first-story shear was calculated by summing the floor inertial forces (product of floor mass and floor acceleration) and compared to the recorded first-story shear force.

## 4.5 Testing Program

The testing on the earthquake simulator at the University at Buffalo utilized the slender five-story model structure described above. The testing program involved a number of actual horizontal and vertical ground motions having a variety of frequency content and

Table 4-2: List of data acquisition channels (with reference to Figure 4-4)

Channel	Notation	Instrument	Unit	Response Measured
1	Time	CLOCK	sec	Time
2	ABW	ACCL	g	Base Horizontal Acceleration - South West
3	ABE	ACCL	g	Base Horizontal Acceleration - South East
4	A1W	ACCL	g	First Floor Horizontal Acceleration - South West
5	A1E	ACCL	g	First Floor Horizontal Acceleration - South East
6	A2W	ACCL	g	Second Floor Horizontal Acceleration - South West
7	A2E	ACCL	g	Second Floor Horizontal Acceleration - South East
8	A3W	ACCL	g	Third Floor Horizontal Acceleration - South West
9	A3E	ACCL	g	Third Floor Horizontal Acceleration - South East
10	A4W	ACCL	g	Fourth Floor Horizontal Acceleration - South West
11	A4E	ACCL	g	Fourth Floor Horizontal Acceleration - South East
12	A5W	ACCL	g	Fifth Floor Horizontal Acceleration - South West
13	A5E	ACCL	g	Fifth Floor Horizontal Acceleration - South East
14	AT	ACCL	g	Table Horizontal Acceleration
15	ABCEW	ACCL	g	Base Horizontal Acceleration – C.M. (EW)
16	ABCNS	ACCL	g	Base Horizontal Acceleration – C.M. (NS)
17	ABCV	ACCL	g	Base Vertical Acceleration – C.M.
18	D5W	DT	inch	Fifth Floor Displacement - South West Corner
19	D5E	DT	inch	Fifth Floor Displacement - South East Corner
20	D4W	DT	inch	Fourth Floor Displacement - South West Corner
21	D3W	DT	inch	Third Floor Displacement - South West Corner
22	D3E	DT	inch	Third Floor Displacement - South East Corner
23	D2W	DT	inch	Second Floor Displacement - South West Corner
24	D1W	DT	inch	First Floor Displacement - South West Corner

Table 4-2: List of data acquisition channels (cont.)

Channel	Notation	Instrument	Unit	Response Measured
25	D1E	DT	inch	First Floor Displacement - South East Corner
26	DRBW	DT	inch	Base Relative Displacement - South West
27	DRBE	DT	inch	Base Relative Displacement - South East
28	DBW	DT	inch	Base Displacement - South West
29	DBE	DT	inch	Base Displacement - South East
30	DBEW	DT	inch	Transverse Base Displacement - East
31	ALAT	ACCL	g	Table Horizontal Acceleration
32	SHEAR	LOAD CELL	kips	First Story Shear Force
34	DTH	DT	inch	Table Horizontal Displacement – South Center

amplitude. Table 4-3 lists the earthquake motions used for the simulator testing together with their peak ground motion characteristics at the prototype (full) scale. Each record was compressed in time by a factor of two to conform to the similitude requirements of Table 4-1.

Figures 4-5 through 4-13 present the recorded histories of the table motion in nine tests with these earthquake inputs. The acceleration and displacement records were measured directly, whereas the velocity record was calculated by differentiating the displacement record. Each of these figures presents the 5-percent damped response spectrum (in prototype scale) of the table motion, and the spectrum of the target history. It can be observed that the shake table reproduced motions that are in acceptable agreement with the target motions in the period range of the isolated model structure.

The isolation system was rotated below the base plate for testing in different directions. Specifically, tests were undertaken at 0-degree, 45-degree, and 90-degree angle of the lower bearing beam with respect to the direction of horizontal excitation. A complete list of tests conducted is presented in Table 4-4. In this table, *V* denotes the vertical earthquake component.

Table 4-3: List of earthquake motions and their characteristics in prototype scale.

Notation	Excitation	Component	Peak Ground Motion		
			Disp. (mm)	Vel. (mm/s)	Accel. (g)
El Centro S00E	Imperial Valley, 1940	S00E	109	335	0.34
El Centro V	Imperial Valley, 1940	Vertical	92	107	0.21
Taft N21E	Kern County, 1952	N21E	67	157	0.16
Taft V	Kern County, 1952	Vertical	45	66	0.11
Newhall 90°	Northridge-Newhall, LA County Fire Station, 1994	90°	176	748	0.58
Newhall 360°	Northridge-Newhall, LA County Fire Station, 1994	360°	305	947	0.59
Newhall V	Northridge-Newhall, LA County Fire Station, 1994	Vertical	163	315	0.55
Sylmar 90°	Northridge-Sylmar, Parking Lot, 1994	90°	152	769	0.60
Sylmar V	Northridge-Sylmar, Parking Lot, 1994	Vertical	85	191	0.54
Kobe N-S	Kobe Station, Japan, 1995	N-S	207	914	0.83
Kobe V	Kobe Station, Japan, 1995	Vertical	103	383	0.34
Pacoima S74W	San Fernando, Pacoima Dam, 1971	S74W	108	568	1.08
Pacoima S16E	San Fernando, Pacoima Dam, 1971	S16E	365	1132	1.17
Pacoima V	San Fernando, Pacoima Dam, 1971	Vertical	182	565	0.71
Hachinohe N-S	Tokachi, Hachinohe, Japan, 1968	N-S	119	357	0.23

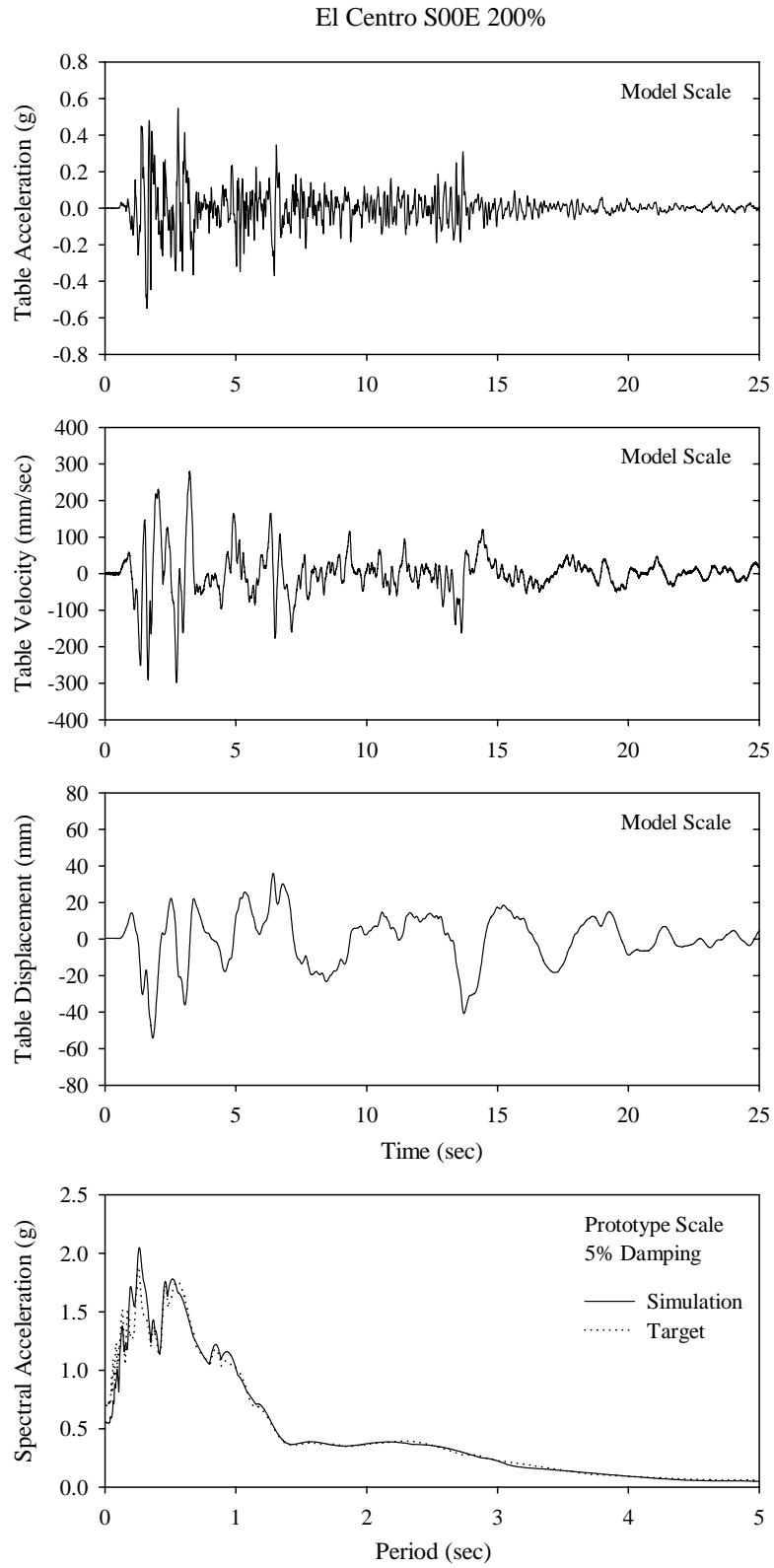


Figure 4-5: Histories and response spectra of shake table motion for El Centro S00E 200% excitation.

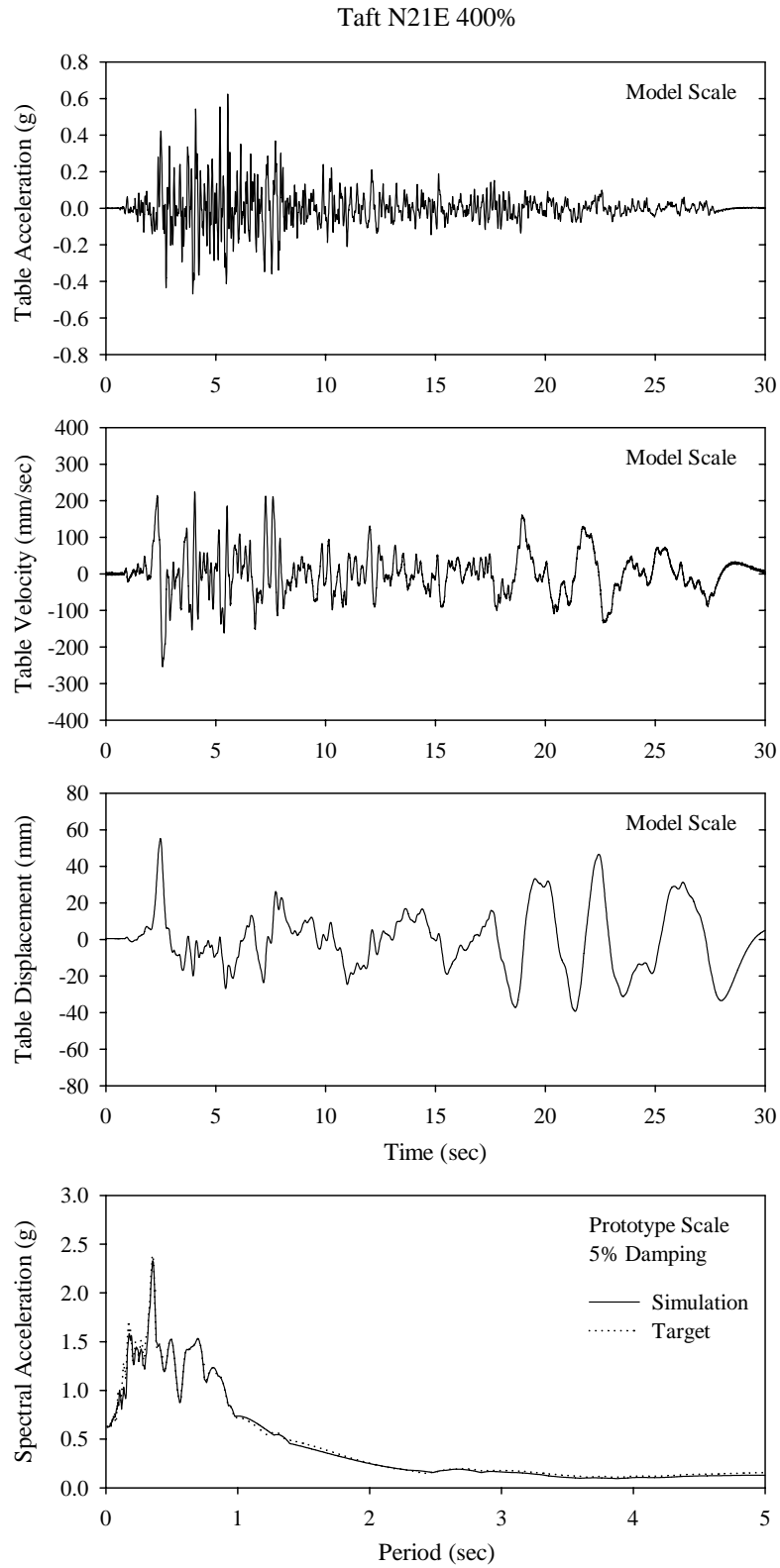


Figure 4-6: Histories and response spectra of shake table motion for Taft N21E 400% excitation.

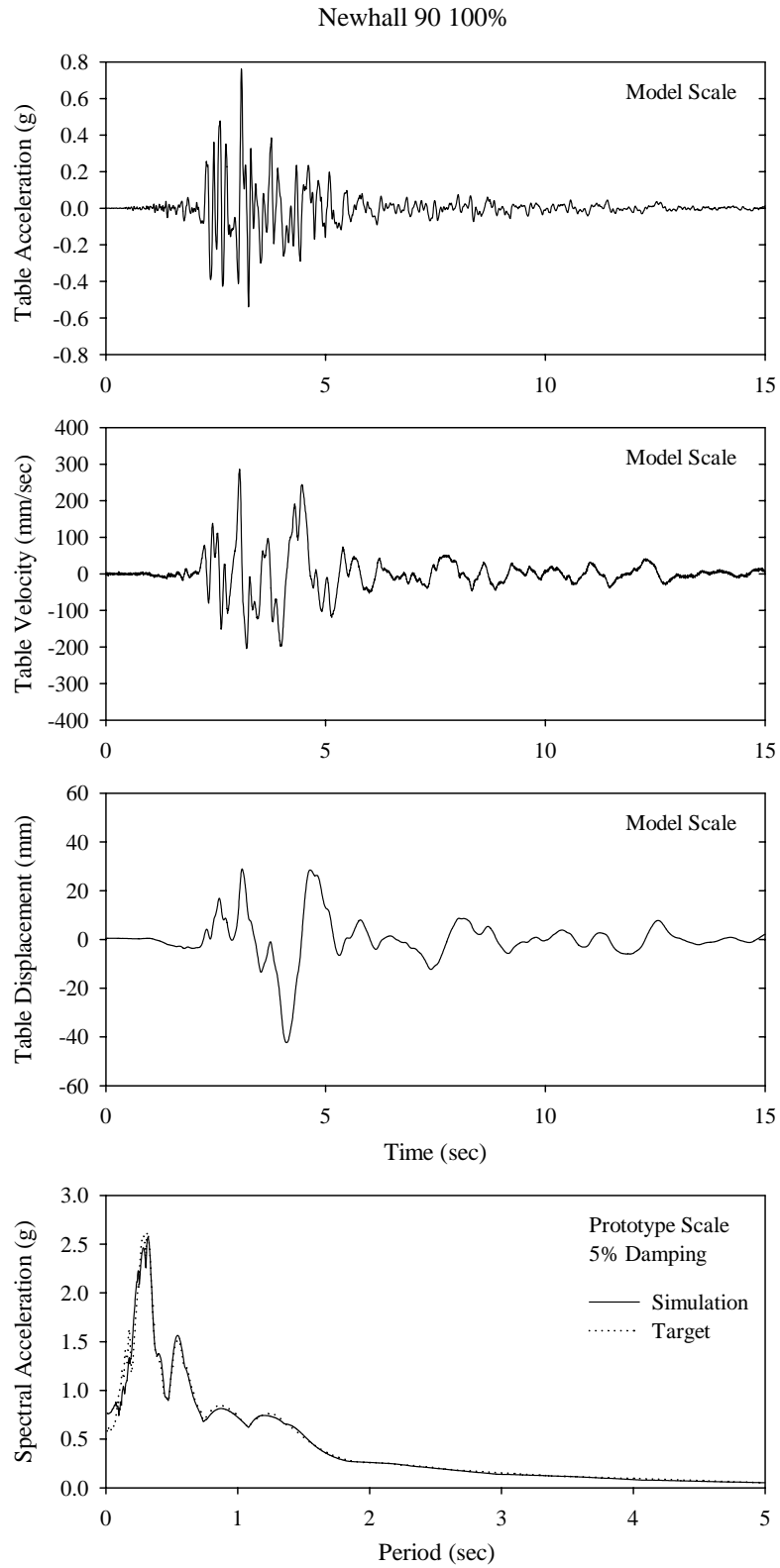


Figure 4-7: Histories and response spectra of shake table motion for Newhall 90 100% excitation.

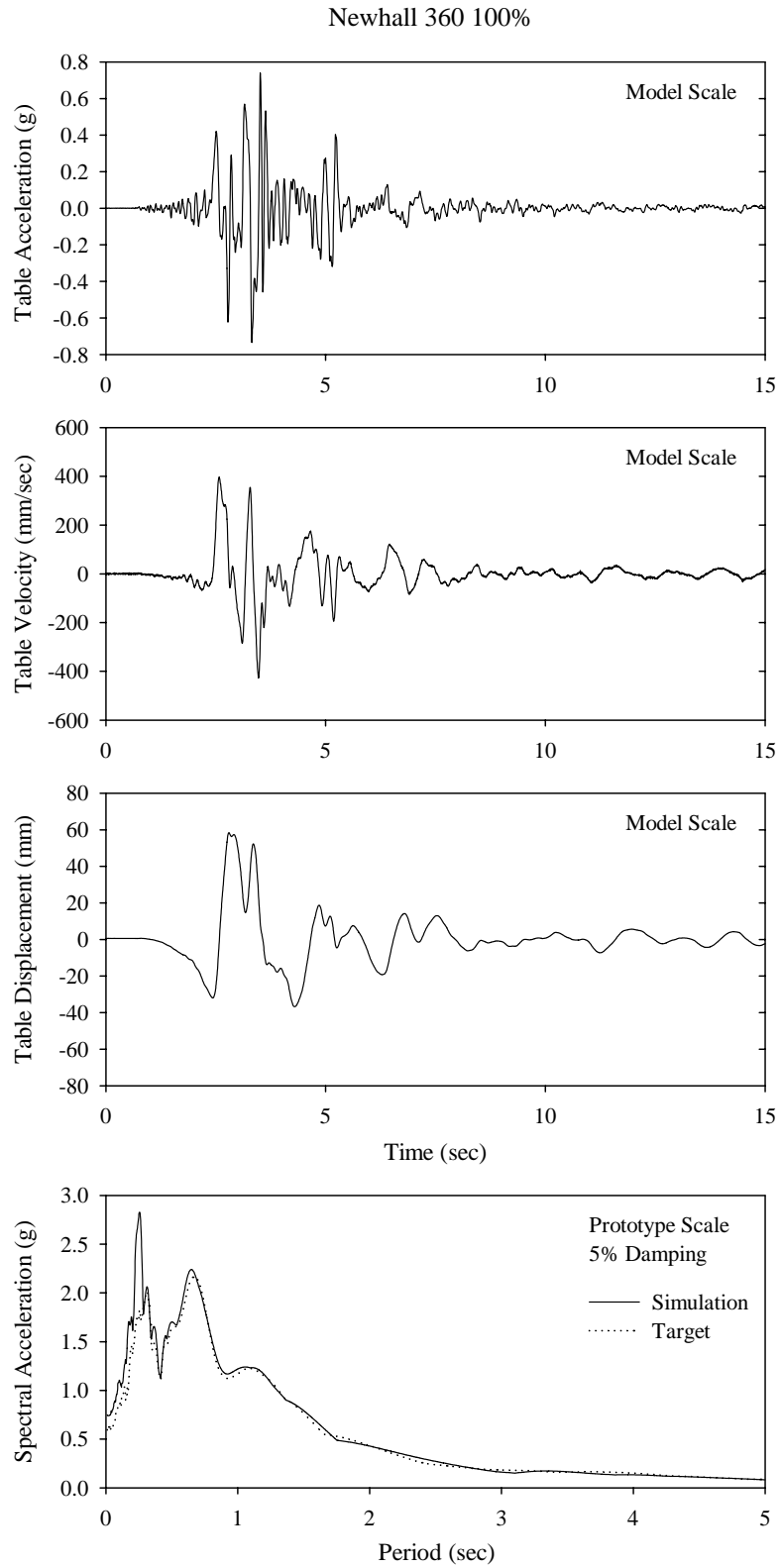


Figure 4-8: Histories and response spectra of shake table motion for Newhall 360 100% excitation.

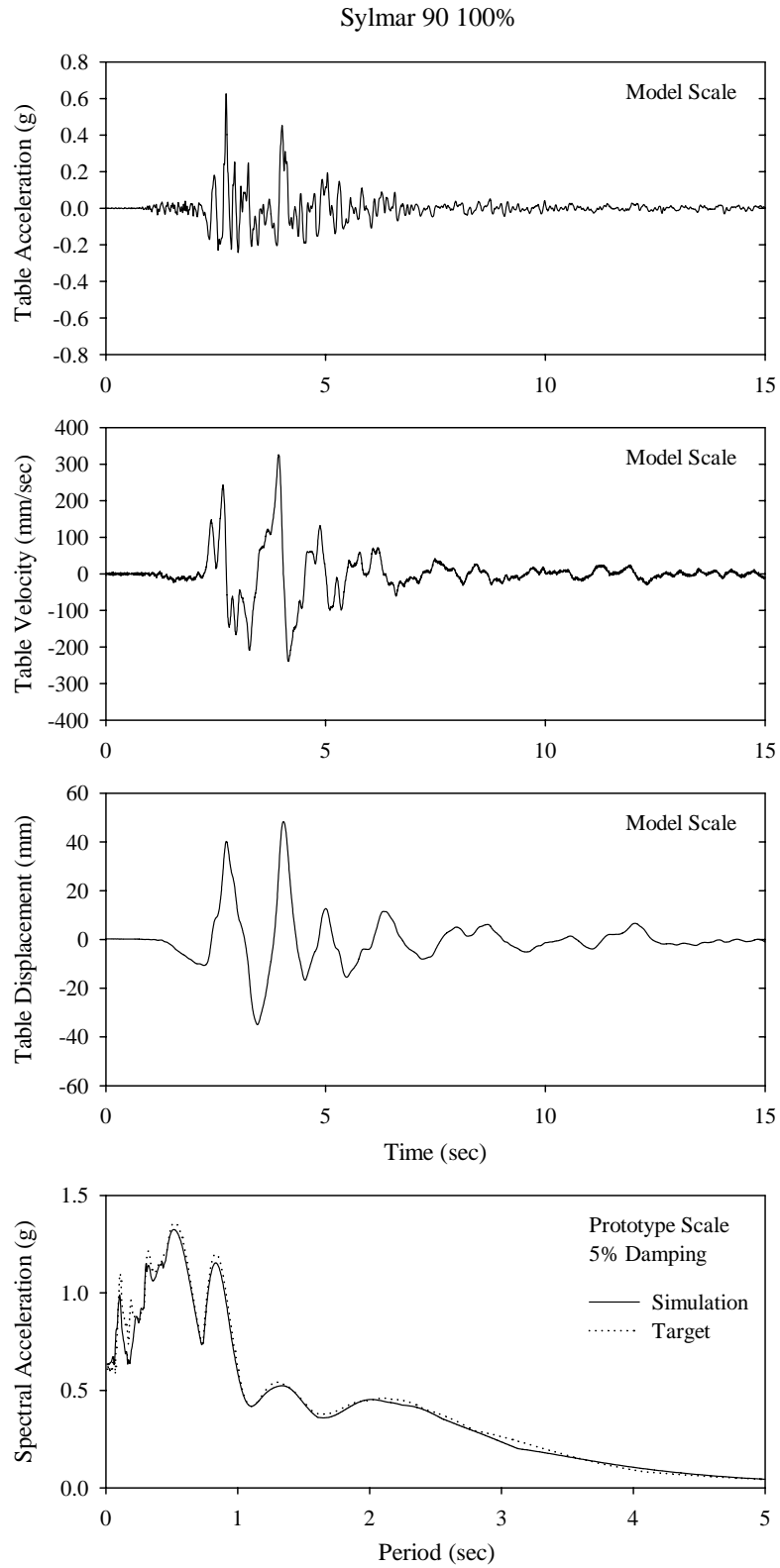


Figure 4-9: Histories and response spectra of shake table motion for Sylmar 90 100% excitation.

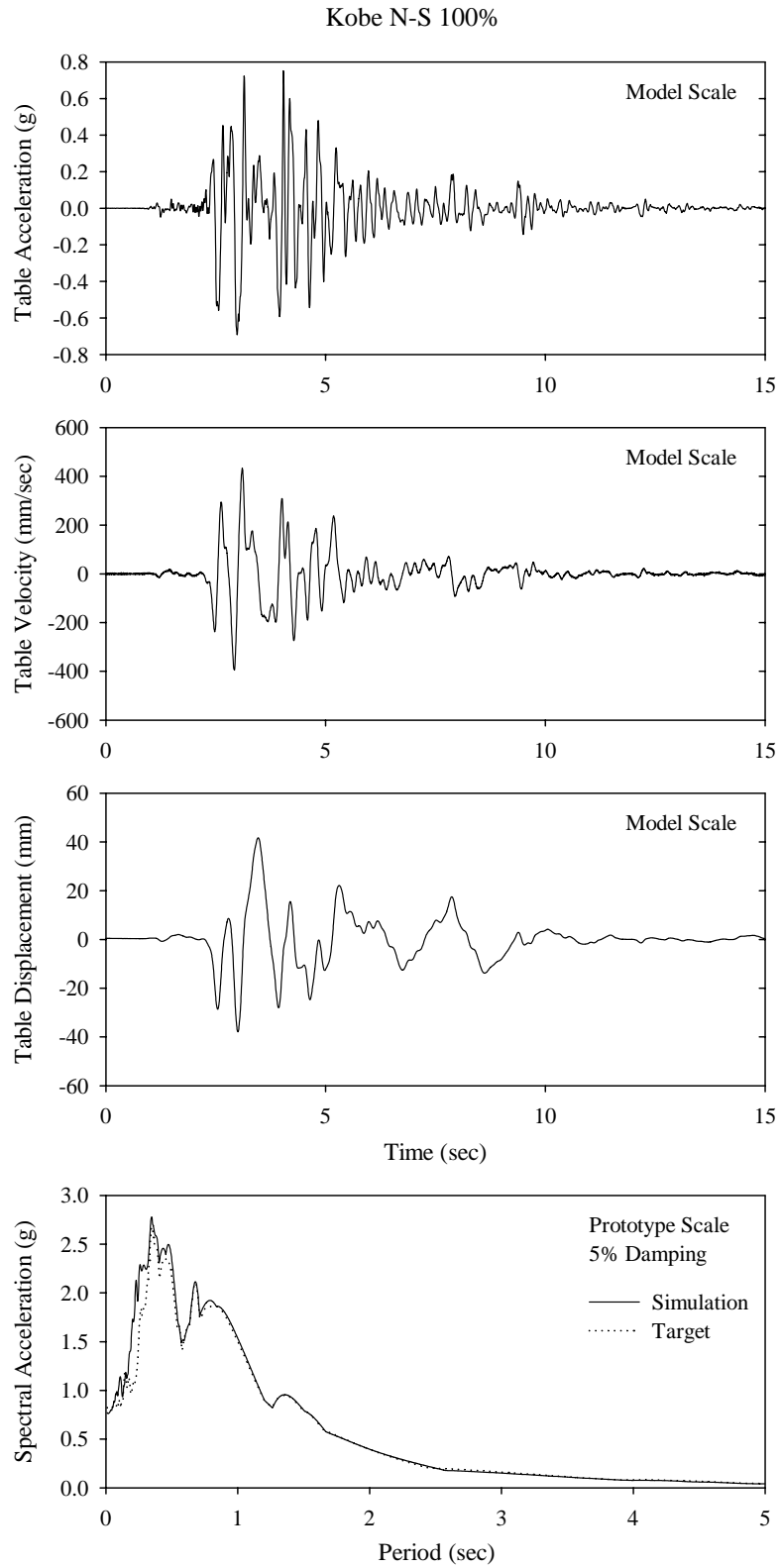


Figure 4-10: Histories and response spectra of shake table motion for Kobe N-S 100% excitation.

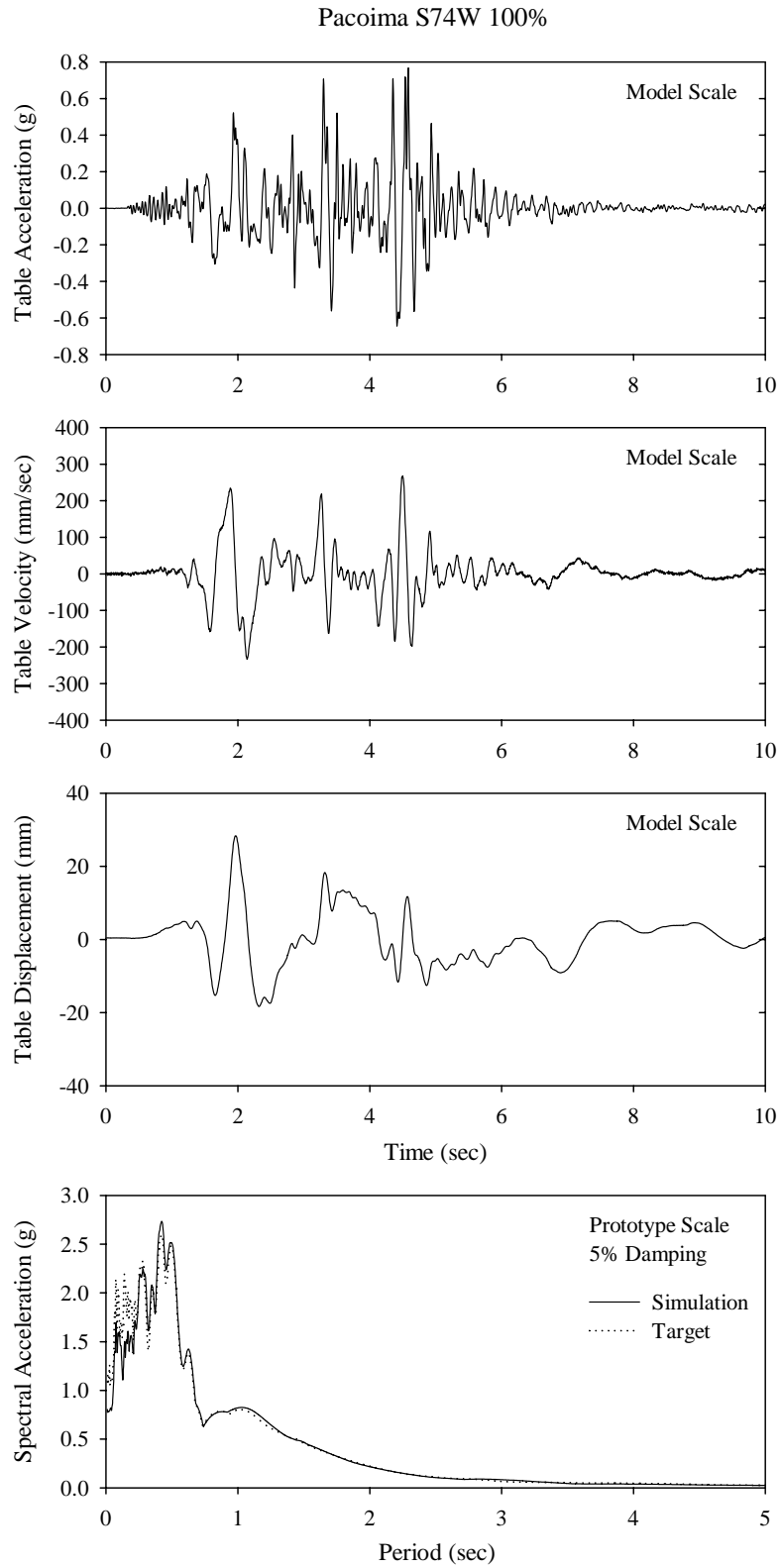


Figure 4-11: Histories and response spectra of shake table motion for Pacoima S74W 100% excitation.

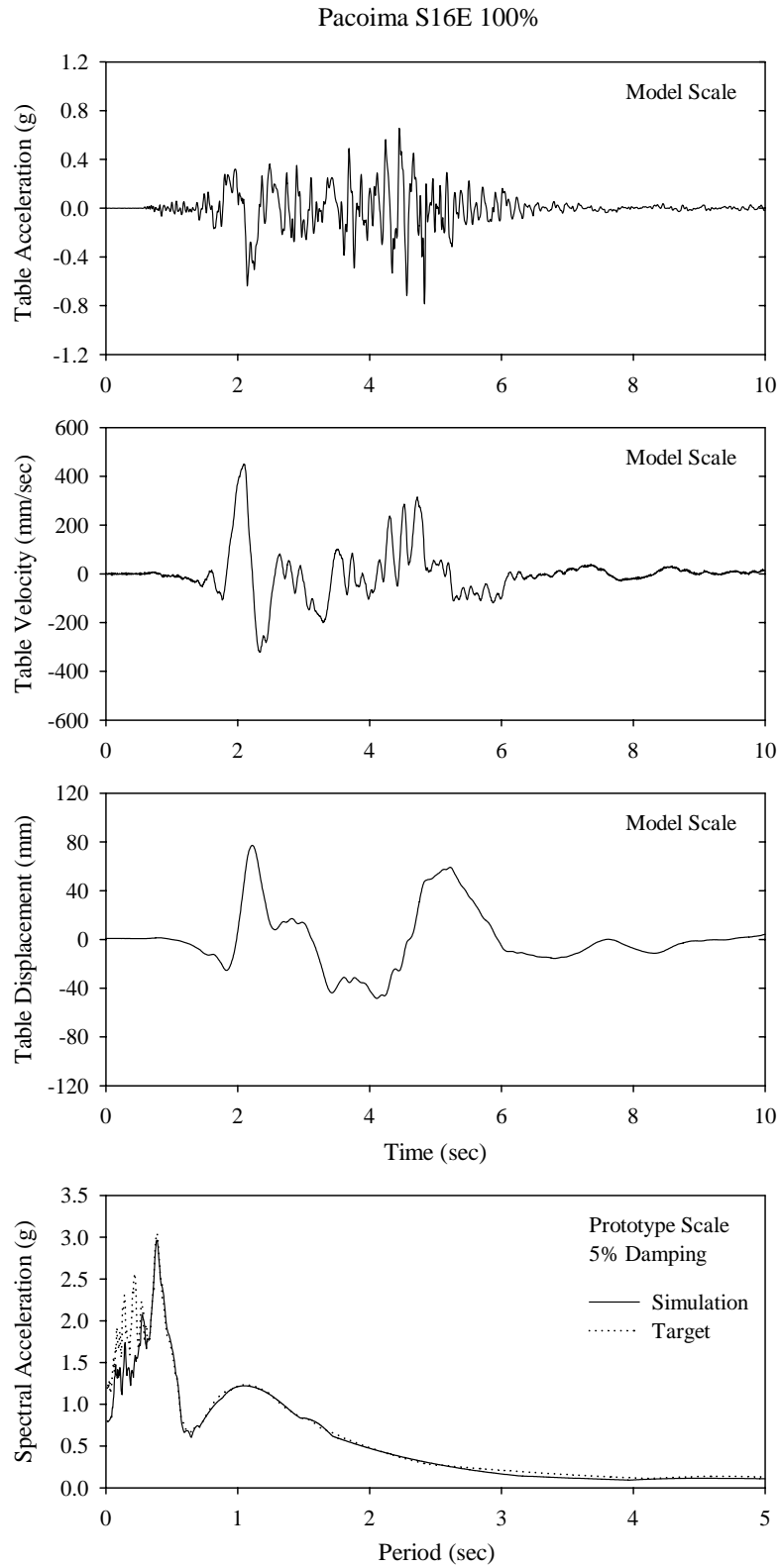


Figure 4-12: Histories and response spectra of shake table motion for Pacoima S16E 100% excitation.

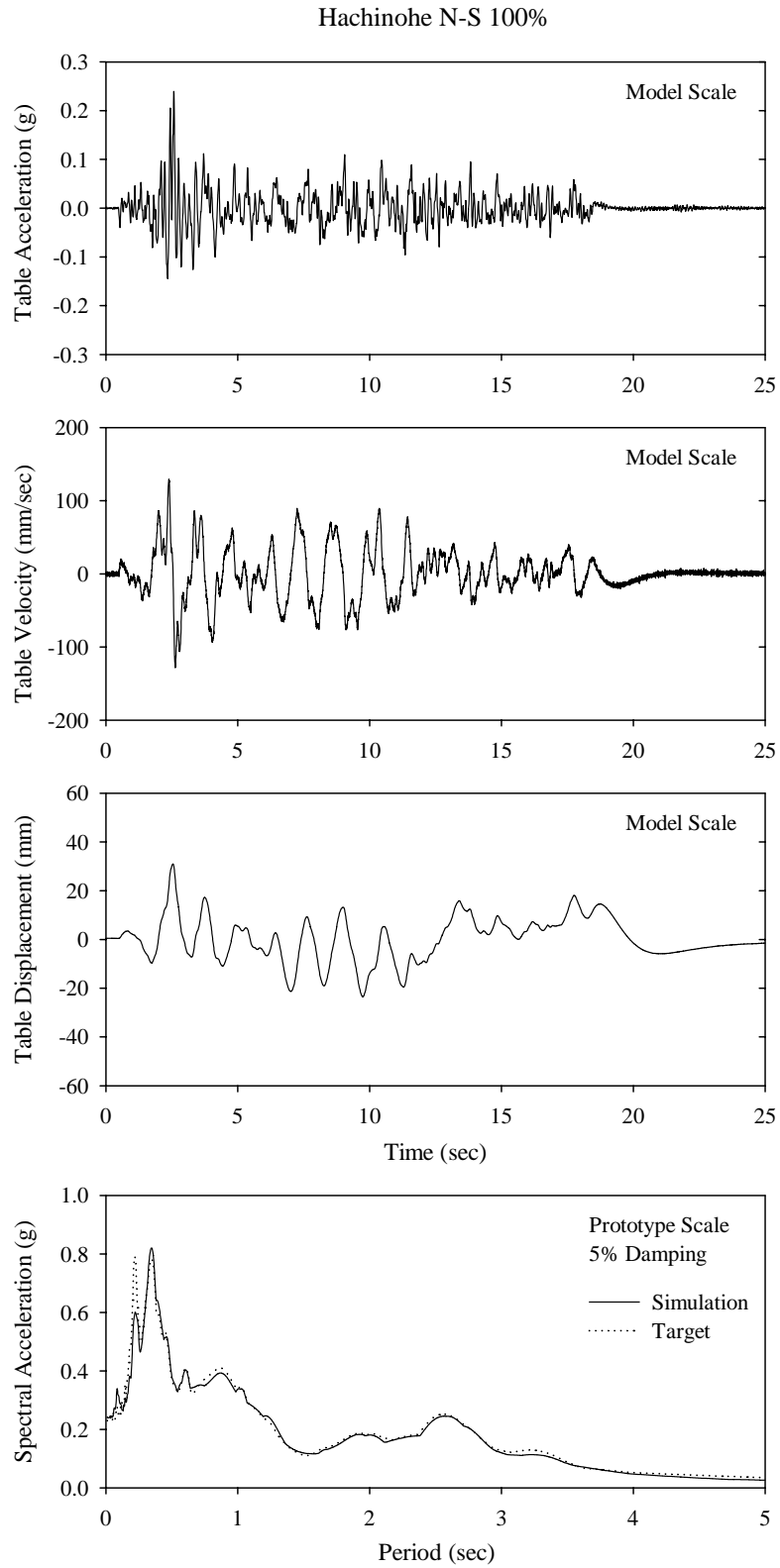


Figure 4-13: Histories and response spectra of shake table motion for Hachinohe N-S 100% excitation.

Table 4-4: List of earthquake simulator tests conducted on the 5-story model structure.

Excitation	Component	Intensity	Fixed Base	Isolated		
				Isolator Orientation		
				0°	90°	45°
El Centro	S00E	33%	√	-	-	-
		50%	-	√	-	-
100%		-	√	-	√	
200%		-	√	√	√	
	S00E + V	200%	-	√	√	√
Pacoima	S74W	100%	-	√	-	-
	S74W + V	100%	-	√	-	-
Pacoima	S16E	75%	-	√	-	-
		100%	-	√	√	√
		125%	-	-	√	√
		150%	-	-	√	-
	S16E + V	100%	-	√	√	√
Taft	N21E	50%	√	-	-	-
		100%	√	-	-	-
		400%	-	√	-	-
	N21E + V	400%	-	√	-	-
Hachinohe	N-S	100%	-	√	-	-
Sylmar	90°	100%	-	√	√	√
	90° + V	100%	-	√	√	√
Newhall	90°	100%	-	√	-	-
	90° + V	100%	-	√	-	-
Newhall	360°	100%	-	√	√	√
	360° + V	100%	-	√	√	√
Kobe	N-S	100%	-	√	-	-
	N-S + V	100%	-	√	-	-

#### 4.6 Identification of Dynamic Characteristics of Model Structure

The testing program involved identification tests aimed at determining the dynamic characteristics of the non-isolated 5-story superstructure. The fixed-base condition was attained by locking the rigid base to the shake table via side plates, thereby preventing any relative motion of the base and table. The tests were conducted using banded white noise excitation with acceleration amplitude of 0.05g and frequency content in the range of 0 to 40 Hz.

The shapes, frequencies, and damping ratios of modes within the tested frequency range were determined using modal identification techniques. The method is based on the experimentally-recorded floor acceleration histories and frequency response of the floor transfer functions (Bracci et al., 1992). The transfer function is defined as an output structural response normalized by a superimposed input base motion in the frequency domain. In particular, the transfer function for the  $j$ -th floor was obtained as the ratio of the Fourier transform of recorded horizontal acceleration of the  $j$ -th floor to the Fourier transform of the recorded base acceleration.

Equation (4-1) shows the general equation of motion of a base excited multi-degree-of-freedom lumped mass structure.

$$[M]\{\ddot{u}\} + [C]\{\dot{u}\} + [K]\{u\} = -[M]\{R\}\ddot{u}_g(t) \quad (4-1)$$

where  $[M]$  is the mass matrix,  $[C]$  is the damping matrix,  $[K]$  is the stiffness matrix;  $\{\ddot{u}\}$ ,  $\{\dot{u}\}$ , and  $\{u\}$  are the vectors of relative acceleration, velocity, and displacement of the degrees of freedom, respectively;  $\{R\}$  is a unit vector; and  $\ddot{u}_g(t)$  is the ground (base) acceleration history.

Expressing the displacement vector in terms of modal coordinates,  $y_k$ :

$$\{u\} = \sum_{k=1}^N \{\phi_k\} y_k \quad (4-2)$$

where  $\{\phi_k\}$  is the  $k$ -th mode shape and  $N$  is the number of degrees of freedom.

The amplitude of the acceleration transfer function of degree of freedom  $j$  may be obtained as the amplitude of the ratio of the Fourier Transforms of the acceleration of degree-of-freedom  $j$  to the acceleration of the ground:

$$H_j(\omega) = \left| \sum_{k=1}^N \frac{-\Gamma_k(2i\omega\xi_k\omega_k + \omega_k^2)}{\omega_k^2 - \omega^2 + 2i\omega\xi_k\omega_k} \phi_{jk} \right| \quad (4-3)$$

where  $\omega_k$  and  $\xi_k$  are the  $k$ -th mode frequency and damping ratio,  $\phi_{jk}$  is the component

of mode shape  $\phi_k$  corresponding to the degree of freedom  $j$ ,  $\omega$  is frequency, and  $\Gamma_k$  is the  $k$ -th modal participation factor given by

$$\Gamma_k = \frac{\{\phi_k\}^T [M] \{R\}}{\{\phi_k\}^T [M] \{\phi_k\}} \quad (4-4)$$

For a lightly damped structure, the  $k$ -th peak of the amplitude of the transfer function occurs at frequency  $\omega_k$ . Furthermore, if we assume well separated modes, the term in front of  $\phi_{jk}$  in Equation (4-3) can be neglected for all frequencies  $\omega \neq \omega_k$ . Accordingly, Equation (4-3) simplifies to

$$H_j(\omega_k) = \frac{\Gamma_k (1 + 4\xi_k^2)}{2\xi_k} \phi_{jk} \quad (4-5)$$

It should be noted that the peak of the  $j$ -th transfer function at the  $k$ -th natural frequency is proportional to the magnitude of the  $k$ -th mode shape corresponding to the  $j$ -th degree of freedom. The constant of proportionality is a function of the damping ratio and modal participation factor for the  $k$ -th mode. Since the constant of proportionality is the same for all degrees of freedom for the  $k$ -th mode, the ratio of the peaks in the transfer functions for the different degrees of freedom at the  $k$ -th natural frequency are equal to the ratio of the mode shapes for the  $k$ -th mode.

Thus the position and magnitude of the peaks of experimental transfer functions of all degrees of freedom directly yield the frequencies and mode shapes. The phase angles for the mode shapes can also be determined experimentally from the Fourier Transform of the story accelerations as a function of the natural frequencies as

$$\theta(\omega_i) = \tan^{-1} \left( \frac{I(\omega_i)}{R(\omega_i)} \right) \quad (4-6)$$

where  $I(\omega_i)$  and  $R(\omega_i)$  are the imaginary and the real parts of the Fourier Amplitude of the  $j$ -th story acceleration at the  $i$ -th frequency  $\omega_i$ , respectively. Therefore, by comparing the phase angles for each story at the natural frequencies, the mode shape

phases can be determined.

In addition, the corresponding damping ratios for the  $k$ -th mode,  $\xi_k$ , can be estimated from the experimentally determined  $j$ -th story transfer function magnitude,  $k$ -th mass normalized mode shape at the  $j$ -th degree of freedom, and the  $k$ -th modal participation factor as

$$\xi_k = \sqrt{\left[ \left( \frac{2|H_j(\omega_k)|}{\phi_{jk}\Gamma_k} \right)^2 - 4 \right]^{-1}} \quad (4-7)$$

Figure 4-14 presents the experimentally obtained acceleration transfer function amplitudes for banded (0-40 Hz) white noise base excitation. These transfer functions were used to extract the dynamic characteristics reported in Table 4-5.

The dynamic characteristics of the fixed-base structure were also analytically determined using the program SAP2000 (Computers and Structures, 1998). The first three mode shapes are graphically portrayed in Figure 4-15 and all extracted data pertinent to the superstructure identification (natural frequencies, damping ratios, and mode shapes) are listed in Table 4-5. The agreement between experimentally derived and analytically calculated modal characteristics is excellent.

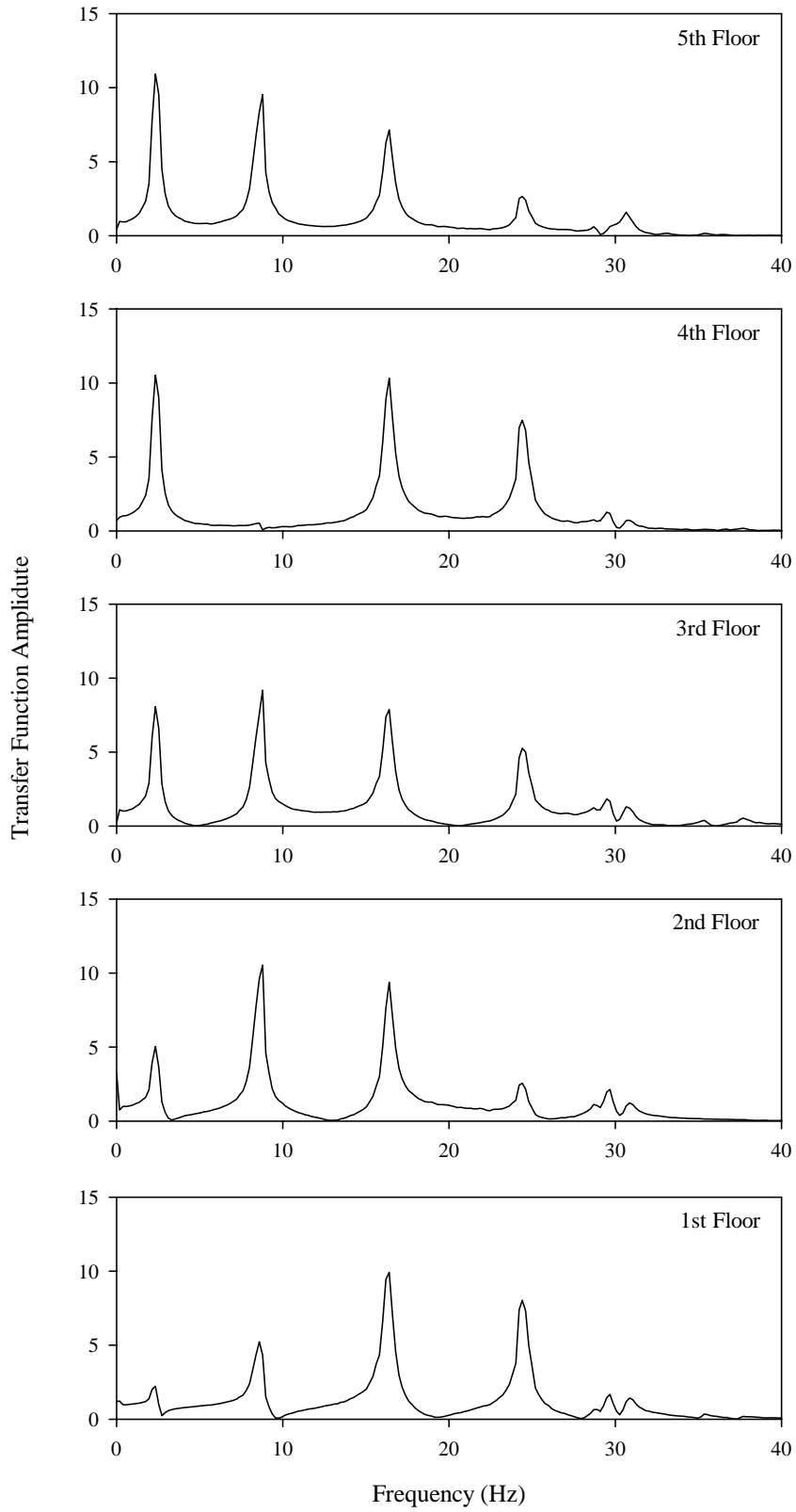


Figure 4-14: Floor transfer function amplitudes for banded (0-40 Hz) white noise base excitation.

Table 4-5: Dynamic characteristics of fixed-base model structure.

Mode	Method	Frequency (Hz)	Damping Ratio	Mode Shape				
				Floor 1	Floor 2	Floor 3	Floor 4	Floor 5
1	Experimental	2.3	0.061	0.200	0.460	0.740	0.960	1.000
	Analytical	2.4	-	0.120	0.380	0.640	0.850	1.000
2	Experimental	8.6	0.019	-0.526	-1.000	-0.807	0.044	0.877
	Analytical	8.2	-	-0.481	-1.000	-0.837	0.010	0.962
3	Experimental	16.4	0.011	1.000	0.903	-0.779	-1.000	0.690
	Analytical	16.4	-	1.000	0.958	-0.742	-0.983	0.833
4	Experimental	24.2	0.016	-1.000	0.333	0.637	-0.943	0.333
	Analytical	26.3	-	-1.000	0.272	0.653	-0.922	0.385
5	Experimental	29.7	0.018	0.810	-1.000	0.895	-0.551	0.223
	Analytical	34.6	-	0.914	-1.000	0.898	-0.578	0.178

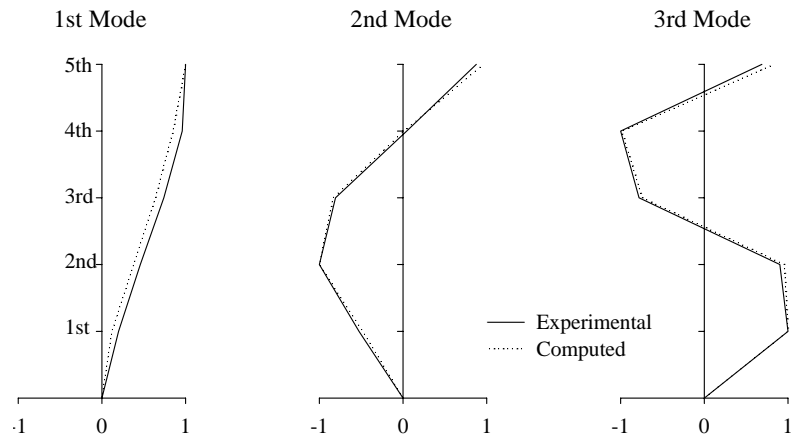


Figure 4-15: Schematic of influential mode shapes of fixed-base model structure.



## SECTION 5

### EARTHQUAKE SIMULATOR TESTING RESULTS

#### 5.1 Introduction

The results of the earthquake simulator testing program described in Section 4 are presented in this section. The range of tests performed on the model structure provides evidence for the effectiveness of the newly introduced isolator in uplift prevention. In addition, the experimental response data form the basis for comparison with and validation of the analytical predictions presented in Section 7.

#### 5.2 Test Results

The experimental results for the five-story isolated model structure are summarized in Tables 5-1 through 5-3. These tables present the experimentally recorded peak structure response in three different bearing orientations, namely at 0-, 45-, and 90-degree angle of lower bearing beam with respect to the direction of excitation. The excitation is identified with a percentage figure which denotes a scaling factor on the actual acceleration record.

The parameters reported in Tables 5-1 to 5-3 refer to peak shake table motion, peak isolation system response, and peak superstructure response. In particular, the quantities reported concern:

1. Peak values of horizontal shake table motion in terms of acceleration, velocity, and displacement. The accelerations and displacements are products of direct instrument recordings, as opposed to the velocities which were derived from the displacement records by numerical differentiation.
2. Peak isolation system response in terms of:
  - *Isolation system displacement*: the initial, maximum, minimum, travel, and permanent values of the average of east and west base displacement with respect to the shake table. The displacement transducers monitoring the base displacement were not initialized prior to each test, thus yielding correct information on the initial and permanent displacement of the isolation system.

Apparently, the initial displacement in any test is identical to the permanent displacement from the immediate previous test. Figure 5-1 exemplifies a typical isolation system displacement history. The maximum travel displacement of the isolation system is readily calculated as

$$U_{travel,max} = \max \{ U_{max} - U_{in}, |U_{min} - U_{in}| \} \quad (5-1)$$

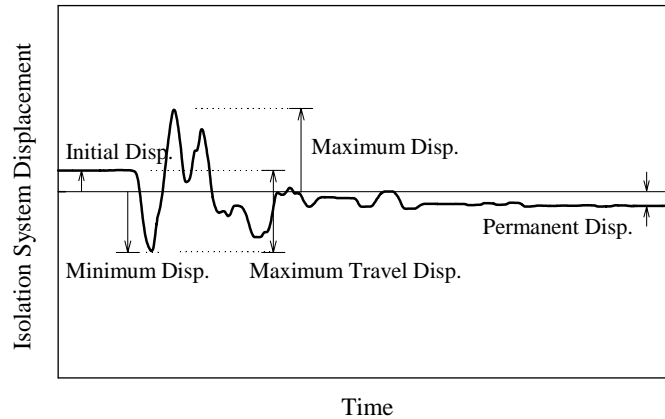


Figure 5-1: Typical isolation system displacement history.

- *Base shear*: the force at the isolation system level calculated as the peak value of the sum of recorded 1st-story shear and base inertial force. The inertial force at base level was calculated as the product of the base reactive mass and the average of the ABE and ABW recordings of base acceleration.
- *Bearing axial load*: the maximum and minimum values of total axial load in bearing due to both static load and dynamic load from overturning moment effects and vertical input motion. The axial load in the isolator was calculated based on Equation (2-11). The additional axial force due to overturning moment effects,  $N_{OM}$ , was obtained by using the overturning moment,  $M_o$ , calculated from records of floor acceleration as follows:

$$N_{OM} = \pm \frac{M_o}{L} = \pm \frac{\sum_{j=1}^5 F_j^I h_j}{L} \quad (5-2)$$

where  $F_j^I = m_j a_j$  is the inertia force of floor  $j$ , with  $m_j$  and  $a_j$  being the floor

mass and recorded floor acceleration, respectively;  $h_j$  is the height of floor  $j$  with respect to the base; and  $L$  is the frame span. Negative values indicate compression and positive values indicate tension.

3. Peak superstructure response in terms of:

- *1st-story shear*: the peak value of the recorded 1st-story shear from strain gauge load cells.
- *Story drift*: the peak value of the difference between the average displacement time histories of two adjacent floors, normalized by the story height.

To assess the accuracy of important recordings, measurements were contrasted with corresponding calculated quantities. For example, to check the direct acceleration measurements, recorded floor absolute displacements were double-differentiated to obtain floor acceleration histories. In addition, the first-story shear was calculated by summing up floor inertia forces (product of floor mass and floor acceleration above and inclusive of the first story) and compared to the recorded first-story shear from strain gauge load cells. Along the same lines, the isolation system shear (base shear) was calculated based solely on floor/base acceleration recordings and compared to the value obtained by adding the recorded 1st-story shear and base inertia force. The aforementioned comparisons provide satisfactory evidence of the fidelity of the experimental results.

### **5.3 Interpretation of Results**

During the initial phase of testing of the five-story model in its isolated condition it was observed that the system had undergone rocking. This was attributed to small imperfections inflicted upon the isolation system during installation. That is, the four isolators were not evenly aligned vertically below the rigid base. The problem was promptly resolved by inserting metallic shims between the isolators and the base plate.

Due to the light weight of the model structure, the bearing pressures were very small, and modest changes in axial load produced a large variation in the frictional properties of the isolation system. Indeed, in view of Equation (3-2) and supportive evidence from testing

Table 5-1: Experimentally recorded peak structure response for isolator angle of 0°.

Test	Excitation	Horizontal Table Motion			Isolation System Response										Superstructure Response	
		Accel. (g)	Vel. (mm/s)	Disp. (mm)	Displacement				Base Shear/Weight (-)	Bearing Axial Load		1st-story Shear/Weight (-)	Story <sup>1</sup> Drift/Height (%)			
					Initial (mm)	Max. (mm)	Min. (mm)	Travel (mm)		Perm. (mm)	Max. (kN)			Min. (kN)		
IELH50A	El Centro S00E 50%	0.21	82	13	-14.5	-2.7	-21.2	11.8	-7.5	0.07	42.83	10.41	0.10	0.25 (2)		
IELH100A	El Centro S00E 100%	0.35	158	27	0.1	9.2	-23.7	23.8	-0.4	0.08	45.51	7.73	0.12	0.33 (2)		
IELH200A	El Centro S00E 200%	0.56	301	55	-0.4	31.2	-55.1	54.7	-7.5	0.11	51.35	1.88	0.16	0.40 (2)		
IELB200A	El Centro S00E+V 200%	0.55	299	54	1.0	23.0	-51.8	52.8	0.2	0.13	58.02	0.49	0.17	0.45 (2)		
ITFH400A	Taft N21E 400%	0.64	257	56	3.5	41.5	-17.3	38.0	-1.8	0.12	53.64	-0.40	0.16	0.64 (2)		
ITFB400A	Taft N21E+V 400%	0.63	259	56	-1.7	40.7	-19.4	42.5	-2.2	0.15	61.48	-10.82	0.21	0.77 (2)		
IN9H100A	Newhall 90° 100%	0.79	287	43	4.9	22.1	-27.8	32.7	-2.8	0.13	49.20	4.04	0.15	0.43 (2)		
IN9B100A	Newhall 90°+V 100%	0.78	289	43	-2.8	20.2	-27.4	24.6	-0.3	0.14	58.39	-2.82	0.16	0.48 (4)		
IN3H100A	Newhall 360° 100%	0.76	428	58	-0.3	49.0	-41.3	49.4	-2.1	0.16	58.63	-5.39	0.21	0.59 (4)		
IN3B100A	Newhall 360°+V 100%	0.74	428	58	-2.1	46.8	-44.5	48.9	-1.1	0.16	66.38	-16.29	0.22	0.64 (4)		
ISYH100A	Sylmar 90° 100%	0.64	332	49	1.3	57.7	-22.8	56.4	3.9	0.16	57.81	-4.57	0.17	0.51 (4)		
ISYB100A	Sylmar 90°+V 100%	0.65	332	49	3.9	56.4	-23.9	52.6	4.9	0.16	71.47	-9.52	0.22	0.46 (3)		
IKBH100A	Kobe N-S 100%	0.75	434	42	-1.1	26.4	-37.8	36.7	-0.3	0.14	59.17	-5.93	0.18	0.81 (2)		
IKBB100A	Kobe N-S+V 100%	0.76	432	42	-0.3	31.8	-32.2	32.0	0.7	0.17	72.79	-5.96	0.22	0.67 (2)		
IP7H100A	Pacoima S74W 100%	0.77	268	28	0.2	26.0	-30.7	30.9	-1.0	0.12	51.87	1.36	0.15	0.36 (2)		
IP7B100A	Pacoima S74W+V 100%	0.75	270	28	-0.9	27.2	-29.0	28.1	-5.7	0.15	69.26	-24.33	0.16	0.50 (3)		
IP1H75A	Pacoima S16E 75%	0.64	348	59	-4.3	43.9	-49.7	48.2	1.0	0.13	48.06	5.17	0.15	0.35 (2)		
IP1H100A	Pacoima S16E 100%	0.80	461	79	1.0	56.5	-72.5	73.5	3.9	0.14	50.56	2.67	0.16	0.37 (2)		
IP1B100A	Pacoima S16E+V 100%	0.80	460	78	3.9	61.2	-68.1	72.0	3.6	0.21	66.71	-1.90	0.17	0.51 (3)		
IHAH100A	Hachinohe N-S 100%	0.24	131	31	-2.2	15.3	-5.6	17.6	1.3	0.11	46.55	6.68	0.14	0.35 (4)		

<sup>1</sup> Value in parenthesis is story at which peak value was recorded.

Table 5-2: Experimentally recorded peak structure response for isolator angle of 90°.

Test	Excitation	Horizontal Table Motion			Isolation System Response								Superstructure Response	
		Accel. (g)	Vel. (mm/s)	Disp. (mm)	Displacement				Base Shear/Weight (-)	Bearing Axial Load		1st-story Shear/Weight (-)	Story <sup>1</sup> Drift/Height (%)	
					Initial (mm)	Max. (mm)	Min. (mm)	Travel (mm)		Perm. (mm)	Max. (kN)			Min. (kN)
IELH100B	El Centro S00E 100%	0.33	149	26	0.0	8.8	-16.1	16.1	1.8	0.18	52.86	0.38	0.19	0.45 (2)
IELH200C	El Centro S00E 200%	0.56	288	53	9.9	20.0	-52.2	62.1	-4.7	0.11	53.61	-0.37	0.17	0.52 (2)
IELB200C	El Centro S00E+V 200%	0.54	291	53	-4.7	18.6	-45.9	41.1	-4.1	0.14	63.50	-5.01	0.22	0.45 (2)
IN3H100C	Newhall 360° 100%	0.75	419	57	10.1	43.8	-32.0	42.0	-1.7	0.14	63.45	-10.21	0.24	0.69 (2)
IN3B100C	Newhall 360°+V 100%	0.72	417	57	-1.7	43.5	-41.4	45.1	-2.9	0.16	63.11	-19.30	0.22	0.66 (2)
ISYH100C	Sylmar 90° 100%	0.62	327	48	4.6	54.5	-21.9	49.9	8.1	0.15	60.01	-6.77	0.18	0.51 (2)
ISYB100C	Sylmar 90°+V 100%	0.64	325	48	8.1	54.6	-20.1	46.5	10.1	0.19	79.66	-24.07	0.24	0.46 (3)
IPIH100C	Pacoima S16E 100%	0.79	457	77	5.7	49.2	-67.5	73.3	3.9	0.16	51.33	1.91	0.18	0.40 (2)
IPIH125C	Pacoima S16E 125%	1.01	565	97	-2.9	66.0	-94.5	91.6	7.9	0.19	58.19	-4.95	0.17	0.50 (2)
IPIB100C	Pacoima S16E+V 100%	0.79	451	77	3.9	54.8	-64.6	68.6	4.6	0.23	80.14	-9.05	0.20	0.55 (3)

<sup>1</sup> Value in parenthesis is story at which peak value was recorded.

Table 5-3: Experimentally recorded peak structure response for isolator angle of 45°.

Test	Excitation	Horizontal Table Motion			Isolation System Response								Superstructure Response	
		Accel. (g)	Vel. (mm/s)	Disp. (mm)	Displacement				Base Shear/Weight (-)	Bearing Axial Load		1st-story Shear/Weight (-)	Story <sup>1</sup> Drift/Height (%)	
					Initial (mm)	Max. (mm)	Min. (mm)	Travel (mm)		Perm. (mm)	Max. (kN)			Min. (kN)
IELH200G	El Centro S00E 200%	0.57	304	55	-7.8	19.8	-54.3	46.5	-1.5	0.14	56.30	-3.07	0.19	0.95 (2)
IELB200G	El Centro S00E+V 200%	0.56	303	54	-1.5	18.0	-52.5	51.0	-0.8	0.15	61.70	-3.28	0.22	0.79 (2)
IN3H100G	Newhall 360° 100%	0.76	435	59	11.5	44.7	-32.4	43.9	-7.7	0.15	66.48	-13.25	0.21	1.32 (3)
IN3B100G	Newhall 360°+V 100%	0.76	431	60	-7.8	43.1	-48.5	50.9	-0.9	0.17	72.71	-21.88	0.24	0.85 (2)
ISYH100G	Sylmar 90° 100%	0.64	337	50	-2.6	61.5	-18.6	64.2	10.7	0.17	57.04	-3.80	0.17	0.63 (2)
ISYB100G	Sylmar 90°+V 100%	0.66	335	50	10.7	61.0	-16.1	50.3	11.5	0.17	85.75	-16.99	0.24	0.72 (2)
IPIH100G	Pacoima S16E 100%	0.79	466	80	-0.8	49.3	-71.1	70.3	-3.1	0.17	52.25	0.99	0.19	0.91 (2)
IPIH125G	Pacoima S16E 125%	1.04	580	100	-1.0	63.3	-92.8	91.8	3.4	0.18	58.16	-4.92	0.18	1.11 (2)
IPIH150G	Pacoima S16E 150%	1.30	671	115	-4.9	74.4	-116.3	111.3	5.1	0.19	63.57	-10.33	0.19	1.17 (2)
IPIB100G	Pacoima S16E+V 100%	0.78	462	79	-3.1	56.8	-68.0	64.9	-2.6	0.25	79.81	-13.65	0.20	1.17 (2)

<sup>1</sup> Value in parenthesis is story at which peak value was recorded.

of individual isolator presented in Section 3, the lower the bearing pressure, the less stable the frictional properties. This peculiarity of noticeable uncertainty in frictional properties refers only to the laboratory model at hand and does not apply for real-life applications, where the design is carried out for high loads.

Because of the low contact pressure, the XY-FP isolators exhibited initially high sliding coefficient of friction, in the range of 0.12-0.15, limiting the isolation system performance. Accordingly, in order to render the isolation system more effective to facilitate larger displacements, successive lubrication of the bearing sliding interface was attempted during the testing program. The lubrication process resulted in a coefficient of friction in the range of 0.06 to 0.10. However, by virtue of the superficial application of the lubricant, the reduction in friction was not permanent and the coefficient of friction gradually increased with repeated testing as lubricant was lost, thus necessitating repetitive lubrication.

In general, the shake table produced motions that are in acceptable agreement with the target motions in the period range of the isolated model structure. However, it is worth noting that the recorded histories of the table motion were not accurately reproduced among tests with inputs that were specified to be identical. This can be seen from the peak values of the generated table motion presented in Tables 5-1 through 5-3. This ambiguity can be explained along the lines of shake table-structure interaction.

Furthermore, the shake table underwent perceptible vertical motion even when only horizontal table motion was imposed. Again, this can be interpreted as evidence of shake table-structure interaction during testing. The implications of this phenomenon were, in effect, to increase the severity of the testing by aggravating the earthquake induced axial load (compression and tension) on the bearings.

One can observe from Tables 5-1 through 5-3 that the permanent displacement of the isolation system along the excitation direction was small and not cumulative in successive tests. Figure 5-2 depicts graphically the history of the permanent displacements from testing in different isolator orientations. Evidently, the tested XY-FP isolator provided sufficient restoring force and prevented permanent displacements to accumulate to unacceptable levels.

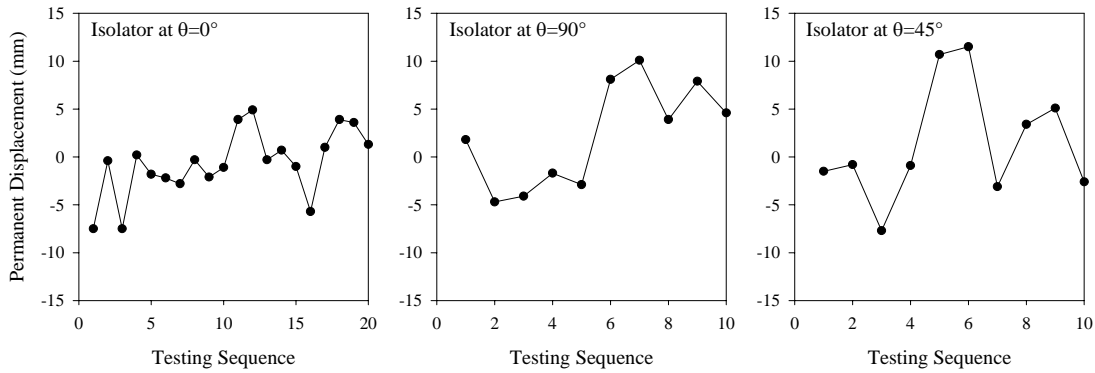


Figure 5-2: History of permanent displacements from testing in different isolator orientations.

Figures 5-3 through 5-7 depict representative results from the range of tests performed on the model structure. The graphs present histories of the isolation system displacement, the normalized 1st-story shear, the bearing axial force, and the shear force-displacement loops for the isolation system. These results provide evidence of the effectiveness of the newly introduced XY-FP isolator in different orientations. Clearly, the new isolator is capable of developing tension, thereby providing uplift restraint.

Of particular interest is the axial force histories associated with the isolators, herein plotted per isolator pair. Due to the slenderness of the structure (height to width aspect ratio approximately 4.5), large overturning moment effects were induced under strong base excitation. This was manifested as considerable variation in axial force, on the order of 100%. The effect of overturning moment is more pronounced in Figures 5-5 through 5-7 where the fluctuations in the bearing axial forces caused by overturning moments were large enough to cause reversal of the axial force from compression to tension.

Figure 5-7 provides evidence of the effect of the vertical component of ground motion on the response of the isolated structure. These results demonstrate that the vertical ground motion component has a minor effect on the isolation system displacement, yet a non-negligible effect on the isolation system force response, a deviation on the order of 15%, reflected primarily in the way form of the isolation system hysteresis loop. Analogous observations have been reported for the case of structures seismically isolated with conventional FP bearings (e.g., Constantinou et al., 1993; Al-Hussaini et al., 1994;

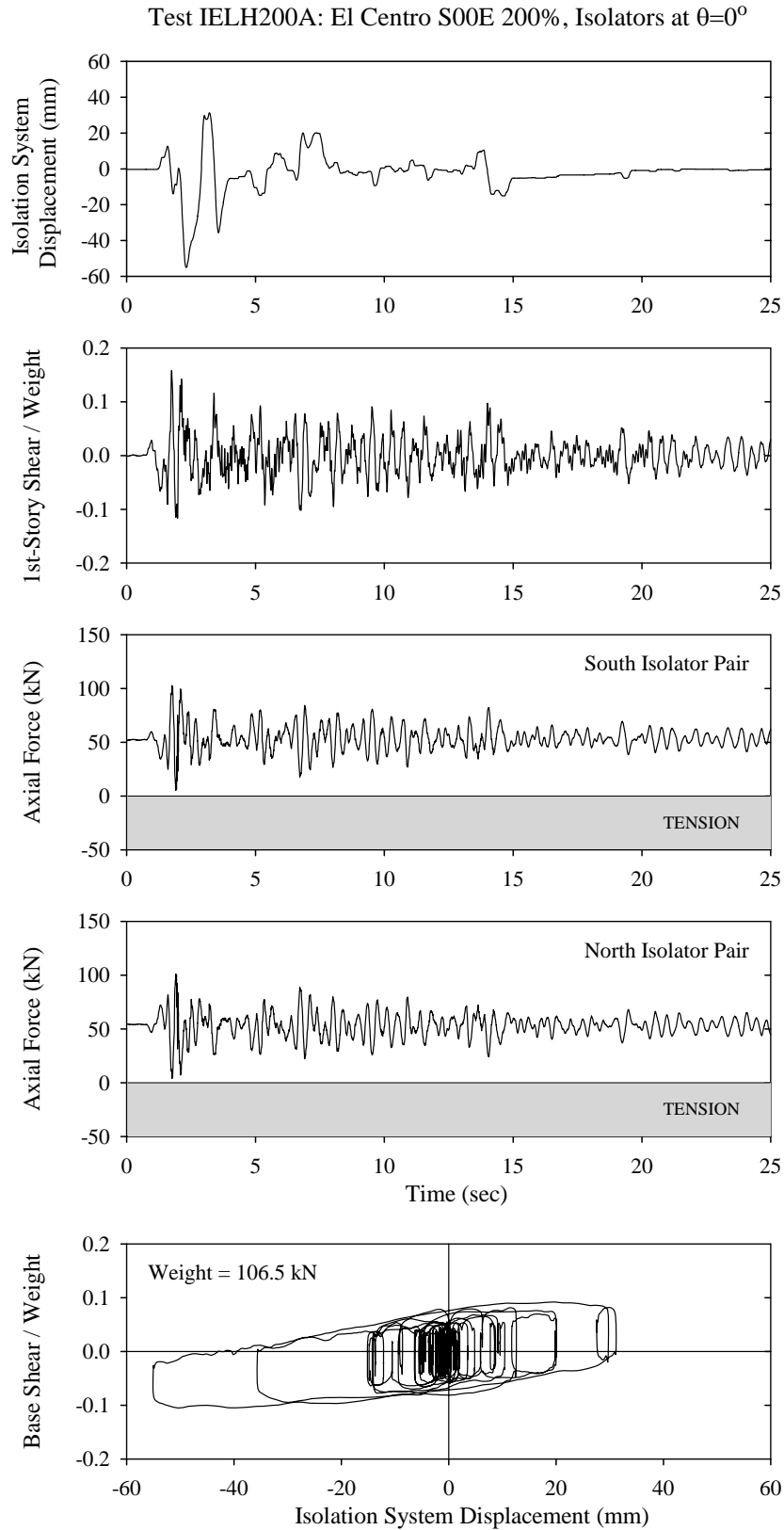


Figure 5-3: Experimental results in El Centro S00E 200% for bearing orientation of  $0^\circ$ .

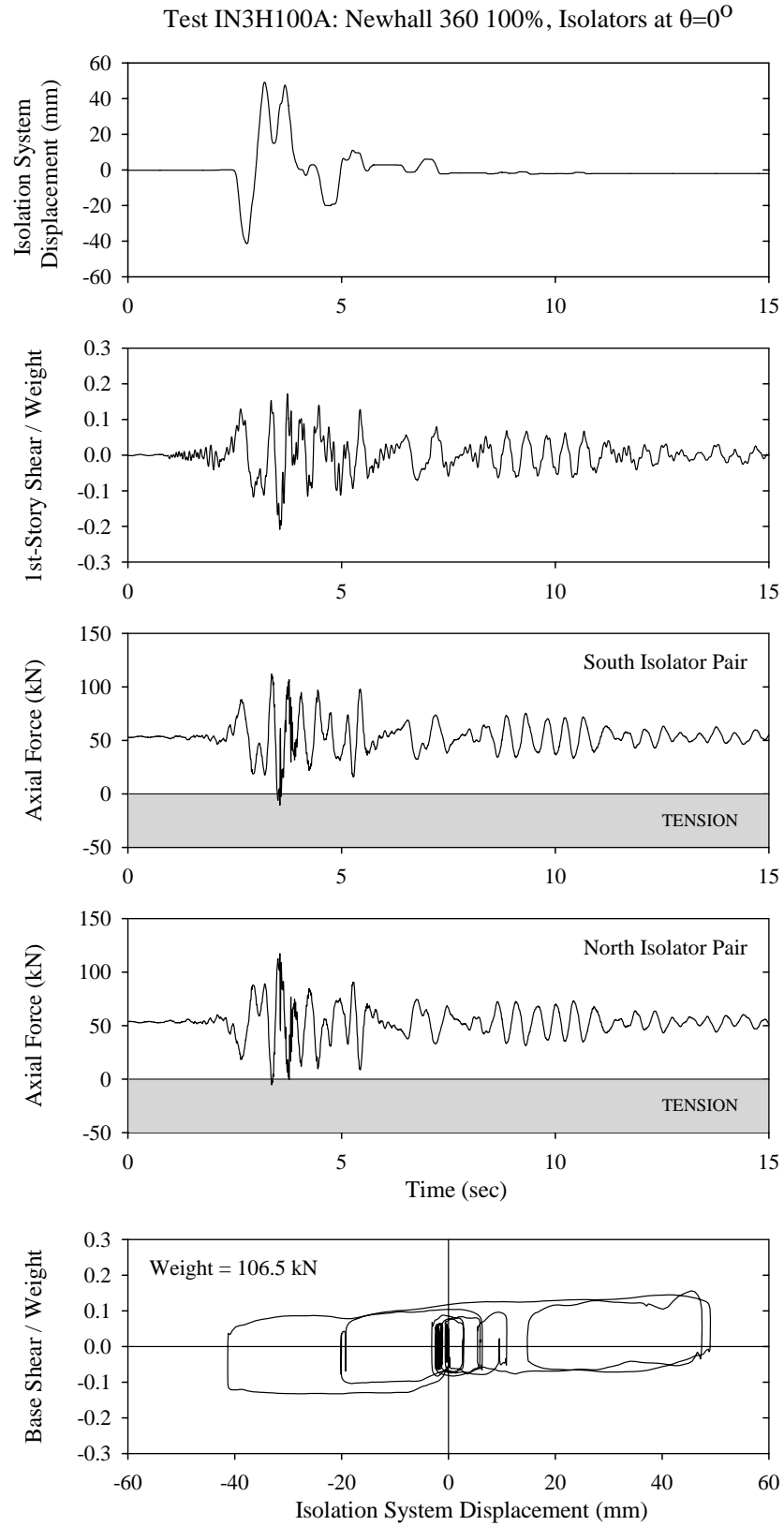


Figure 5-4: Experimental results in Newhall 360 100% for bearing orientation of  $0^\circ$ .

Test IN3H100C: Newhall 360 100%, Isolators at  $\theta=90^\circ$

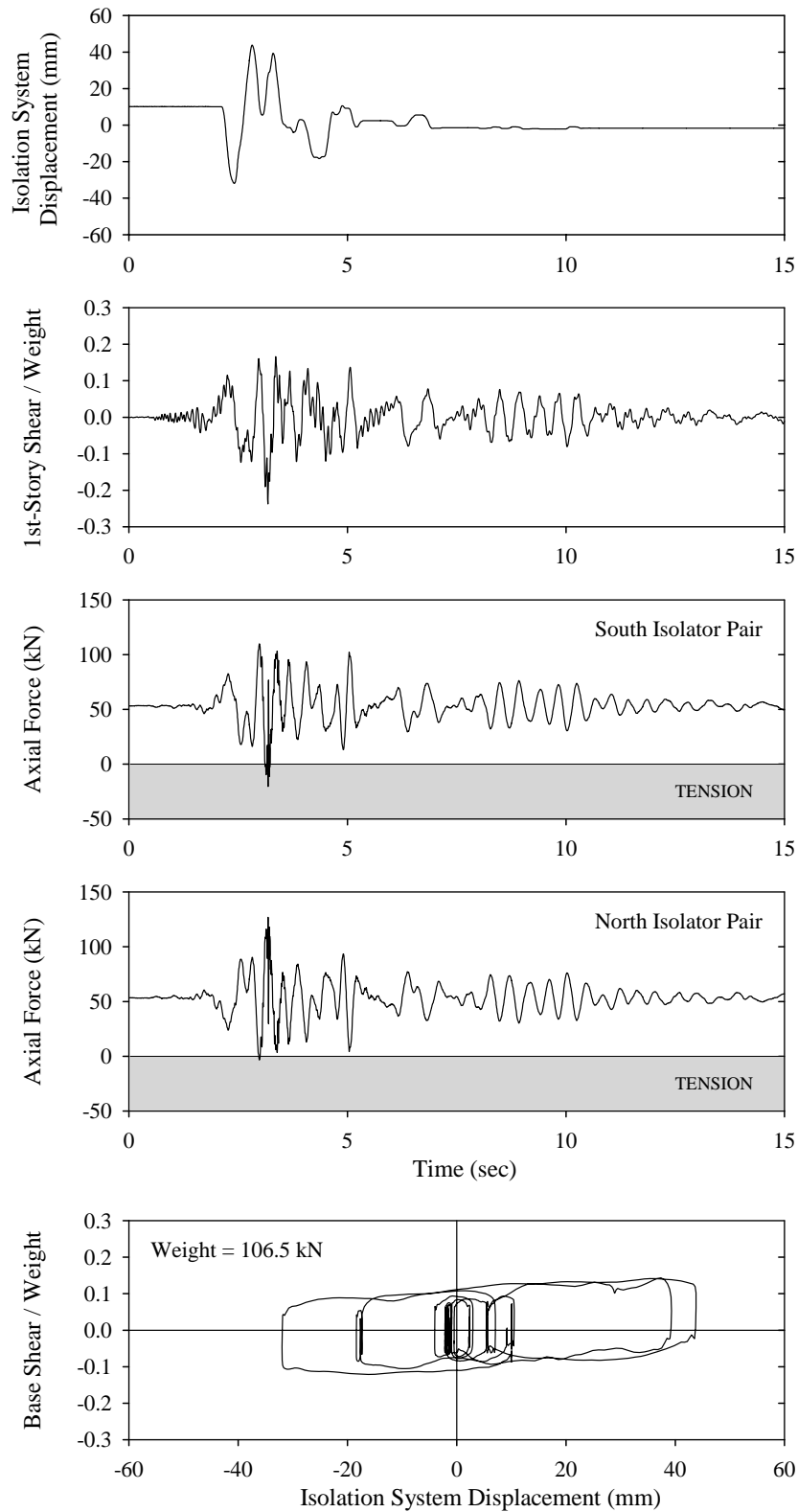


Figure 5-5: Experimental results in Newhall 360 100% for bearing orientation of  $90^\circ$ .

Test IN3H100G: Newhall 360 100%, Isolators at  $\theta=45^\circ$

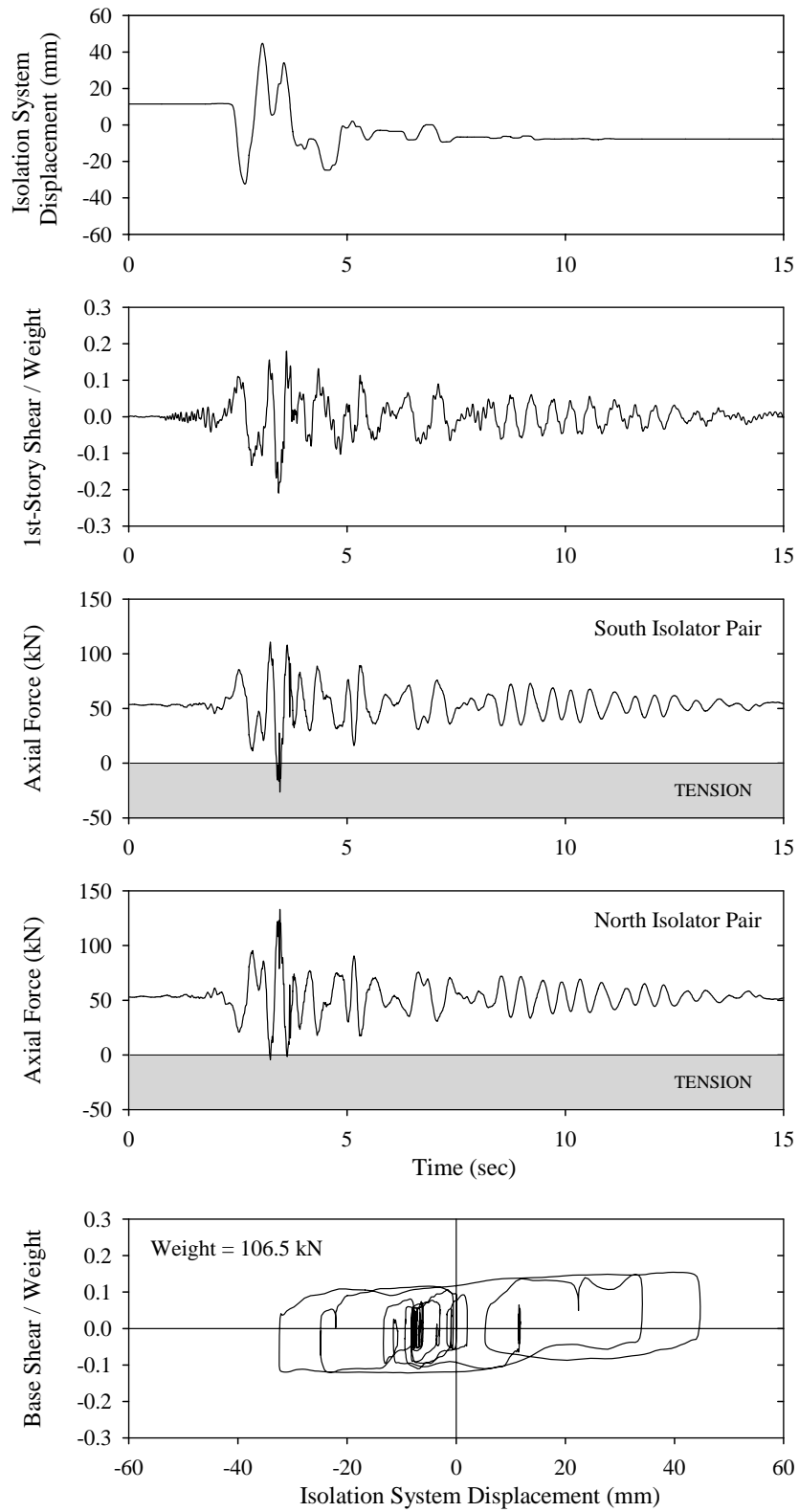


Figure 5-6: Experimental results in Newhall 360 100% for bearing orientation of  $45^\circ$ .

Tests IP7H100A & IP7B100A: Pacoima S74W & S74W+V 100%, Isolators at  $\theta=0^\circ$

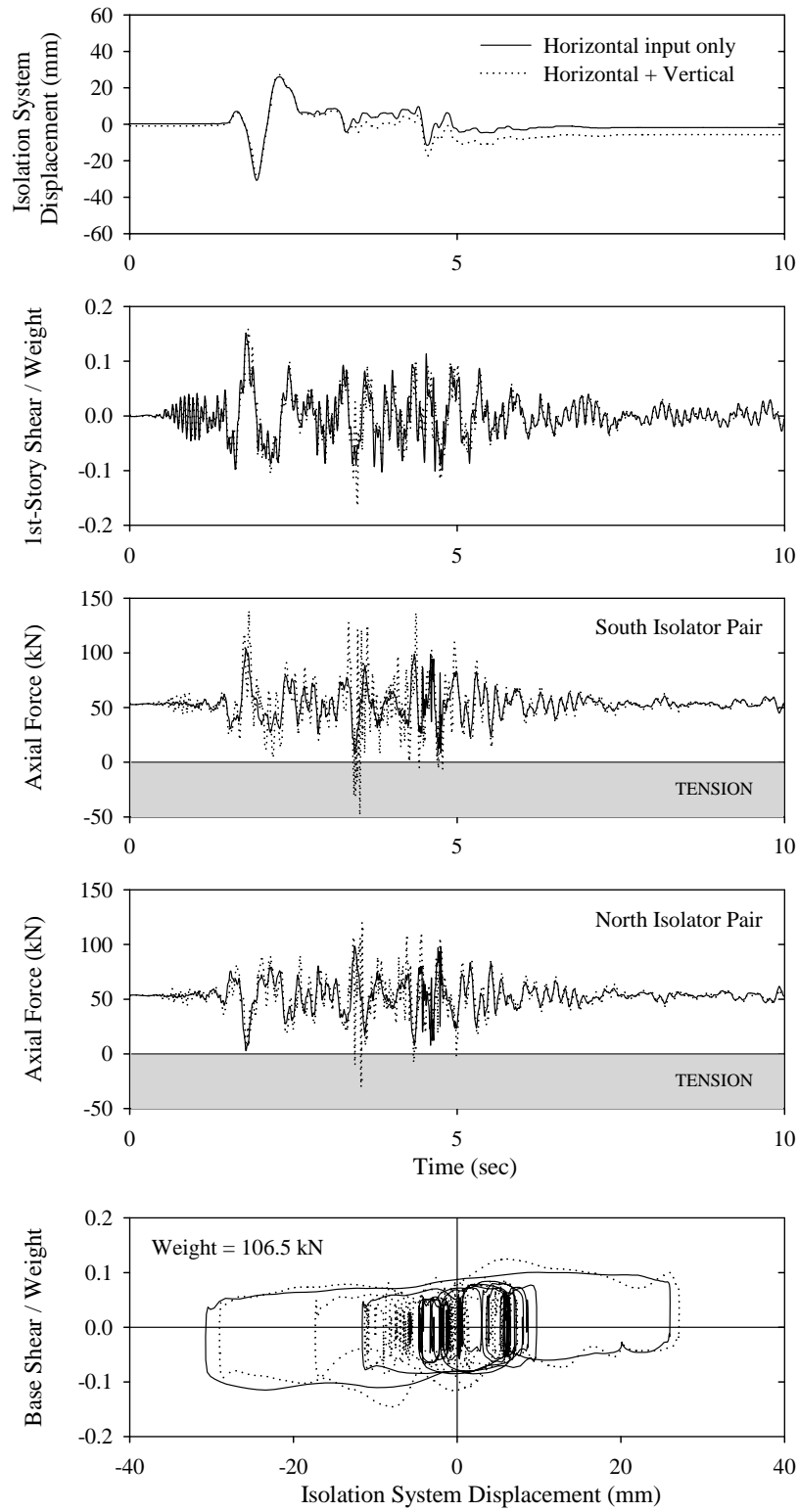


Figure 5-7: Comparison of experimental results in Pacoima S74W 100% and Pacoima S74W+Vertical 100% excitations for bearing orientation of  $0^\circ$ .

Kasalanati et al., 1999; Mosqueda et al., 2004). The effect of the vertical component of ground motion is pronounced in the local response of the isolators. In effect, the vertical ground acceleration modifies the axial load on the bearing (Equation (2-11)), and therefore impacts both the restoring force and the friction force in the bearing constitutive relationship (Equation (2-7)). A parallel implication of the variation of the bearing pressure at the sliding interface is the modification of the coefficient of friction (see section 3.2). Figure 5-7 demonstrates that the amplification of the bearing axial force due to the vertical input may prove large enough to cause tension to develop in the bearing.

It is worth observing that the peak axial load on the bearing occurs at a large lateral displacement but not exactly at the instant of peak isolation displacement. Upon noting that the bearing axial load is directly related to overturning moment, and hence to floor accelerations, the aforementioned discrepancy can be attributed to the fact that floor acceleration response was out of phase (higher mode response). Similar observations on floor acceleration profiles and their impact on the response of FP-isolated structures were also reported by Mokha et al. (1990) and Al-Hussaini et al. (1994).

## **SECTION 6**

### **MODIFICATION OF PROGRAM 3D-BASIS-ME**

#### **6.1 Introduction**

Section 6 outlines the modifications made to computer program 3D-BASIS-ME (Tsopeles et al., 1994). While maintaining the key features of the program, the following enhancements are incorporated: (i) a new hysteretic element capable of modeling the behavior of the XY-FP isolator; (ii) a capability of accounting for initial non-zero displacement of the isolators; and (iii) a more accurate description of the additional bearing axial forces due to global overturning moment effects.

#### **6.2 Overview of Program 3D-BASIS**

The 3D-BASIS suite of computer programs was developed for the nonlinear dynamic analysis of three-dimensional seismically isolated structures. Capable of modeling various types of isolation devices with strong nonlinearities, 3D-BASIS provides a versatile tool for analysis and design of complex structures with modern isolation systems. As such, the program contributed in the verification and development of new standards for design of base isolated structures and facilitated the advancement of practical application of base isolation.

Rooted in the core philosophy of its predecessors, 3D-BASIS-ME represents an enhanced version of program 3D-BASIS-M (Tsopeles et al. 1991), which is a further extension of the original program 3D-BASIS (Nagarajaiah et al. 1989, 1991b and 1993).

Program 3D-BASIS-M is an improvement on the original version by offering the capability to analyze multiple superstructures on a single isolation basemat. This could be exploited, for example, in dynamic analysis of isolated structures consisting of several parts separated by thermal expansion joints, or isolated liquid storage tanks in which the liquid-tank system is modeled by two multi-degree-of freedom systems representing the impulsive and convective effects, respectively.

Program 3D-BASIS-ME augments the potential of its predecessor by introducing new

elements for modeling Friction Pendulum (FP) bearings, high damping rubber bearings with stiffening behavior, and nonlinear viscous dampers. Furthermore, it accounts for the effects of vertical ground motion and overturning moment on the behavior of sliding bearings.

Assumed to remain elastic at all times, the superstructure in 3D-BASIS-ME can be modeled via (i) a shear-type representation, or (ii) a full three-dimensional representation. In the shear-type representation, the stiffness matrix of the superstructure is internally constructed by the program, based on input story translational stiffnesses, rotational stiffness, and eccentricities of center of resistance with respect to the center of mass for each floor. It is assumed that the centers of mass of all floors lie on a common vertical axis, floors are rigid, and walls and columns are inextensible. In the full three-dimensional representation, the dynamic characteristics of the superstructure in terms of frequencies and mode shapes are determined externally by other computer programs and imported to program 3D-BASIS-ME. In this way, the extensibility of the vertical elements, arbitrary location of centers of mass, and floor flexibility may be implicitly accounted for. In both options, each floor mass is lumped into a single point mass having three degrees of freedom (two lateral and one torsional) in the horizontal plane.

The isolation system is modeled with spatial distribution and explicit nonlinear force-displacement characteristics of the individual isolators. The isolation devices are considered rigid in the vertical direction and are assumed to have negligible resistance to torsion. 3D-BASIS-ME has the following elements for modeling the behavior of an isolator: (i) linear elastic element; (ii) linear and nonlinear viscous element for fluid viscous dampers or other devices displaying viscous behavior; (iii) hysteretic element for elastomeric bearings and steel dampers; (iv) stiffening (biaxial) hysteretic element for high damping rubber bearings; (v) hysteretic element for flat sliding bearings; and (vi) hysteretic element for spherical sliding (FP) bearings.

The algorithm selected for the 3D-BASIS series is based on the solution of the equations of motion using a combination of Newmark's integration method and a fourth-order Runge-Kutta scheme, complemented by a pseudo-load formulation and time marching procedure for accuracy and efficiency. The algorithm has been proven to be suitable for

analyzing highly nonlinear sliding isolation systems (Nagarajaiah et al., 1989, 1990, 1991a, 1991b).

### **6.3 Enhancements Introduced in Program 3D-BASIS-ME**

While maintaining the key features of the program, the following enhancements were incorporated into 3D-BASIS-ME: (i) a new hysteretic element capable of modeling the behavior of the XY-FP isolator; (ii) a capability of accounting for initial non-zero displacement of the isolators; and (iii) a more accurate description of the additional bearing axial forces due to overturning moment effects.

#### **6.3.1 New Hysteretic Element for XY-FP Isolator**

The mathematical model of the new XY-FP isolator has been established in Section 2.3. The force-displacement constitutive relationship, neglecting the interaction between lateral force and friction force, is given by Equation (2-10). To accommodate the mechanical behavior of the new XY-FP isolator, a new hysteretic element was incorporated into 3D-BASIS-ME. The new element is synthesized by two independent uniaxial hysteretic elements allowing different frictional interface properties along the principal isolator directions. It should be emphasized that, contrary to the element representing the conventional FP isolator, the new element is capable of developing tension. Moreover, different frictional interface properties can be assumed under compressive and tensile isolator normal force.

In general, under harmonic or transient dynamic loading each sliding bearing undergoes different motion requiring multiple stick-slip conditions. Accordingly, the use of Coulomb model (Su et al., 1987; Mostaghel and Khodaverdian, 1987; Younis et al., 1983; Goodman, 1963) under these conditions is complicated. Hence the Bouc-Wen plasticity model (Park et al., 1986; Wen, 1976) was adopted in modeling the XY-FP isolator because of its computational efficiency, which stems from the fact that tracing of the hysteresis loops in this model is not necessary.

The horizontal forces in the XY-FP element in 3D-BASIS-ME are given by

$$\begin{Bmatrix} F_1 \\ F_2 \end{Bmatrix} = \begin{bmatrix} N/R_1 & 0 \\ 0 & N/R_2 \end{bmatrix} \begin{Bmatrix} U_1 \\ U_2 \end{Bmatrix} + \begin{bmatrix} \mu_1 |N| & 0 \\ 0 & \mu_2 |N| \end{bmatrix} \begin{Bmatrix} Z_1 \\ Z_2 \end{Bmatrix} \quad (6-1)$$

where  $R_1$  and  $R_2$  are the radii of curvature of the lower and upper concave beams, respectively;  $\mu_1$  and  $\mu_2$  are the associated sliding friction coefficients;  $U_1$  and  $U_2$  are the displacements in local axis 1 and 2, respectively;  $N$  is the normal force on the bearing, positive when compressive; and  $Z_1$  and  $Z_2$  are hysteretic dimensionless quantities governed by the following differential equations:

$$\begin{Bmatrix} \dot{Z}_1 Y_1 \\ \dot{Z}_2 Y_2 \end{Bmatrix} = A \begin{bmatrix} 1 & 0 \\ 0 & 1 \end{bmatrix} \begin{Bmatrix} \dot{U}_1 \\ \dot{U}_2 \end{Bmatrix} - \begin{bmatrix} |Z_1|^\eta (\gamma \operatorname{sgn}(\dot{U}_1 Z_1) + \beta) & 0 \\ 0 & |Z_2|^\eta (\gamma \operatorname{sgn}(\dot{U}_2 Z_2) + \beta) \end{bmatrix} \begin{Bmatrix} \dot{U}_1 \\ \dot{U}_2 \end{Bmatrix} \quad (6-2)$$

where  $\dot{U}_1$  and  $\dot{U}_2$  are the velocities in local axis 1 and 2, respectively;  $A$ ,  $\beta$ ,  $\gamma$ , and  $\eta$  are dimensionless quantities that control the shape of the hysteresis loop; and  $Y_1$  and  $Y_2$  represent displacement quantities.

Constantinou et al. (1990) have shown that when  $A=1$  and  $\beta+\gamma=1$ , the model of Equation (6-2) reduces to a model of viscoplasticity that was proposed by Ozdemir (1976). In this case,  $Y_1$  and  $Y_2$  represent the yield displacements, while parameter  $\eta$  controls the mode of transition into the inelastic range. The model exhibits rate dependency, which reduces with increasing values of the exponent,  $\eta$ , and/or increasing values of the ductility ratio (maximum value of  $U/Y$ ).

The conditions of separation and reattachment (stick-slip) are accounted for by variables  $Z_1$  and  $Z_2$  in Equation (6-2). In this respect, quantity  $Z_i$  may be regarded as a continuous approximation to the unit step function,  $\operatorname{sgn}(\dot{U}_i)$  in Equation (2-10). It should be noted that  $Z_i = \pm 1$  during the sliding phase, whereas  $|Z_i| < 1$  during the sticking phase (elastic behavior with very high stiffness).

A limitation of the employed plasticity model is its inability to reproduce truly rigid-plastic behavior. However, since Teflon-steel interfaces undergo very small elastic displacement before sliding, small value of yield displacement  $Y$ , in the range of 0.13-

0.50 mm (0.005-0.02 in.) can be reasonably assumed and, hence, the viscoplasticity model can be used (Constantinou et al., 1990). The model exhibits insignificant rate dependency for such low yield displacement and resulting ductility ratio, and for parameter values of  $\eta = 2$ ,  $\beta = 0.1$ , and  $\gamma = 0.9$  suggested by Constantinou et al. (1990).

It should be emphasized that Equation (6-2) is uncoupled, representing two independent uniaxial hysteretic elements along the principal directions of the isolator. Accordingly, the biaxial interaction between forces in the two orthogonal directions is nonexistent, rendering the interaction surface to be square, as opposed to the circular interaction surface for the biaxial behavior of the spherical FP isolator (Figure 6-1).

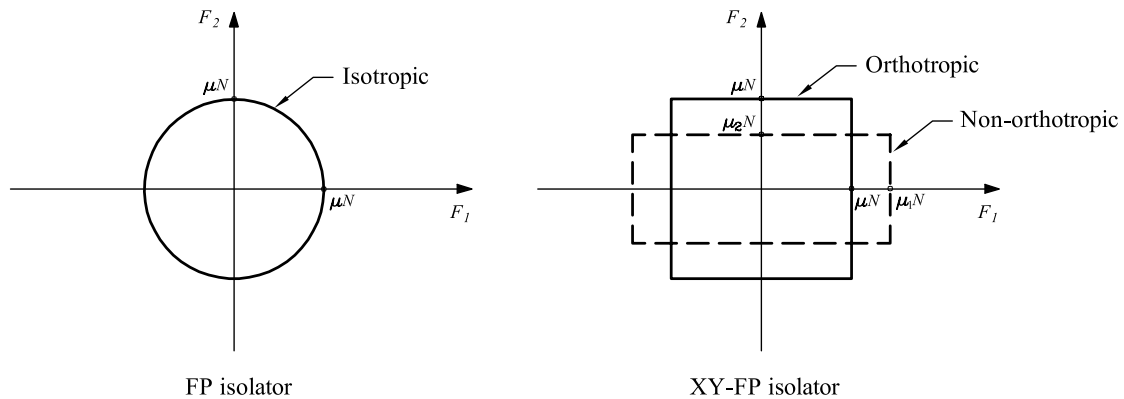


Figure 6-1: Force interaction curves for XY-FP and FP isolators.

Recall that in the case of the conventional FP isolator, an arbitrary uni-directional motion entails a collinear resisting force. On the contrary, in the case of the XY-FP isolator, application of a horizontal force in an arbitrary direction results in a bi-directional motion realized along the two isolator beams. This is true even for orthotropic interface conditions, namely for identical frictional and geometric properties along the two component beams. An exception to this is when the applied force is either along a local axis or at 45 degrees with respect to a local axis, wherein uni-directional motion results along the corresponding force direction.

In Equation (6-1), the normal force,  $N$ , on an isolation bearing is, in general, a varying function of time due to the vertical component of ground motion and the overturning moment effects. For vertically rigid structures, the normal force on the XY-FP bearing at

any given time is given by

$$N = W \left( 1 + \frac{\ddot{u}_{gv}}{g} + \frac{N_{OM}}{W} \right) \quad (6-3)$$

where  $W$  is the weight acting on the isolator;  $\ddot{u}_{gv}$  is the vertical ground acceleration, positive when directed upward; and  $N_{OM}$  is the additional axial force due to overturning moment effects, positive when compressive.

The new element for the XY-FP isolator in 3D-BASIS-ME requires a user-supplied subroutine, function FOVM, to calculate the additional axial force due to overturning moment effects. The function – called by the main program at each time step – returns to the main program the additional axial load FOVM on each bearing due to overturning moment effects. The definition of the additional force FOVM due to the overturning moments OVMX and OVMY is illustrated in Figure 6-2, in which FOVM is the normal force due to overturning moment, positive when compressive; OVMX and OVMY are the overturning moments about X- and Y-axis, respectively, positive in the direction shown in the figure (Tsopelas et al., 1994).

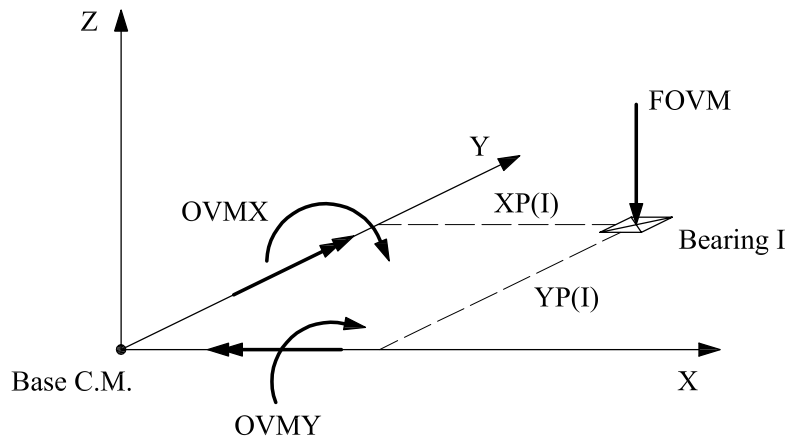


Figure 6-2: Definition of overturning moments OVMX and OVMY, and additional force FOVM.

Contrary to the element representing the conventional FP isolator, the new element is capable of capturing the uplift-restraint property of the XY-FP isolator allowing potential reversal of the bearing axial force from compression to tension.

Moreover, the dependency of the coefficient of friction on sliding velocity and bearing pressure is explicitly modeled in 3D-BASIS-ME according to Equations (3-1) and(3-2), respectively.

Output data pertaining to the new element representing the XY-FP isolator are given in file *ISOL8*. The output file contains response histories of individual XY-FP isolators, in terms of (a) isolator shear forces in both local and global axes; (b) isolator axial forces; and (c) isolator displacements in both local and global axes.

### **6.3.2 Account for initial non-zero displacement of the isolators**

The potentiality of permanent displacements in sliding isolation systems with reduced restoring force capability, or lack thereof, is often of concern, as the permanent displacements may accumulate to unacceptable levels in successive earthquakes (Roussis et al., 2002, 2003; Constantinou et al., 1991). Building codes and guide specifications for seismic isolation design, attempt to account for this possibility by either specifying minimum stiffness requirements or by penalizing systems with insufficient stiffness.

To accommodate monitoring of the history of residual displacements in successive analyses, 3D-BASIS-ME was modified to account for initial non-zero displacements of the isolation system resulting from the permanent displacements in the immediate previous analysis. This option, available for the new XY-FP element, allows for input of the initial state of the isolation system in terms of the initial displacements along the X and Y directions and initial rotation of the center of mass of the base.

### **6.3.3 A more accurate description of the additional bearing axial forces due to overturning moment effects**

A user-supplied subroutine, FOVM, is available in program 3D-BASIS-ME which accounts for the variability of axial forces in the isolation bearings due to overturning moment effects (Tsopelas et al., 1994). The function, which shall be modified by the user before each run, updates and returns to the main program the additional axial load FOVM on bearing  $i$  at every time step. The function assumes a unique relation between overturning moments and additional axial load on bearings. It should be noted that this is a simplification of a complex phenomenon, yet it is a commonly used engineering

approximation.

In order to provide a more accurate representation of bearing axial forces, 3D-BASIS-ME was modified to include a direct relationship between floor inertia forces and additional axial load on bearings. At each time step of integration, the horizontal inertia forces,  $\{F_I\}$ , are calculated from the floor accelerations and multiplied by a coefficient matrix,  $[T]$ , to obtain the corresponding variation of vertical loads on the bearings due to overturning moment effects,  $\{N_{OM}\}$ . The additional vertical load may be expressed as

$$\{N_{OM}\} = [T]\{F_I\} \quad (6-4)$$

where  $\{N_{OM}\}_{n \times 1} = [N_{OM,1} \quad N_{OM,2} \quad \dots \quad N_{OM,n}]^T$  is the vector of bearing axial forces;  $[T]_{n \times 2i}$  is a coefficient matrix relating additional bearing axial forces to floor inertia forces;  $\{F_I\}_{2i \times 1} = [F_{I,ix} \quad F_{I,iy} \quad \dots \quad F_{I,1x} \quad F_{I,1y}]^T$  is the vector of floor inertia forces;  $n$  is the number of bearings; and  $i$  is the number of floors.

The coefficient matrix,  $[T]$ , is evaluated externally by other computer programs and imported into program 3D-BASIS-ME through the file *tmatrix.dat*. It shall be calculated from linear static analyses of the structure supported on hinge supports and subjected to horizontally acting unit loads at the different floor levels. For example, the  $i$ -th column of matrix  $[T]$  is calculated as the local frame column loads upon application of a unit lateral force at the center of mass of the  $i$ -th floor, with the lateral forces of the remaining floors being zero. It should be noted that matrix  $[T]$  in Equation (6-4) is single-valued in the case of the XY-FP isolator, regardless of whether the isolator is in tension or compression.

The same equation is used in the program for establishing the relationship between the axial forces on isolators and floor inertial forces for conventional FP isolators. It should be noted that matrix  $[T]$  is not single-valued in the case of FP isolators when uplift can occur, since different load distributions exist depending on what combination of isolators undergo uplift. Nevertheless, the single-valued matrix (which assumes that bearings can

sustain tension) is used in the program, and when a tensile value is detected, it is replaced by zero. This is an approximation because it does not account for redistribution of loads. However, the error involved is not significant, since typically the force that needs to be redistributed is small by comparison to the total weight, and only a small number of isolators undergo uplift at any instant of time.



## SECTION 7

### ANALYTICAL PREDICTION OF RESPONSE

#### 7.1 Introduction

The dynamic response of the five-story seismically isolated model structure was predicted analytically using 3D-BASIS-ME. The validity of the analytical model, with reference to the newly introduced element representing the XY-FP isolator, is investigated by comparison of analytical predictions with experimental results and conclusions on the accuracy of the analysis methods are derived.

#### 7.2 Analytical Model

The dynamic response of the five-story structure was analytically predicted using the 3D-BASIS-ME computer program. Assumed to remain elastic at all times, the 5-story superstructure model in 3D-BASIS utilized a three-dimensional representation. Each floor mass was lumped into a single point mass having three degrees of freedom (two lateral and one torsional) in the horizontal plane. The weight distribution, including the tributary weight from beams and columns, was estimated to be 37.8 kN (8.5 kip) at the base, 13.7 kN (3.08 kip) at the first and second floors, 13.8 kN (3.11 kip) at the third and fourth floors, and 13.6 kN (3.05 kip) at the top floor, for a total weight of the model of 106.5 kN (24 kip). The dynamic characteristics required as input to 3D-BASIS-ME for the superstructure modeling were obtained from identification tests of the non-isolated frame (Table 4-5). A total of three modes were used, with assumed damping ratios of 0.06 in the first mode and 0.02 in the other two modes.

The isolation system was modeled with spatial distribution and explicit nonlinear force-displacement characteristics of the individual isolation devices. To accommodate the mechanical behavior of the XY-FP isolator, a new hysteretic element was incorporated into the program. Acknowledging that the bi-directional motion admits decoupling along the principal axes of the bearing, the new element is developed as two independent uniaxial hysteretic elements in the orthogonal directions. The element accounts for the conditions of separation and reattachment (stick-slip) along the sliding interface. It should

be emphasized that, contrary to the element representing the conventional FP isolator, the new element is capable of developing tension. Moreover, different frictional interface properties can be assumed along the principal isolator directions under compressive and tensile isolator normal force. A detailed description of the analytical model of the new isolator incorporated in 3D-BASIS-ME is given in Section 6.3.1.

In modeling the isolation system in 3D-BASIS-ME, the frictional properties along the principal isolator directions under compressive and tensile isolator normal force were assumed to be identical. Owing to successive lubrication of the bearing sliding interface, and by virtue of the superficial application of the lubricant, the coefficient of friction varied during the earthquake simulator testing program. Accordingly, the isolators were modeled using values of coefficient of friction parameter  $f_{\max}$  in the range of 0.06 to 0.10, based on the experimental results. In addition, the isolators were assigned the following properties: radius of curvature  $R = 990.6$  mm (39 in.),  $a = 0.031$  s/mm (0.8 s/in),  $f_{\min} = 0.03$ , and a gravity load of 26.62 kN (5.98 kip). Moreover, a value for the yield displacement equal to 0.28 mm (0.011 in.) was assumed based on the mechanical properties of the sliding interface (Constantinou et al., 1990).

The analysis accounted for (i) the variability of axial load in the isolators due to the vertical component of ground motion and the overturning moment effects; (ii) the dependency of friction on velocity; (iii) different orientations of the isolator with respect to the excitation (global-X) direction; and (iv) the initial non-zero displacement of the isolators (the permanent displacement from the previous test).

### **7.3 Comparison of Experimental and Analytical Results**

The validity of 3D-BASIS model, especially with reference to the newly introduced element representing the XY-FP isolator, was investigated by comparison of analytical predictions with experimental results. Appendix C presents comparisons of experimental and analytical results produced by program 3D-BASIS-ME. A representative sample of results from Appendix C is presented in Figures 7-1 through 7-5.

These figures depict results for horizontal and vertical input ground motions and for bearing orientation of 0, 90, and 45 degrees with respect to the horizontal excitation

direction. The comparison is made in terms of histories of the isolation system displacement, the 1st-story shear force, the bearing axial force, and the shear force-displacement loops of the isolation system.

The comparison made in terms of the axial force histories associated with the isolators is instrumental in validating the analytical techniques under extreme dynamic conditions. The fluctuations in the fast-varying axial forces were predicted sufficiently accurately in the analysis on account of capturing the effects of overturning and the vertical component of ground motion. The experimental results shown in Figures 7-1 through 7-5, indicative of the phenomenon of uplift restraint, provide an effective means of verifying the accuracy of analytical predictions under highly nonlinear conditions.

Figures 7-2 to 7-5 compare experimental and analytical results for combined horizontal and vertical components of Newhall 100% and Sylmar 100% excitations for bearing orientations of  $0^\circ$ ,  $90^\circ$ , and  $45^\circ$ . The analysis, by accounting for the vertical motion effects, captures correctly the wavy form of the isolation system shear force-displacement loops.

Evidently, there is good agreement between analytical and experimental results, with the analytical prediction not restricted to only peak response values but capable of reproducing almost every detail of the observed response history. Accordingly, the presented experimental results attest to the accuracy of the analytical model of the new isolator incorporated in 3D-BASIS-ME. This demonstrates that the behavior of XY-FP isolator is well understood to allow for accurate prediction of the response of isolated structures incorporating the new isolation bearing.

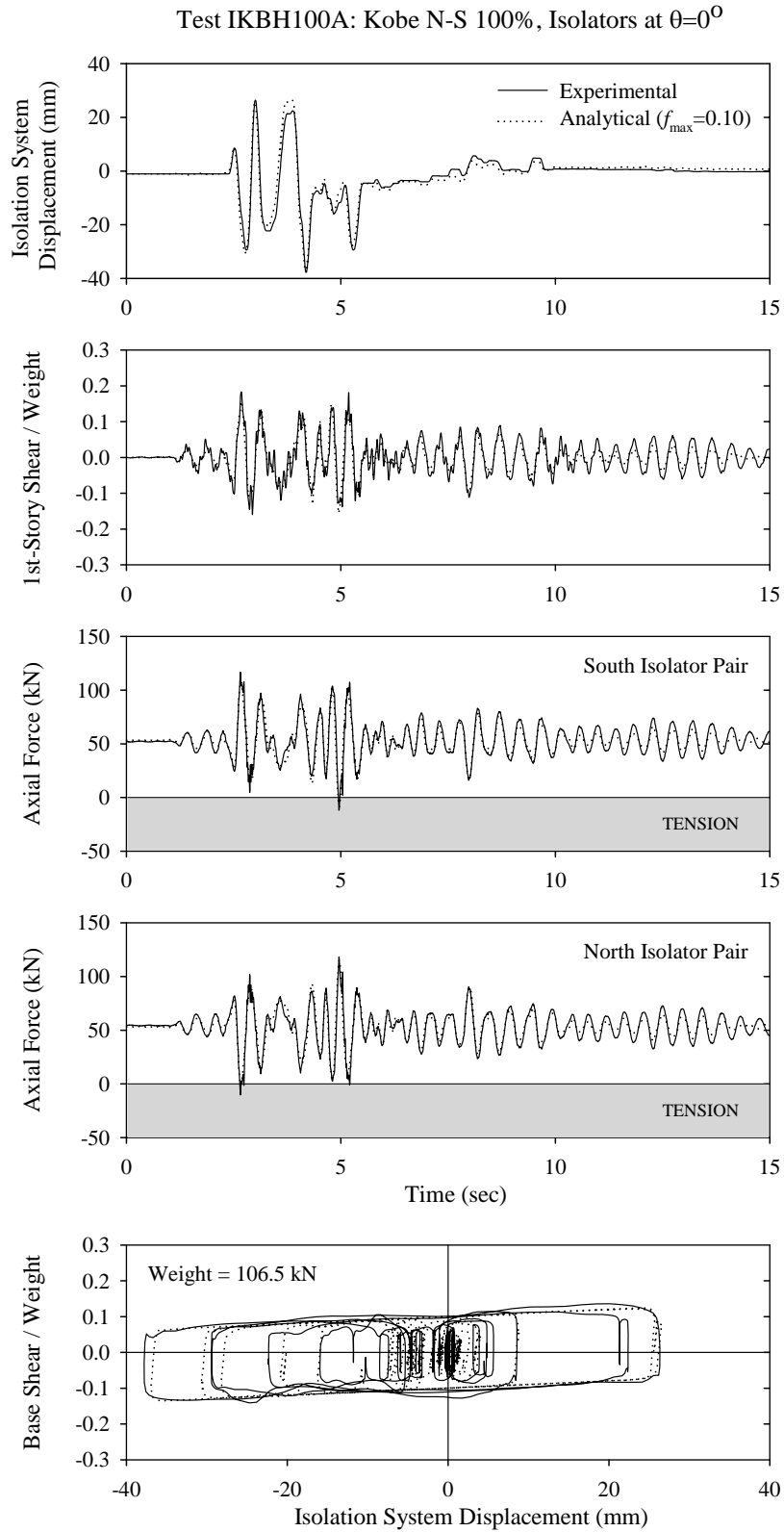


Figure 7-1: Comparison of experimental and analytical results for bearing orientation of  $0^\circ$  for 100% Kobe N-S excitation.

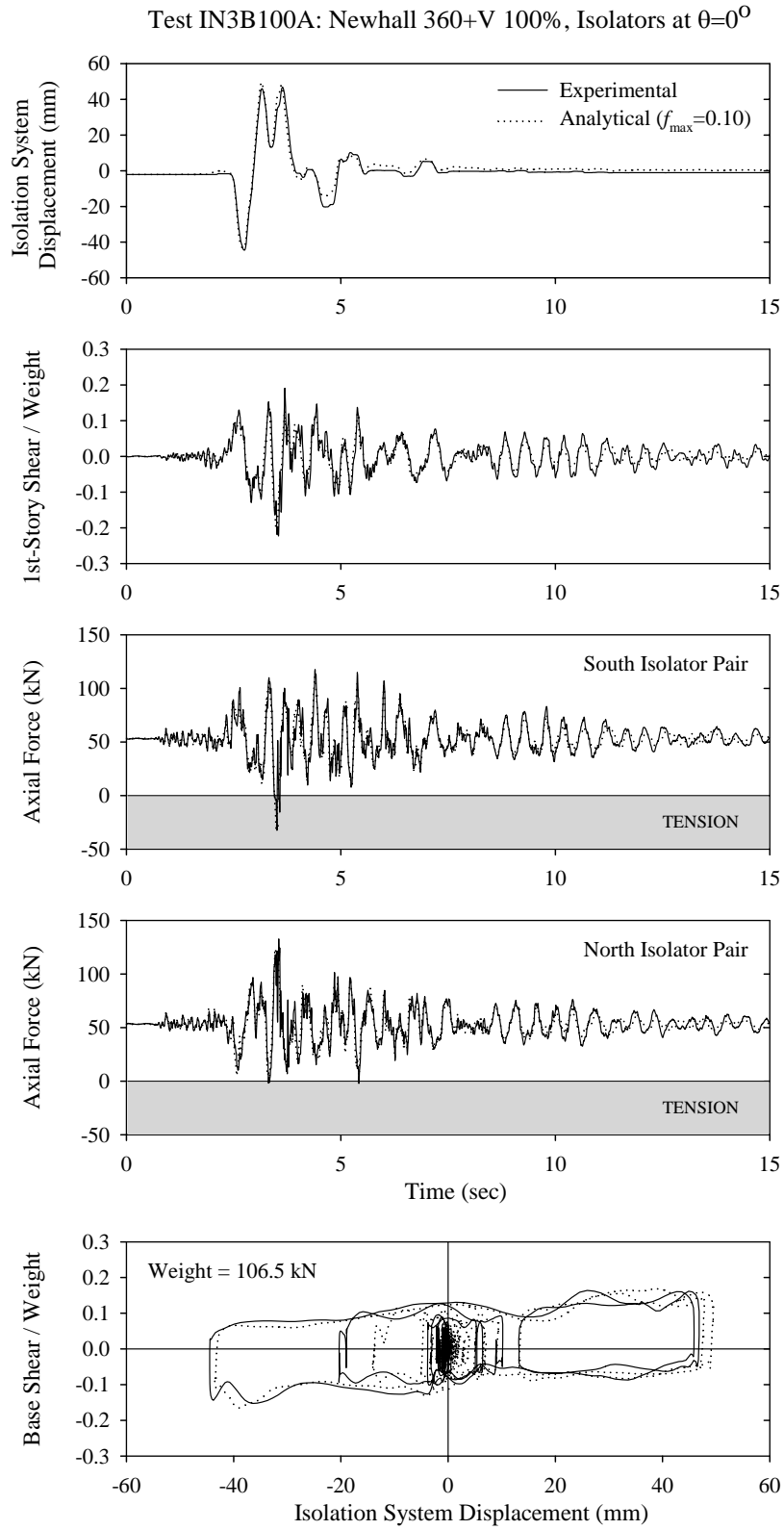


Figure 7-2: Comparison of experimental and analytical results for bearing orientation of  $0^\circ$  for 100% Newhall 360+vertical excitation.

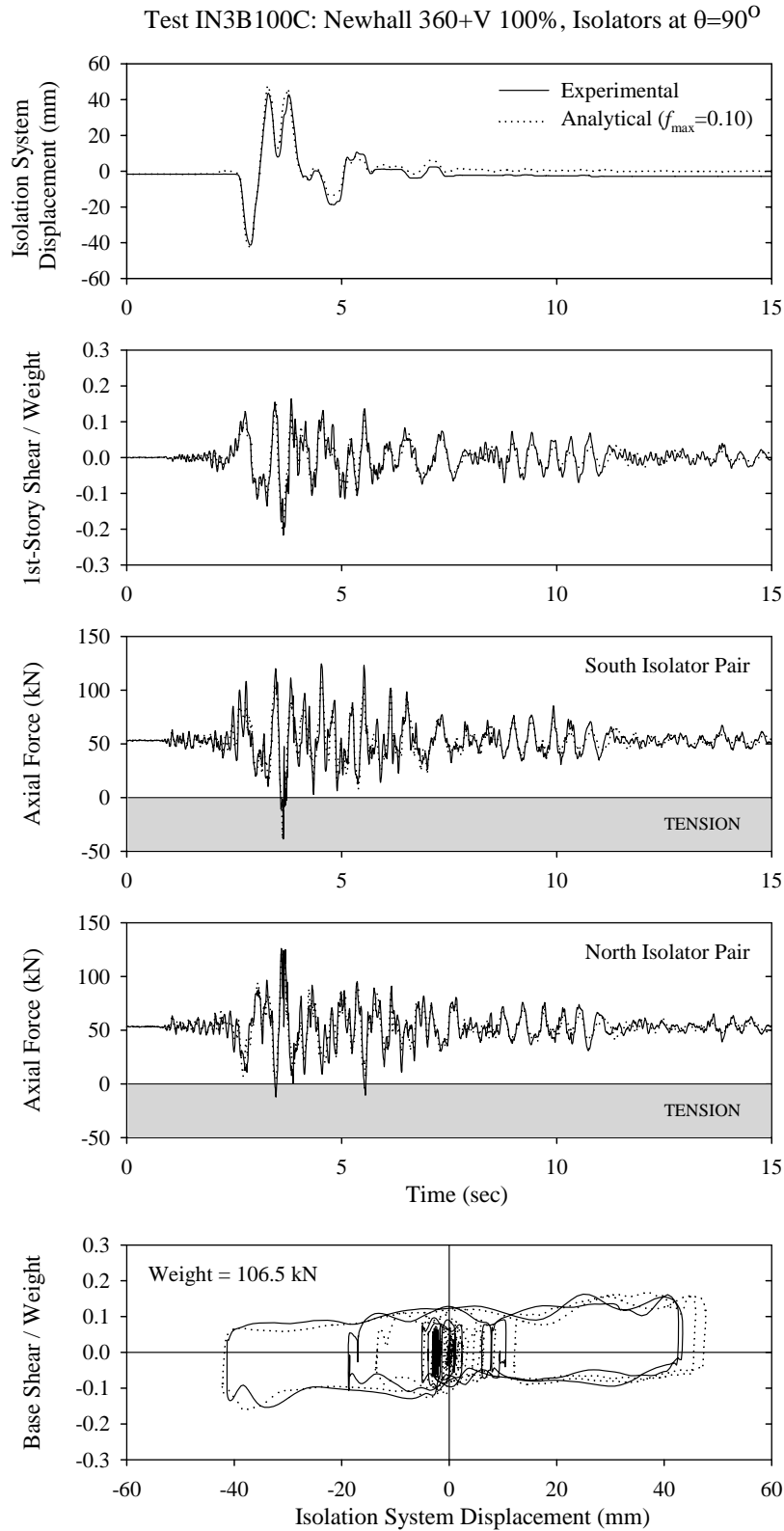


Figure 7-3: Comparison of experimental and analytical results for bearing orientation of  $90^\circ$  for 100% Newhall 360+vertical excitation.

Test ISYB100G: Sylmar 90+V 100%, Isolators at  $\theta=45^\circ$

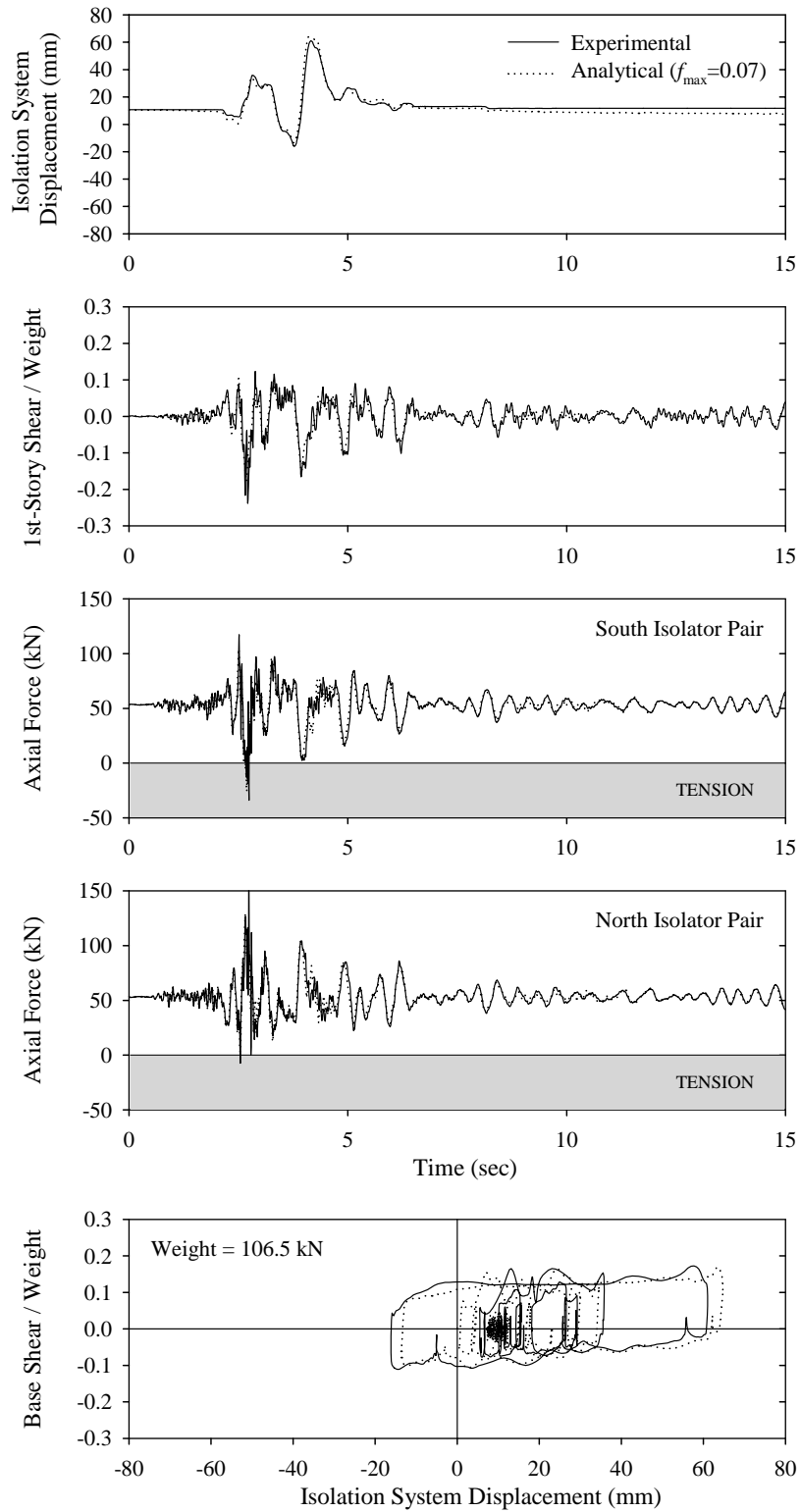


Figure 7-4: Comparison of experimental and analytical results for bearing orientation of  $45^\circ$  for 100% Sylmar 90+vertical excitation.

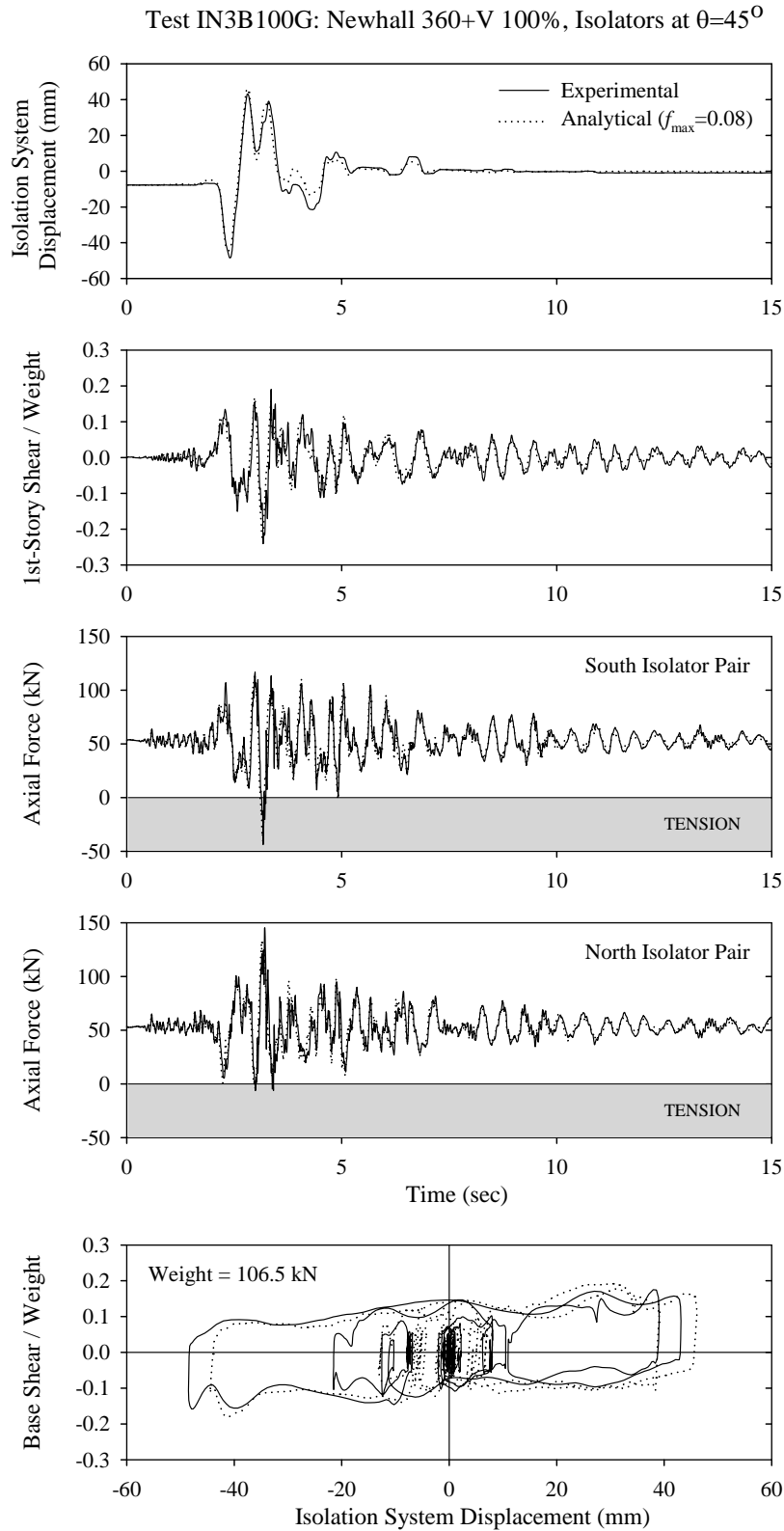


Figure 7-5: Comparison of experimental and analytical results for bearing orientation of  $45^\circ$  for 100% Newhall 360+vertical excitation.

## SECTION 8

### A CASE STUDY

#### 8.1 Introduction

Section 8 presents a case study which involves analysis of a seismically isolated structure and assessment of the impact of XY-FP bearing on its response. The structure utilized in the analysis is the new Acropolis Museum in Athens, Greece, currently under construction, directly at the foot of the Acropolis facing the Parthenon.

In this section, nonlinear response-history analysis of the seismically isolated structure subjected to bi-directional horizontal seismic excitation was performed using programs SAP2000 and 3D-BASIS-ME. First, a comparison is made between results from SAP2000 and 3DBASIS-ME analysis based on an isolation system model consisting solely of Friction Pendulum (FP) isolators. Then, results from 3D-BASIS-ME analysis of the model with only FP isolators are compared to results from analysis of the model with isolators prone to uplift being replaced with XY-FP isolators. The input motions used in the analysis were arbitrarily scaled so that they cause significant uplift in the FP isolators or significant tension in the XY-FP isolators, in order to ascertain the impact of use of the XY-FP isolators in a real structure.

#### 8.2 Description of Seismically Isolated Structure

The new museum of the Acropolis was designed as a four-story building above ground with up to four underground levels, of which one is for parking and one is for mechanical equipment (Figure 8-1). In plan the building is quadrilateral with sides measuring about 60 m, 75 m, 40 m, and 100 m (Figure 8-2). The structural system is reinforced concrete frame mixed with shear walls. The distribution of gravity-carrying elements of the structure is highly asymmetric due to the existence of archaeological findings that cannot be moved or disturbed. The total seismic weight of the superstructure is  $W_{tot} = 407$  MN.

Figure 8-2 presents a plan view of the isolated structure with the basic dimensions and bearing locations shown. The most heavily and the least loaded bearings (gravity load

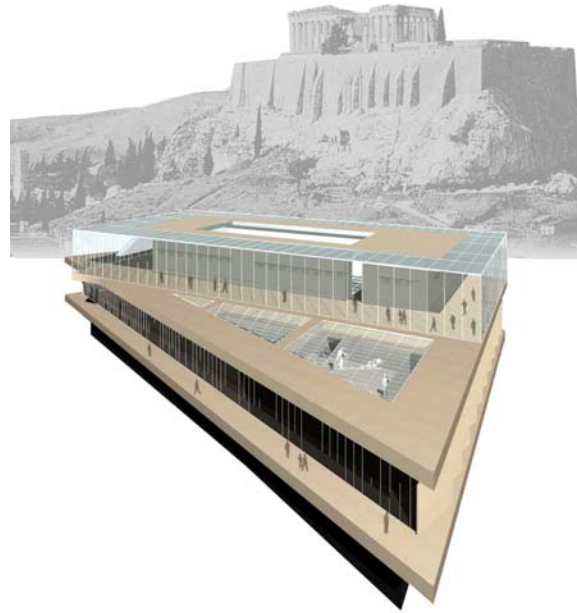


Figure 8-1: View of the new Acropolis Museum in Athens, Greece directly at the foot of the Acropolis. ([http://www.archpedia.com/Projects-Bernard-Tschumi\\_01.html](http://www.archpedia.com/Projects-Bernard-Tschumi_01.html))

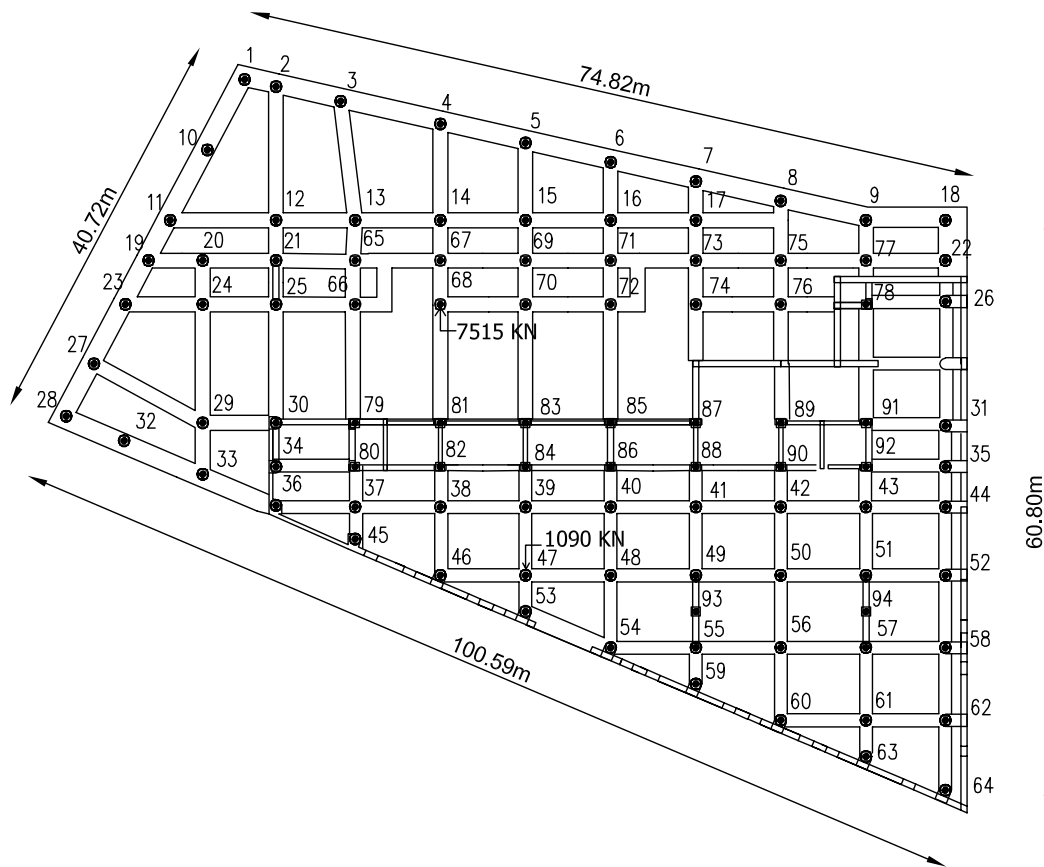


Figure 8-2: Plan view of isolated structure.

consisting of dead load plus half of live load) are identified and the values of the load are shown on the plan. It may be noted that there is a substantial range of gravity loads on the bearings.

The structure will be seismically isolated using 94 conventional FP bearings. The isolators were designed to have a displacement capacity of 250 mm, with radius of curvature  $R = 2235$  mm, and nominal value of the coefficient of friction under dynamic conditions equal to 0.04. Upper and lower bound values of the coefficient of friction when considering uncertainty in properties, aging, temperature, and contamination effects were determined to be 0.055 and 0.035, respectively.

### 8.3 Analytical Model in SAP2000 and 3D-BASIS-ME

The seismically isolated structure with conventional FP isolators was analyzed in programs SAP2000 and 3DBASIS-ME. Furthermore, exploiting the newly developed capability of 3DBASIS-ME to model the behavior of the uplift-restraint XY-FP isolator (Section 6.3.1), analyses were performed on the seismically isolated structure with isolators prone to uplift being replaced with XY-FP isolators.

Nonlinear response-history analysis, based on the Fast Nonlinear Analysis (FNA) method, was performed in SAP2000 (Computers and Structures, 1998), utilizing a three-dimensional model (Figure 8-3). The model mass, represented as lumped masses at joints, was distributed at six levels along the height of the model. The properties of the structure are given in Table 8-1.

Figure 8-4 illustrates the spatial distribution of the 94 seismic isolation bearings. The FP bearings were modeled in SAP2000 using the *NLLINK* element *Isolator2* property. Each of these elements was assigned the following properties: radius of sliding surface  $R = 2.235$  m; friction coefficient (fast)  $f_{\max} = 0.055$ ; friction coefficient (slow)  $f_{\min} = 0.03$ ; rate  $\alpha = 50$  s/m; and an initial stiffness  $k = 67007$  kN/m. A damping ratio of 0.04 was specified for the 18 modes used in the analysis.

The gravity load on the bearings is typically generated in SAP2000 from loads applied to the superstructure. In this case the gravity load was specified as span force load along the

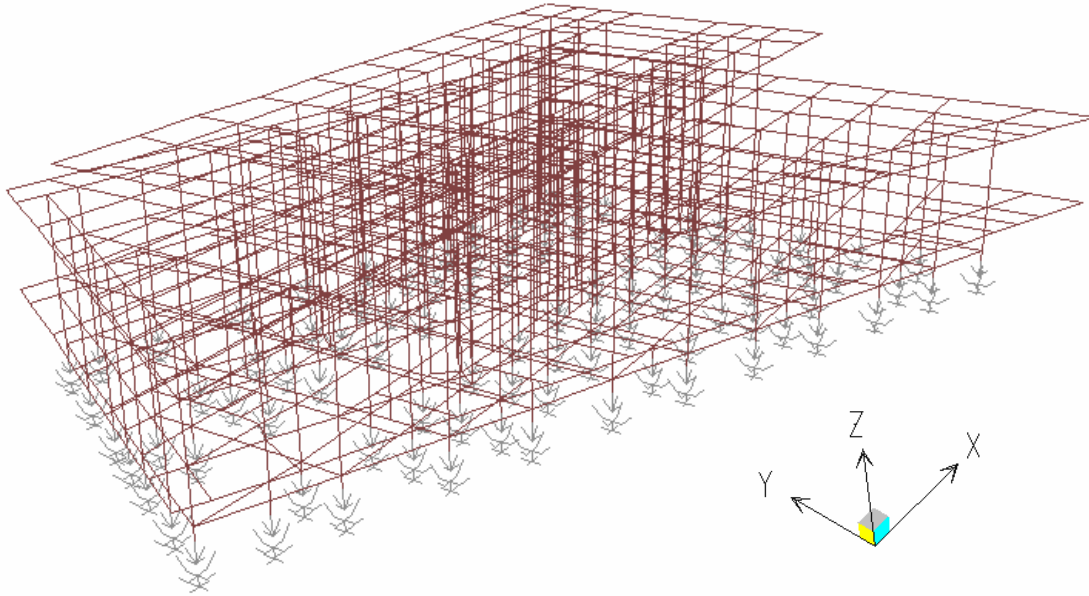


Figure 8-3: Schematic of SAP2000 model of the seismically isolated building used in the case study.

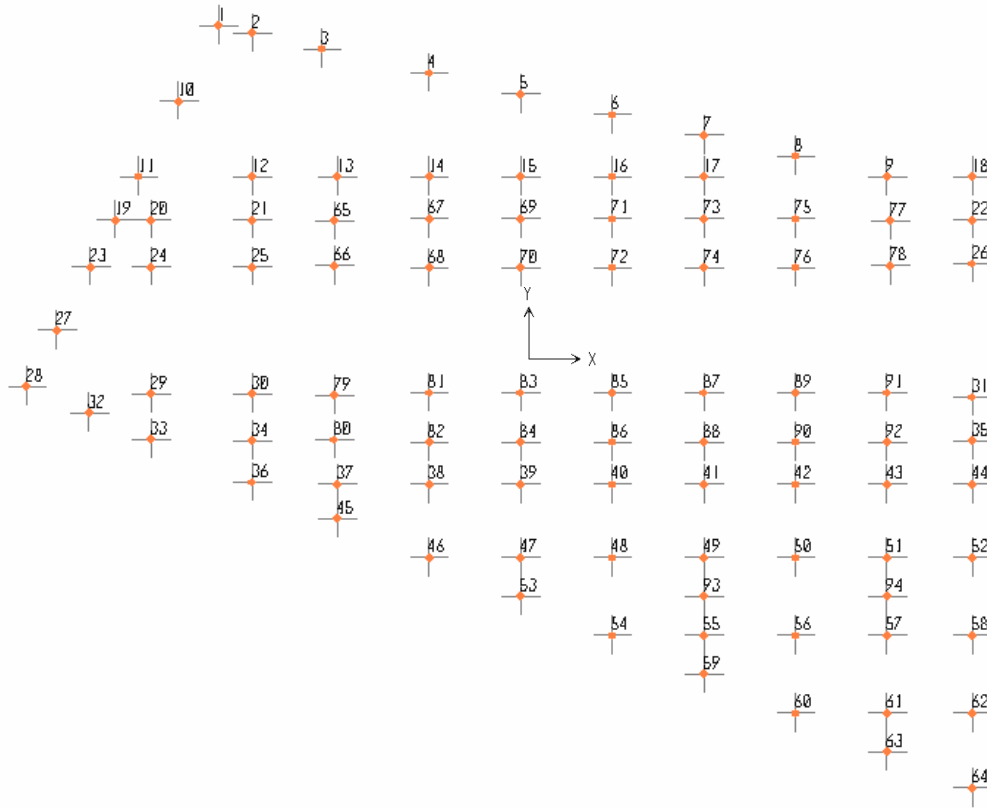


Figure 8-4: Plan view of the base of the building model in SAP2000 showing the spatial distribution of seismic isolation bearings.

Table 8-1: Properties of analyzed structure.

Level	Height (m)	Mass			Eccentricities	
		$M_x$ (kN-s <sup>2</sup> /m)	$M_y$ (kN-s <sup>2</sup> /m)	$I_z$ (kN-s <sup>2</sup> /m)	X (m)	Y (m)
6	21.4	3512	3512	3125987	2.3	2.4
5	19.4	2208	2208	1063811	2.6	2.8
4	15.3	11049	11049	10627050	2.1	-1.2
3	10.5	6207	6207	4201263	-8.4	6.9
2	5.2	9504	9504	9501796	0.7	-1.7
1 (Base)	0.0	9054	9054	8039340	0.0	0.0

frame members. These forces were applied quasistatically, that is, dynamically over a long time duration, utilizing a ramp function with a duration of 10 sec (5 sec build-up time and 5 sec constant unit load) and a large modal damping ratio (= 0.99) to prevent oscillations.

The dynamic response of the isolated structure was also predicted analytically using program 3D-BASIS-ME. The superstructure model in 3D-BASIS utilized a three-dimensional representation. Each floor mass was lumped into a single point mass having three degrees of freedom (two lateral and one torsional) in the horizontal plane. The assumed mass distribution is given in Table 8-1. The dynamic characteristics required as input to 3D-BASIS-ME for the superstructure modeling were obtained using program SAP2000. A total of 15 modes were used with assumed damping ratio of 0.04. The periods of free vibration for the first five modes are presented in Table 8-2.

Table 8-2: Periods of free vibration of the fixed-base structure.

Mode	Period (sec)
1	0.401
2	0.295
3	0.208
4	0.123
5	0.080

The isolation system with the spatial distribution shown in Figure 8-4 was explicitly modeled with nonlinear force-displacement characteristics of the individual isolation devices. In modeling the FP bearings in 3D-BASIS-ME, the following parameters were used:  $R = 2.235$  m,  $f_{\max} = 0.055$ ,  $f_{\min} = 0.03$ ,  $\alpha = 50$  s/m, and  $Y = 0.004$  m. The assumed yield displacement is consistent with the isolator model in SAP2000 upon accounting for the flexibility of the (short) columns above the isolators. Further, the gravity load on each isolator was obtained from static analysis in SAP2000. The aforementioned parameters were also assigned to the XY-FP isolators with the frictional properties along the principal isolator directions under compressive and tensile isolator normal force assumed to be identical. The dependency of friction coefficient on instantaneous pressure was neglected in the analysis.

The analysis in program 3D-BASIS-ME accounted for the variability of axial load in isolators due to overturning moment effects via a user-supplied subroutine that was modified to include a direct relationship between floor inertia forces and additional axial load on bearings (Section 6.3.3). The required coefficient matrix,  $[T]$ , was evaluated externally by program SAP2000 from linear static analyses of the structure supported on hinge supports and subjected to horizontally acting unit loads at the different floor levels. The same coefficient matrix,  $[T]$ , was utilized in modeling the structure with both XY-FP isolators and conventional FP isolators. In the case of the uplift-restraint XY-FP isolators, where there is a continuous transition from compression to tension and vice versa, matrix  $[T]$  accurately predicts the additional axial load on the isolators due to overturning moment effects. On the contrary, the prediction of the isolator axial load based on matrix  $[T]$  is an approximation when uplift occurs on conventional FP isolators. In such a case, while the total axial load of the isolator in uplift is replaced by zero, no redistribution of forces is accounted for. The error involved is small (as seen in the presented results in Section 8.4), since the phenomenon of uplift occurs instantaneously and only a small portion of isolators undergo uplift at any instant of time. In fact, the analytical prediction in terms of isolator loads is conservative, as the calculated total axial loads are slightly larger than the actual ones. It should be noted that,

by virtue of the three-dimensional formulation, SAP2000 allows for direct consideration of overturning moment effects.

The structure was analyzed using three pairs of bi-directional seismic excitations. Each component was amplified by a factor so as to accentuate the overturning moment effects and increase the possibility of uplift occurrence. It should be noted that the scaled motions represented earthquakes significantly stronger than the maximum earthquake for the site of the Museum of the Acropolis. Table 8-3 lists the earthquake motions used in the analysis along with their peak ground motion characteristics and scale factors. A total of six seismic input combinations were considered by interchanging pair components in X and Y directions.

Table 8-3: Selected ground motions and scale factors used in analysis.

Ground Motion	Station	Component	PGA (g)	PGV (cm/s)	PGD (cm)	Scale Factor
1940 El Centro	117 (USGS)	180	0.34	33.45	10.87	2.0
		270	0.21	36.92	19.78	
1952 Kern County	1095 (USGS)	021	0.16	15.30	9.25	4.0
		111	0.18	17.50	8.99	
1934 Lower California	117 (USGS)	180	0.16	20.85	4.20	4.5
		270	0.18	11.56	3.66	

## 8.4 Analysis Results

Nonlinear response-history analysis of the seismically isolated structure subjected to bi-directional seismic excitations was performed using programs SAP2000 and 3D-BASIS-ME. First, a comparison is made between results from SAP2000 and 3DBASIS-ME analysis based on an isolation system model consisting solely of FP isolators. Moreover, results from 3DBASIS-ME analysis of the model with FP isolators only are compared to results from analysis of the model with isolators subject to uplift being replaced with XY-FP isolators.

Only the upper bound on the coefficient of sliding friction,  $f = 0.055$ , is considered in

the analysis, as it yields the maximum forces on the superstructure and hence the most unfavorable overturning moment effects.

Presented in Appendix D are results generated by programs SAP2000 and 3DBASIS-ME from analyses of the model with only FP isolators. A representative sample of these results is depicted in Figures 8-5 through 8-10 in terms of isolation system response, superstructure response, and individual bearing response in X and Y directions in Lower California 270-180 450% excitation. The generated results serve the purpose of demonstrating that programs SAP2000 and 3D-BASIS-ME produce comparable output.

The local frame action and the large overturning forces generated by the strong input excitations resulted in large variations in the vertical loads on the bearings. These variations were large enough (compared to the static dead load on the bearings) to reduce the bearing load to zero and cause local uplift in the bearings (Figures 8-9 and 8-10). Table 8-4 presents information on the isolators that undergo uplift (with reference to Figure 8-4) in the six seismic input combinations used in the analysis. Graphical representation of the number of isolators experienced uplift at each time instant is given in Figure 8-11. It can be observed that even under such extreme loading conditions only a small fraction (about 15%) of the isolators undergo uplift at each time instant.

In assessing the impact of the XY-FP bearing on the response of the seismically isolated structure, results from a 3DBASIS-ME analysis of the model with FP isolators only are compared to results from analysis of the model with isolators prone to uplift (per Table 8-4) being replaced with XY-FP isolators. Appendix E contains comparison of 3D-BASIS-ME analysis results of the two models in terms of superstructure response, isolation system response, and individual bearing response in X and Y directions for the selected ground motions listed in Table 8-3.

Figures 8-12 through 8-17 depict representative results from the range of analyses performed for the El Centro 180-270 200% excitation. In particular, Figures 8-12 and 8-13 provide information on the superstructure response in X and Y directions, respectively, in terms of histories of total floor acceleration, total floor velocity, and story drift for the floor/story at which the maximum response occurs, as well as histories of the normalized first-story shear force. Figures 8-14 and 8-15 present histories of the isolation

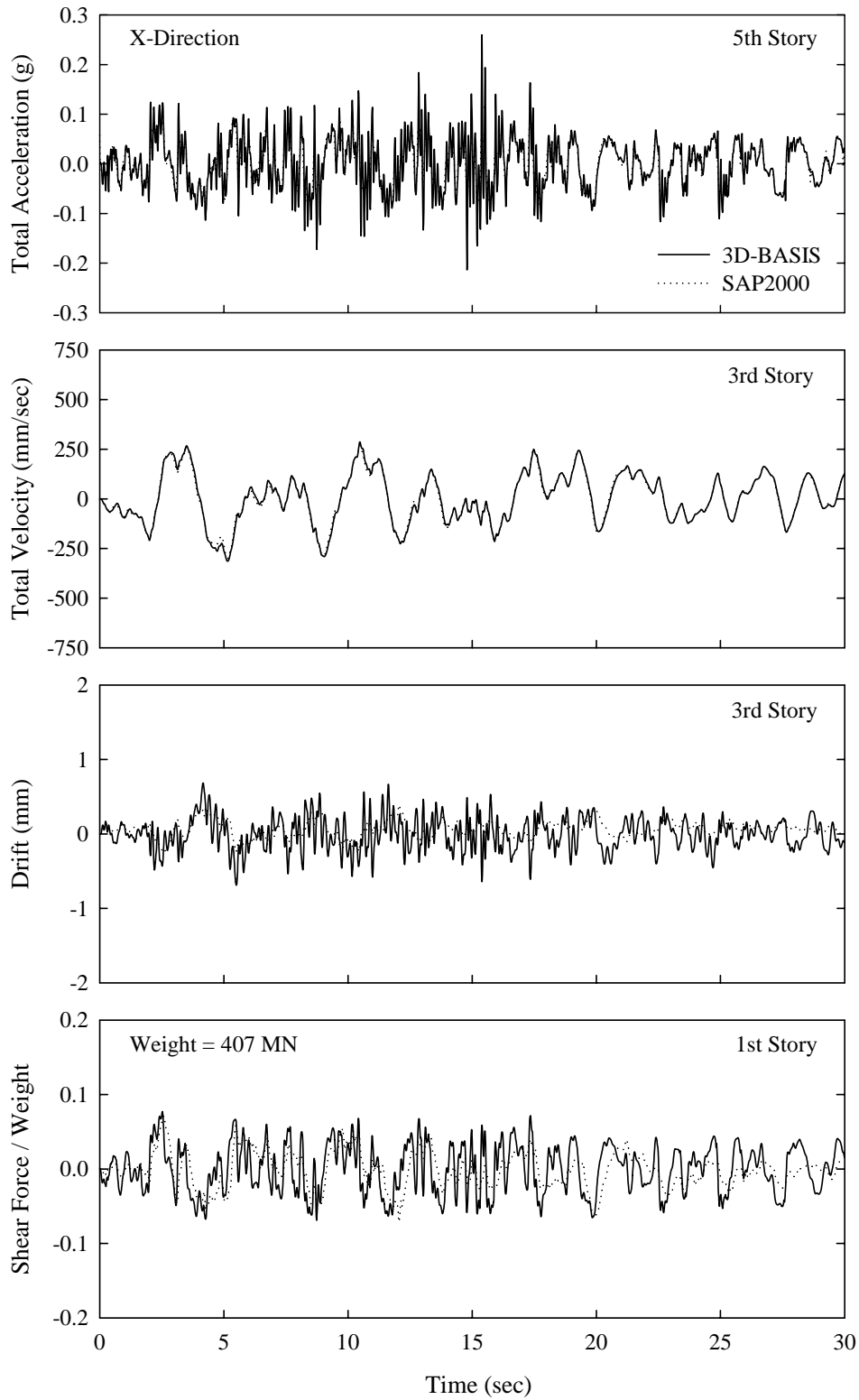


Figure 8-5: Comparison of SAP2000 and 3D-BASIS-ME generated results in terms of superstructure response in X direction for the model with 94 FP isolators in scaled (factor 4.5) Lower California 270-180 excitation.

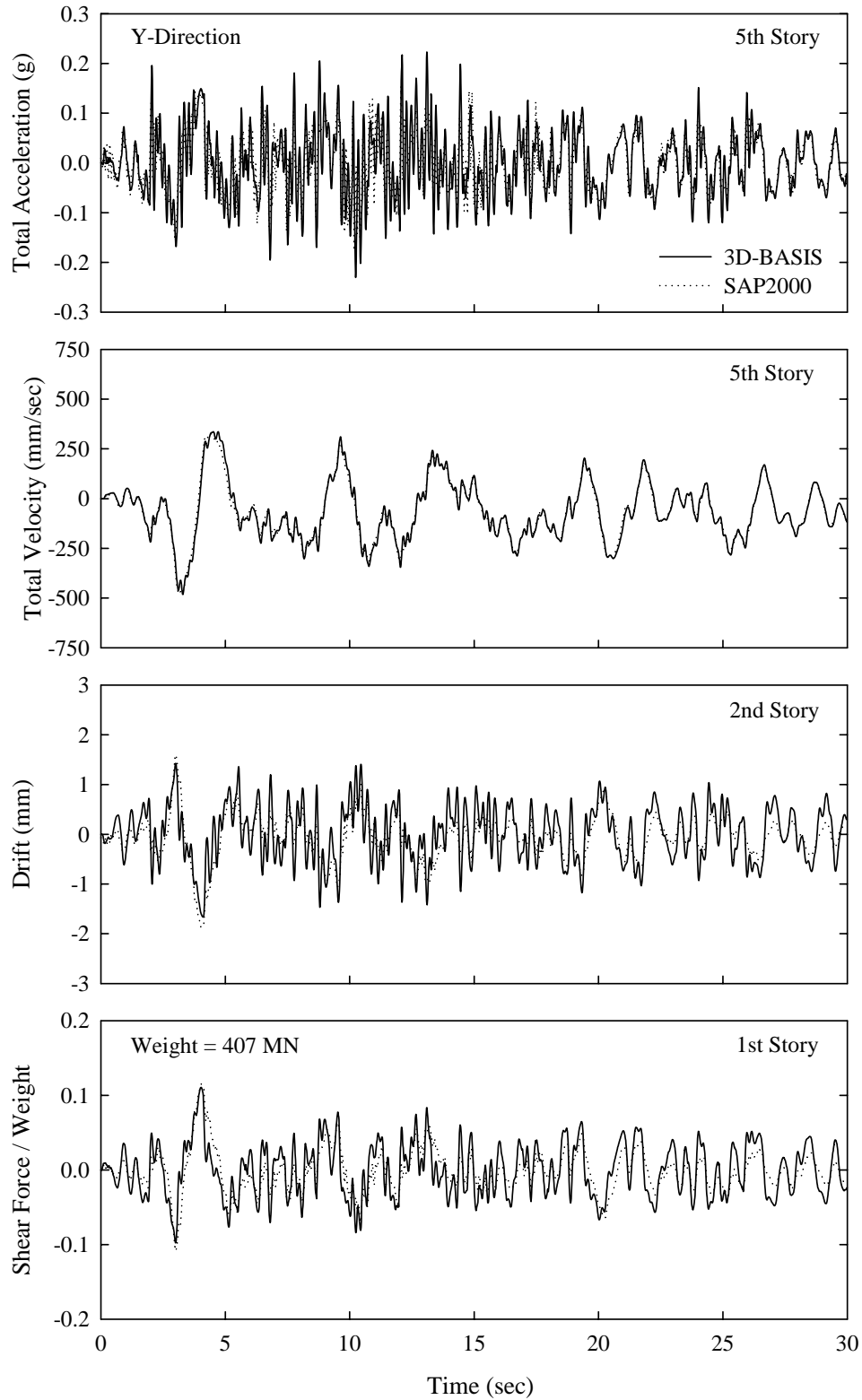


Figure 8-6: Comparison of SAP2000 and 3D-BASIS-ME generated results in terms of superstructure response in Y direction for the model with 94 FP isolators in scaled (factor 4.5) Lower California 270-180 excitation.

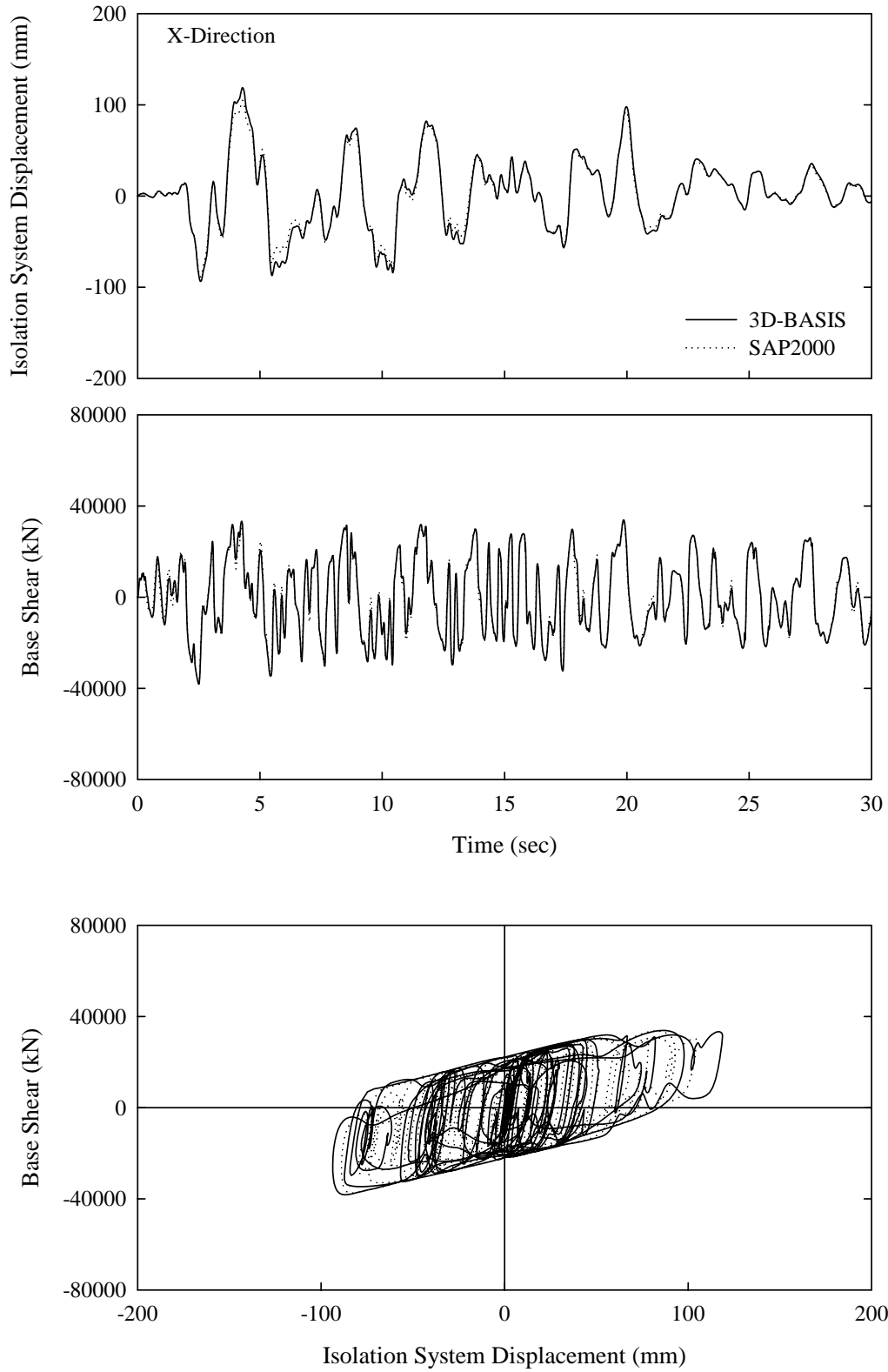


Figure 8-7: Comparison of SAP2000 and 3D-BASIS-ME generated results in terms of isolation system response in X direction for the model with 94 FP isolators in scaled (factor 4.5) Lower California 270-180 excitation.

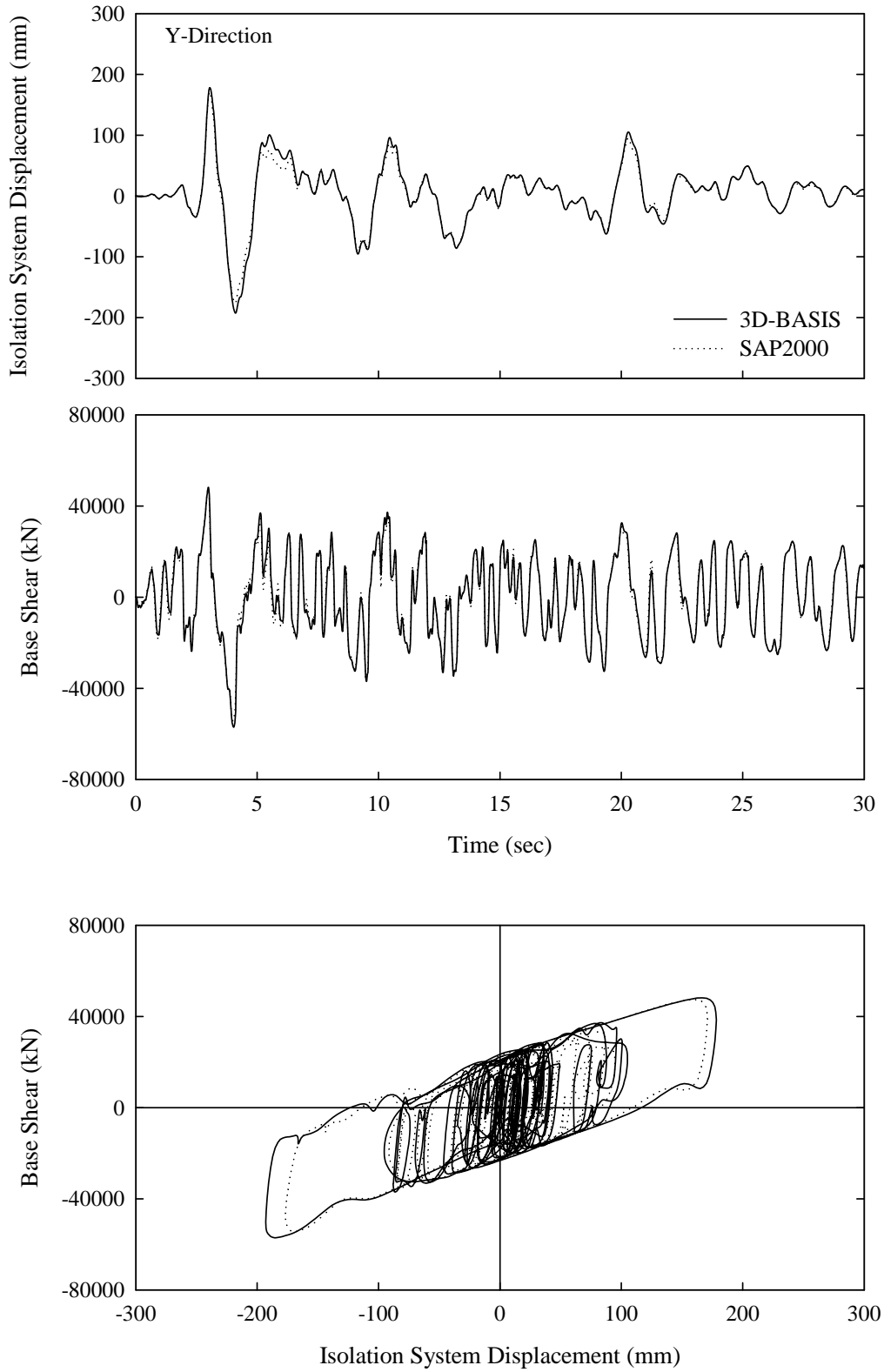


Figure 8-8: Comparison of SAP2000 and 3D-BASIS-ME generated results in terms of isolation system response in Y direction for the model with 94 FP isolators in scaled (factor 4.5) Lower California 270-180 excitation.

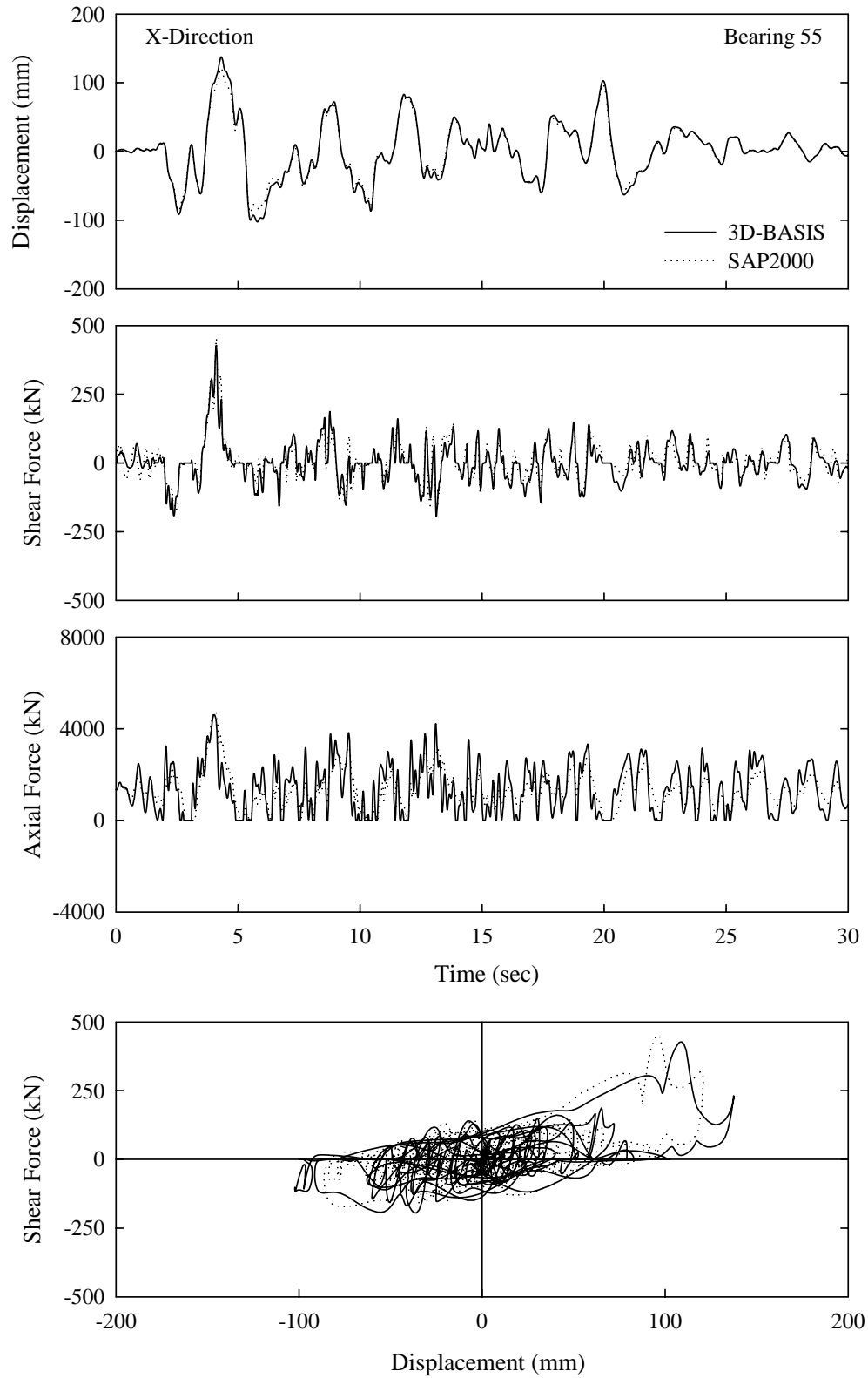


Figure 8-9: Comparison of SAP2000 and 3D-BASIS-ME generated results in terms of response of bearing No. 55 in X direction for the model with 94 FP isolators in scaled (factor 4.5) Lower California 270-180 excitation.

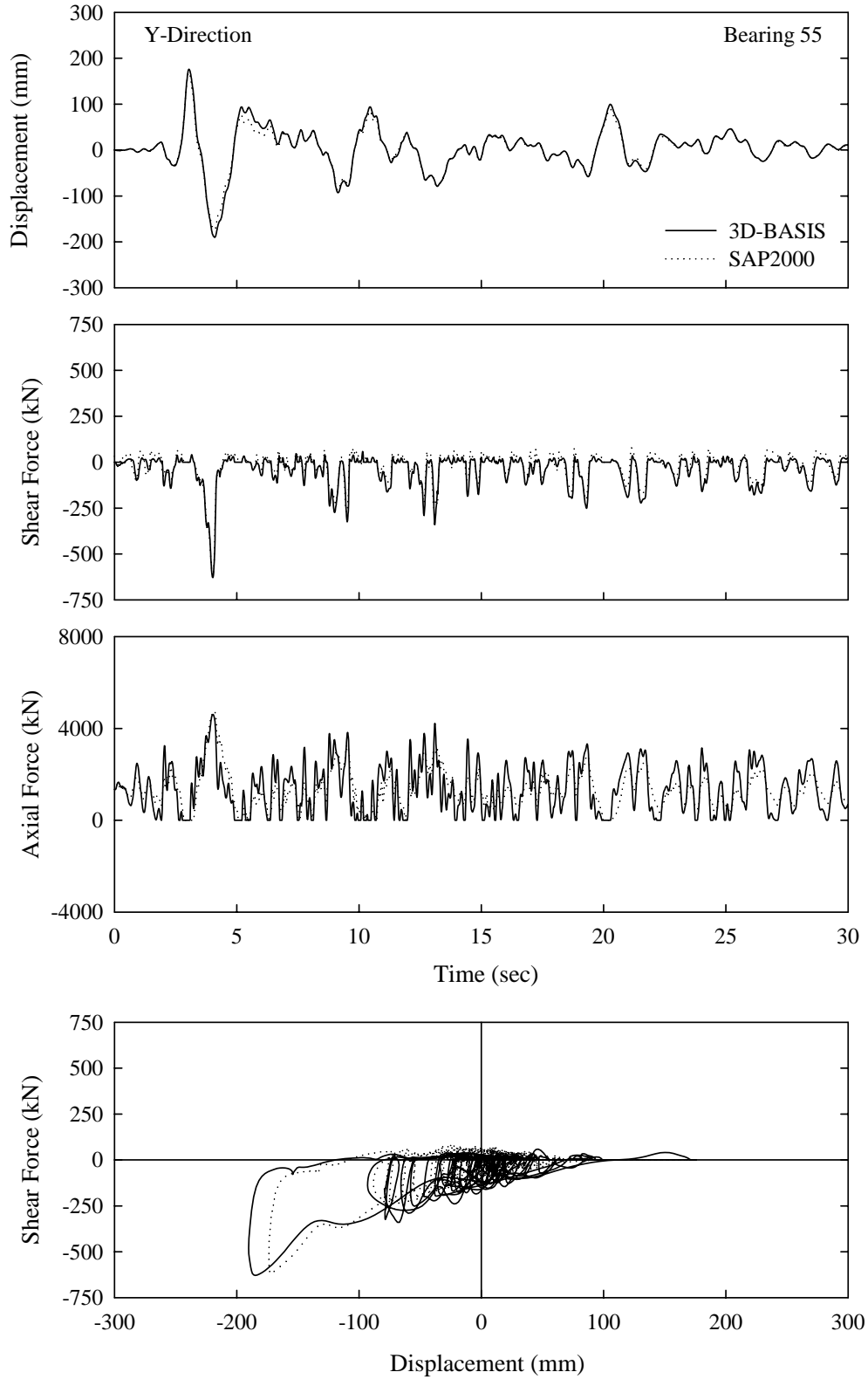


Figure 8-10: Comparison of SAP2000 and 3D-BASIS-ME generated results in terms of response of bearing No. 55 in Y direction for the model with 94 FP isolators in scaled (factor 4.5) Lower California 270-180 excitation.

Table 8-4: FP isolators undergoing uplift identified from 3D-BASIS-ME analysis.

Bearing ID	El Centro 200%		Kern County 400%		Lower CA 450%	
	180-270	270-180	021-111	111-021	180-270	270-180
21	√	√	√	√	-	√
30	√	√	√	√	-	√
34	-	√	-	-	-	-
49	√	√	√	√	√	√
51	√	√	√	√	-	-
55	√	√	√	√	√	√
57	√	√	√	√	-	√
65	√	√	√	√	√	√
66	-	-	√	-	-	√
67	√	√	√	√	√	√
68	√	√	-	-	-	-
69	√	√	√	√	√	√
70	√	√	-	-	-	-
71	√	√	√	√	√	√
73	√	√	√	√	-	-
75	√	-	-	-	-	-
77	√	-	√	-	-	-
79	√	√	√	√	√	√
80	-	-	√	-	-	√
81	√	√	√	√	-	-
82	√	√	√	√	-	√
83	√	√	√	√	-	√
84	√	√	√	√	√	√
85	√	-	√	-	-	-
86	√	√	√	√	√	√
87	√	-	-	-	-	-
88	√	√	-	-	-	√
92	√	√	-	-	-	-
<b>Total #</b>	25	22	21	17	9	17

system displacement, isolation system shear force, and the associated shear force-displacement loops in X and Y directions, respectively. Individual bearing results for a typical bearing that experienced considerable and successive uplift/tension (bearing No. 67) are shown in Figures 8-16 and 8-17 in terms of histories of bearing displacement, shear force, axial force, and shear force-displacement loops in X and Y directions,

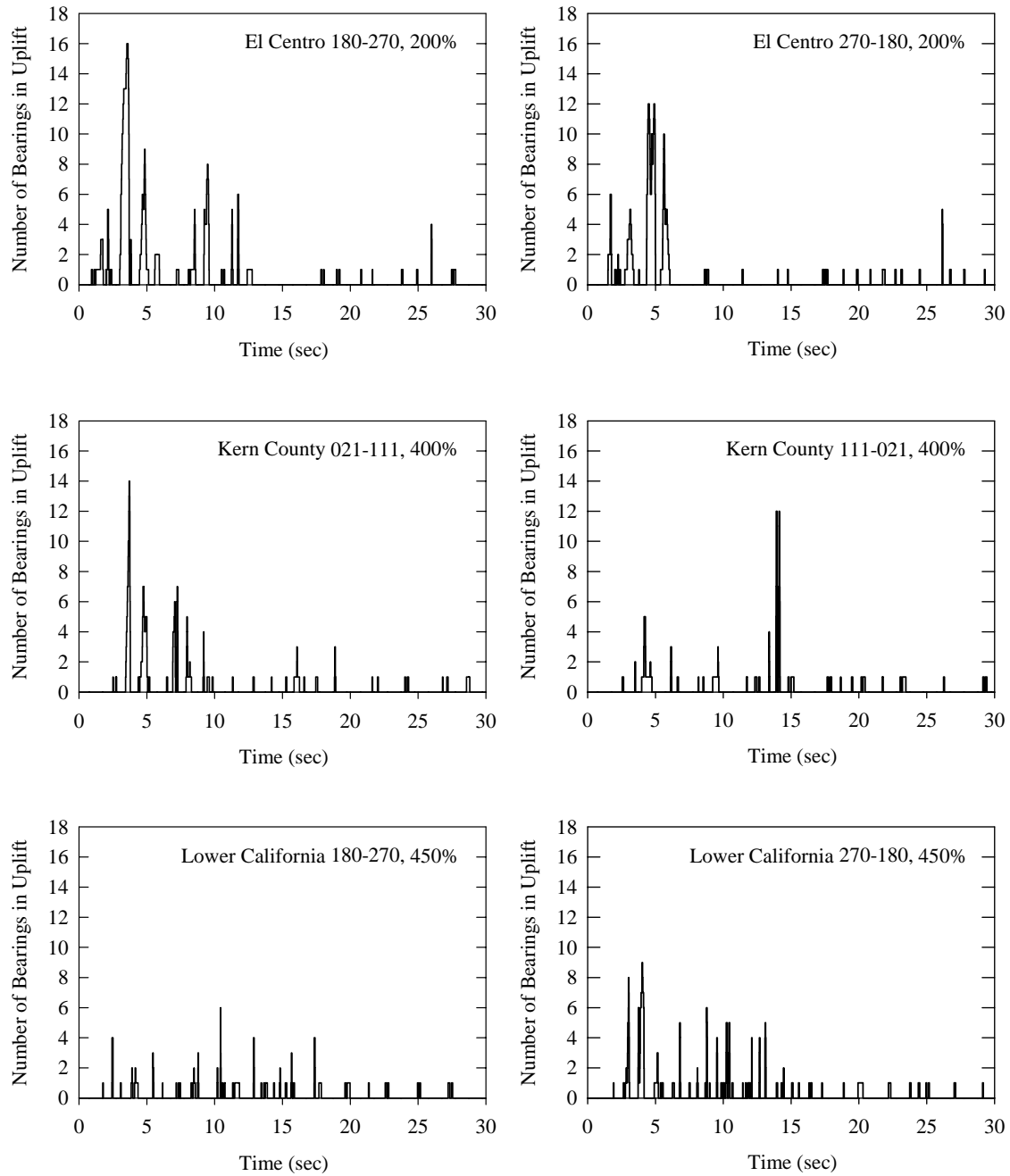


Figure 8-11: Number of bearings in uplift per time instant.

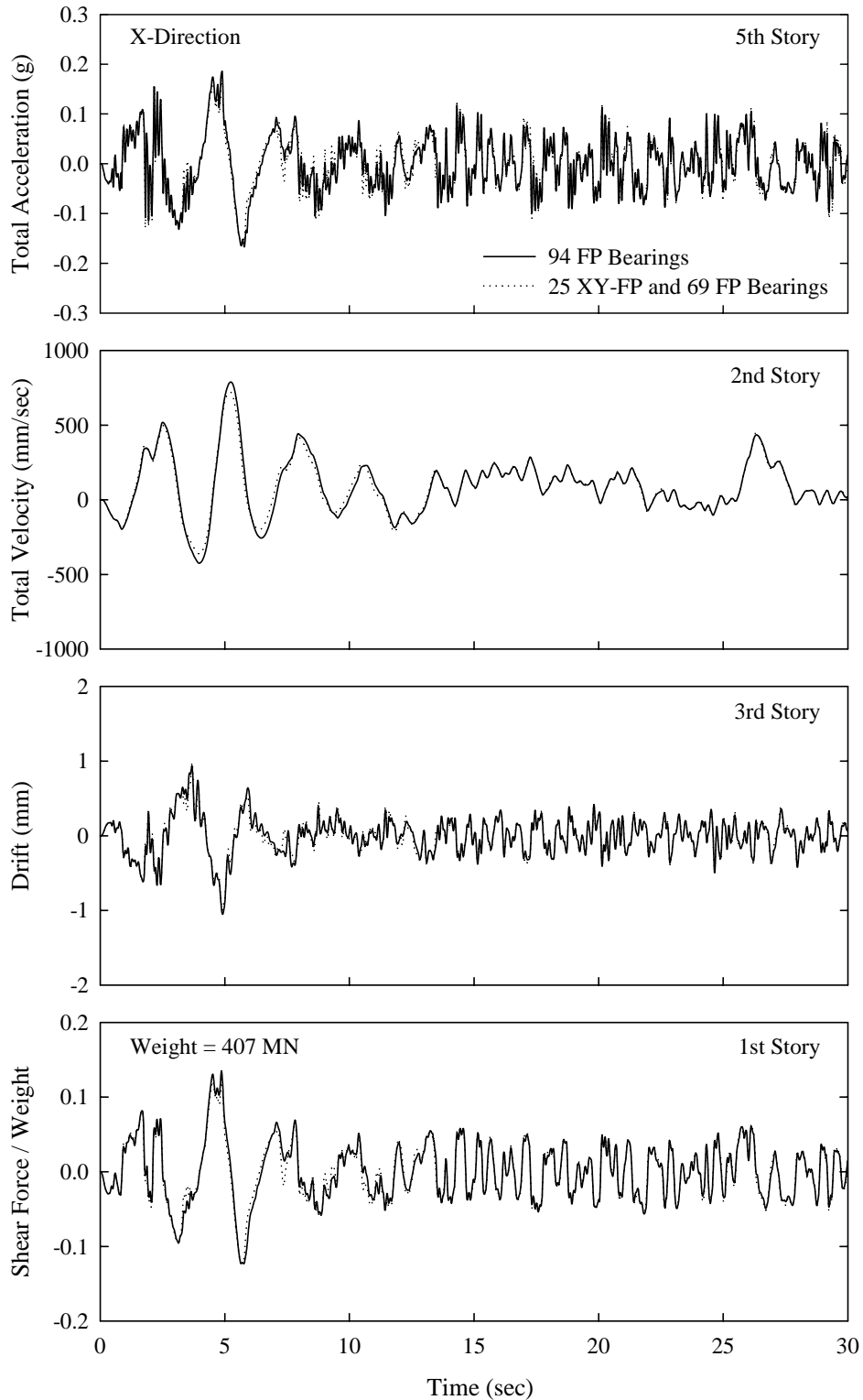


Figure 8-12: Comparison of 3D-BASIS-ME generated results in terms of superstructure response in X direction between the model with 94 FP isolators and the model with 25 XY-FP + 69 FP isolators in scaled (factor 2.0) El Centro 180-270 excitation.

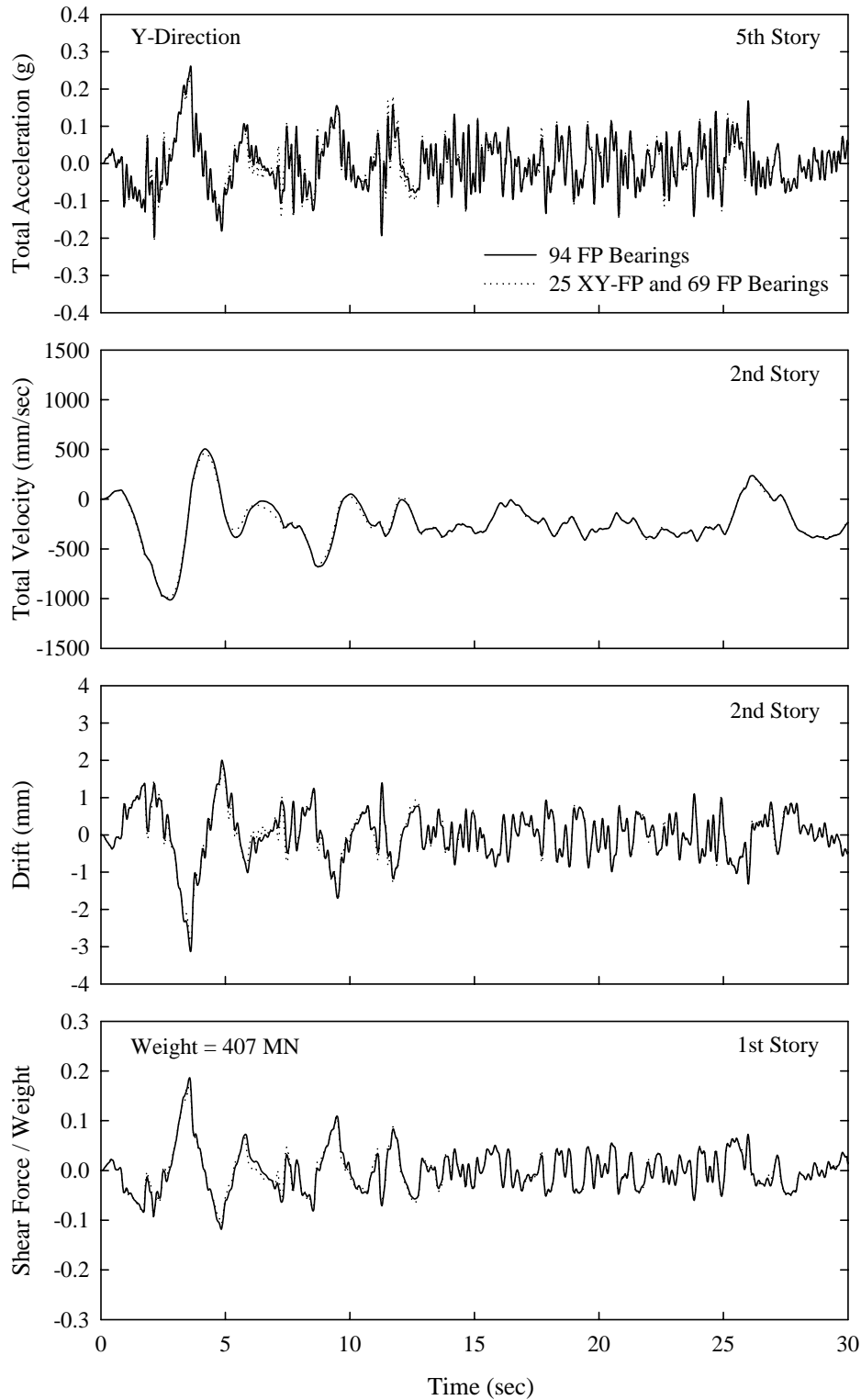


Figure 8-13: Comparison of 3D-BASIS-ME generated results in terms of superstructure response in Y direction between the model with 94 FP isolators and the model with 25 XY-FP + 69 FP isolators in scaled (factor 2.0) El Centro 180-270 excitation.

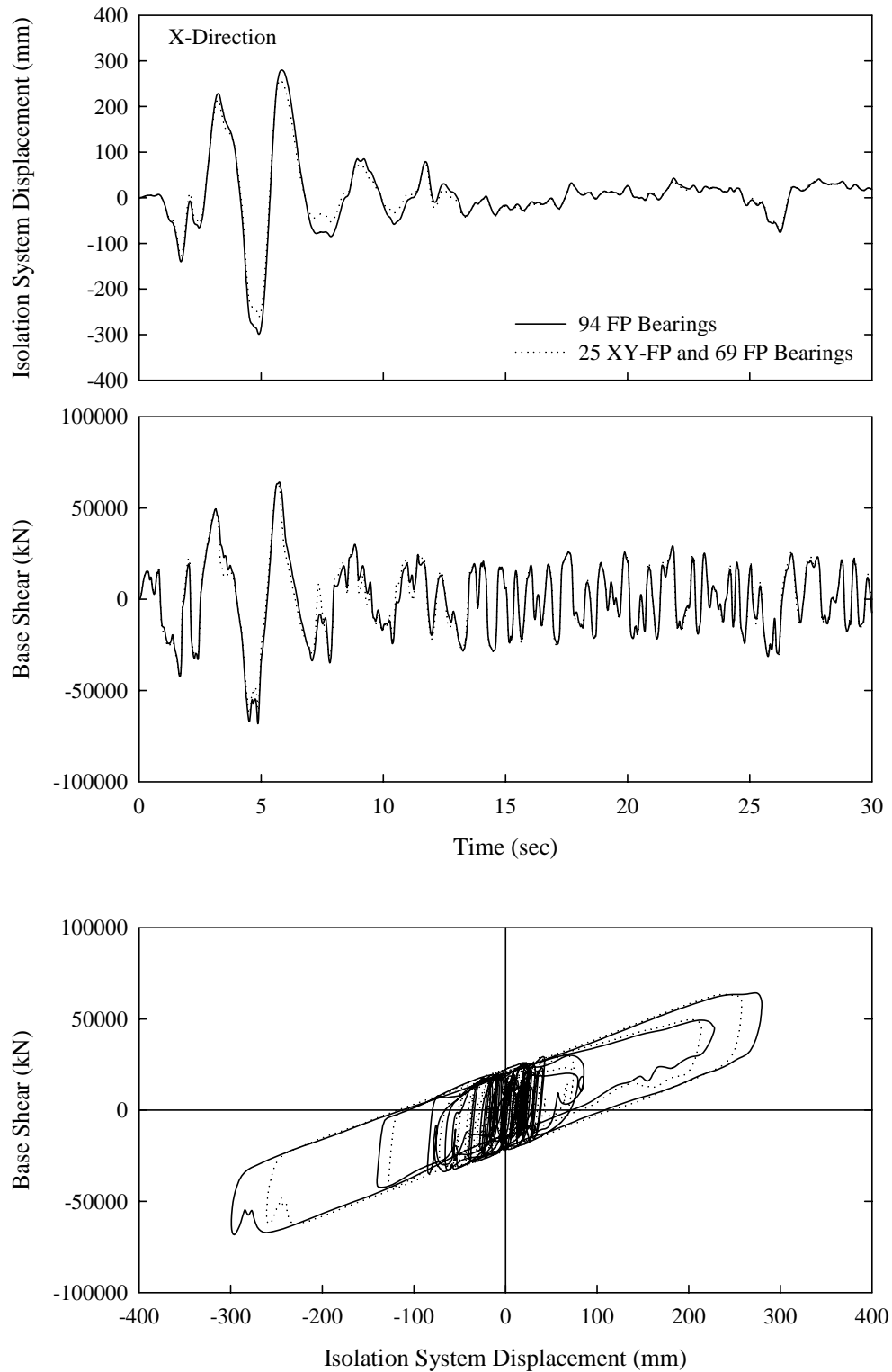


Figure 8-14: Comparison of 3D-BASIS-ME generated results in terms of isolation system response in X direction between the model with 94 FP isolators and the model with 25 XY-FP + 69 FP isolators in scaled (factor 2.0) El Centro 180-270 excitation.

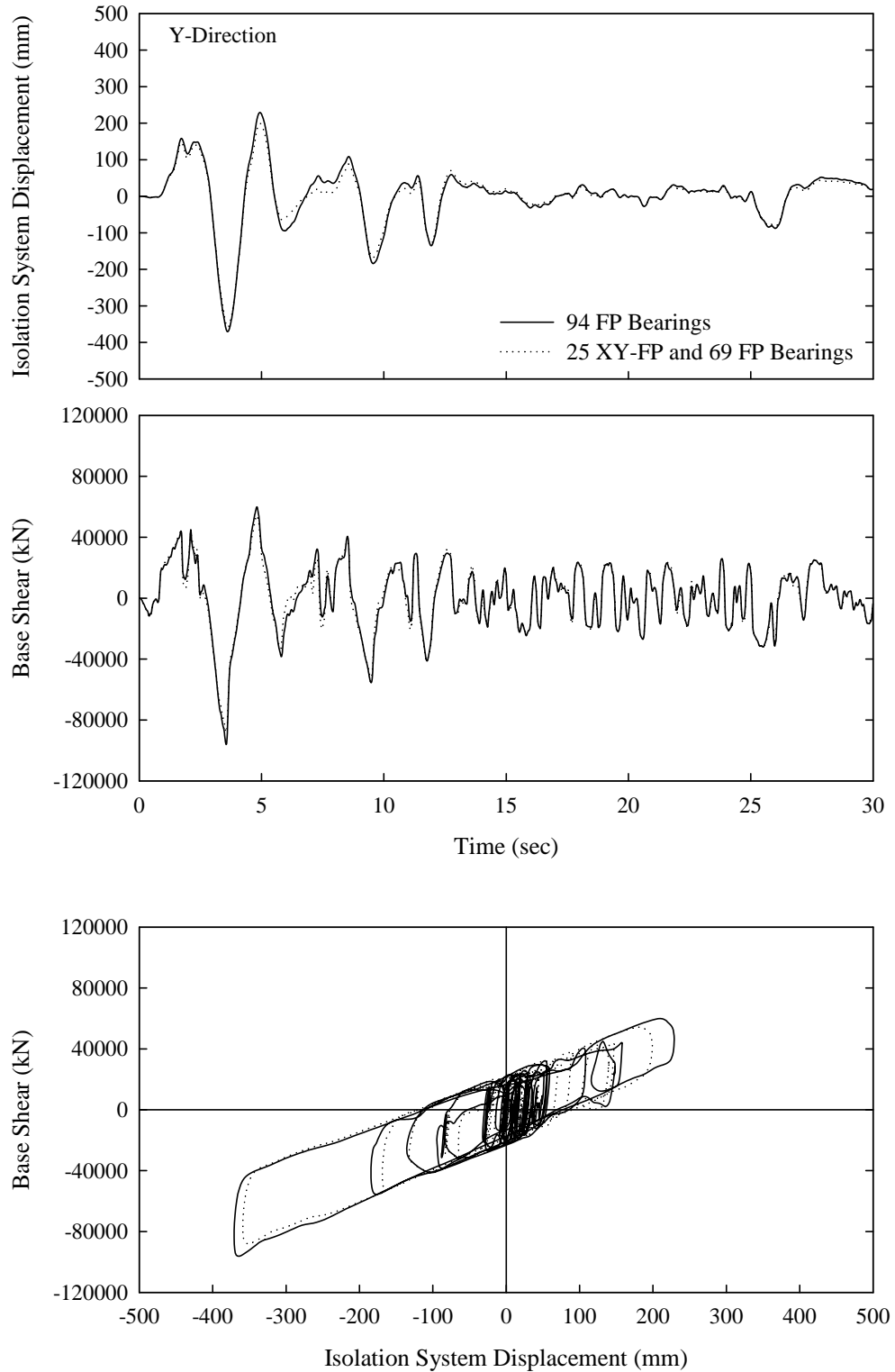


Figure 8-15: Comparison of 3D-BASIS-ME generated results in terms of isolation system response in Y direction between the model with 94 FP isolators and the model with 25 XY-FP + 69 FP isolators in scaled (factor 2.0) El Centro 180-270 excitation.

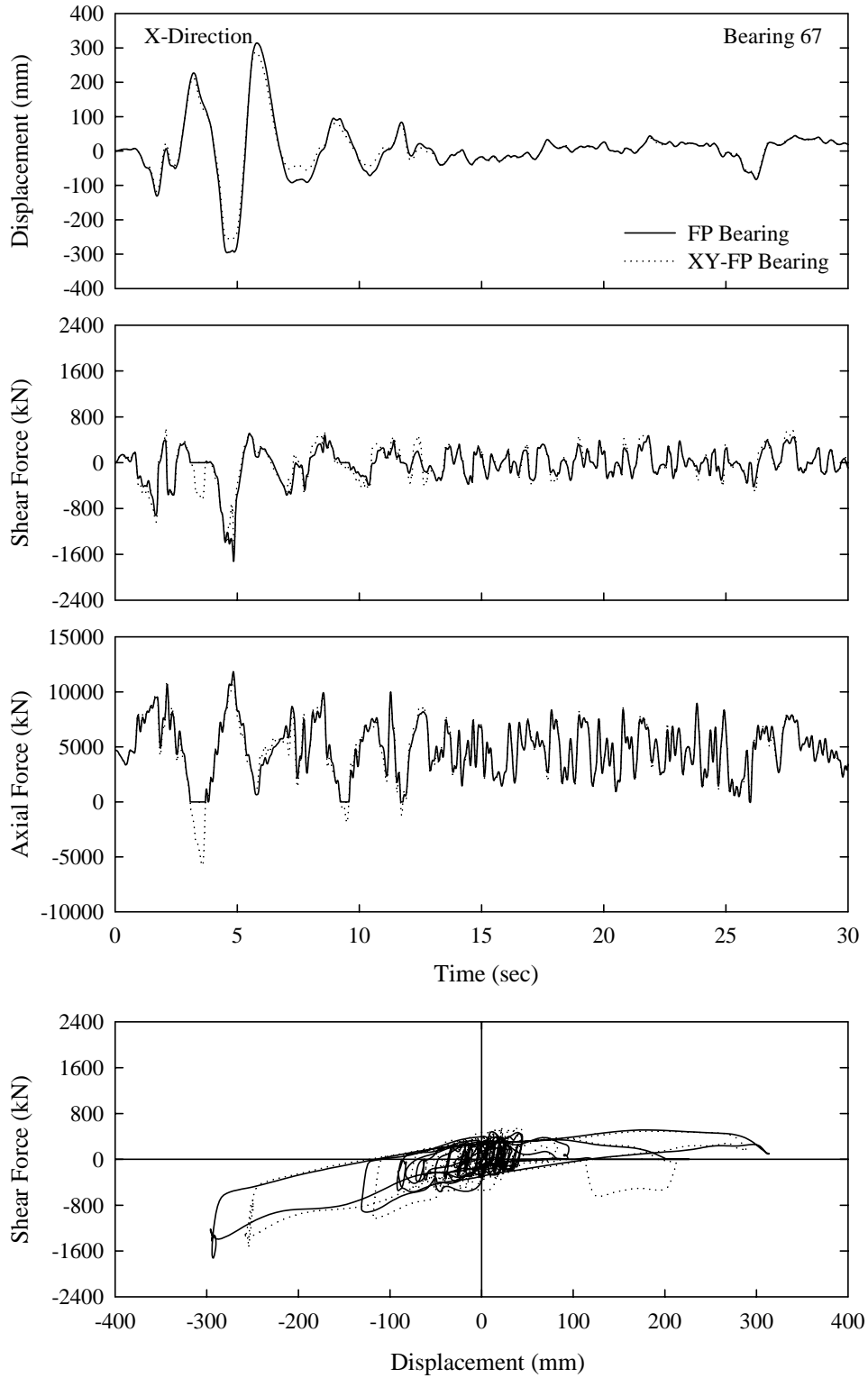


Figure 8-16: Comparison of 3D-BASIS-ME generated results in terms of response of bearing No. 67 in X direction between the model with 94 FP isolators and the model with 25 XY-FP + 69 FP isolators in scaled (factor 2.0) El Centro 180-270 excitation.

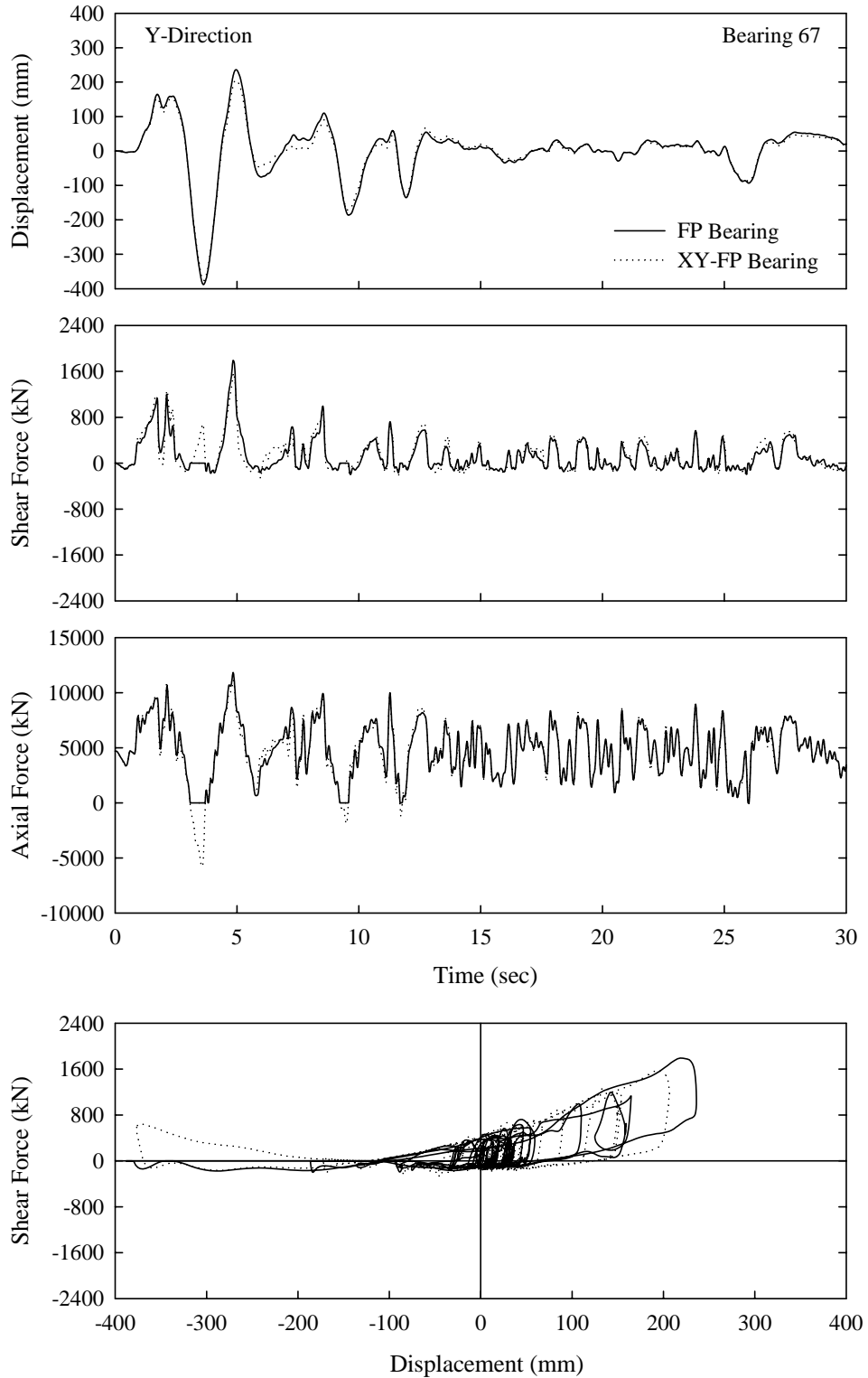


Figure 8-17: Comparison of 3D-BASIS-ME generated results in terms of response of bearing No. 67 in Y direction between the model with 94 FP isolators and the model with 25 XY-FP + 69 FP isolators in scaled (factor 2.0) El Centro 180-270 excitation.

respectively. Of particular interest is the axial force histories associated with the isolator. Due to strong seismic excitation large overturning moment effects were induced on a number of bearings, manifested as considerable variation in the axial force histories. For the isolator in question, the fluctuation in the bearing axial force was large enough, on the order of 200%, to cause reversal of the bearing axial force from compression to tension. Nevertheless, the development of tension in individual isolators, and by extension the increase of isolation system friction force (as discussed in Section 2.3), does not have any measurable effect on either the isolation system response (Figures 8-14 and 8-15) or the superstructure response (Figures 8-12 and 8-13). This is attributed to the fact that, typically, only a small number of the bearings (no more than 15%) are subjected to tension at any instant of time.

The increase in global friction force due to tension development in XY-FP isolators may prove significant in rare cases in which adverse conditions prevail in terms of the number of bearings sustaining tension at any instant of time and the magnitude of the developed tensile force. A narrow building seismically isolated with only two rows of bearings (e.g., the Excel Minami-Koshigaya building in Japan (Sumitomo Construction, 1990)) under horizontal base excitation in the transverse direction, exemplifies these conditions. Indeed, by allowing 50% of the uplift-restraint bearings to sustain tension and provided that the bearing tensile force is significantly larger than the acting weight, the increase in global friction force can potentially impact the response of structural and non-structural systems. Nevertheless, even under such adverse conditions, the capability to predict the response is made available through the newly-developed and verified analytical model of XY-FP isolator.



## SECTION 9

### SUMMARY AND CONCLUSIONS

This report aimed at extending the scope of seismic isolation by studying a novel sliding isolation bearing capable of sustaining tension. With its appealing conceptual simplicity and its proven effectiveness, the new uplift-restraint isolator, termed the XY-FP isolator, has the potential to facilitate the application of seismic isolation even under the most extreme of conditions, including but not limited to near-fault strong ground motions and uplift-prone structural systems.

This study primarily focused on: (i) introducing the concept and establishing the principles of operation and mathematical model of the new XY-FP isolator; (ii) developing an understanding of the mechanical behavior of the XY-FP isolator through testing of a single isolator; (iii) generating experimental results through testing of a quarter-scale steel-frame model structure on the earthquake simulator at the University at Buffalo to validate the effectiveness of these isolators in preventing uplift; (iv) modifying the computer program 3D-BASIS-ME to include an element representative of the mechanical behavior of the new XY-FP isolator; and (v) assessing the validity and accuracy of analytical methods to predict the behavior of such systems.

Even though a number of uplift prevention systems in seismic isolation have been proposed (and some have been implemented), their potential has been hindered by limitations stemmed from their intrinsic complexity, unpredictability, and/or deficiency to provide effective uplift prevention. Moreover, a number of such systems have not been tested and their impact on the behavior of the isolation system has not been assessed. Accordingly, a need evolved to develop acceptable isolators with tension (or uplift restraint) capability and to better understand the phenomena of uplift or tension of isolators and their impact on the performance of structural and non-structural systems.

Studied in this report is an effective uplift-restraint isolation bearing synthesized by two opposing concave stainless steel-faced beams to form a bi-directional (XY) motion mechanism. The salient features that distinguish the XY-FP isolator from the conventional Friction Pendulum (FP) isolator include: (i) effective uplift prevention

regardless of the state of displacement in the bearing; (ii) decoupling of the bi-directional horizontal motion along two orthogonal directions; and (iii) capability of providing distinct stiffness and energy dissipation along the principal directions of the bearing. Additional benefits can be derived from the unique morphology of the new bearing. In particular, by encompassing much less structural material, the isolator offers a lighter and more economical alternative to the standard FP bearing, and by extension a higher manufacturing quality. Moreover, it provides an architecturally flexible solution in terms of integration into a structural system for cases where space considerations are important.

A displacement-control testing program on a single XY-FP isolator was conducted to expand our understanding of its mechanical behavior and to extract various frictional characteristics of interest, under compressive and tensile normal load. The testing included a range of isolator orientation angles, normal loads (compressive and tensile), and peak sliding velocities. The generated results reveal the dependency of the coefficient of friction both on the apparent pressure and on the velocity of sliding. The studies also verified that, given the frictional properties of the two isolator component beams, the equivalent coefficient of friction can be calculated in any direction.

The testing program on the earthquake simulator at the University at Buffalo involved a five-story base-isolated model structure and a number of recorded horizontal and vertical ground motions with a wide range of both frequency content and amplitude. The isolation system, comprised of four uplift-prevention XY-FP isolators, was installed beneath a base and rotated for testing in different directions (0-, 45-, and 90-degree angle). This series of tests represent the only available experimental data on XY-FP isolators.

In this testing configuration, the bearing pressure was very small, and modest changes in axial load produced a large variation in the frictional properties of the isolation system. The small weight of the model structure and the four-bearing condition are “extreme” for building structures; much smaller variations in frictional response are to be expected in real-life applications.

Of particular interest are the results pertaining to the axial force histories associated with the isolators. Due to the slenderness of the structure (height to width aspect ratio approximately 4.5), large overturning moment effects were induced on the bearings under

strong base excitation. This was manifested as considerable variation in axial force, on the order of 100%, which in some cases proved large enough to cause reversal of the bearing axial force from compression to tension.

Results from a number of tests conducted with combined horizontal and vertical excitations provided evidence of the effect of the vertical component of ground motion on the response of the isolated structure. The results demonstrated that the vertical ground motion component had a minor effect on the isolation system displacement, yet a non-negligible effect on the isolation system force response, a deviation on the order of 15%, reflected primarily in the wavy form of the isolation system hysteresis loop. The effect of the vertical component of ground motion was pronounced in the local response of the isolators. In effect, the vertical ground acceleration modified significantly the axial load on the bearings, causing, in some cases, tension to develop in the bearing.

The range of tests performed on the model structure demonstrated the validity of the concept and provided evidence for the effectiveness of the XY-FP isolator in uplift prevention. Clearly, the new isolator is capable of developing tension, thereby providing uplift restraint. In addition, the experimental response formed the basis for comparison with and validation of the analytical predictions.

A comprehensive mathematical model capable of accommodating the mechanical behavior of the XY-FP isolator was developed and implemented in program 3D-BASIS-ME. In doing so, a new hysteretic element representing the XY-FP isolator was incorporated in 3D-BASIS-ME. The element is synthesized by two independent uniaxial hysteretic elements allowing different frictional interface properties along the principal isolator directions. It should be emphasized that, contrary to the element representing the conventional FP isolator, the new element is capable of developing tension and therefore providing uplift restraint. Moreover, different frictional interface properties can be assumed under compressive and tensile isolator normal force. This enhancement augments the potential of 3D-BASIS-ME by providing a versatile tool for analysis of seismically isolated structures with XY-FP isolators.

The dynamic response of the five-story seismically isolated model was predicted analytically using 3D-BASIS-ME. The analysis accounted for the variability of the

isolator axial load due to the vertical component of ground motion and the overturning moment effects, the dependency of friction coefficient on velocity, different isolator orientations, and the initial non-zero displacement of the isolators.

The validity of the 3D-BASIS-ME analytical model with reference to the newly introduced element representing the XY-FP isolator was investigated by comparison of analytical predictions with experimental results. The maximum deviation between peak experimental and analytical response quantities was on the order of 15% or less. The good agreement attests to the accuracy of the analytical model, evident even under extreme dynamic conditions entailing tension in the isolators. This demonstrates that the behavior of the XY-FP isolator is sufficiently well understood to allow for accurate prediction of the response of isolated structures incorporating the proposed isolation devices.

A case study involved analysis of the new Acropolis Museum in Athens, Greece and assessment of the impact of XY-FP isolator on its response. Nonlinear response-history analysis of the seismically isolated structure subjected to bi-directional horizontal seismic excitation was performed using programs SAP2000 and 3D-BASIS-ME. The seismically isolated structure with solely conventional FP isolators was analyzed in program 3DBASIS-ME to identify the isolators that undergo uplift. Additional analysis of the structure with an analogous isolation system model was performed in program SAP2000 as a means for comparison. The generated results demonstrate that programs SAP2000 and 3D-BASIS-ME produce comparable output.

In addition, 3D-BASIS-ME analysis was performed on the seismically isolated structure with isolators prone to uplift being replaced with XY-FP isolators. These results demonstrate that tension in individual XY-FP isolators, and by extension the increase of isolation system friction force, did not have any appreciable effect on either the total isolation system response or the superstructure response. This is attributed to the fact that, typically, only a small number of the bearings (no more than 15%) are subjected to tension at any instant of time.

The increase in global friction force due to tension development in XY-FP isolators may prove significant in rare cases in which adverse conditions prevail in terms of the number

of bearings sustaining tension at any instant of time and the magnitude of the developed tensile force. A narrow building seismically isolated with only two rows of bearings under horizontal base excitation in the transverse direction, exemplifies these conditions. Indeed, by allowing 50% of the uplift-restraint bearings to sustain tension, and provided that the bearing tensile force is significantly larger than the acting weight, the increase in global friction force can potentially impact the response of structural and non-structural systems. Nevertheless, even under such adverse conditions, the capability to predict the response is made available through the newly developed and verified analytical model of XY-FP isolator.



## SECTION 10

### REFERENCES

Al-Hussaini, T.M., Zayas, V.A., and Constantinou, M.C. (1994), "Seismic Isolation of Multi-Story Frame Structures Using Spherical Sliding Isolation System," *Report No. NCEER-94-0007*, National Center for Earthquake Engineering Research, State University of New York, Buffalo, NY.

Bracci, J.M., Reinhorn, A.M., and Mander, J.B. (1992), "Seismic Resistance of Reinforced Concrete Frame Structures Designed Only for Gravity Loads: Part I - Design and Properties of a One-Third Scale Model Structure," *Report No. NCEER-92-0027*, National Center for Earthquake Engineering Research, State University of New York, Buffalo, NY.

Chang, K.C., Lai, M.L., Soong, T.T., Hao, D.S., and Yeh, Y.C. (1993), "Seismic Behavior and Design Guidelines for Steel Frame Structures with Added Viscoelastic Dampers," *Report No. NCEER-93-0009*, National Center for Earthquake Engineering Research, State University of New York, Buffalo, NY.

Computers and Structures Inc. (1998), "SAP2000: Integrated Finite Element Analysis and Design of Structures," Version 7.5, Berkeley, CA.

Constantinou, M.C. (1998), "Application of Seismic Isolation Systems in Greece," *Proceedings of '98 Structural Engineers World Congress*, Paper T175-3, San Francisco, CA.

Constantinou, M.C., Mokha, A., and Reinhorn, A.M. (1990), "Teflon Bearings in Base Isolation II: Modeling," *Journal of Structural Engineering*, ASCE, 116(2), 455-474.

Constantinou, M.C., Tsopelas, P.C., Kasalanati, A., and Wolff, E. (1999), "Property Modification Factors for Seismic Isolation Bearings," *Report No. MCEER-990012*, Multidisciplinary Center for Earthquake Engineering Research, State University of New York, Buffalo, NY.

Constantinou, M.C., Tsopelas, P., Kim, Y-S., and Okamoto, S. (1993), "NCEER-TAISEI Corporation Research Program on Sliding Seismic Isolation Systems for Bridges-Experimental and Analytical Study of Friction Pendulum System (FPS)," *Report No. NCEER 93-0020*, National Center for Earthquake Engineering Research, State University of New York, Buffalo, NY.

Goodman, T.P. (1963), "Analysis of Two Dimensional Motion Resisted by Coulomb Friction," *Journal of Engineering for Industry*, 85, 17-26.

Griffith, M.C., Kelly, J.M., Coveney, V.A., and Koh, C.G. (1988a), "Experimental Evaluation of Seismic Isolation of Medium-Rise Structures Subject to Uplift," *Report No. UCB/EERC-88/02*, Earthquake Engineering Research Center, University of California, Berkeley, CA.

Griffith, M.C., Aiken, I.D., and Kelly, J.M. (1988b), "Experimental Evaluation of Seismic Isolation of a 9-Story Braced Steel Frame Subject to Uplift," *Report No. UCB/EERC-88/05*, Earthquake Engineering Research Center, University of California, Berkeley, CA.

Griffith, M.C., Aiken, I.D., and Kelly, J.M. (1990), "Displacement Control and Uplift Restraint for Base-Isolated Structures," *Journal of Structural Engineering*, ASCE 116(4), 1135-1148.

Honeck, W., Walters, M., Sattary, V., and Rodler, P. (1993), "Seismic Isolation of the Oakland City Hall," *Proceedings of ATC-17-1 Seminar on Seismic Isolation, Passive Energy Dissipation, and Active Control*, San Francisco, CA, March 11-12, 1993, Vol. I, 221-232.

Kasalanati, A. and Constantinou, M.C. (1999), "Experimental Study of Bridge Elastomeric and Other Isolation and Energy Dissipation Systems with Emphasis on Uplift Prevention and High Velocity Near-Source Seismic Excitation," *Report No. MCEER-99-0004*, Multidisciplinary Center for Earthquake Engineering Research, State University of New York, Buffalo, NY.

Kelly, J.M., Griffith, M.C., and Aiken, I.D. (1987), "A Displacement Control and Uplift Restraint Device for Base Isolated Structures," *Report No. UCB/EERC-87/03*, Earthquake Engineering Research Center, University of California, Berkeley, CA.

Logiadis, I.S.E. (1996), "Application of Vertical Unbonded Tensioned Prestressed Tendons in the Seismic Isolation of Structures," *Dissertation*, Technische Universitat Munchen (in German).

Mokha, A., Constantinou, M.C., and Reinhorn, A.M. (1988), "Teflon Bearings in Aseismic Base Isolation: Experimental Studies and Mathematical Modeling," *Report NCEER-88-0038*, National Center for Earthquake Engineering Research, State University of New York, Buffalo, NY.

Mokha, A.S., Constantinou, M.C., and Reinhorn, A.M. (1990), "Experimental Study and Analytical Prediction of Earthquake Response of a Sliding Isolation System with Spherical Surface," *Report NCEER-90-0020*, National Center for Earthquake Engineering Research, State University of New York, Buffalo, NY.

Mosqueda, G., Whittaker, A.S., and Fenves, G.L. (2004), "Characterization and Modeling of Friction Pendulum Bearings Subjected to Multiple Components of Excitation," *Journal of Structural Engineering*, ASCE, 130(3), 433-442.

Mostaghel, N. and Khodaverdian, M. (1987), "Dynamics of Resilient-Friction Base Isolator (R-FBI)," *Earthquake Engineering and Structural Dynamics*, 15(3), 379-390.

Naeim, F. and Kelly, J.M. (1999), *Design of Seismic Isolated Structures – From Theory to Practice*, John Wiley & Sons Inc., NY.

Nagarajaiah, S., Reinhorn, A.M., and Constantinou, M.C. (1989), "Nonlinear Dynamic Analysis of Three Dimensional Base Isolated Structures (3D-BASIS)," *Report No. NCEER-89-0019*, National Center for Earthquake Engineering Research, State University of New York, Buffalo, NY.

Nagarajaiah, S., Reinhorn, A.M., and Constantinou, M.C. (1992), "Experimental Study of Sliding Isolated Structures with Uplift Restraint," *Journal of Structural Engineering*,

ASCE, 118(6), 1666–1682.

Nagarajaiah, S., Reinhorn, A.M., and Constantinou, M.C. (1991a), “Nonlinear Dynamic Analysis of Three Dimensional Base Isolated Structures,” *Journal of Structural Engineering*, ASCE, 117(7), 2035-2054.

Nagarajaiah, S., Reinhorn, A.M., and Constantinou, M.C. (1991b), “Nonlinear Dynamic Analysis of Three Dimensional Base Isolated Structures, Part II,” *Report No. NCEER-91-0005*, National Center for Earthquake Engineering Research, State University of New York, Buffalo, NY.

Nagarajaiah, S., Li, C., Reinhorn, A.M., and Constantinou, M.C. (1993), “3D-BASIS-TABS: Computer Program for Nonlinear Dynamic Analysis of SD-Base-Isolated Structures,” *Report No. NCEER-93-0011*, National Center for Earthquake Engineering Research, State University of New York, Buffalo, NY.

Ozdemir, H. (1976), “Nonlinear Transient Dynamic Analysis of Yielding Structures,” *Ph.D. Thesis*, Department of Civil Engineering, University of California, at Berkeley, CA.

Park, Y.J., Wen, Y.K., and Ang, A.H.S. (1986), “Random Vibration of Hysteretic Systems under Bidirectional Ground Motions,” *Earthquake Engineering and Structural Dynamics*, 14(4), 543-557.

Ramirez, O.M., Constantinou, M.C., Kircher, C.A., Whittaker, A.S., Johnson, M.W., and Gomez, J.D. (2001), “Development and Evaluation of Simplified Procedures for Analysis and Design of Buildings with Passive Energy Dissipation Systems,” *Report No. MCEER-00-0010*, Multidisciplinary Center for Earthquake Engineering Research, State University of New York, Buffalo, NY.

Roussis, P.C. (2004), “Experimental and Analytical Studies of Structures Seismically Isolated with an Uplift-Restraint Isolation System,” *Ph.D. Dissertation*, Department of Civil, Structural and Environmental Engineering, University at Buffalo, State University of New York, Buffalo, NY.

Roussis, P.C., Constantinou, M.C., Erdik, M., Durukal, E., and Dicleli, M. (2003), "Assessment of Performance of Seismic Isolation System of Bolu Viaduct," *Journal of Bridge Engineering*, ASCE, 8(4), 182-190.

Roussis, P.C., Constantinou, M.C., Erdik, M., Durukal, E., and Dicleli, M. (2002), "Assessment of Performance of Bolu Viaduct in the 1999 Duzce Earthquake in Turkey," *Report No. MCEER-02-0001*, Multidisciplinary Center for Earthquake Engineering Research, Buffalo, NY.

Skinner, R.I., Robinson, W.H., and McVerry, G.H. (1993), *An Introduction to Seismic Isolation*, John Wiley & Sons Inc., NY.

Soong, T.T. and Constantinou, M.C. (1994), *Passive and Active Structural Vibration Control in Civil Engineering*, Springer-Verlag, Wien.

Su, L., Ahmadi, G., and Tadjbakhsh, I.G. (1987), "A Comparative Study of Base Isolation Systems," *Report No. MIE-150*, Clarkson University, Potsdam, NY.

Sumitomo Construction (1990), "Base-Isolated Buildings by Sumitomo Construction," Report by Sumitomo Construction Co.Ltd., Tokyo, Japan.

Tsopelas, P.C., Nagarajaiah, S., Constantinou, M.C., and Reinhorn, A.M. (1991), "3D-BASIS-M: Nonlinear Dynamic Analysis of Multiple Building Base Isolated Structures," *Report No. NCEER91-0014*, National Center for Earthquake Engineering Research, State University of New York, Buffalo, NY.

Tsopelas, P.C., Constantinou, M.C., and Reinhorn, A.M. (1994), "3D-BASIS-ME: Computer Program for Nonlinear Dynamic Analysis of Seismically Isolated Single and Multiple Structures and Liquid Storage Tanks," *Report No. MCEER-94-0010*, Multidisciplinary Center for Earthquake Engineering Research, State University of New York, Buffalo, NY.

Wen, Y.K. (1976), "Method of Random Vibration of Hysteretic Systems," *Journal of Engineering Mechanics Division*, ASCE, 102(2), 249-263.

Younis, C., Tadjbakhsh, I.G., and Saibel, E.A. (1983), "Analysis of General Plane Motion with Coulomb Friction," *Wear*, 91, 319-331.

Zayas, V., Low, S.S., and Mahin, S.A. (1987), "The FPS Earthquake Resisting System, Experimental Report," *Report No. UBC/EERC-87/01*, Earthquake Engineering Research Center, University of California, Berkeley, CA.

## **Multidisciplinary Center for Earthquake Engineering Research List of Technical Reports**

The Multidisciplinary Center for Earthquake Engineering Research (MCEER) publishes technical reports on a variety of subjects related to earthquake engineering written by authors funded through MCEER. These reports are available from both MCEER Publications and the National Technical Information Service (NTIS). Requests for reports should be directed to MCEER Publications, Multidisciplinary Center for Earthquake Engineering Research, State University of New York at Buffalo, Red Jacket Quadrangle, Buffalo, New York 14261. Reports can also be requested through NTIS, 5285 Port Royal Road, Springfield, Virginia 22161. NTIS accession numbers are shown in parenthesis, if available.

- NCEER-87-0001 "First-Year Program in Research, Education and Technology Transfer," 3/5/87, (PB88-134275, A04, MF-A01).
- NCEER-87-0002 "Experimental Evaluation of Instantaneous Optimal Algorithms for Structural Control," by R.C. Lin, T.T. Soong and A.M. Reinhorn, 4/20/87, (PB88-134341, A04, MF-A01).
- NCEER-87-0003 "Experimentation Using the Earthquake Simulation Facilities at University at Buffalo," by A.M. Reinhorn and R.L. Ketter, to be published.
- NCEER-87-0004 "The System Characteristics and Performance of a Shaking Table," by J.S. Hwang, K.C. Chang and G.C. Lee, 6/1/87, (PB88-134259, A03, MF-A01). This report is available only through NTIS (see address given above).
- NCEER-87-0005 "A Finite Element Formulation for Nonlinear Viscoplastic Material Using a Q Model," by O. Gyebe and G. Dasgupta, 11/2/87, (PB88-213764, A08, MF-A01).
- NCEER-87-0006 "Symbolic Manipulation Program (SMP) - Algebraic Codes for Two and Three Dimensional Finite Element Formulations," by X. Lee and G. Dasgupta, 11/9/87, (PB88-218522, A05, MF-A01).
- NCEER-87-0007 "Instantaneous Optimal Control Laws for Tall Buildings Under Seismic Excitations," by J.N. Yang, A. Akbarpour and P. Ghaemmaghami, 6/10/87, (PB88-134333, A06, MF-A01). This report is only available through NTIS (see address given above).
- NCEER-87-0008 "IDARC: Inelastic Damage Analysis of Reinforced Concrete Frame - Shear-Wall Structures," by Y.J. Park, A.M. Reinhorn and S.K. Kunnath, 7/20/87, (PB88-134325, A09, MF-A01). This report is only available through NTIS (see address given above).
- NCEER-87-0009 "Liquefaction Potential for New York State: A Preliminary Report on Sites in Manhattan and Buffalo," by M. Budhu, V. Vijayakumar, R.F. Giese and L. Baumgras, 8/31/87, (PB88-163704, A03, MF-A01). This report is available only through NTIS (see address given above).
- NCEER-87-0010 "Vertical and Torsional Vibration of Foundations in Inhomogeneous Media," by A.S. Veletsos and K.W. Dotson, 6/1/87, (PB88-134291, A03, MF-A01). This report is only available through NTIS (see address given above).
- NCEER-87-0011 "Seismic Probabilistic Risk Assessment and Seismic Margins Studies for Nuclear Power Plants," by Howard H.M. Hwang, 6/15/87, (PB88-134267, A03, MF-A01). This report is only available through NTIS (see address given above).
- NCEER-87-0012 "Parametric Studies of Frequency Response of Secondary Systems Under Ground-Acceleration Excitations," by Y. Yong and Y.K. Lin, 6/10/87, (PB88-134309, A03, MF-A01). This report is only available through NTIS (see address given above).
- NCEER-87-0013 "Frequency Response of Secondary Systems Under Seismic Excitation," by J.A. HoLung, J. Cai and Y.K. Lin, 7/31/87, (PB88-134317, A05, MF-A01). This report is only available through NTIS (see address given above).
- NCEER-87-0014 "Modelling Earthquake Ground Motions in Seismically Active Regions Using Parametric Time Series Methods," by G.W. Ellis and A.S. Cakmak, 8/25/87, (PB88-134283, A08, MF-A01). This report is only available through NTIS (see address given above).

- NCEER-87-0015 "Detection and Assessment of Seismic Structural Damage," by E. DiPasquale and A.S. Cakmak, 8/25/87, (PB88-163712, A05, MF-A01). This report is only available through NTIS (see address given above).
- NCEER-87-0016 "Pipeline Experiment at Parkfield, California," by J. Isenberg and E. Richardson, 9/15/87, (PB88-163720, A03, MF-A01). This report is available only through NTIS (see address given above).
- NCEER-87-0017 "Digital Simulation of Seismic Ground Motion," by M. Shinozuka, G. Deodatis and T. Harada, 8/31/87, (PB88-155197, A04, MF-A01). This report is available only through NTIS (see address given above).
- NCEER-87-0018 "Practical Considerations for Structural Control: System Uncertainty, System Time Delay and Truncation of Small Control Forces," J.N. Yang and A. Akbarpour, 8/10/87, (PB88-163738, A08, MF-A01). This report is only available through NTIS (see address given above).
- NCEER-87-0019 "Modal Analysis of Nonclassically Damped Structural Systems Using Canonical Transformation," by J.N. Yang, S. Sarkani and F.X. Long, 9/27/87, (PB88-187851, A04, MF-A01).
- NCEER-87-0020 "A Nonstationary Solution in Random Vibration Theory," by J.R. Red-Horse and P.D. Spanos, 11/3/87, (PB88-163746, A03, MF-A01).
- NCEER-87-0021 "Horizontal Impedances for Radially Inhomogeneous Viscoelastic Soil Layers," by A.S. Veletsos and K.W. Dotson, 10/15/87, (PB88-150859, A04, MF-A01).
- NCEER-87-0022 "Seismic Damage Assessment of Reinforced Concrete Members," by Y.S. Chung, C. Meyer and M. Shinozuka, 10/9/87, (PB88-150867, A05, MF-A01). This report is available only through NTIS (see address given above).
- NCEER-87-0023 "Active Structural Control in Civil Engineering," by T.T. Soong, 11/11/87, (PB88-187778, A03, MF-A01).
- NCEER-87-0024 "Vertical and Torsional Impedances for Radially Inhomogeneous Viscoelastic Soil Layers," by K.W. Dotson and A.S. Veletsos, 12/87, (PB88-187786, A03, MF-A01).
- NCEER-87-0025 "Proceedings from the Symposium on Seismic Hazards, Ground Motions, Soil-Liquefaction and Engineering Practice in Eastern North America," October 20-22, 1987, edited by K.H. Jacob, 12/87, (PB88-188115, A23, MF-A01). This report is available only through NTIS (see address given above).
- NCEER-87-0026 "Report on the Whittier-Narrows, California, Earthquake of October 1, 1987," by J. Pantelic and A. Reinhorn, 11/87, (PB88-187752, A03, MF-A01). This report is available only through NTIS (see address given above).
- NCEER-87-0027 "Design of a Modular Program for Transient Nonlinear Analysis of Large 3-D Building Structures," by S. Srivastav and J.F. Abel, 12/30/87, (PB88-187950, A05, MF-A01). This report is only available through NTIS (see address given above).
- NCEER-87-0028 "Second-Year Program in Research, Education and Technology Transfer," 3/8/88, (PB88-219480, A04, MF-A01).
- NCEER-88-0001 "Workshop on Seismic Computer Analysis and Design of Buildings With Interactive Graphics," by W. McGuire, J.F. Abel and C.H. Conley, 1/18/88, (PB88-187760, A03, MF-A01). This report is only available through NTIS (see address given above).
- NCEER-88-0002 "Optimal Control of Nonlinear Flexible Structures," by J.N. Yang, F.X. Long and D. Wong, 1/22/88, (PB88-213772, A06, MF-A01).
- NCEER-88-0003 "Substructuring Techniques in the Time Domain for Primary-Secondary Structural Systems," by G.D. Manolis and G. Juhn, 2/10/88, (PB88-213780, A04, MF-A01).
- NCEER-88-0004 "Iterative Seismic Analysis of Primary-Secondary Systems," by A. Singhal, L.D. Lutes and P.D. Spanos, 2/23/88, (PB88-213798, A04, MF-A01).

- NCEER-88-0005 "Stochastic Finite Element Expansion for Random Media," by P.D. Spanos and R. Ghanem, 3/14/88, (PB88-213806, A03, MF-A01).
- NCEER-88-0006 "Combining Structural Optimization and Structural Control," by F.Y. Cheng and C.P. Pantelides, 1/10/88, (PB88-213814, A05, MF-A01).
- NCEER-88-0007 "Seismic Performance Assessment of Code-Designed Structures," by H.H-M. Hwang, J-W. Jaw and H-J. Shau, 3/20/88, (PB88-219423, A04, MF-A01). This report is only available through NTIS (see address given above).
- NCEER-88-0008 "Reliability Analysis of Code-Designed Structures Under Natural Hazards," by H.H-M. Hwang, H. Ushiba and M. Shinozuka, 2/29/88, (PB88-229471, A07, MF-A01). This report is only available through NTIS (see address given above).
- NCEER-88-0009 "Seismic Fragility Analysis of Shear Wall Structures," by J-W Jaw and H.H-M. Hwang, 4/30/88, (PB89-102867, A04, MF-A01).
- NCEER-88-0010 "Base Isolation of a Multi-Story Building Under a Harmonic Ground Motion - A Comparison of Performances of Various Systems," by F-G Fan, G. Ahmadi and I.G. Tadjbakhsh, 5/18/88, (PB89-122238, A06, MF-A01). This report is only available through NTIS (see address given above).
- NCEER-88-0011 "Seismic Floor Response Spectra for a Combined System by Green's Functions," by F.M. Lavelle, L.A. Bergman and P.D. Spanos, 5/1/88, (PB89-102875, A03, MF-A01).
- NCEER-88-0012 "A New Solution Technique for Randomly Excited Hysteretic Structures," by G.Q. Cai and Y.K. Lin, 5/16/88, (PB89-102883, A03, MF-A01).
- NCEER-88-0013 "A Study of Radiation Damping and Soil-Structure Interaction Effects in the Centrifuge," by K. Weissman, supervised by J.H. Prevost, 5/24/88, (PB89-144703, A06, MF-A01).
- NCEER-88-0014 "Parameter Identification and Implementation of a Kinematic Plasticity Model for Frictional Soils," by J.H. Prevost and D.V. Griffiths, to be published.
- NCEER-88-0015 "Two- and Three- Dimensional Dynamic Finite Element Analyses of the Long Valley Dam," by D.V. Griffiths and J.H. Prevost, 6/17/88, (PB89-144711, A04, MF-A01).
- NCEER-88-0016 "Damage Assessment of Reinforced Concrete Structures in Eastern United States," by A.M. Reinhorn, M.J. Seidel, S.K. Kunnath and Y.J. Park, 6/15/88, (PB89-122220, A04, MF-A01). This report is only available through NTIS (see address given above).
- NCEER-88-0017 "Dynamic Compliance of Vertically Loaded Strip Foundations in Multilayered Viscoelastic Soils," by S. Ahmad and A.S.M. Israil, 6/17/88, (PB89-102891, A04, MF-A01).
- NCEER-88-0018 "An Experimental Study of Seismic Structural Response With Added Viscoelastic Dampers," by R.C. Lin, Z. Liang, T.T. Soong and R.H. Zhang, 6/30/88, (PB89-122212, A05, MF-A01). This report is available only through NTIS (see address given above).
- NCEER-88-0019 "Experimental Investigation of Primary - Secondary System Interaction," by G.D. Manolis, G. Juhn and A.M. Reinhorn, 5/27/88, (PB89-122204, A04, MF-A01).
- NCEER-88-0020 "A Response Spectrum Approach For Analysis of Nonclassically Damped Structures," by J.N. Yang, S. Sarkani and F.X. Long, 4/22/88, (PB89-102909, A04, MF-A01).
- NCEER-88-0021 "Seismic Interaction of Structures and Soils: Stochastic Approach," by A.S. Veletsos and A.M. Prasad, 7/21/88, (PB89-122196, A04, MF-A01). This report is only available through NTIS (see address given above).
- NCEER-88-0022 "Identification of the Serviceability Limit State and Detection of Seismic Structural Damage," by E. DiPasquale and A.S. Cakmak, 6/15/88, (PB89-122188, A05, MF-A01). This report is available only through NTIS (see address given above).

- NCEER-88-0023 "Multi-Hazard Risk Analysis: Case of a Simple Offshore Structure," by B.K. Bhartia and E.H. Vanmarcke, 7/21/88, (PB89-145213, A05, MF-A01).
- NCEER-88-0024 "Automated Seismic Design of Reinforced Concrete Buildings," by Y.S. Chung, C. Meyer and M. Shinozuka, 7/5/88, (PB89-122170, A06, MF-A01). This report is available only through NTIS (see address given above).
- NCEER-88-0025 "Experimental Study of Active Control of MDOF Structures Under Seismic Excitations," by L.L. Chung, R.C. Lin, T.T. Soong and A.M. Reinhorn, 7/10/88, (PB89-122600, A04, MF-A01).
- NCEER-88-0026 "Earthquake Simulation Tests of a Low-Rise Metal Structure," by J.S. Hwang, K.C. Chang, G.C. Lee and R.L. Ketter, 8/1/88, (PB89-102917, A04, MF-A01).
- NCEER-88-0027 "Systems Study of Urban Response and Reconstruction Due to Catastrophic Earthquakes," by F. Kozin and H.K. Zhou, 9/22/88, (PB90-162348, A04, MF-A01).
- NCEER-88-0028 "Seismic Fragility Analysis of Plane Frame Structures," by H.H-M. Hwang and Y.K. Low, 7/31/88, (PB89-131445, A06, MF-A01).
- NCEER-88-0029 "Response Analysis of Stochastic Structures," by A. Kardara, C. Bucher and M. Shinozuka, 9/22/88, (PB89-174429, A04, MF-A01).
- NCEER-88-0030 "Nonnormal Accelerations Due to Yielding in a Primary Structure," by D.C.K. Chen and L.D. Lutes, 9/19/88, (PB89-131437, A04, MF-A01).
- NCEER-88-0031 "Design Approaches for Soil-Structure Interaction," by A.S. Veletsos, A.M. Prasad and Y. Tang, 12/30/88, (PB89-174437, A03, MF-A01). This report is available only through NTIS (see address given above).
- NCEER-88-0032 "A Re-evaluation of Design Spectra for Seismic Damage Control," by C.J. Turkstra and A.G. Tallin, 11/7/88, (PB89-145221, A05, MF-A01).
- NCEER-88-0033 "The Behavior and Design of Noncontact Lap Splices Subjected to Repeated Inelastic Tensile Loading," by V.E. Sagan, P. Gergely and R.N. White, 12/8/88, (PB89-163737, A08, MF-A01).
- NCEER-88-0034 "Seismic Response of Pile Foundations," by S.M. Mamoon, P.K. Banerjee and S. Ahmad, 11/1/88, (PB89-145239, A04, MF-A01).
- NCEER-88-0035 "Modeling of R/C Building Structures With Flexible Floor Diaphragms (IDARC2)," by A.M. Reinhorn, S.K. Kunnath and N. Panahshahi, 9/7/88, (PB89-207153, A07, MF-A01).
- NCEER-88-0036 "Solution of the Dam-Reservoir Interaction Problem Using a Combination of FEM, BEM with Particular Integrals, Modal Analysis, and Substructuring," by C-S. Tsai, G.C. Lee and R.L. Ketter, 12/31/88, (PB89-207146, A04, MF-A01).
- NCEER-88-0037 "Optimal Placement of Actuators for Structural Control," by F.Y. Cheng and C.P. Pantelides, 8/15/88, (PB89-162846, A05, MF-A01).
- NCEER-88-0038 "Teflon Bearings in Aseismic Base Isolation: Experimental Studies and Mathematical Modeling," by A. Mokha, M.C. Constantinou and A.M. Reinhorn, 12/5/88, (PB89-218457, A10, MF-A01). This report is available only through NTIS (see address given above).
- NCEER-88-0039 "Seismic Behavior of Flat Slab High-Rise Buildings in the New York City Area," by P. Weidlinger and M. Ettouney, 10/15/88, (PB90-145681, A04, MF-A01).
- NCEER-88-0040 "Evaluation of the Earthquake Resistance of Existing Buildings in New York City," by P. Weidlinger and M. Ettouney, 10/15/88, to be published.
- NCEER-88-0041 "Small-Scale Modeling Techniques for Reinforced Concrete Structures Subjected to Seismic Loads," by W. Kim, A. El-Attar and R.N. White, 11/22/88, (PB89-189625, A05, MF-A01).

- NCEER-88-0042 "Modeling Strong Ground Motion from Multiple Event Earthquakes," by G.W. Ellis and A.S. Cakmak, 10/15/88, (PB89-174445, A03, MF-A01).
- NCEER-88-0043 "Nonstationary Models of Seismic Ground Acceleration," by M. Grigoriu, S.E. Ruiz and E. Rosenblueth, 7/15/88, (PB89-189617, A04, MF-A01).
- NCEER-88-0044 "SARCF User's Guide: Seismic Analysis of Reinforced Concrete Frames," by Y.S. Chung, C. Meyer and M. Shinozuka, 11/9/88, (PB89-174452, A08, MF-A01).
- NCEER-88-0045 "First Expert Panel Meeting on Disaster Research and Planning," edited by J. Pantelic and J. Stoyke, 9/15/88, (PB89-174460, A05, MF-A01).
- NCEER-88-0046 "Preliminary Studies of the Effect of Degrading Infill Walls on the Nonlinear Seismic Response of Steel Frames," by C.Z. Chrysostomou, P. Gergely and J.F. Abel, 12/19/88, (PB89-208383, A05, MF-A01).
- NCEER-88-0047 "Reinforced Concrete Frame Component Testing Facility - Design, Construction, Instrumentation and Operation," by S.P. Pessiki, C. Conley, T. Bond, P. Gergely and R.N. White, 12/16/88, (PB89-174478, A04, MF-A01).
- NCEER-89-0001 "Effects of Protective Cushion and Soil Compliancy on the Response of Equipment Within a Seismically Excited Building," by J.A. HoLung, 2/16/89, (PB89-207179, A04, MF-A01).
- NCEER-89-0002 "Statistical Evaluation of Response Modification Factors for Reinforced Concrete Structures," by H.H-M. Hwang and J-W. Jaw, 2/17/89, (PB89-207187, A05, MF-A01).
- NCEER-89-0003 "Hysteretic Columns Under Random Excitation," by G-Q. Cai and Y.K. Lin, 1/9/89, (PB89-196513, A03, MF-A01).
- NCEER-89-0004 "Experimental Study of 'Elephant Foot Bulge' Instability of Thin-Walled Metal Tanks," by Z-H. Jia and R.L. Ketter, 2/22/89, (PB89-207195, A03, MF-A01).
- NCEER-89-0005 "Experiment on Performance of Buried Pipelines Across San Andreas Fault," by J. Isenberg, E. Richardson and T.D. O'Rourke, 3/10/89, (PB89-218440, A04, MF-A01). This report is available only through NTIS (see address given above).
- NCEER-89-0006 "A Knowledge-Based Approach to Structural Design of Earthquake-Resistant Buildings," by M. Subramani, P. Gergely, C.H. Conley, J.F. Abel and A.H. Zaghaw, 1/15/89, (PB89-218465, A06, MF-A01).
- NCEER-89-0007 "Liquefaction Hazards and Their Effects on Buried Pipelines," by T.D. O'Rourke and P.A. Lane, 2/1/89, (PB89-218481, A09, MF-A01).
- NCEER-89-0008 "Fundamentals of System Identification in Structural Dynamics," by H. Imai, C-B. Yun, O. Maruyama and M. Shinozuka, 1/26/89, (PB89-207211, A04, MF-A01).
- NCEER-89-0009 "Effects of the 1985 Michoacan Earthquake on Water Systems and Other Buried Lifelines in Mexico," by A.G. Ayala and M.J. O'Rourke, 3/8/89, (PB89-207229, A06, MF-A01).
- NCEER-89-R010 "NCEER Bibliography of Earthquake Education Materials," by K.E.K. Ross, Second Revision, 9/1/89, (PB90-125352, A05, MF-A01). This report is replaced by NCEER-92-0018.
- NCEER-89-0011 "Inelastic Three-Dimensional Response Analysis of Reinforced Concrete Building Structures (IDARC-3D), Part I - Modeling," by S.K. Kunnath and A.M. Reinhorn, 4/17/89, (PB90-114612, A07, MF-A01). This report is available only through NTIS (see address given above).
- NCEER-89-0012 "Recommended Modifications to ATC-14," by C.D. Poland and J.O. Malley, 4/12/89, (PB90-108648, A15, MF-A01).
- NCEER-89-0013 "Repair and Strengthening of Beam-to-Column Connections Subjected to Earthquake Loading," by M. Corazao and A.J. Durrani, 2/28/89, (PB90-109885, A06, MF-A01).

- NCEER-89-0014 "Program EXKAL2 for Identification of Structural Dynamic Systems," by O. Maruyama, C-B. Yun, M. Hoshiya and M. Shinozuka, 5/19/89, (PB90-109877, A09, MF-A01).
- NCEER-89-0015 "Response of Frames With Bolted Semi-Rigid Connections, Part I - Experimental Study and Analytical Predictions," by P.J. DiCorso, A.M. Reinhorn, J.R. Dickerson, J.B. Radzinski and W.L. Harper, 6/1/89, to be published.
- NCEER-89-0016 "ARMA Monte Carlo Simulation in Probabilistic Structural Analysis," by P.D. Spanos and M.P. Mignolet, 7/10/89, (PB90-109893, A03, MF-A01).
- NCEER-89-P017 "Preliminary Proceedings from the Conference on Disaster Preparedness - The Place of Earthquake Education in Our Schools," Edited by K.E.K. Ross, 6/23/89, (PB90-108606, A03, MF-A01).
- NCEER-89-0017 "Proceedings from the Conference on Disaster Preparedness - The Place of Earthquake Education in Our Schools," Edited by K.E.K. Ross, 12/31/89, (PB90-207895, A012, MF-A02). This report is available only through NTIS (see address given above).
- NCEER-89-0018 "Multidimensional Models of Hysteretic Material Behavior for Vibration Analysis of Shape Memory Energy Absorbing Devices, by E.J. Graesser and F.A. Cozzarelli, 6/7/89, (PB90-164146, A04, MF-A01).
- NCEER-89-0019 "Nonlinear Dynamic Analysis of Three-Dimensional Base Isolated Structures (3D-BASIS)," by S. Nagarajaiah, A.M. Reinhorn and M.C. Constantinou, 8/3/89, (PB90-161936, A06, MF-A01). This report has been replaced by NCEER-93-0011.
- NCEER-89-0020 "Structural Control Considering Time-Rate of Control Forces and Control Rate Constraints," by F.Y. Cheng and C.P. Pantelides, 8/3/89, (PB90-120445, A04, MF-A01).
- NCEER-89-0021 "Subsurface Conditions of Memphis and Shelby County," by K.W. Ng, T-S. Chang and H-H.M. Hwang, 7/26/89, (PB90-120437, A03, MF-A01).
- NCEER-89-0022 "Seismic Wave Propagation Effects on Straight Jointed Buried Pipelines," by K. Elhadi and M.J. O'Rourke, 8/24/89, (PB90-162322, A10, MF-A02).
- NCEER-89-0023 "Workshop on Serviceability Analysis of Water Delivery Systems," edited by M. Grigoriu, 3/6/89, (PB90-127424, A03, MF-A01).
- NCEER-89-0024 "Shaking Table Study of a 1/5 Scale Steel Frame Composed of Tapered Members," by K.C. Chang, J.S. Hwang and G.C. Lee, 9/18/89, (PB90-160169, A04, MF-A01).
- NCEER-89-0025 "DYNA1D: A Computer Program for Nonlinear Seismic Site Response Analysis - Technical Documentation," by Jean H. Prevost, 9/14/89, (PB90-161944, A07, MF-A01). This report is available only through NTIS (see address given above).
- NCEER-89-0026 "1:4 Scale Model Studies of Active Tendon Systems and Active Mass Dampers for Aseismic Protection," by A.M. Reinhorn, T.T. Soong, R.C. Lin, Y.P. Yang, Y. Fukao, H. Abe and M. Nakai, 9/15/89, (PB90-173246, A10, MF-A02). This report is available only through NTIS (see address given above).
- NCEER-89-0027 "Scattering of Waves by Inclusions in a Nonhomogeneous Elastic Half Space Solved by Boundary Element Methods," by P.K. Hadley, A. Askar and A.S. Cakmak, 6/15/89, (PB90-145699, A07, MF-A01).
- NCEER-89-0028 "Statistical Evaluation of Deflection Amplification Factors for Reinforced Concrete Structures," by H.H.M. Hwang, J-W. Jaw and A.L. Ch'ng, 8/31/89, (PB90-164633, A05, MF-A01).
- NCEER-89-0029 "Bedrock Accelerations in Memphis Area Due to Large New Madrid Earthquakes," by H.H.M. Hwang, C.H.S. Chen and G. Yu, 11/7/89, (PB90-162330, A04, MF-A01).
- NCEER-89-0030 "Seismic Behavior and Response Sensitivity of Secondary Structural Systems," by Y.Q. Chen and T.T. Soong, 10/23/89, (PB90-164658, A08, MF-A01).
- NCEER-89-0031 "Random Vibration and Reliability Analysis of Primary-Secondary Structural Systems," by Y. Ibrahim, M. Grigoriu and T.T. Soong, 11/10/89, (PB90-161951, A04, MF-A01).

- NCEER-89-0032 "Proceedings from the Second U.S. - Japan Workshop on Liquefaction, Large Ground Deformation and Their Effects on Lifelines, September 26-29, 1989," Edited by T.D. O'Rourke and M. Hamada, 12/1/89, (PB90-209388, A22, MF-A03).
- NCEER-89-0033 "Deterministic Model for Seismic Damage Evaluation of Reinforced Concrete Structures," by J.M. Bracci, A.M. Reinhorn, J.B. Mander and S.K. Kunnath, 9/27/89, (PB91-108803, A06, MF-A01).
- NCEER-89-0034 "On the Relation Between Local and Global Damage Indices," by E. DiPasquale and A.S. Cakmak, 8/15/89, (PB90-173865, A05, MF-A01).
- NCEER-89-0035 "Cyclic Undrained Behavior of Nonplastic and Low Plasticity Silts," by A.J. Walker and H.E. Stewart, 7/26/89, (PB90-183518, A10, MF-A01).
- NCEER-89-0036 "Liquefaction Potential of Surficial Deposits in the City of Buffalo, New York," by M. Budhu, R. Giese and L. Baumgrass, 1/17/89, (PB90-208455, A04, MF-A01).
- NCEER-89-0037 "A Deterministic Assessment of Effects of Ground Motion Incoherence," by A.S. Veletsos and Y. Tang, 7/15/89, (PB90-164294, A03, MF-A01).
- NCEER-89-0038 "Workshop on Ground Motion Parameters for Seismic Hazard Mapping," July 17-18, 1989, edited by R.V. Whitman, 12/1/89, (PB90-173923, A04, MF-A01).
- NCEER-89-0039 "Seismic Effects on Elevated Transit Lines of the New York City Transit Authority," by C.J. Costantino, C.A. Miller and E. Heymsfield, 12/26/89, (PB90-207887, A06, MF-A01).
- NCEER-89-0040 "Centrifugal Modeling of Dynamic Soil-Structure Interaction," by K. Weissman, Supervised by J.H. Prevost, 5/10/89, (PB90-207879, A07, MF-A01).
- NCEER-89-0041 "Linearized Identification of Buildings With Cores for Seismic Vulnerability Assessment," by I-K. Ho and A.E. Aktan, 11/1/89, (PB90-251943, A07, MF-A01).
- NCEER-90-0001 "Geotechnical and Lifeline Aspects of the October 17, 1989 Loma Prieta Earthquake in San Francisco," by T.D. O'Rourke, H.E. Stewart, F.T. Blackburn and T.S. Dickerman, 1/90, (PB90-208596, A05, MF-A01).
- NCEER-90-0002 "Nonnormal Secondary Response Due to Yielding in a Primary Structure," by D.C.K. Chen and L.D. Lutes, 2/28/90, (PB90-251976, A07, MF-A01).
- NCEER-90-0003 "Earthquake Education Materials for Grades K-12," by K.E.K. Ross, 4/16/90, (PB91-251984, A05, MF-A05). This report has been replaced by NCEER-92-0018.
- NCEER-90-0004 "Catalog of Strong Motion Stations in Eastern North America," by R.W. Busby, 4/3/90, (PB90-251984, A05, MF-A01).
- NCEER-90-0005 "NCEER Strong-Motion Data Base: A User Manual for the GeoBase Release (Version 1.0 for the Sun3)," by P. Friberg and K. Jacob, 3/31/90 (PB90-258062, A04, MF-A01).
- NCEER-90-0006 "Seismic Hazard Along a Crude Oil Pipeline in the Event of an 1811-1812 Type New Madrid Earthquake," by H.H.M. Hwang and C-H.S. Chen, 4/16/90, (PB90-258054, A04, MF-A01).
- NCEER-90-0007 "Site-Specific Response Spectra for Memphis Sheahan Pumping Station," by H.H.M. Hwang and C.S. Lee, 5/15/90, (PB91-108811, A05, MF-A01).
- NCEER-90-0008 "Pilot Study on Seismic Vulnerability of Crude Oil Transmission Systems," by T. Ariman, R. Dobry, M. Grigoriu, F. Kozin, M. O'Rourke, T. O'Rourke and M. Shinozuka, 5/25/90, (PB91-108837, A06, MF-A01).
- NCEER-90-0009 "A Program to Generate Site Dependent Time Histories: EQGEN," by G.W. Ellis, M. Srinivasan and A.S. Cakmak, 1/30/90, (PB91-108829, A04, MF-A01).
- NCEER-90-0010 "Active Isolation for Seismic Protection of Operating Rooms," by M.E. Talbott, Supervised by M. Shinozuka, 6/8/9, (PB91-110205, A05, MF-A01).

- NCEER-90-0011 "Program LINEARID for Identification of Linear Structural Dynamic Systems," by C-B. Yun and M. Shinozuka, 6/25/90, (PB91-110312, A08, MF-A01).
- NCEER-90-0012 "Two-Dimensional Two-Phase Elasto-Plastic Seismic Response of Earth Dams," by A.N. Yiagos, Supervised by J.H. Prevost, 6/20/90, (PB91-110197, A13, MF-A02).
- NCEER-90-0013 "Secondary Systems in Base-Isolated Structures: Experimental Investigation, Stochastic Response and Stochastic Sensitivity," by G.D. Manolis, G. Juhn, M.C. Constantinou and A.M. Reinhorn, 7/1/90, (PB91-110320, A08, MF-A01).
- NCEER-90-0014 "Seismic Behavior of Lightly-Reinforced Concrete Column and Beam-Column Joint Details," by S.P. Pessiki, C.H. Conley, P. Gergely and R.N. White, 8/22/90, (PB91-108795, A11, MF-A02).
- NCEER-90-0015 "Two Hybrid Control Systems for Building Structures Under Strong Earthquakes," by J.N. Yang and A. Danielians, 6/29/90, (PB91-125393, A04, MF-A01).
- NCEER-90-0016 "Instantaneous Optimal Control with Acceleration and Velocity Feedback," by J.N. Yang and Z. Li, 6/29/90, (PB91-125401, A03, MF-A01).
- NCEER-90-0017 "Reconnaissance Report on the Northern Iran Earthquake of June 21, 1990," by M. Mehrain, 10/4/90, (PB91-125377, A03, MF-A01).
- NCEER-90-0018 "Evaluation of Liquefaction Potential in Memphis and Shelby County," by T.S. Chang, P.S. Tang, C.S. Lee and H. Hwang, 8/10/90, (PB91-125427, A09, MF-A01).
- NCEER-90-0019 "Experimental and Analytical Study of a Combined Sliding Disc Bearing and Helical Steel Spring Isolation System," by M.C. Constantinou, A.S. Mokha and A.M. Reinhorn, 10/4/90, (PB91-125385, A06, MF-A01). This report is available only through NTIS (see address given above).
- NCEER-90-0020 "Experimental Study and Analytical Prediction of Earthquake Response of a Sliding Isolation System with a Spherical Surface," by A.S. Mokha, M.C. Constantinou and A.M. Reinhorn, 10/11/90, (PB91-125419, A05, MF-A01).
- NCEER-90-0021 "Dynamic Interaction Factors for Floating Pile Groups," by G. Gazetas, K. Fan, A. Kaynia and E. Kausel, 9/10/90, (PB91-170381, A05, MF-A01).
- NCEER-90-0022 "Evaluation of Seismic Damage Indices for Reinforced Concrete Structures," by S. Rodriguez-Gomez and A.S. Cakmak, 9/30/90, PB91-171322, A06, MF-A01).
- NCEER-90-0023 "Study of Site Response at a Selected Memphis Site," by H. Desai, S. Ahmad, E.S. Gazetas and M.R. Oh, 10/11/90, (PB91-196857, A03, MF-A01).
- NCEER-90-0024 "A User's Guide to Strongmo: Version 1.0 of NCEER's Strong-Motion Data Access Tool for PCs and Terminals," by P.A. Friberg and C.A.T. Susch, 11/15/90, (PB91-171272, A03, MF-A01).
- NCEER-90-0025 "A Three-Dimensional Analytical Study of Spatial Variability of Seismic Ground Motions," by L-L. Hong and A.H.-S. Ang, 10/30/90, (PB91-170399, A09, MF-A01).
- NCEER-90-0026 "MUMOID User's Guide - A Program for the Identification of Modal Parameters," by S. Rodriguez-Gomez and E. DiPasquale, 9/30/90, (PB91-171298, A04, MF-A01).
- NCEER-90-0027 "SARCF-II User's Guide - Seismic Analysis of Reinforced Concrete Frames," by S. Rodriguez-Gomez, Y.S. Chung and C. Meyer, 9/30/90, (PB91-171280, A05, MF-A01).
- NCEER-90-0028 "Viscous Dampers: Testing, Modeling and Application in Vibration and Seismic Isolation," by N. Makris and M.C. Constantinou, 12/20/90 (PB91-190561, A06, MF-A01).
- NCEER-90-0029 "Soil Effects on Earthquake Ground Motions in the Memphis Area," by H. Hwang, C.S. Lee, K.W. Ng and T.S. Chang, 8/2/90, (PB91-190751, A05, MF-A01).

- NCEER-91-0001 "Proceedings from the Third Japan-U.S. Workshop on Earthquake Resistant Design of Lifeline Facilities and Countermeasures for Soil Liquefaction, December 17-19, 1990," edited by T.D. O'Rourke and M. Hamada, 2/1/91, (PB91-179259, A99, MF-A04).
- NCEER-91-0002 "Physical Space Solutions of Non-Proportionally Damped Systems," by M. Tong, Z. Liang and G.C. Lee, 1/15/91, (PB91-179242, A04, MF-A01).
- NCEER-91-0003 "Seismic Response of Single Piles and Pile Groups," by K. Fan and G. Gazetas, 1/10/91, (PB92-174994, A04, MF-A01).
- NCEER-91-0004 "Damping of Structures: Part 1 - Theory of Complex Damping," by Z. Liang and G. Lee, 10/10/91, (PB92-197235, A12, MF-A03).
- NCEER-91-0005 "3D-BASIS - Nonlinear Dynamic Analysis of Three Dimensional Base Isolated Structures: Part II," by S. Nagarajaiah, A.M. Reinhorn and M.C. Constantinou, 2/28/91, (PB91-190553, A07, MF-A01). This report has been replaced by NCEER-93-0011.
- NCEER-91-0006 "A Multidimensional Hysteretic Model for Plasticity Deforming Metals in Energy Absorbing Devices," by E.J. Graesser and F.A. Cozzarelli, 4/9/91, (PB92-108364, A04, MF-A01).
- NCEER-91-0007 "A Framework for Customizable Knowledge-Based Expert Systems with an Application to a KBES for Evaluating the Seismic Resistance of Existing Buildings," by E.G. Ibarra-Anaya and S.J. Fennes, 4/9/91, (PB91-210930, A08, MF-A01).
- NCEER-91-0008 "Nonlinear Analysis of Steel Frames with Semi-Rigid Connections Using the Capacity Spectrum Method," by G.G. Deierlein, S-H. Hsieh, Y-J. Shen and J.F. Abel, 7/2/91, (PB92-113828, A05, MF-A01).
- NCEER-91-0009 "Earthquake Education Materials for Grades K-12," by K.E.K. Ross, 4/30/91, (PB91-212142, A06, MF-A01). This report has been replaced by NCEER-92-0018.
- NCEER-91-0010 "Phase Wave Velocities and Displacement Phase Differences in a Harmonically Oscillating Pile," by N. Makris and G. Gazetas, 7/8/91, (PB92-108356, A04, MF-A01).
- NCEER-91-0011 "Dynamic Characteristics of a Full-Size Five-Story Steel Structure and a 2/5 Scale Model," by K.C. Chang, G.C. Yao, G.C. Lee, D.S. Hao and Y.C. Yeh, 7/2/91, (PB93-116648, A06, MF-A02).
- NCEER-91-0012 "Seismic Response of a 2/5 Scale Steel Structure with Added Viscoelastic Dampers," by K.C. Chang, T.T. Soong, S-T. Oh and M.L. Lai, 5/17/91, (PB92-110816, A05, MF-A01).
- NCEER-91-0013 "Earthquake Response of Retaining Walls; Full-Scale Testing and Computational Modeling," by S. Alampalli and A-W.M. Elgamal, 6/20/91, to be published.
- NCEER-91-0014 "3D-BASIS-M: Nonlinear Dynamic Analysis of Multiple Building Base Isolated Structures," by P.C. Tsopelas, S. Nagarajaiah, M.C. Constantinou and A.M. Reinhorn, 5/28/91, (PB92-113885, A09, MF-A02).
- NCEER-91-0015 "Evaluation of SEAOC Design Requirements for Sliding Isolated Structures," by D. Theodossiou and M.C. Constantinou, 6/10/91, (PB92-114602, A11, MF-A03).
- NCEER-91-0016 "Closed-Loop Modal Testing of a 27-Story Reinforced Concrete Flat Plate-Core Building," by H.R. Somaprasad, T. Toksoy, H. Yoshiyuki and A.E. Aktan, 7/15/91, (PB92-129980, A07, MF-A02).
- NCEER-91-0017 "Shake Table Test of a 1/6 Scale Two-Story Lightly Reinforced Concrete Building," by A.G. El-Attar, R.N. White and P. Gergely, 2/28/91, (PB92-222447, A06, MF-A02).
- NCEER-91-0018 "Shake Table Test of a 1/8 Scale Three-Story Lightly Reinforced Concrete Building," by A.G. El-Attar, R.N. White and P. Gergely, 2/28/91, (PB93-116630, A08, MF-A02).
- NCEER-91-0019 "Transfer Functions for Rigid Rectangular Foundations," by A.S. Veletsos, A.M. Prasad and W.H. Wu, 7/31/91, to be published.

- NCEER-91-0020 "Hybrid Control of Seismic-Excited Nonlinear and Inelastic Structural Systems," by J.N. Yang, Z. Li and A. Daniellians, 8/1/91, (PB92-143171, A06, MF-A02).
- NCEER-91-0021 "The NCEER-91 Earthquake Catalog: Improved Intensity-Based Magnitudes and Recurrence Relations for U.S. Earthquakes East of New Madrid," by L. Seeber and J.G. Armbruster, 8/28/91, (PB92-176742, A06, MF-A02).
- NCEER-91-0022 "Proceedings from the Implementation of Earthquake Planning and Education in Schools: The Need for Change - The Roles of the Changemakers," by K.E.K. Ross and F. Winslow, 7/23/91, (PB92-129998, A12, MF-A03).
- NCEER-91-0023 "A Study of Reliability-Based Criteria for Seismic Design of Reinforced Concrete Frame Buildings," by H.H.M. Hwang and H-M. Hsu, 8/10/91, (PB92-140235, A09, MF-A02).
- NCEER-91-0024 "Experimental Verification of a Number of Structural System Identification Algorithms," by R.G. Ghanem, H. Gavin and M. Shinozuka, 9/18/91, (PB92-176577, A18, MF-A04).
- NCEER-91-0025 "Probabilistic Evaluation of Liquefaction Potential," by H.H.M. Hwang and C.S. Lee, 11/25/91, (PB92-143429, A05, MF-A01).
- NCEER-91-0026 "Instantaneous Optimal Control for Linear, Nonlinear and Hysteretic Structures - Stable Controllers," by J.N. Yang and Z. Li, 11/15/91, (PB92-163807, A04, MF-A01).
- NCEER-91-0027 "Experimental and Theoretical Study of a Sliding Isolation System for Bridges," by M.C. Constantinou, A. Kartoum, A.M. Reinhorn and P. Bradford, 11/15/91, (PB92-176973, A10, MF-A03).
- NCEER-92-0001 "Case Studies of Liquefaction and Lifeline Performance During Past Earthquakes, Volume 1: Japanese Case Studies," Edited by M. Hamada and T. O'Rourke, 2/17/92, (PB92-197243, A18, MF-A04).
- NCEER-92-0002 "Case Studies of Liquefaction and Lifeline Performance During Past Earthquakes, Volume 2: United States Case Studies," Edited by T. O'Rourke and M. Hamada, 2/17/92, (PB92-197250, A20, MF-A04).
- NCEER-92-0003 "Issues in Earthquake Education," Edited by K. Ross, 2/3/92, (PB92-222389, A07, MF-A02).
- NCEER-92-0004 "Proceedings from the First U.S. - Japan Workshop on Earthquake Protective Systems for Bridges," Edited by I.G. Buckle, 2/4/92, (PB94-142239, A99, MF-A06).
- NCEER-92-0005 "Seismic Ground Motion from a Haskell-Type Source in a Multiple-Layered Half-Space," A.P. Theoharis, G. Deodatis and M. Shinozuka, 1/2/92, to be published.
- NCEER-92-0006 "Proceedings from the Site Effects Workshop," Edited by R. Whitman, 2/29/92, (PB92-197201, A04, MF-A01).
- NCEER-92-0007 "Engineering Evaluation of Permanent Ground Deformations Due to Seismically-Induced Liquefaction," by M.H. Baziar, R. Dobry and A-W.M. Elgamel, 3/24/92, (PB92-222421, A13, MF-A03).
- NCEER-92-0008 "A Procedure for the Seismic Evaluation of Buildings in the Central and Eastern United States," by C.D. Poland and J.O. Malley, 4/2/92, (PB92-222439, A20, MF-A04).
- NCEER-92-0009 "Experimental and Analytical Study of a Hybrid Isolation System Using Friction Controllable Sliding Bearings," by M.Q. Feng, S. Fujii and M. Shinozuka, 5/15/92, (PB93-150282, A06, MF-A02).
- NCEER-92-0010 "Seismic Resistance of Slab-Column Connections in Existing Non-Ductile Flat-Plate Buildings," by A.J. Durrani and Y. Du, 5/18/92, (PB93-116812, A06, MF-A02).
- NCEER-92-0011 "The Hysteretic and Dynamic Behavior of Brick Masonry Walls Upgraded by Ferrocement Coatings Under Cyclic Loading and Strong Simulated Ground Motion," by H. Lee and S.P. Prawl, 5/11/92, to be published.
- NCEER-92-0012 "Study of Wire Rope Systems for Seismic Protection of Equipment in Buildings," by G.F. Demetriades, M.C. Constantinou and A.M. Reinhorn, 5/20/92, (PB93-116655, A08, MF-A02).

- NCEER-92-0013 "Shape Memory Structural Dampers: Material Properties, Design and Seismic Testing," by P.R. Witting and F.A. Cozzarelli, 5/26/92, (PB93-116663, A05, MF-A01).
- NCEER-92-0014 "Longitudinal Permanent Ground Deformation Effects on Buried Continuous Pipelines," by M.J. O'Rourke, and C. Nordberg, 6/15/92, (PB93-116671, A08, MF-A02).
- NCEER-92-0015 "A Simulation Method for Stationary Gaussian Random Functions Based on the Sampling Theorem," by M. Grigoriu and S. Balopoulou, 6/11/92, (PB93-127496, A05, MF-A01).
- NCEER-92-0016 "Gravity-Load-Designed Reinforced Concrete Buildings: Seismic Evaluation of Existing Construction and Detailing Strategies for Improved Seismic Resistance," by G.W. Hoffmann, S.K. Kunnath, A.M. Reinhorn and J.B. Mander, 7/15/92, (PB94-142007, A08, MF-A02).
- NCEER-92-0017 "Observations on Water System and Pipeline Performance in the Limón Area of Costa Rica Due to the April 22, 1991 Earthquake," by M. O'Rourke and D. Ballantyne, 6/30/92, (PB93-126811, A06, MF-A02).
- NCEER-92-0018 "Fourth Edition of Earthquake Education Materials for Grades K-12," Edited by K.E.K. Ross, 8/10/92, (PB93-114023, A07, MF-A02).
- NCEER-92-0019 "Proceedings from the Fourth Japan-U.S. Workshop on Earthquake Resistant Design of Lifeline Facilities and Countermeasures for Soil Liquefaction," Edited by M. Hamada and T.D. O'Rourke, 8/12/92, (PB93-163939, A99, MF-E11).
- NCEER-92-0020 "Active Bracing System: A Full Scale Implementation of Active Control," by A.M. Reinhorn, T.T. Soong, R.C. Lin, M.A. Riley, Y.P. Wang, S. Aizawa and M. Higashino, 8/14/92, (PB93-127512, A06, MF-A02).
- NCEER-92-0021 "Empirical Analysis of Horizontal Ground Displacement Generated by Liquefaction-Induced Lateral Spreads," by S.F. Bartlett and T.L. Youd, 8/17/92, (PB93-188241, A06, MF-A02).
- NCEER-92-0022 "IDARC Version 3.0: Inelastic Damage Analysis of Reinforced Concrete Structures," by S.K. Kunnath, A.M. Reinhorn and R.F. Lobo, 8/31/92, (PB93-227502, A07, MF-A02).
- NCEER-92-0023 "A Semi-Empirical Analysis of Strong-Motion Peaks in Terms of Seismic Source, Propagation Path and Local Site Conditions, by M. Kamiyama, M.J. O'Rourke and R. Flores-Berrones, 9/9/92, (PB93-150266, A08, MF-A02).
- NCEER-92-0024 "Seismic Behavior of Reinforced Concrete Frame Structures with Nonductile Details, Part I: Summary of Experimental Findings of Full Scale Beam-Column Joint Tests," by A. Beres, R.N. White and P. Gergely, 9/30/92, (PB93-227783, A05, MF-A01).
- NCEER-92-0025 "Experimental Results of Repaired and Retrofitted Beam-Column Joint Tests in Lightly Reinforced Concrete Frame Buildings," by A. Beres, S. El-Borgi, R.N. White and P. Gergely, 10/29/92, (PB93-227791, A05, MF-A01).
- NCEER-92-0026 "A Generalization of Optimal Control Theory: Linear and Nonlinear Structures," by J.N. Yang, Z. Li and S. Vongchavalitkul, 11/2/92, (PB93-188621, A05, MF-A01).
- NCEER-92-0027 "Seismic Resistance of Reinforced Concrete Frame Structures Designed Only for Gravity Loads: Part I - Design and Properties of a One-Third Scale Model Structure," by J.M. Bracci, A.M. Reinhorn and J.B. Mander, 12/1/92, (PB94-104502, A08, MF-A02).
- NCEER-92-0028 "Seismic Resistance of Reinforced Concrete Frame Structures Designed Only for Gravity Loads: Part II - Experimental Performance of Subassemblages," by L.E. Aycaardi, J.B. Mander and A.M. Reinhorn, 12/1/92, (PB94-104510, A08, MF-A02).
- NCEER-92-0029 "Seismic Resistance of Reinforced Concrete Frame Structures Designed Only for Gravity Loads: Part III - Experimental Performance and Analytical Study of a Structural Model," by J.M. Bracci, A.M. Reinhorn and J.B. Mander, 12/1/92, (PB93-227528, A09, MF-A01).

- NCEER-92-0030 "Evaluation of Seismic Retrofit of Reinforced Concrete Frame Structures: Part I - Experimental Performance of Retrofitted Subassemblages," by D. Choudhuri, J.B. Mander and A.M. Reinhorn, 12/8/92, (PB93-198307, A07, MF-A02).
- NCEER-92-0031 "Evaluation of Seismic Retrofit of Reinforced Concrete Frame Structures: Part II - Experimental Performance and Analytical Study of a Retrofitted Structural Model," by J.M. Bracci, A.M. Reinhorn and J.B. Mander, 12/8/92, (PB93-198315, A09, MF-A03).
- NCEER-92-0032 "Experimental and Analytical Investigation of Seismic Response of Structures with Supplemental Fluid Viscous Dampers," by M.C. Constantinou and M.D. Symans, 12/21/92, (PB93-191435, A10, MF-A03). This report is available only through NTIS (see address given above).
- NCEER-92-0033 "Reconnaissance Report on the Cairo, Egypt Earthquake of October 12, 1992," by M. Khater, 12/23/92, (PB93-188621, A03, MF-A01).
- NCEER-92-0034 "Low-Level Dynamic Characteristics of Four Tall Flat-Plate Buildings in New York City," by H. Gavin, S. Yuan, J. Grossman, E. Pekelis and K. Jacob, 12/28/92, (PB93-188217, A07, MF-A02).
- NCEER-93-0001 "An Experimental Study on the Seismic Performance of Brick-Infilled Steel Frames With and Without Retrofit," by J.B. Mander, B. Nair, K. Wojtkowski and J. Ma, 1/29/93, (PB93-227510, A07, MF-A02).
- NCEER-93-0002 "Social Accounting for Disaster Preparedness and Recovery Planning," by S. Cole, E. Pantoja and V. Razak, 2/22/93, (PB94-142114, A12, MF-A03).
- NCEER-93-0003 "Assessment of 1991 NEHRP Provisions for Nonstructural Components and Recommended Revisions," by T.T. Soong, G. Chen, Z. Wu, R-H. Zhang and M. Grigoriu, 3/1/93, (PB93-188639, A06, MF-A02).
- NCEER-93-0004 "Evaluation of Static and Response Spectrum Analysis Procedures of SEAOC/UBC for Seismic Isolated Structures," by C.W. Winters and M.C. Constantinou, 3/23/93, (PB93-198299, A10, MF-A03).
- NCEER-93-0005 "Earthquakes in the Northeast - Are We Ignoring the Hazard? A Workshop on Earthquake Science and Safety for Educators," edited by K.E.K. Ross, 4/2/93, (PB94-103066, A09, MF-A02).
- NCEER-93-0006 "Inelastic Response of Reinforced Concrete Structures with Viscoelastic Braces," by R.F. Lobo, J.M. Bracci, K.L. Shen, A.M. Reinhorn and T.T. Soong, 4/5/93, (PB93-227486, A05, MF-A02).
- NCEER-93-0007 "Seismic Testing of Installation Methods for Computers and Data Processing Equipment," by K. Kosar, T.T. Soong, K.L. Shen, J.A. HoLung and Y.K. Lin, 4/12/93, (PB93-198299, A07, MF-A02).
- NCEER-93-0008 "Retrofit of Reinforced Concrete Frames Using Added Dampers," by A. Reinhorn, M. Constantinou and C. Li, to be published.
- NCEER-93-0009 "Seismic Behavior and Design Guidelines for Steel Frame Structures with Added Viscoelastic Dampers," by K.C. Chang, M.L. Lai, T.T. Soong, D.S. Hao and Y.C. Yeh, 5/1/93, (PB94-141959, A07, MF-A02).
- NCEER-93-0010 "Seismic Performance of Shear-Critical Reinforced Concrete Bridge Piers," by J.B. Mander, S.M. Waheed, M.T.A. Chaudhary and S.S. Chen, 5/12/93, (PB93-227494, A08, MF-A02).
- NCEER-93-0011 "3D-BASIS-TABS: Computer Program for Nonlinear Dynamic Analysis of Three Dimensional Base Isolated Structures," by S. Nagarajaiah, C. Li, A.M. Reinhorn and M.C. Constantinou, 8/2/93, (PB94-141819, A09, MF-A02).
- NCEER-93-0012 "Effects of Hydrocarbon Spills from an Oil Pipeline Break on Ground Water," by O.J. Helweg and H.H.M. Hwang, 8/3/93, (PB94-141942, A06, MF-A02).
- NCEER-93-0013 "Simplified Procedures for Seismic Design of Nonstructural Components and Assessment of Current Code Provisions," by M.P. Singh, L.E. Suarez, E.E. Matheu and G.O. Maldonado, 8/4/93, (PB94-141827, A09, MF-A02).
- NCEER-93-0014 "An Energy Approach to Seismic Analysis and Design of Secondary Systems," by G. Chen and T.T. Soong, 8/6/93, (PB94-142767, A11, MF-A03).

- NCEER-93-0015 "Proceedings from School Sites: Becoming Prepared for Earthquakes - Commemorating the Third Anniversary of the Loma Prieta Earthquake," Edited by F.E. Winslow and K.E.K. Ross, 8/16/93, (PB94-154275, A16, MF-A02).
- NCEER-93-0016 "Reconnaissance Report of Damage to Historic Monuments in Cairo, Egypt Following the October 12, 1992 Dahshur Earthquake," by D. Sykora, D. Look, G. Croci, E. Karaesmen and E. Karaesmen, 8/19/93, (PB94-142221, A08, MF-A02).
- NCEER-93-0017 "The Island of Guam Earthquake of August 8, 1993," by S.W. Swan and S.K. Harris, 9/30/93, (PB94-141843, A04, MF-A01).
- NCEER-93-0018 "Engineering Aspects of the October 12, 1992 Egyptian Earthquake," by A.W. Elgamal, M. Amer, K. Adalier and A. Abul-Fadl, 10/7/93, (PB94-141983, A05, MF-A01).
- NCEER-93-0019 "Development of an Earthquake Motion Simulator and its Application in Dynamic Centrifuge Testing," by I. Krstelj, Supervised by J.H. Prevost, 10/23/93, (PB94-181773, A-10, MF-A03).
- NCEER-93-0020 "NCEER-Taisei Corporation Research Program on Sliding Seismic Isolation Systems for Bridges: Experimental and Analytical Study of a Friction Pendulum System (FPS)," by M.C. Constantinou, P. Tsopelas, Y-S. Kim and S. Okamoto, 11/1/93, (PB94-142775, A08, MF-A02).
- NCEER-93-0021 "Finite Element Modeling of Elastomeric Seismic Isolation Bearings," by L.J. Billings, Supervised by R. Shepherd, 11/8/93, to be published.
- NCEER-93-0022 "Seismic Vulnerability of Equipment in Critical Facilities: Life-Safety and Operational Consequences," by K. Porter, G.S. Johnson, M.M. Zadeh, C. Scawthorn and S. Eder, 11/24/93, (PB94-181765, A16, MF-A03).
- NCEER-93-0023 "Hokkaido Nansei-oki, Japan Earthquake of July 12, 1993, by P.I. Yanev and C.R. Scawthorn, 12/23/93, (PB94-181500, A07, MF-A01).
- NCEER-94-0001 "An Evaluation of Seismic Serviceability of Water Supply Networks with Application to the San Francisco Auxiliary Water Supply System," by I. Markov, Supervised by M. Grigoriu and T. O'Rourke, 1/21/94, (PB94-204013, A07, MF-A02).
- NCEER-94-0002 "NCEER-Taisei Corporation Research Program on Sliding Seismic Isolation Systems for Bridges: Experimental and Analytical Study of Systems Consisting of Sliding Bearings, Rubber Restoring Force Devices and Fluid Dampers," Volumes I and II, by P. Tsopelas, S. Okamoto, M.C. Constantinou, D. Ozaki and S. Fujii, 2/4/94, (PB94-181740, A09, MF-A02 and PB94-181757, A12, MF-A03).
- NCEER-94-0003 "A Markov Model for Local and Global Damage Indices in Seismic Analysis," by S. Rahman and M. Grigoriu, 2/18/94, (PB94-206000, A12, MF-A03).
- NCEER-94-0004 "Proceedings from the NCEER Workshop on Seismic Response of Masonry Infills," edited by D.P. Abrams, 3/1/94, (PB94-180783, A07, MF-A02).
- NCEER-94-0005 "The Northridge, California Earthquake of January 17, 1994: General Reconnaissance Report," edited by J.D. Goltz, 3/11/94, (PB94-193943, A10, MF-A03).
- NCEER-94-0006 "Seismic Energy Based Fatigue Damage Analysis of Bridge Columns: Part I - Evaluation of Seismic Capacity," by G.A. Chang and J.B. Mander, 3/14/94, (PB94-219185, A11, MF-A03).
- NCEER-94-0007 "Seismic Isolation of Multi-Story Frame Structures Using Spherical Sliding Isolation Systems," by T.M. Al-Hussaini, V.A. Zayas and M.C. Constantinou, 3/17/94, (PB94-193745, A09, MF-A02).
- NCEER-94-0008 "The Northridge, California Earthquake of January 17, 1994: Performance of Highway Bridges," edited by I.G. Buckle, 3/24/94, (PB94-193851, A06, MF-A02).
- NCEER-94-0009 "Proceedings of the Third U.S.-Japan Workshop on Earthquake Protective Systems for Bridges," edited by I.G. Buckle and I. Friedland, 3/31/94, (PB94-195815, A99, MF-A06).

- NCEER-94-0010 "3D-BASIS-ME: Computer Program for Nonlinear Dynamic Analysis of Seismically Isolated Single and Multiple Structures and Liquid Storage Tanks," by P.C. Tsopelas, M.C. Constantinou and A.M. Reinhorn, 4/12/94, (PB94-204922, A09, MF-A02).
- NCEER-94-0011 "The Northridge, California Earthquake of January 17, 1994: Performance of Gas Transmission Pipelines," by T.D. O'Rourke and M.C. Palmer, 5/16/94, (PB94-204989, A05, MF-A01).
- NCEER-94-0012 "Feasibility Study of Replacement Procedures and Earthquake Performance Related to Gas Transmission Pipelines," by T.D. O'Rourke and M.C. Palmer, 5/25/94, (PB94-206638, A09, MF-A02).
- NCEER-94-0013 "Seismic Energy Based Fatigue Damage Analysis of Bridge Columns: Part II - Evaluation of Seismic Demand," by G.A. Chang and J.B. Mander, 6/1/94, (PB95-18106, A08, MF-A02).
- NCEER-94-0014 "NCEER-Taisei Corporation Research Program on Sliding Seismic Isolation Systems for Bridges: Experimental and Analytical Study of a System Consisting of Sliding Bearings and Fluid Restoring Force/Damping Devices," by P. Tsopelas and M.C. Constantinou, 6/13/94, (PB94-219144, A10, MF-A03).
- NCEER-94-0015 "Generation of Hazard-Consistent Fragility Curves for Seismic Loss Estimation Studies," by H. Hwang and J-R. Huo, 6/14/94, (PB95-181996, A09, MF-A02).
- NCEER-94-0016 "Seismic Study of Building Frames with Added Energy-Absorbing Devices," by W.S. Pong, C.S. Tsai and G.C. Lee, 6/20/94, (PB94-219136, A10, A03).
- NCEER-94-0017 "Sliding Mode Control for Seismic-Excited Linear and Nonlinear Civil Engineering Structures," by J. Yang, J. Wu, A. Agrawal and Z. Li, 6/21/94, (PB95-138483, A06, MF-A02).
- NCEER-94-0018 "3D-BASIS-TABS Version 2.0: Computer Program for Nonlinear Dynamic Analysis of Three Dimensional Base Isolated Structures," by A.M. Reinhorn, S. Nagarajaiah, M.C. Constantinou, P. Tsopelas and R. Li, 6/22/94, (PB95-182176, A08, MF-A02).
- NCEER-94-0019 "Proceedings of the International Workshop on Civil Infrastructure Systems: Application of Intelligent Systems and Advanced Materials on Bridge Systems," Edited by G.C. Lee and K.C. Chang, 7/18/94, (PB95-252474, A20, MF-A04).
- NCEER-94-0020 "Study of Seismic Isolation Systems for Computer Floors," by V. Lambrou and M.C. Constantinou, 7/19/94, (PB95-138533, A10, MF-A03).
- NCEER-94-0021 "Proceedings of the U.S.-Italian Workshop on Guidelines for Seismic Evaluation and Rehabilitation of Unreinforced Masonry Buildings," Edited by D.P. Abrams and G.M. Calvi, 7/20/94, (PB95-138749, A13, MF-A03).
- NCEER-94-0022 "NCEER-Taisei Corporation Research Program on Sliding Seismic Isolation Systems for Bridges: Experimental and Analytical Study of a System Consisting of Lubricated PTFE Sliding Bearings and Mild Steel Dampers," by P. Tsopelas and M.C. Constantinou, 7/22/94, (PB95-182184, A08, MF-A02).
- NCEER-94-0023 "Development of Reliability-Based Design Criteria for Buildings Under Seismic Load," by Y.K. Wen, H. Hwang and M. Shinozuka, 8/1/94, (PB95-211934, A08, MF-A02).
- NCEER-94-0024 "Experimental Verification of Acceleration Feedback Control Strategies for an Active Tendon System," by S.J. Dyke, B.F. Spencer, Jr., P. Quast, M.K. Sain, D.C. Kaspari, Jr. and T.T. Soong, 8/29/94, (PB95-212320, A05, MF-A01).
- NCEER-94-0025 "Seismic Retrofitting Manual for Highway Bridges," Edited by I.G. Buckle and I.F. Friedland, published by the Federal Highway Administration (PB95-212676, A15, MF-A03).
- NCEER-94-0026 "Proceedings from the Fifth U.S.-Japan Workshop on Earthquake Resistant Design of Lifeline Facilities and Countermeasures Against Soil Liquefaction," Edited by T.D. O'Rourke and M. Hamada, 11/7/94, (PB95-220802, A99, MF-E08).

- NCEER-95-0001 “Experimental and Analytical Investigation of Seismic Retrofit of Structures with Supplemental Damping: Part 1 - Fluid Viscous Damping Devices,” by A.M. Reinhorn, C. Li and M.C. Constantinou, 1/3/95, (PB95-266599, A09, MF-A02).
- NCEER-95-0002 “Experimental and Analytical Study of Low-Cycle Fatigue Behavior of Semi-Rigid Top-And-Seat Angle Connections,” by G. Pekcan, J.B. Mander and S.S. Chen, 1/5/95, (PB95-220042, A07, MF-A02).
- NCEER-95-0003 “NCEER-ATC Joint Study on Fragility of Buildings,” by T. Anagnos, C. Rojahn and A.S. Kiremidjian, 1/20/95, (PB95-220026, A06, MF-A02).
- NCEER-95-0004 “Nonlinear Control Algorithms for Peak Response Reduction,” by Z. Wu, T.T. Soong, V. Gattulli and R.C. Lin, 2/16/95, (PB95-220349, A05, MF-A01).
- NCEER-95-0005 “Pipeline Replacement Feasibility Study: A Methodology for Minimizing Seismic and Corrosion Risks to Underground Natural Gas Pipelines,” by R.T. Eguchi, H.A. Seligson and D.G. Honegger, 3/2/95, (PB95-252326, A06, MF-A02).
- NCEER-95-0006 “Evaluation of Seismic Performance of an 11-Story Frame Building During the 1994 Northridge Earthquake,” by F. Naeim, R. DiSulio, K. Benuska, A. Reinhorn and C. Li, to be published.
- NCEER-95-0007 “Prioritization of Bridges for Seismic Retrofitting,” by N. Basöz and A.S. Kiremidjian, 4/24/95, (PB95-252300, A08, MF-A02).
- NCEER-95-0008 “Method for Developing Motion Damage Relationships for Reinforced Concrete Frames,” by A. Singhal and A.S. Kiremidjian, 5/11/95, (PB95-266607, A06, MF-A02).
- NCEER-95-0009 “Experimental and Analytical Investigation of Seismic Retrofit of Structures with Supplemental Damping: Part II - Friction Devices,” by C. Li and A.M. Reinhorn, 7/6/95, (PB96-128087, A11, MF-A03).
- NCEER-95-0010 “Experimental Performance and Analytical Study of a Non-Ductile Reinforced Concrete Frame Structure Retrofitted with Elastomeric Spring Dampers,” by G. Pekcan, J.B. Mander and S.S. Chen, 7/14/95, (PB96-137161, A08, MF-A02).
- NCEER-95-0011 “Development and Experimental Study of Semi-Active Fluid Damping Devices for Seismic Protection of Structures,” by M.D. Symans and M.C. Constantinou, 8/3/95, (PB96-136940, A23, MF-A04).
- NCEER-95-0012 “Real-Time Structural Parameter Modification (RSPM): Development of Innervated Structures,” by Z. Liang, M. Tong and G.C. Lee, 4/11/95, (PB96-137153, A06, MF-A01).
- NCEER-95-0013 “Experimental and Analytical Investigation of Seismic Retrofit of Structures with Supplemental Damping: Part III - Viscous Damping Walls,” by A.M. Reinhorn and C. Li, 10/1/95, (PB96-176409, A11, MF-A03).
- NCEER-95-0014 “Seismic Fragility Analysis of Equipment and Structures in a Memphis Electric Substation,” by J-R. Huo and H.H.M. Hwang, 8/10/95, (PB96-128087, A09, MF-A02).
- NCEER-95-0015 “The Hanshin-Awaji Earthquake of January 17, 1995: Performance of Lifelines,” Edited by M. Shinozuka, 11/3/95, (PB96-176383, A15, MF-A03).
- NCEER-95-0016 “Highway Culvert Performance During Earthquakes,” by T.L. Youd and C.J. Beckman, available as NCEER-96-0015.
- NCEER-95-0017 “The Hanshin-Awaji Earthquake of January 17, 1995: Performance of Highway Bridges,” Edited by I.G. Buckle, 12/1/95, to be published.
- NCEER-95-0018 “Modeling of Masonry Infill Panels for Structural Analysis,” by A.M. Reinhorn, A. Madan, R.E. Valles, Y. Reichmann and J.B. Mander, 12/8/95, (PB97-110886, MF-A01, A06).
- NCEER-95-0019 “Optimal Polynomial Control for Linear and Nonlinear Structures,” by A.K. Agrawal and J.N. Yang, 12/11/95, (PB96-168737, A07, MF-A02).

- NCEER-95-0020 "Retrofit of Non-Ductile Reinforced Concrete Frames Using Friction Dampers," by R.S. Rao, P. Gergely and R.N. White, 12/22/95, (PB97-133508, A10, MF-A02).
- NCEER-95-0021 "Parametric Results for Seismic Response of Pile-Supported Bridge Bents," by G. Mylonakis, A. Nikolaou and G. Gazetas, 12/22/95, (PB97-100242, A12, MF-A03).
- NCEER-95-0022 "Kinematic Bending Moments in Seismically Stressed Piles," by A. Nikolaou, G. Mylonakis and G. Gazetas, 12/23/95, (PB97-113914, MF-A03, A13).
- NCEER-96-0001 "Dynamic Response of Unreinforced Masonry Buildings with Flexible Diaphragms," by A.C. Costley and D.P. Abrams, 10/10/96, (PB97-133573, MF-A03, A15).
- NCEER-96-0002 "State of the Art Review: Foundations and Retaining Structures," by I. Po Lam, to be published.
- NCEER-96-0003 "Ductility of Rectangular Reinforced Concrete Bridge Columns with Moderate Confinement," by N. Wehbe, M. Saiidi, D. Sanders and B. Douglas, 11/7/96, (PB97-133557, A06, MF-A02).
- NCEER-96-0004 "Proceedings of the Long-Span Bridge Seismic Research Workshop," edited by I.G. Buckle and I.M. Friedland, to be published.
- NCEER-96-0005 "Establish Representative Pier Types for Comprehensive Study: Eastern United States," by J. Kulicki and Z. Prucz, 5/28/96, (PB98-119217, A07, MF-A02).
- NCEER-96-0006 "Establish Representative Pier Types for Comprehensive Study: Western United States," by R. Imbsen, R.A. Schamber and T.A. Osterkamp, 5/28/96, (PB98-118607, A07, MF-A02).
- NCEER-96-0007 "Nonlinear Control Techniques for Dynamical Systems with Uncertain Parameters," by R.G. Ghanem and M.I. Bujakov, 5/27/96, (PB97-100259, A17, MF-A03).
- NCEER-96-0008 "Seismic Evaluation of a 30-Year Old Non-Ductile Highway Bridge Pier and Its Retrofit," by J.B. Mander, B. Mahmoodzadegan, S. Bhadra and S.S. Chen, 5/31/96, (PB97-110902, MF-A03, A10).
- NCEER-96-0009 "Seismic Performance of a Model Reinforced Concrete Bridge Pier Before and After Retrofit," by J.B. Mander, J.H. Kim and C.A. Ligozio, 5/31/96, (PB97-110910, MF-A02, A10).
- NCEER-96-0010 "IDARC2D Version 4.0: A Computer Program for the Inelastic Damage Analysis of Buildings," by R.E. Valles, A.M. Reinhorn, S.K. Kunnath, C. Li and A. Madan, 6/3/96, (PB97-100234, A17, MF-A03).
- NCEER-96-0011 "Estimation of the Economic Impact of Multiple Lifeline Disruption: Memphis Light, Gas and Water Division Case Study," by S.E. Chang, H.A. Seligson and R.T. Eguchi, 8/16/96, (PB97-133490, A11, MF-A03).
- NCEER-96-0012 "Proceedings from the Sixth Japan-U.S. Workshop on Earthquake Resistant Design of Lifeline Facilities and Countermeasures Against Soil Liquefaction, Edited by M. Hamada and T. O'Rourke, 9/11/96, (PB97-133581, A99, MF-A06).
- NCEER-96-0013 "Chemical Hazards, Mitigation and Preparedness in Areas of High Seismic Risk: A Methodology for Estimating the Risk of Post-Earthquake Hazardous Materials Release," by H.A. Seligson, R.T. Eguchi, K.J. Tierney and K. Richmond, 11/7/96, (PB97-133565, MF-A02, A08).
- NCEER-96-0014 "Response of Steel Bridge Bearings to Reversed Cyclic Loading," by J.B. Mander, D-K. Kim, S.S. Chen and G.J. Premus, 11/13/96, (PB97-140735, A12, MF-A03).
- NCEER-96-0015 "Highway Culvert Performance During Past Earthquakes," by T.L. Youd and C.J. Beckman, 11/25/96, (PB97-133532, A06, MF-A01).
- NCEER-97-0001 "Evaluation, Prevention and Mitigation of Pounding Effects in Building Structures," by R.E. Valles and A.M. Reinhorn, 2/20/97, (PB97-159552, A14, MF-A03).
- NCEER-97-0002 "Seismic Design Criteria for Bridges and Other Highway Structures," by C. Rojahn, R. Mayes, D.G. Anderson, J. Clark, J.H. Hom, R.V. Nutt and M.J. O'Rourke, 4/30/97, (PB97-194658, A06, MF-A03).

- NCEER-97-0003 "Proceedings of the U.S.-Italian Workshop on Seismic Evaluation and Retrofit," Edited by D.P. Abrams and G.M. Calvi, 3/19/97, (PB97-194666, A13, MF-A03).
- NCEER-97-0004 "Investigation of Seismic Response of Buildings with Linear and Nonlinear Fluid Viscous Dampers," by A.A. Seleemah and M.C. Constantinou, 5/21/97, (PB98-109002, A15, MF-A03).
- NCEER-97-0005 "Proceedings of the Workshop on Earthquake Engineering Frontiers in Transportation Facilities," edited by G.C. Lee and I.M. Friedland, 8/29/97, (PB98-128911, A25, MR-A04).
- NCEER-97-0006 "Cumulative Seismic Damage of Reinforced Concrete Bridge Piers," by S.K. Kunnath, A. El-Bahy, A. Taylor and W. Stone, 9/2/97, (PB98-108814, A11, MF-A03).
- NCEER-97-0007 "Structural Details to Accommodate Seismic Movements of Highway Bridges and Retaining Walls," by R.A. Imbsen, R.A. Schamber, E. Thorkildsen, A. Kartoum, B.T. Martin, T.N. Rosser and J.M. Kulicki, 9/3/97, (PB98-108996, A09, MF-A02).
- NCEER-97-0008 "A Method for Earthquake Motion-Damage Relationships with Application to Reinforced Concrete Frames," by A. Singhal and A.S. Kiremidjian, 9/10/97, (PB98-108988, A13, MF-A03).
- NCEER-97-0009 "Seismic Analysis and Design of Bridge Abutments Considering Sliding and Rotation," by K. Fishman and R. Richards, Jr., 9/15/97, (PB98-108897, A06, MF-A02).
- NCEER-97-0010 "Proceedings of the FHWA/NCEER Workshop on the National Representation of Seismic Ground Motion for New and Existing Highway Facilities," edited by I.M. Friedland, M.S. Power and R.L. Mayes, 9/22/97, (PB98-128903, A21, MF-A04).
- NCEER-97-0011 "Seismic Analysis for Design or Retrofit of Gravity Bridge Abutments," by K.L. Fishman, R. Richards, Jr. and R.C. Divito, 10/2/97, (PB98-128937, A08, MF-A02).
- NCEER-97-0012 "Evaluation of Simplified Methods of Analysis for Yielding Structures," by P. Tsopelas, M.C. Constantinou, C.A. Kircher and A.S. Whittaker, 10/31/97, (PB98-128929, A10, MF-A03).
- NCEER-97-0013 "Seismic Design of Bridge Columns Based on Control and Repairability of Damage," by C-T. Cheng and J.B. Mander, 12/8/97, (PB98-144249, A11, MF-A03).
- NCEER-97-0014 "Seismic Resistance of Bridge Piers Based on Damage Avoidance Design," by J.B. Mander and C-T. Cheng, 12/10/97, (PB98-144223, A09, MF-A02).
- NCEER-97-0015 "Seismic Response of Nominally Symmetric Systems with Strength Uncertainty," by S. Balopoulou and M. Grigoriu, 12/23/97, (PB98-153422, A11, MF-A03).
- NCEER-97-0016 "Evaluation of Seismic Retrofit Methods for Reinforced Concrete Bridge Columns," by T.J. Wipf, F.W. Klaiber and F.M. Russo, 12/28/97, (PB98-144215, A12, MF-A03).
- NCEER-97-0017 "Seismic Fragility of Existing Conventional Reinforced Concrete Highway Bridges," by C.L. Mullen and A.S. Cakmak, 12/30/97, (PB98-153406, A08, MF-A02).
- NCEER-97-0018 "Loss Assessment of Memphis Buildings," edited by D.P. Abrams and M. Shinozuka, 12/31/97, (PB98-144231, A13, MF-A03).
- NCEER-97-0019 "Seismic Evaluation of Frames with Infill Walls Using Quasi-static Experiments," by K.M. Mosalam, R.N. White and P. Gergely, 12/31/97, (PB98-153455, A07, MF-A02).
- NCEER-97-0020 "Seismic Evaluation of Frames with Infill Walls Using Pseudo-dynamic Experiments," by K.M. Mosalam, R.N. White and P. Gergely, 12/31/97, (PB98-153430, A07, MF-A02).
- NCEER-97-0021 "Computational Strategies for Frames with Infill Walls: Discrete and Smeared Crack Analyses and Seismic Fragility," by K.M. Mosalam, R.N. White and P. Gergely, 12/31/97, (PB98-153414, A10, MF-A02).

- NCEER-97-0022 "Proceedings of the NCEER Workshop on Evaluation of Liquefaction Resistance of Soils," edited by T.L. Youd and I.M. Idriss, 12/31/97, (PB98-155617, A15, MF-A03).
- MCEER-98-0001 "Extraction of Nonlinear Hysteretic Properties of Seismically Isolated Bridges from Quick-Release Field Tests," by Q. Chen, B.M. Douglas, E.M. Maragakis and I.G. Buckle, 5/26/98, (PB99-118838, A06, MF-A01).
- MCEER-98-0002 "Methodologies for Evaluating the Importance of Highway Bridges," by A. Thomas, S. Eshenaur and J. Kulicki, 5/29/98, (PB99-118846, A10, MF-A02).
- MCEER-98-0003 "Capacity Design of Bridge Piers and the Analysis of Overstrength," by J.B. Mander, A. Dutta and P. Goel, 6/1/98, (PB99-118853, A09, MF-A02).
- MCEER-98-0004 "Evaluation of Bridge Damage Data from the Loma Prieta and Northridge, California Earthquakes," by N. Basoz and A. Kiremidjian, 6/2/98, (PB99-118861, A15, MF-A03).
- MCEER-98-0005 "Screening Guide for Rapid Assessment of Liquefaction Hazard at Highway Bridge Sites," by T. L. Youd, 6/16/98, (PB99-118879, A06, not available on microfiche).
- MCEER-98-0006 "Structural Steel and Steel/Concrete Interface Details for Bridges," by P. Ritchie, N. Kauh and J. Kulicki, 7/13/98, (PB99-118945, A06, MF-A01).
- MCEER-98-0007 "Capacity Design and Fatigue Analysis of Confined Concrete Columns," by A. Dutta and J.B. Mander, 7/14/98, (PB99-118960, A14, MF-A03).
- MCEER-98-0008 "Proceedings of the Workshop on Performance Criteria for Telecommunication Services Under Earthquake Conditions," edited by A.J. Schiff, 7/15/98, (PB99-118952, A08, MF-A02).
- MCEER-98-0009 "Fatigue Analysis of Unconfined Concrete Columns," by J.B. Mander, A. Dutta and J.H. Kim, 9/12/98, (PB99-123655, A10, MF-A02).
- MCEER-98-0010 "Centrifuge Modeling of Cyclic Lateral Response of Pile-Cap Systems and Seat-Type Abutments in Dry Sands," by A.D. Gadre and R. Dobry, 10/2/98, (PB99-123606, A13, MF-A03).
- MCEER-98-0011 "IDARC-BRIDGE: A Computational Platform for Seismic Damage Assessment of Bridge Structures," by A.M. Reinhorn, V. Simeonov, G. Mylonakis and Y. Reichman, 10/2/98, (PB99-162919, A15, MF-A03).
- MCEER-98-0012 "Experimental Investigation of the Dynamic Response of Two Bridges Before and After Retrofitting with Elastomeric Bearings," by D.A. Wendichansky, S.S. Chen and J.B. Mander, 10/2/98, (PB99-162927, A15, MF-A03).
- MCEER-98-0013 "Design Procedures for Hinge Restrainers and Hinge Sear Width for Multiple-Frame Bridges," by R. Des Roches and G.L. Fenves, 11/3/98, (PB99-140477, A13, MF-A03).
- MCEER-98-0014 "Response Modification Factors for Seismically Isolated Bridges," by M.C. Constantinou and J.K. Quarshie, 11/3/98, (PB99-140485, A14, MF-A03).
- MCEER-98-0015 "Proceedings of the U.S.-Italy Workshop on Seismic Protective Systems for Bridges," edited by I.M. Friedland and M.C. Constantinou, 11/3/98, (PB2000-101711, A22, MF-A04).
- MCEER-98-0016 "Appropriate Seismic Reliability for Critical Equipment Systems: Recommendations Based on Regional Analysis of Financial and Life Loss," by K. Porter, C. Scawthorn, C. Taylor and N. Blais, 11/10/98, (PB99-157265, A08, MF-A02).
- MCEER-98-0017 "Proceedings of the U.S. Japan Joint Seminar on Civil Infrastructure Systems Research," edited by M. Shinozuka and A. Rose, 11/12/98, (PB99-156713, A16, MF-A03).
- MCEER-98-0018 "Modeling of Pile Footings and Drilled Shafts for Seismic Design," by I. PoLam, M. Kapuskar and D. Chaudhuri, 12/21/98, (PB99-157257, A09, MF-A02).

- MCEER-99-0001 "Seismic Evaluation of a Masonry Infilled Reinforced Concrete Frame by Pseudodynamic Testing," by S.G. Buonopane and R.N. White, 2/16/99, (PB99-162851, A09, MF-A02).
- MCEER-99-0002 "Response History Analysis of Structures with Seismic Isolation and Energy Dissipation Systems: Verification Examples for Program SAP2000," by J. Scheller and M.C. Constantinou, 2/22/99, (PB99-162869, A08, MF-A02).
- MCEER-99-0003 "Experimental Study on the Seismic Design and Retrofit of Bridge Columns Including Axial Load Effects," by A. Dutta, T. Kokorina and J.B. Mander, 2/22/99, (PB99-162877, A09, MF-A02).
- MCEER-99-0004 "Experimental Study of Bridge Elastomeric and Other Isolation and Energy Dissipation Systems with Emphasis on Uplift Prevention and High Velocity Near-source Seismic Excitation," by A. Kasalanati and M. C. Constantinou, 2/26/99, (PB99-162885, A12, MF-A03).
- MCEER-99-0005 "Truss Modeling of Reinforced Concrete Shear-flexure Behavior," by J.H. Kim and J.B. Mander, 3/8/99, (PB99-163693, A12, MF-A03).
- MCEER-99-0006 "Experimental Investigation and Computational Modeling of Seismic Response of a 1:4 Scale Model Steel Structure with a Load Balancing Supplemental Damping System," by G. Pekcan, J.B. Mander and S.S. Chen, 4/2/99, (PB99-162893, A11, MF-A03).
- MCEER-99-0007 "Effect of Vertical Ground Motions on the Structural Response of Highway Bridges," by M.R. Button, C.J. Cronin and R.L. Mayes, 4/10/99, (PB2000-101411, A10, MF-A03).
- MCEER-99-0008 "Seismic Reliability Assessment of Critical Facilities: A Handbook, Supporting Documentation, and Model Code Provisions," by G.S. Johnson, R.E. Sheppard, M.D. Quilici, S.J. Eder and C.R. Scawthorn, 4/12/99, (PB2000-101701, A18, MF-A04).
- MCEER-99-0009 "Impact Assessment of Selected MCEER Highway Project Research on the Seismic Design of Highway Structures," by C. Rojahn, R. Mayes, D.G. Anderson, J.H. Clark, D'Appolonia Engineering, S. Gloyd and R.V. Nutt, 4/14/99, (PB99-162901, A10, MF-A02).
- MCEER-99-0010 "Site Factors and Site Categories in Seismic Codes," by R. Dobry, R. Ramos and M.S. Power, 7/19/99, (PB2000-101705, A08, MF-A02).
- MCEER-99-0011 "Restrainer Design Procedures for Multi-Span Simply-Supported Bridges," by M.J. Randall, M. Saiidi, E. Maragakis and T. Isakovic, 7/20/99, (PB2000-101702, A10, MF-A02).
- MCEER-99-0012 "Property Modification Factors for Seismic Isolation Bearings," by M.C. Constantinou, P. Tsopelas, A. Kasalanati and E. Wolff, 7/20/99, (PB2000-103387, A11, MF-A03).
- MCEER-99-0013 "Critical Seismic Issues for Existing Steel Bridges," by P. Ritchie, N. Kauh and J. Kulicki, 7/20/99, (PB2000-101697, A09, MF-A02).
- MCEER-99-0014 "Nonstructural Damage Database," by A. Kao, T.T. Soong and A. Vender, 7/24/99, (PB2000-101407, A06, MF-A01).
- MCEER-99-0015 "Guide to Remedial Measures for Liquefaction Mitigation at Existing Highway Bridge Sites," by H.G. Cooke and J. K. Mitchell, 7/26/99, (PB2000-101703, A11, MF-A03).
- MCEER-99-0016 "Proceedings of the MCEER Workshop on Ground Motion Methodologies for the Eastern United States," edited by N. Abrahamson and A. Becker, 8/11/99, (PB2000-103385, A07, MF-A02).
- MCEER-99-0017 "Quindío, Colombia Earthquake of January 25, 1999: Reconnaissance Report," by A.P. Asfura and P.J. Flores, 10/4/99, (PB2000-106893, A06, MF-A01).
- MCEER-99-0018 "Hysteretic Models for Cyclic Behavior of Deteriorating Inelastic Structures," by M.V. Sivaselvan and A.M. Reinhorn, 11/5/99, (PB2000-103386, A08, MF-A02).

- MCEER-99-0019 "Proceedings of the 7<sup>th</sup> U.S.- Japan Workshop on Earthquake Resistant Design of Lifeline Facilities and Countermeasures Against Soil Liquefaction," edited by T.D. O'Rourke, J.P. Bardet and M. Hamada, 11/19/99, (PB2000-103354, A99, MF-A06).
- MCEER-99-0020 "Development of Measurement Capability for Micro-Vibration Evaluations with Application to Chip Fabrication Facilities," by G.C. Lee, Z. Liang, J.W. Song, J.D. Shen and W.C. Liu, 12/1/99, (PB2000-105993, A08, MF-A02).
- MCEER-99-0021 "Design and Retrofit Methodology for Building Structures with Supplemental Energy Dissipating Systems," by G. Pekcan, J.B. Mander and S.S. Chen, 12/31/99, (PB2000-105994, A11, MF-A03).
- MCEER-00-0001 "The Marmara, Turkey Earthquake of August 17, 1999: Reconnaissance Report," edited by C. Scawthorn; with major contributions by M. Bruneau, R. Eguchi, T. Holzer, G. Johnson, J. Mander, J. Mitchell, W. Mitchell, A. Papageorgiou, C. Scaethorn, and G. Webb, 3/23/00, (PB2000-106200, A11, MF-A03).
- MCEER-00-0002 "Proceedings of the MCEER Workshop for Seismic Hazard Mitigation of Health Care Facilities," edited by G.C. Lee, M. Ettouney, M. Grigoriu, J. Hauer and J. Nigg, 3/29/00, (PB2000-106892, A08, MF-A02).
- MCEER-00-0003 "The Chi-Chi, Taiwan Earthquake of September 21, 1999: Reconnaissance Report," edited by G.C. Lee and C.H. Loh, with major contributions by G.C. Lee, M. Bruneau, I.G. Buckle, S.E. Chang, P.J. Flores, T.D. O'Rourke, M. Shinozuka, T.T. Soong, C-H. Loh, K-C. Chang, Z-J. Chen, J-S. Hwang, M-L. Lin, G-Y. Liu, K-C. Tsai, G.C. Yao and C-L. Yen, 4/30/00, (PB2001-100980, A10, MF-A02).
- MCEER-00-0004 "Seismic Retrofit of End-Sway Frames of Steel Deck-Truss Bridges with a Supplemental Tendon System: Experimental and Analytical Investigation," by G. Pekcan, J.B. Mander and S.S. Chen, 7/1/00, (PB2001-100982, A10, MF-A02).
- MCEER-00-0005 "Sliding Fragility of Unrestrained Equipment in Critical Facilities," by W.H. Chong and T.T. Soong, 7/5/00, (PB2001-100983, A08, MF-A02).
- MCEER-00-0006 "Seismic Response of Reinforced Concrete Bridge Pier Walls in the Weak Direction," by N. Abo-Shadi, M. Saiidi and D. Sanders, 7/17/00, (PB2001-100981, A17, MF-A03).
- MCEER-00-0007 "Low-Cycle Fatigue Behavior of Longitudinal Reinforcement in Reinforced Concrete Bridge Columns," by J. Brown and S.K. Kunnath, 7/23/00, (PB2001-104392, A08, MF-A02).
- MCEER-00-0008 "Soil Structure Interaction of Bridges for Seismic Analysis," I. PoLam and H. Law, 9/25/00, (PB2001-105397, A08, MF-A02).
- MCEER-00-0009 "Proceedings of the First MCEER Workshop on Mitigation of Earthquake Disaster by Advanced Technologies (MEDAT-1), edited by M. Shinozuka, D.J. Inman and T.D. O'Rourke, 11/10/00, (PB2001-105399, A14, MF-A03).
- MCEER-00-0010 "Development and Evaluation of Simplified Procedures for Analysis and Design of Buildings with Passive Energy Dissipation Systems," by O.M. Ramirez, M.C. Constantinou, C.A. Kircher, A.S. Whittaker, M.W. Johnson, J.D. Gomez and C. Chrysostomou, 11/16/01, (PB2001-105523, A23, MF-A04).
- MCEER-00-0011 "Dynamic Soil-Foundation-Structure Interaction Analyses of Large Caissons," by C-Y. Chang, C-M. Mok, Z-L. Wang, R. Settgast, F. Waggoner, M.A. Ketchum, H.M. Gonnermann and C-C. Chin, 12/30/00, (PB2001-104373, A07, MF-A02).
- MCEER-00-0012 "Experimental Evaluation of Seismic Performance of Bridge Restrainers," by A.G. Vlassis, E.M. Maragakis and M. Saiid Saiidi, 12/30/00, (PB2001-104354, A09, MF-A02).
- MCEER-00-0013 "Effect of Spatial Variation of Ground Motion on Highway Structures," by M. Shinozuka, V. Saxena and G. Deodatis, 12/31/00, (PB2001-108755, A13, MF-A03).
- MCEER-00-0014 "A Risk-Based Methodology for Assessing the Seismic Performance of Highway Systems," by S.D. Werner, C.E. Taylor, J.E. Moore, II, J.S. Walton and S. Cho, 12/31/00, (PB2001-108756, A14, MF-A03).

- MCEER-01-0001 "Experimental Investigation of P-Delta Effects to Collapse During Earthquakes," by D. Vian and M. Bruneau, 6/25/01, (PB2002-100534, A17, MF-A03).
- MCEER-01-0002 "Proceedings of the Second MCEER Workshop on Mitigation of Earthquake Disaster by Advanced Technologies (MEDAT-2)," edited by M. Bruneau and D.J. Inman, 7/23/01, (PB2002-100434, A16, MF-A03).
- MCEER-01-0003 "Sensitivity Analysis of Dynamic Systems Subjected to Seismic Loads," by C. Roth and M. Grigoriu, 9/18/01, (PB2003-100884, A12, MF-A03).
- MCEER-01-0004 "Overcoming Obstacles to Implementing Earthquake Hazard Mitigation Policies: Stage 1 Report," by D.J. Alesch and W.J. Petak, 12/17/01, (PB2002-107949, A07, MF-A02).
- MCEER-01-0005 "Updating Real-Time Earthquake Loss Estimates: Methods, Problems and Insights," by C.E. Taylor, S.E. Chang and R.T. Eguchi, 12/17/01, (PB2002-107948, A05, MF-A01).
- MCEER-01-0006 "Experimental Investigation and Retrofit of Steel Pile Foundations and Pile Bents Under Cyclic Lateral Loadings," by A. Shama, J. Mander, B. Blabac and S. Chen, 12/31/01, (PB2002-107950, A13, MF-A03).
- MCEER-02-0001 "Assessment of Performance of Bolu Viaduct in the 1999 Duzce Earthquake in Turkey" by P.C. Roussis, M.C. Constantinou, M. Erdik, E. Durukal and M. Dicleli, 5/8/02, (PB2003-100883, A08, MF-A02).
- MCEER-02-0002 "Seismic Behavior of Rail Counterweight Systems of Elevators in Buildings," by M.P. Singh, Rildova and L.E. Suarez, 5/27/02. (PB2003-100882, A11, MF-A03).
- MCEER-02-0003 "Development of Analysis and Design Procedures for Spread Footings," by G. Mylonakis, G. Gazetas, S. Nikolaou and A. Chauncey, 10/02/02, (PB2004-101636, A13, MF-A03, CD-A13).
- MCEER-02-0004 "Bare-Earth Algorithms for Use with SAR and LIDAR Digital Elevation Models," by C.K. Huyck, R.T. Eguchi and B. Houshmand, 10/16/02, (PB2004-101637, A07, CD-A07).
- MCEER-02-0005 "Review of Energy Dissipation of Compression Members in Concentrically Braced Frames," by K.Lee and M. Bruneau, 10/18/02, (PB2004-101638, A10, CD-A10).
- MCEER-03-0001 "Experimental Investigation of Light-Gauge Steel Plate Shear Walls for the Seismic Retrofit of Buildings" by J. Berman and M. Bruneau, 5/2/03, (PB2004-101622, A10, MF-A03, CD-A10).
- MCEER-03-0002 "Statistical Analysis of Fragility Curves," by M. Shinozuka, M.Q. Feng, H. Kim, T. Uzawa and T. Ueda, 6/16/03, (PB2004-101849, A09, CD-A09).
- MCEER-03-0003 "Proceedings of the Eighth U.S.-Japan Workshop on Earthquake Resistant Design of Lifeline Facilities and Countermeasures Against Liquefaction," edited by M. Hamada, J.P. Bardet and T.D. O'Rourke, 6/30/03, (PB2004-104386, A99, CD-A99).
- MCEER-03-0004 "Proceedings of the PRC-US Workshop on Seismic Analysis and Design of Special Bridges," edited by L.C. Fan and G.C. Lee, 7/15/03, (PB2004-104387, A14, CD-A14).
- MCEER-03-0005 "Urban Disaster Recovery: A Framework and Simulation Model," by S.B. Miles and S.E. Chang, 7/25/03, (PB2004-104388, A07, CD-A07).
- MCEER-03-0006 "Behavior of Underground Piping Joints Due to Static and Dynamic Loading," by R.D. Meis, M. Maragakis and R. Siddharthan, 11/17/03.
- MCEER-03-0007 "Seismic Vulnerability of Timber Bridges and Timber Substructures," by A.A. Shama, J.B. Mander, I.M. Friedland and D.R. Allicock, 12/15/03.
- MCEER-04-0001 "Experimental Study of Seismic Isolation Systems with Emphasis on Secondary System Response and Verification of Accuracy of Dynamic Response History Analysis Methods," by E. Wolff and M. Constantinou, 1/16/04.

- MCEER-04-0002 “Tension, Compression and Cyclic Testing of Engineered Cementitious Composite Materials,” by K. Kesner and S.L. Billington, 3/1/04.
- MCEER-04-0003 “Cyclic Testing of Braces Laterally Restrained by Steel Studs to Enhance Performance During Earthquakes,” by O.C. Celik, J.W. Berman and M. Bruneau, 3/16/04.
- MCEER-04-0004 “Methodologies for Post Earthquake Building Damage Detection Using SAR and Optical Remote Sensing: Application to the August 17, 1999 Marmara, Turkey Earthquake,” by C.K. Huyck, B.J. Adams, S. Cho, R.T. Eguchi, B. Mansouri and B. Houshmand, 6/15/04.
- MCEER-04-0005 “Nonlinear Structural Analysis Towards Collapse Simulation: A Dynamical Systems Approach,” by M.V. Sivaselvan and A.M. Reinhorn, 6/16/04.
- MCEER-04-0006 “Proceedings of the Second PRC-US Workshop on Seismic Analysis and Design of Special Bridges,” edited by G.C. Lee and L.C. Fan, 6/25/04.
- MCEER-04-0007 “Seismic Vulnerability Evaluation of Axially Loaded Steel Built-up Laced Members,” by K. Lee and M. Bruneau, 6/30/04.
- MCEER-04-0008 “Evaluation of Accuracy of Simplified Methods of Analysis and Design of Buildings with Damping Systems for Near-Fault and for Soft-Soil Seismic Motions,” by E.A. Pavlou and M.C. Constantinou, 8/16/04.
- MCEER-04-0009 “Assessment of Geotechnical Issues in Acute Care Facilities in California,” by M. Lew, T.D. O’Rourke, R. Dobry and M. Koch, 9/15/04.
- MCEER-04-0010 “Scissor-Jack-Damper Energy Dissipation System,” by A.N. Sigaher-Boyle and M.C. Constantinou, 12/1/04.
- MCEER-04-0011 “Seismic Retrofit of Bridge Steel Truss Piers Using a Controlled Rocking Approach,” by M. Pollino and M. Bruneau, 12/20/04.
- MCEER-05-0001 “Experimental and Analytical Studies of Structures Seismically Isolated with an Uplift-Restraint Isolation System,” by P.C. Roussis and M.C. Constantinou, 1/10/05.



MULTIDISCIPLINARY CENTER FOR EARTHQUAKE ENGINEERING RESEARCH

*A National Center of Excellence in Advanced Technology Applications*

University at Buffalo, State University of New York

Red Jacket Quadrangle ■ Buffalo, New York 14261

Phone: (716) 645-3391 ■ Fax: (716) 645-3399

E-mail: [mceer@mceermail.buffalo.edu](mailto:mceer@mceermail.buffalo.edu) ■ WWW Site <http://mceer.buffalo.edu>



University at Buffalo *The State University of New York*

ISSN 1520-295X